Delivery of Atomised Carbon Substrates for In Situ Bioremediation of Chlorinated Solvents using Medical Jet Nebulisers

Nicholas David Glew

ACKNOWLEDGEMENTS

I would like to acknowledge a number of people for their assistance and support during the period of research and writing of this thesis. Many thanks go to Mark Dyer and Philippe Sentenac for supervising me throughout the research. Without their insight and guidance, this project would have not have been realised. I also owe many thanks to all the technical staff at the University of Strathclyde for their help with various practical issues throughout the course of the research.

A great deal of time, effort and money has been spent on this project by Tauw bv, The Netherlands. I must thank in particular, Emile Marnette, Charles Pils and Chris Shuren. In addition I must thank the Institute of Civil Engineers for financial support on this project.

Above all I owe a the biggest debt of gratitude to my family. To my Mum and Dad for their support through all my education to get to this point. I am very grateful for all you have done for me. Most of all to Jude and Ethan for their unwavering support, understanding and love during all the many hours I worked on this project, without you this thesis would never have been possible.

ABSTRACT

Chlorinated solvents are a group of volatile organic compounds frequently utilised in many commercial applications including metal degreasing, paint stripping and fabric cleaning. Casual and accidental release have led to chlorinated solvents representing one of the most widespread contaminants in the industrialised world. Many of these contaminants pose a serious risk to human health and may persist to depths in the subsurface that preclude ex-situ remediation techniques. Established in situ remediation technologies can be hampered by a variety of technical as well as economical factors.

Laboratory studies have shown that indigenous bacteria, such as *dehaloccocoides ethenogenes*, are able to completely dechlorinate the solvents to innocuous daughter products under anaerobic conditions in a process that has become broadly known as in situ bioremediation. This technique can present a rapid, economical and effective solution for remediating contaminated sites however a major obstacle to its successful implementation is the delivery of an energy source, in the form of an organic substrate, to the bacteria in the subsurface. Current delivery techniques can be hampered by insufficient distribution of the substrate in the subsurface, leading to unreliable bioremediation.

A novel injection technique has been investigated whereby the substrates are atomised and delivered to the subsurface in the form of fine droplets. This technique has been pioneered using the so-called LINER® system, however pilot studies suggest that the transportation of droplets in the subsurface is not yet fully understood. A series of detailed laboratory experiments have therefore been carried out to ascertain the possibility of adapting current nebuliser technology to substrate delivery. Results indicate the possibility of delivering atomised liquids into fully-saturated, granular soils under laboratory conditions. Transportation of an atomised tracer dye was exhibited in a large-scale, fully-saturated coarse-grained sand column however droplet distribution was generally limited to the region directly surrounding the injection filter.

TABLE OF CONTENTS

LIST OF FIGURES

LIST OF TABLES

LIST OF EQUATIONS

NOMENCLATURE

LC_{50}	Lethal Concentration$_{50}$
LTEL	Long Term Exposure Limit
STEL	Short Term Exposure Limit
PCE	Perchloroethylene (tetrachloroethylene)
TCE	Trichloroethylene
K_d	distribution factor
TCA	Trichloroethane
LC_{50}	Lethal Concentration$_{50}$
d	droplet diameter
$\bar{d}$	mean droplet diameter
$d_{0.1}$	droplet diameter at which 10% spray volume lies below
$d_{0.5}$, MMD	droplet diameter at which 50% spray volume lies below
$d_{0.632}$	droplet diameter at which 63.2% spray volume lies below
$d_{0.9}$	droplet diameter at which 90% spray volume lies below
$d_{0.999}$	droplet diameter at which 99.9% spray volume lies below
d_{peak}	peak droplet diameter
d_m	maximum droplet diameter
d_0	minimum droplet diameter
d_{ng}	geometric number mean diameter
d_{sg}	geometric surface mean diameter
d_{vg}	geometric volume mean diameter
N	number of droplets
Q	fraction of liquid less than *d*
d_{32}, SMD	Sauter mean diameter
s_g	geometric standard deviation
s_n	standard deviation
V	volume
X	characteristic diameter in Rosin-Rammler expression
Δ	relative span factor

CHAPTER 1. INTRODUCTION

1.1. *Background to the Research*

Chlorinated aliphatic hydrocarbons (CAH's), in particular chlorinated ethenes, are a group of halogenated volatile organic compounds (VOC's), commonly known as chlorinated solvents, that have seen widespread use in commercial cleaning industries for over three decades (USEPA, 2000). Chlorinated solvents are produced by the substitution of one or several hydrocarbon atoms with chlorine atoms on naturally occurring hydrocarbons such as methane, ethane and ethane (USEPA, 2000) for use in a wide range of commercial applications including metal degreasing, paint stripping and dry cleaning of textiles. Frequently used chlorinated solvents include tetrachloroethylene (PCE), trichloroethylene (TCE) and vinyl chloride (VC). Accidental and casual release to the environment have led to chlorinated solvents representing one of the most common groundwater pollutants in many industrialised countries (Westrick *et al*, 1984, Freedman and Gossett, 1989, De Bruin *et al*, 1992, DiStefano *et al*, 1992, Kao and Prosser, 1999, USEPA, 2000). Many chlorinated solvents and their degradation intermediates, such as *cis*-dichloroethylene, represent a serious risk to the environment and human health. In the USA alone, there are approximately 400,000 sites contaminated with chlorinated solvents and the total cost for remediation has been estimated at $45billion (USEPA, 1997). Figure 1.1 shows the molecular structures of common chlorinated solvents. It should be noted that cis-dichloroethene is caused by biological transformation of trichloroethene.

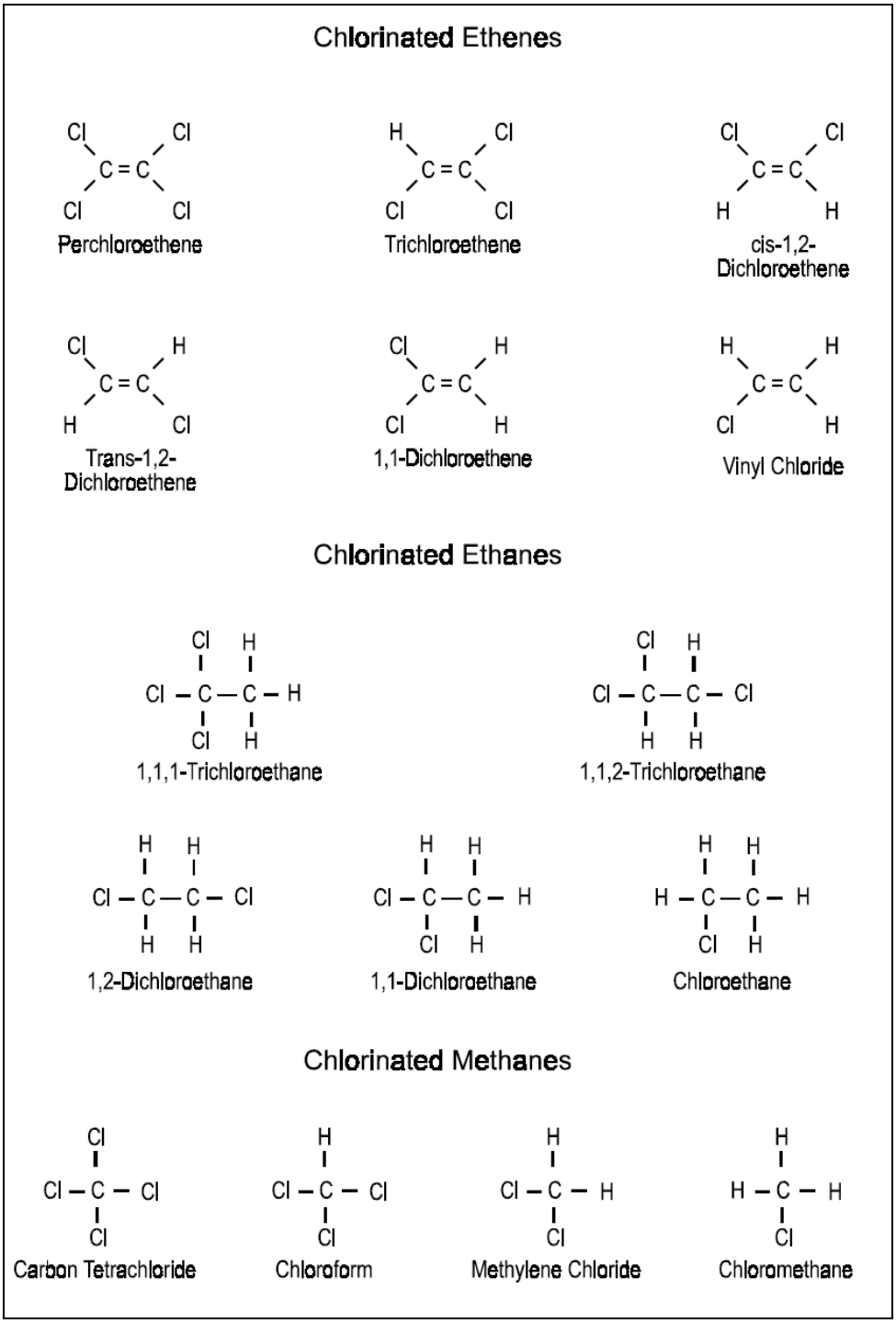

FIGURE 1.1. MOLECULAR STRUCTURES OF COMMON CHLORINATED SOLVENTS (USEPA, 2000).

As most of the solvents exist in an oxidised state, with the exception of vinyl chloride, they are typically not treatable using aerobic oxidation techniques however they can be reduced under anaerobic conditions by chemical or biological techniques. In situ bioremediation is one such technique.

Chlorinated solvent released to the environment is typically transported to the subsurface in the form of a dense non-aqueous phase liquid (DNAPL). Here it generally dissolves in the groundwater aquifer where its transport is governed by advection, diffusion, dispersion which may lead to the contamination of drinking water supplies. Strong partitioning to the solid phase makes the DNAPL extremely difficult to move so a source zone often persists in the subsurface. Figure 1.2 illustrates the potential transportation mechanisms influencing chlorinated solvents in the subsurface.

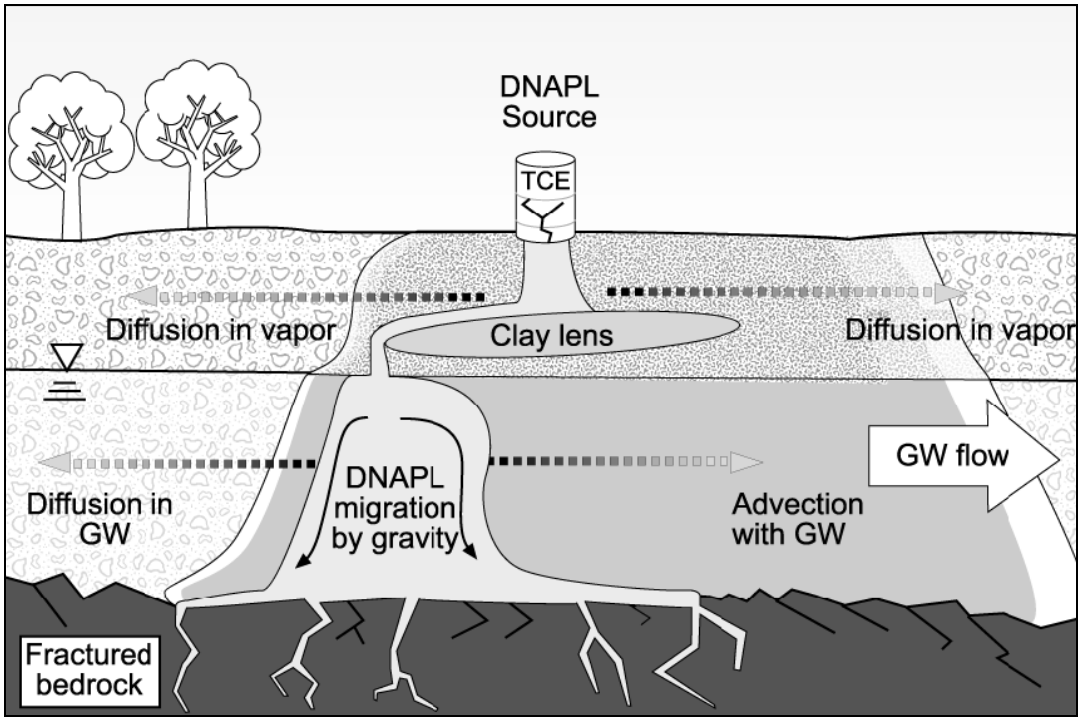

FIGURE 1.2. TRANSPORT MECHANISMS INFLUENCING CHLORINATED SOLVENTS IN THE SUBSURFACE (USEPA, 2000).

Since the identification of the potential pollution issues of these contaminants, techniques have been developed to remediate sites contaminated with chlorinated solvents. These techniques may be ex-situ or in situ and may use chemical, biological or physical processes to lower the aqueous concentration of the contaminant to a regulatory level or to isolate the contaminant from receptors. Currently, the most commonly used remediation strategies are pump-and-treat, thermal desorption, permeable reactive barriers, groundwater recirculation, chemical oxidation and in situ bioremediation.

In situ bioremediation of chlorinated solvents and the delivery of the carbon substrates essential to the bioremediation process will be the focus of this report. Laboratory and field studies have shown that under the correct conditions, aerobic, anaerobic and cometabolic biological processes are able to successfully dechlorinate many chlorinated solvents to innocuous end products such as ethene, ethane and carbon dioxide. Indigenous bacteria in the subsurface are able to use the chlorinated solvents as electron donors or acceptors in redox reactions by which they gain energy to live and propagate in a process known as dehalorespiration. During these reactions the contaminants are sequentially oxidised or reduced to form ethene, ethane or complete mineralisation. One such reaction is known as anaerobic reductive dechlorination which has been shown to successfully dehalogenate chlorinated solvents in laboratory and field studies by a number of researchers. Figure 1.3 shows the anaerobic reductive dechlorination of tetrachloroethylene (PCE) to ethene (ETH).

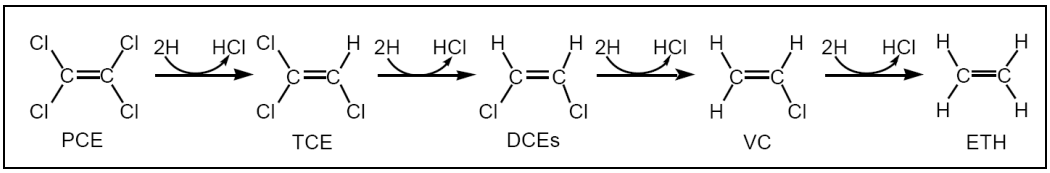

FIGURE 1.3. ANAEROBIC REDUCTIVE DECHLORINATION OF TETRACHLOROETHYLENE TO ETHENE (Maymo-Gatell *et al*, 1997).

In situ bioremediation can be an attractive remediation solution for many sites contaminated with chlorinated solvents. As the technique often uses indigenous bacteria found in the subsurface, required infrastructure at the surface is minimal, meaning relatively low capital and maintenance costs. Under favourable conditions the remediation process can progress relatively rapidly when compared to other techniques (USEPA, 2000). In situ bioremediation also has the advantage of appearing environmentally friendly to the public as it uses natural processes to deal with contamination.

In situ bioremediation is an innovative and relatively novel technology and consequently there are still technical obstacles to its successful implementation at some contaminated sites. One of these obstacles is the reliable and efficient delivery of an energy source to the subsurface to allow the bacteria to live and

propagate and therefore stimulate the dechlorination process. In the case of anaerobic dechlorination the nutrients, in the form of an organic substrate, ferment to provide an electron donor in the form of hydrogen and the contaminant acts as an electron acceptor in the reduction reaction to replace chlorine atoms with hydrogen atoms. Frequently utilised carbon substrates are methanol, lactate, acetate and formate as well as molasses and glucose and currently available techniques for the delivery of these substrates to the subsurface typically involve direct injection or recirculation in the form of a bulk liquid. These injection techniques are often hampered in the field due to inadequate distribution of the substrates in the subsurface, resulting in poor stimulation of the degradation process. The lack of distribution usually arises from poor soil permeability, unexpected variations in stratigraphy or bioclogging, whereby excessive bacterial growth in the region directly surrounding the injection filters blocks pore spaces and prohibits flow of liquid.

A potential solution to overcome this obstacle is to deliver the substrates in the form a fine spray, transported to the subsurface by gas. To produce a sufficiently fine spray, the substrate must be atomised to produce a droplet size small enough to penetrate the pore spaces in the contaminated soil. A wide range of commercial atomisers are available however, and selecting the appropriate droplet size and flow rate can be problematic.

This is a novel technique and consequently there has been no research to date into the transportation of droplets through the subsurface. There is however extensive research on the atomisation of liquids and the commercial applications of common atomisers. The injection of sparging gases in the subsurface has also been extensively researched for use in the volatilization of hydrocarbons and chlorinated solvents.

1.2. *Scope of the Research*

The ultimate aim of the research is to investigate the possibility of delivering carbon substrates to the subsurface in the form of fine droplets for in situ bioremediation of chlorinated solvents using commercially available atomiser technology.

The research will initially comprise of a literature review into previous research carried out into the bioremediation of chlorinated solvents in both laboratory and field studies with particular reference to the use of carbon substrates as electron donors under anaerobic conditions. To the author's knowledge no prior research into the transportation of droplets in geological media has so far been carried out. The theoretical processes involved in the atomisation of liquids and the delivery of gases to the subsurface will be also extensively investigated.

The research will subsequently comprise of an extensive series of laboratory experiments to ascertain the practicality of implementing current atomiser technology to deliver fine droplets to the subsurface.

Small-scale experiments will use a Malvern Mastersizer S laser diffraction particle sizer to extensively investigate the effect on the droplet size distribution of atomised carbon substrates caused by transportation and deposition in small columns of granular soil. These tests will allow initial observations to be made on the feasibility of adapting current atomiser technology to deliver fine droplet to the subsurface. If successful, the experiments will aim to determine the minimum droplet size required to penetrate fine-grained gravel and coarse-grained sand under dry and saturated conditions.

Medium-scale experiments will advance the work of small-scale experiments to quantify the deposition of droplets in geological media. A column will be constructed to investigate the vertical transportation of atomised liquid in a fully-saturated granular soil using a fluorescent tracer dye, rhodamine water tracer. The molar concentration of transported liquid will be quantifiable.

Large-scale experiments will progress the work from medium-scale experiments to more realistically simulate anticipated field conditions. A large column will be constructed to contain fully-saturated granular soil. The column will be constructed in such a way as to allow sampling at a range of heights as well as depths to fully quantify the distribution of atomised liquid in a column of fully-saturated sand.

1.3. *Organisation of the Thesis*

The thesis is divided into eight separate chapters outlined below.

Chapter 1 Introduction to the research
Chapter 2 Review of existing literature
Chapter 3 Theoretical background to the processes of atomisation, sparging
Chapter 4 Experimental methods and materials
Chapter 5 Results obtained from droplet size distribution experiments
Chapter 6 Results obtained from mid-scale column experiments
Chapter 7 Results obtained from large-scale experimental results
Chapter 8 Discussion and conclusions
Chapter 9 Summary and recommendations for future research
Chapter 10 References
Chapter 11 Appendices

CHAPTER 2. LITERATURE REVIEW

2.1. *Chapter Synopsis*

The following chapter presents a review of literature on the remediation of chlorinated solvents using biological techniques. The review presents the conclusions of several laboratory studies into the effectiveness of using microbes to dechlorinate solvents such as tetrachloroethylene and trichloroethylene to innocuous daughter products ethene and ethane as well as the use of substrates to stimulate and enhance the dehalogenation process. The review also presents the findings of field studies into the in situ bioremediation of sites contaminated with chlorinated solvents, in particular the so-called LINER® technique. In addition, the review also presents the findings of research into in situ gas sparging, as this technique will be modified to deliver the atomised substrates to the subsurface.

2.2. *In situ Bioremediation of Chlorinated Solvents*

In situ bioremediation entails the degradation of pollutant chemicals by microbes, fungi and plants in a process whereby the contaminants are transformed to less polluting end products. The treatment of the pollutant is carried out in situ, without the removal of contaminated groundwater from the subsurface. The focus of this research is the reductive dechlorination of chlorinated solvents using anaerobic bacteria which use an organic substrate as an electron donor and the contaminant as an electron acceptor in a process known as halorespiration or dehalorespiration. Laboratory and field studies have shown that aerobic, anaerobic and cometabolic biological processes are able to successfully dechlorinate chlorinated solvents to innocuous end products such as ethene or ethane. In some cases, complete mineralisation of the pollutant is achievable. For in situ bioremediation to be effective the contaminant must be anaerobically degradable, reducing conditions must be achievable, appropriate bacteria must be present in the subsurface and a fermentable source of carbon must be distributed in the contaminated zone (Parsons Corporation, 2004).

Released chlorinated solvent transported to the subsurface and typically exists in the groundwater aquifer as a dense non-aqueous phase liquid (DNAPL). The DNAPL slowly dissolves in the aquifer, where it may persist for long periods of time. This transport mechanism is discussed in more detail in Chapter 3.4.2. Indigenous or exogenous bacteria in the subsurface are able to use the chlorinated solvents as electron donors or acceptors in redox reactions by which they gain energy to live and propagate. During these reactions the contaminants are sequentially oxidised or reduced to form products such as ethene, ethane or complete mineralisation. During anaerobic dechlorination the fermentation of an organic substrate allows hydrogen to be supplied as a direct electron donor to the bacteria.

Bioremediation can be an attractive remediation solution for many contaminated sites as the technique is performed in situ and usually uses indigenous bacteria in the subsurface. Infrastructure required at the surface is minimal, resulting in relatively low installation and maintenance costs. Under favourable conditions, remediation can progress relatively quickly when compared to alternative, established technologies. In situ bioremediation also has the considerable advantage of appearing environmentally friendly to the public as it uses natural processes to deal with contamination.

In situ bioremediation is an innovative technology and therefore there are still technical obstacles to successful implementation at many potential contaminated sites. One of these obstacles is the delivery of sufficient nutrients to the subsurface to stimulate biodegradation of the chlorinated solvents. In the case of anaerobic dechlorination the nutrients act as electron donors as part of a reduction reaction to replace chlorine atoms with hydrogen atoms. Techniques for the delivery of these nutrients to the subsurface are already in existence and typically consist of directly injecting the substrates into the subsurface in the form of a bulk liquid. This technique is often hampered due to insufficient distribution of the substrates in the subsurface caused by bioclogging and variations in stratigraphy.

A potential solution to overcome this obstacle is to deliver the substrates to the subsurface in the form of a fine spray transported by sparging gases. To create a spray, the substrate must be atomised at the surface to produce a droplet size sufficiently small to penetrate the tortuous pore spaces found in granular soils. A wide range of commercial atomisers are available however, and selecting the appropriate droplet size and flow rate can be problematic.

This is a novel technique with limited research to date into the production and transportation of droplets through the subsurface. There is however extensive research on the atomisation of liquids and the commercial applications of common atomisers. The injection of sparging gases in the subsurface has also been extensively researched for use in the volatilization of hydrocarbons and chlorinated solvents.

2.2.1. *Principles of In Situ Bioremediation*

In situ bioremediation involves the use of indigenous or exogenous microbes in the subsurface to dechlorinate chlorinated solvents in the contaminated aquifer. Biodegradation of chlorinated solvents can be achieved directly by using substrates as either electron acceptors (aerobic conditions) or electron donors (anaerobic conditions). In addition, the fortuitous by-products of the metabolisation of another compound may degrade the solvents in a process known as cometabolism. Both direct metabolism and cometabolism can proceed under both aerobic and anaerobic conditions however degradation may limited to less halogenated solvents under aerobic conditions. Direct metabolism involves the dehalogenation of the contaminants by bacteria as electrons are transferred between a substrate and the chlorinated solvent. Cometabolic degradation arises from the fortuitous production of enzymes as the bacteria metabolise a separate compound, often a hydrocarbon. Direct metabolism has been found to dechlorinate chlorinated solvents at rates several orders of magnitude higher than cometabolism (Fetzner, 1998). A number of biological processes can be carried out by a wide variety of microbes. Highly chlorinated molecules such as perchloroethylene are most easily degraded under reducing conditions as they exist in a highly oxidised state. As degradation progresses towards less

chlorinated molecules such as vinyl chloride, oxidising conditions are preferred however degradation may be completed under reducing conditions.

2.2.1.1. *Direct Aerobic Oxidation*

In this process the chlorinated solvent acts as an electron donor and substrate for the microbes and oxygen acts as the electron acceptor. Only those solvents in a reduced state, with less than three chlorine atoms, such as DCE and VC can be degraded by this process. Degradation end products are typically carbon dioxide, water, chloride or free electrons. Under direct aerobic oxidation conditions bacteria belonging to the genera *Mycobacterium*, *Nocardioides* and *Pseudomonas* have been identified as being capable of oxidizing vinyl chloride to carbon dioxide (Field *et al*, 2004). In addition, a strain closely related to *Polaromonas vacuolata* has been found to oxidize cis-DCE to chloride. Figure 2.1 illustrates chlorinated solvent degradation by direct aerobic oxidation.

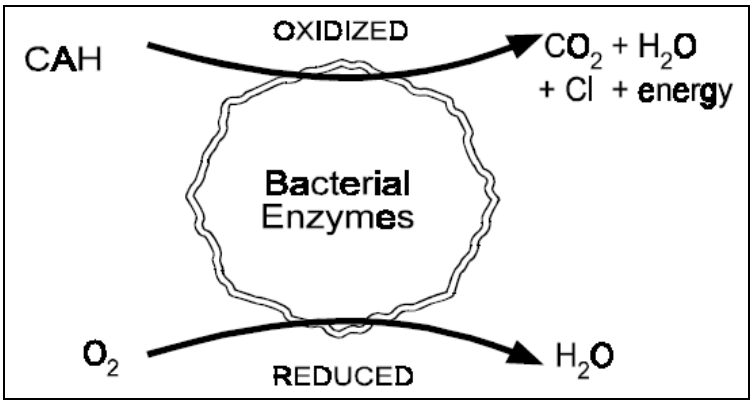

FIGURE 2.1. DIRECT AEROBIC OXIDATION (USEPA, 2000).

2.2.1.2. *Cometabolic Aerobic Oxidation*

In this process the chlorinated solvent is fortuitously oxidised by enzymes such as monooxygenase produced by bacteria during the metabolism of another compound, often a hydrocarbon. Again, cometabolic aerobic oxidation has been shown to degrade solvents with three or less chlorine atoms. This process has been observed during the metabolism of compounds such as methane, ethane, ethene, propane, butane, aromatic hydrocarbons and ammonia. The bacterium *Mycobacterium aurum* has been shown to have the capacity to cometabolise cis-

DCE, trans-DCE and 1,1-DCE. Figure 2.2 illustrates the cometabolic aerobic degradation of CAH's during the metabolism of toluene.

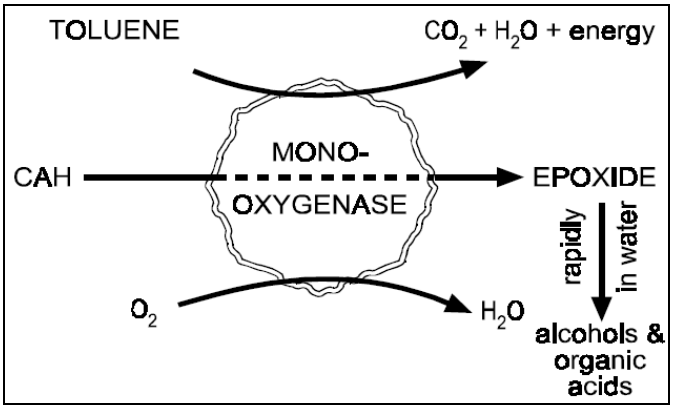

FIGURE 2.2. COMETABOLIC AEROBIC OXIDATION (USEPA, 2000).

2.2.1.3. *Direct Anaerobic Reduction*

As previously discussed, in this process chlorine atoms are sequentially replaced with hydrogen atoms in a reduction reaction. Substrate required as electron donor to produce hydrogen atoms and chlorinated solvent acts as electron acceptor. Direct anaerobic reduction is more suited to degrading highly chlorinated solvents such as PCE and TCE but is capable of complete dechlorination to ethene or carbon dioxide under strongly reducing conditions.

2.2.1.4 *Cometabolic Anaerobic Reduction*

Similarly to cometabolic aerobic oxidation, in this process the chlorinated solvent is degraded by enzymes produced during the metabolism of a separate compound. Methanogens such as *Methanobacterium thermoautotrophicum*, *Methanococcus deltae* and *Methanobacterium thermolithoautotrophicus* have been shown to degrade DCE to acetylene and VC to ethene. Lower chlorinated solvents may also be dehalogenated cometabolically during the direct reduction of higher chlorinated solvents. This has been shown with the dehalogenation of VC with no energy gain by *Dehaloccocoides ethenogenes* during PCE degradation. The solvent does not act as electron acceptor and the bacteria do not

gain energy from the degradation process. Cometabolic and direct degradation can be difficult to distinguish in the field (Grindstaff, 2000).

2.2.2. *Intrinsic In Situ Bioremediation*

This process is also known as monitored natural attenuation or passive bioremediation because the contaminant degradation is monitored rather than actively treated. Natural attenuation is suited to sites where the level of contamination is relatively low or the risk to human receptors is minimal. Natural attenuation sites can operate for many decades and may only seek to contain the contaminant plume rather than completely remediate it. Biological transformation of contaminant is performed by intrinsic subsurface bacteria. Monitored natural attenuation is defined by the USEPA as "*naturally-occurring processes in soil and groundwater environments that act without human intervention to reduce the mass, toxicity, mobility, volume or concentration of contaminants in those media. These in situ processes include biodegradation, dispersion, dilution, adsorption, volatilization and chemical or biological stabilization or destruction of contaminants."* The definition recognises that biological, chemical and physical processes can attenuate contaminants in situ. MNA can only be implemented as a remediation solution if the above factors are sufficient to reduce the risk to humans or the environment to an acceptable level. It can be perceived that MNA is a "do nothing" approach to remediation however the implementation of MNA still requires detailed characterization of the contaminant as well as ongoing assessment of the effectiveness of the natural attenuation. The process of natural attenuation may take many years, decades or even centuries to reduce the concentration of the contaminant to an acceptable level dependant on the characteristics of the contaminant and the subsurface. MNA may be used as the sole remediation strategy at some sites however it is more commonly used as an additional remediation strategy, particularly for chlorinated solvents. Figure 2.3 illustrates a 3-dimensional view of natural attenuation of chlorinated solvents in the subsurface due to biological processes.

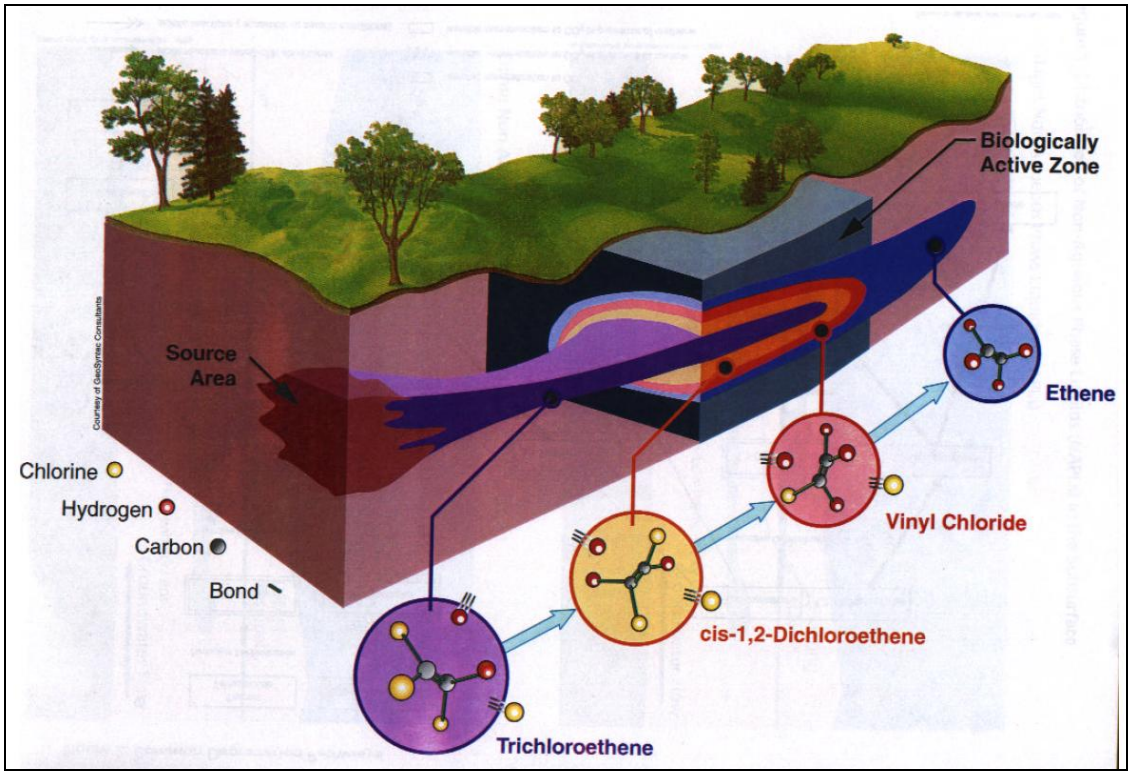

FIGURE 2.3. NATURAL ATTENUATION OF TRICHLOROETHYLENE IN THE SUBSURFACE DUE TO ANAEROBIC DECHLORINATION (ITRC, 1999).

2.2.3. *Enhanced In Situ Bioremediation*

Enhanced bioremediation refers to the addition of nutrients to the subsurface to promote biodegradation of the contaminant. The majority of subsurface bacteria require nutrients in the form of organic substrates such as methanol, ethyl lactate or acetone to live and propagate. A major problem is transporting and distributing the liquid substrates to the bacteria in the subsurface. The hydrogeological conditions and microbial characteristics will significantly influence the implementation of in situ bioremediation at a given contaminated site. Bioremediation of chlorinated solvents is predominantly performed by single-celled prokaryotic bacteria. If the bacteria are indigenous in the subsurface then bioremediation can be performed in situ however an energy source is required for the microbes to live and propagate in the subsurface. This energy is generated in a redox reaction by the transfer of electrons from a donor to an acceptor via the micro-organism and is stored in the form of ATP (adenosine triphosphate) and NAD (nicotinamide adenine dinucleotide). Figure 2.4 shows the basic bioenergetics of a typical microbial system.

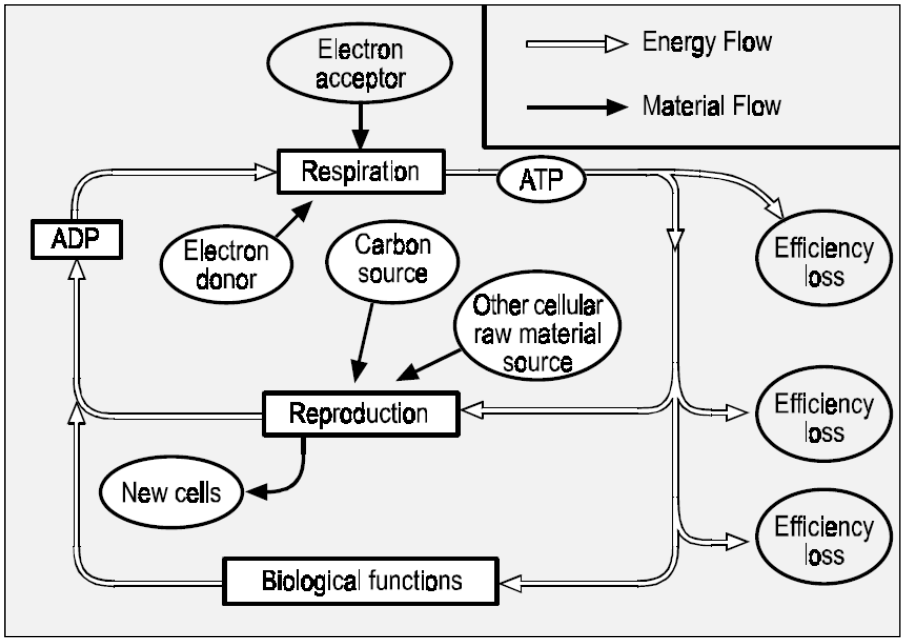

FIGURE 2.4. BIOENERGETICS OF TYPICAL MICROBIAL SYSTEM (USEPA, 2000).

Table 2.1 lists the dominance of bacteria in the subsurface according to the type of electron acceptor they utilise at given redox potentials.

TABLE 2.1. REDOX POTENTIAL AND DEGRADATION MECHANISM (USEPA, 2000).

Dominance	**Electron Acceptor**	**Degradation Mechanism**	**Redox Potential** (V)
More ↓ Less	Oxygen reducing	Aerobic oxidation	+0.82
	Nitrate reducing	Reductive dechlorination	+0.74
	Manganese (IV) reducing		+0.52
	Iron (III) reducing		-0.05
	Sulphate reducing		-0.22
	Carbon dioxide reducing		-0.24

Table 2.2 summarises the potential of biological processes to degrade common chlorinated solvents. It can be seen that only anaerobic processes are able to completely degrade chlorinated solvents on their own however a combination of anaerobic and aerobic processes are also able to transform the pollutants however they would require more than one type of bacterium.

TABLE 2.2. POTENTIAL OF BIOLOGICAL PROCESSES TO DEGRADE COMMON CHLORINATED SOLVENTS (Parsons Corporation, 2000).

	Compound [a/]											
	Chloroethenes				Chloroethanes				Chloromethanes			
Degradation Process	**PCE**	**TCE**	**DCE**	**VC**	**PCA**	**TCA**	**DCA**	**CA**	**CT**	**CF**	**MC**	**CM**
Aerobic Oxidation	N	N	P	Y	N	N	Y	Y	N	N	Y	P
Aerobic Cometabolism	N	Y	Y	Y	P	Y	Y	Y	N	Y	Y	Y
Anaerobic Oxidation	N	N	P	Y	N	N	Y	P	N	N	Y	P
Direct Anaerobic Reductive Dechlorination	Y	Y	Y	Y	Y	Y	Y	Y	Y	Y	Y	Y
Cometabolic Anaerobic Reduction	Y	Y	Y	Y	P	Y	Y	P	Y	Y	Y	P

The stored energy is used proportionally for reproduction and cell maintenance. Under anaerobic conditions the electron donor will take the form of hydrogen fermented from an organic substrate, with the electron acceptor being the contaminant. Bacteria that gain their energy from these redox reactions are known as chemotrophs. A major problem with the reductive dechlorination of PCE and TCE is that without complete metabolism to ethene, high concentrations of *cis*-DCE and VC, which are both potentially more toxic and carcinogenic than PCE or TCE, may remain dissolved in the groundwater aquifer. Certain bacteria are capable of dechlorinating chlorinated solvents as a respiratory process. As the bacteria utilise the dissolved substrate, a local zone of depletion is created around them. Substrate is replenished by diffusive transport (Simoni *et al*, 2001). Figure 2.5 illustrates the idealised degradation of chlorinated solvents in an anaerobic system.

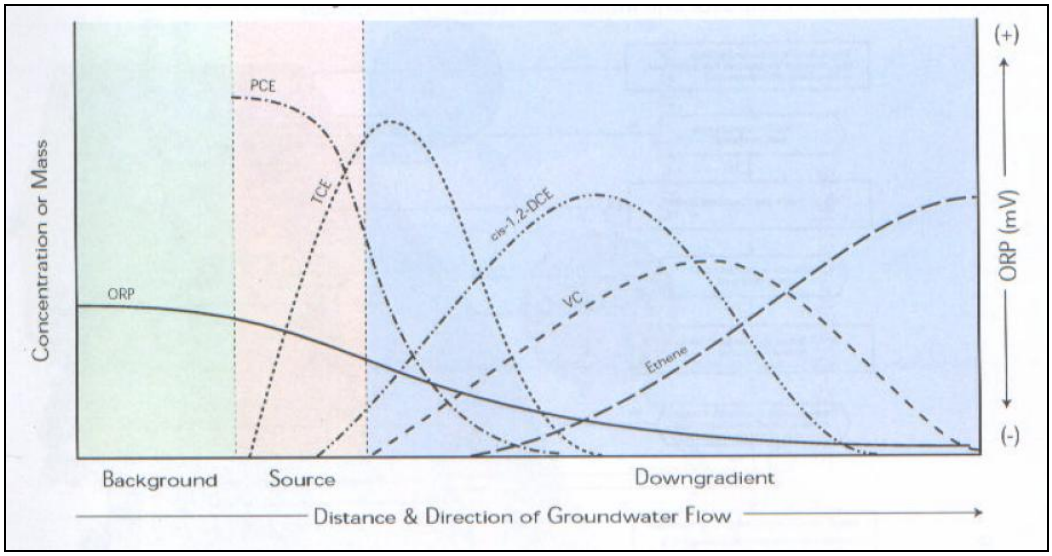

FIGURE 2.5. CHLORINATED SOLVENT DEGRADATION IN AN ANAEROBIC SYSTEM (ITRC, 1999).

2.2.4. *Laboratory Studies of Bioremediation*

Several bacteria have been shown to degrade PCE to its daughter products under anaerobic conditions however they are only able to partially dechlorinate PCE to *cis*-DCE or vinyl chloride (Maymó-Gatell *et al*, 1997). A mixed culture would historically have been be required to completely degrade PCE or TCE to ethene however one recent discovery is that of a bacterial strain capable of completely dechlorinating PCE to ethene under anaerobic conditions.

Freedman and Gossett (1989) conducted laboratory studies to investigate the degradation of PCE to ethene under methanogenic conditions. PCE and TCE solutions of 1.2µM and 8.6µM respectively were added to anaerobic enrichment cultures in 160ml serum bottles at 35°C. First generation cultures were created by placing anaerobic sludge from a wastewater plant into a 15l anaerobic digester, stirred for 20 days at 35°C. Subsequent generation cultures were taken consecutively from the bottles containing the previous generation cultures at a volume of 2-10%. Control samples containing contaminant solution and distilled water were sampled alongside the enrichment cultures. Samples were analysed using a gas chromatograph with a detection limit range of 3.60nmol (for 1,1-DCE) to 14.3nmol (for cis-DCE). The investigation found PCE to be degraded in some first-generation culture bottles. In one sample bottle a total of 9.93µM of

PCE had been degraded by day 55. VC concentration rose to a maximum of 7.64µM and then decreased. By day 85 the concentration of ethene reached a plateau. In another bottle, 84 consecutive additions of PCE were degraded with TCE and cis-DCE being produced until day 31 after which both steadily declined, TCE disappearing first. By day 309, a total of 36.4µM had been degraded with 4.9µM VC remaining. Control samples recorded a reduction of PCE concentration from 618nM to 228nM over the same period. Further studies investigated the use of methanol as an electron donor. The research found that the rate of PCE degradation accelerated when methanol was added to the enrichment cultures at a concentration of 2mg/l. The production of methane indicated that the methanol was being used by the culture. When methanol addition ceased, the rate of degradation significantly decreased. Similar experiments using glucose, formate, acetate as well as hydrogen produced similar results however methanol was found to be the most effective substrate.

Kastner (1991) used laboratory experiments to investigate the importance of the transition from aerobic to anaerobic conditions on the dechlorination of chlorinated solvents. Groundwater samples, contaminated with PCE (98µM) and TCE (111µM) were taken from a contaminated site in Braunschweig, Germany. Two types of bacterium were identified for the tests, namely *Bacillus* sp and *Desulfotomaculum* sp which are not classed as methanogenic bacteria. Dechlorination to cis-DCE was only found to occur after the establishment of reducing conditions in the samples, after approximately 2 to 4 days. A redox potential of -50mV to -150mV was found to start the transformation process when carbon substrates were present in the samples. In cultures that were anaerobic from the beginning, dechlorination ceased at TCE. The transformation of PCE to cis-DCE was thought to coincide with a drop in redox potential caused by the production of sulphide, which also caused the abiotic production of 1,1-DCE. The research concluded that in the absence of methanogens, aerobic or facultative anaerobic bacteria can be used to start the dechlorination process.

DiStefano *et al* (1992) conducted similar experiments to Freedman and Gossett (1989) however the research indicated that dechlorination of tetrachloroethylene to ethene could be achieved in the absence of methanogenesis. The research

concluded that relatively large amounts of PCE could be degraded to ethene in the absence of methanogenesis In fact when PCE concentrations were found to be significantly high, results suggested that methanogens were precluded from dechlorinating the contaminant. This is turn suggested that other microbes were responsible for dehalogenating the PCE.

Gibson and Sewell (1992) conducted studies on the addition of short-chain organic acids and alcohol for the reductive dechlorination of tetrachloroethene by anaerobic microbes. The researchers tested acetate (4mM), lactate, (3mM), propionate (3mM), butyrate (2mM), crotonate (2mM), methanol (4mM), ethanol, (2mM) and isopropanol (3mM) in 20ml bottles containing 30µM PCE. The research found ethanol and lactate to initiate degradation to TCE by the time the first samples were taken at 6 days. Butyrate, crotonate and propionate were also found to degrade the PCE however at a slower rate than ethanol or lactate. Methanol, acetate and isopropanol did not appear to stimulate degradation of the PCE solution however this may have been a result of relatively low amounts of organic carbon in the soil sample from which the aquifer water was taken. The research supported the theory that easily fermentable electron donors such as ethanol and lactate promote relatively rapid degradation of chlorinated solvents and less easily fermentable electron donors such as butyrate and propionate result in slower rates of dechlorination. In the case of methanol, acetate and isopropanol, it was concluded that the relatively low levels of organic carbon were insufficient to support the microbes that normally use these electron donors successfully as substrates. The research highlights the importance of selecting the correct electron donor for specific sites.

De Bruin *et al* (1992) conducted laboratory experiments to investigate the possibility of using electron donors to dechlorinate Tetrachloroethene to ethene. Experiments were performed in a 25cm long, 5.5cm diameter column packed with a mixture of anaerobic sediment and aerobic sludge. To maintain anaerobic conditions, the column was continuously percolated from the bottom with an oxygen depleted mineral solution. Initially, the column was fed with a PCE solution of concentration 0.6µM at a rate of 15ml/h at 20°C using a syringe pump. Lactate was selected as an electron donor and injected into the column at a

concentration of 1mM. The research investigated the influence of several factors, namely contaminant concentration, flow rate and temperature, on the dechlorination process. PCE concentration was increased over time to 9µM, flow rate was increased to 60ml/h and column temperature was reduced to 10°C. A gas chromatograph was used to analyse water samples extracted from the column. The investigation found that after two weeks, no PCE could be detected in the column. The PCE had degraded to TCE, cis-DCE and VC. The flow distance needed to completely dechlorinate the PCE to ethene was the entire length of the column. As the PCE concentration was increased, samples revealed that the contaminant was being reduced to ethene via the aforementioned daughter products and that ethene was being further reduced to ethane. An increase in flow rate resulted in liquid taking 6 hours to be transported the length of the column however despite this reduction in retention time the PCE was still dechlorinated to ethene and the flow distance required to complete reduced to 5cm by day 240. After day 250 a steady state was achieved, allowing mass balance calculations to reveal that approximately 95-98% of the PCE had been dehalogenated to ethane. Decreasing column temperature briefly impaired the bioremediation process, with 2% PCE detected in samples however within one month sample concentrations returned to 20°C levels. The research concluded that the complete reductive dechlorination of PCE to ethane is possible under anaerobic conditions where previous research had indicated that only partial reduction was possible. The maximum possible elimination rate of PCE was calculated to be 3.7µM/l/hr however the research indicated that an electron donor such as lactate was required to eliminate the intermediary products of TCE, cis-DCE and VC.

Maymó-Gatell *et al* (1997) discovered a new strain of bacterium capable of completely dechlorinating PCE to ethene under anaerobic conditions. Laboratory studies showed that *Dehalococcoides ethenogenes* strain 195 cell counts grew for 5 days (growth rate approximately 19.2 hours) in the presence of H_2 and PCE however after 5 days growth stopped. Growth was only recorded in the presence of both H_2 and PCE. PCE could be metabolised to VC at rate of 40µmol/hour/litre culture. The metabolism of VC to ethene followed a first-order kinetics decay rate with the half life for the first 300 hours found to be

approximately 80 hours slowing to 150 hours thereafter. The decay rate of VC is therefore seen to slow after time suggesting that *Dehalococcoides ethenogenes* strain 195 may not be able to indefinitely metabolise VC in the absence of nutrients. Nonetheless the research concluded that a mixed-culture of bacteria were no longer required to dehalogenate PCE completely to ethene, raising the possibility of inoculating contaminated sites with *Dehalococcoides ethenogenes* strain 195 where rates of biodegradation were insufficient to meet regulatory guidelines efficiently.

Fennell and Gossett (1997) compared butyric acid, ethanol, lactic acid, and propionic acid as hydrogen donors for the reductive dechlorination of tetrachloroethene. Long term tests were carried out in 160ml serum bottles containing 100ml of an anaerobic mixed culture that had previously been enriched with methanol, PCE and yeast extract. Initial experiments added PCE and electron donor in a 1:1 ratio in terms of an electron equivalent basis. For butyric acid, ethanol and lactic acid this resulted in 22µmol of electron donor being added for every 11µmol of PCE. Further experiments doubled the volume of electron donor to a 2:1 donor to PCE ratio. Short-term studies were performed intermittently by removing 10ml of culture and adding the appropriate ratio of PCE and electron donor. The research found that all the electron donors were able to dechlorinate PCE to vinyl chloride and ethene in similar amounts over long term studies however short-term studies illustrated marked differences in contaminant degradation for the different donors. Ethanol was found to rapidly degrade PCE for approximately 3½ hours then abruptly slow at both 1:1 and 2:1 donor to PCE ratios. This phenomenon was supported by considerable methane production in the first 3½ hours, followed by a cessation in production. Hydrogen production was found to peak between 1 and 2 hours at approximately 3300nmol. Lactic acid was found to be a much more effective electron donor when added to the PCE at a ratio of 2:1. Maximum hydrogen production was found to be approximately 3000nmol between 1 and 2 hours and PCE dechlorination was found to progress quickly during this time. After lactic acid was completely depleted, the dechlorination process was found to continue, albeit at a lower rate due to the production of propionic acid during the fermentation of the lactic acid. Propionic acid was found to dechlorinate PCE to

VC with some TCE at a relatively slow rate when compared to ethanol and lactic acid. Hydrogen production was found to be very low, peaking at approximately 20nmol after 10 hours. Similar results were obtained when the ratio of donor to PCE was increased to 2:1. Similarly, butyric acid dechlorinated PCE to TCE and VC over a 24 hour testing period. Hydrogen production was found to be steady at approximately 30nmol during the test. Increasing the ratio of donor to PCE to 2:1 resulted in increased hydrogen production to 150nmol and a reduction of TCE when compared to the 1:1 ratio. The research concluded that over the long term all the tested electron donors were able to successfully dechlorinate PCE to ethene. Short term tests revealed more about the mechanisms by which the degradation occurred. The slowly fermenting donors butyric acid and propionic acid supported the activity of dechlorinators while precluding methanogens, resulting in slow dechlorination to vinyl chloride with occasional accumulation of TCE. The rapidly fermenting donors ethanol and lactic acid, particularly at a donor to PCE ratio of 2:1, supported high levels of methanogen activity followed by an abrupt slowdown in dechlorination, leaving significant volumes of PCE to slowly degrade. This is in good agreement with the experiments carried out by Gibson and Sewell (1992).

Gerritse *et al* (1997) found that at high dechlorination rates, degradation of PCE under anaerobic conditions often could not progress past *cis*-DCE when methanol of concentration 20mM was used as an energy source however the addition of formate, acetate and glucose was more successful. They investigated the possibility of using coupled anaerobic and aerobic reduction to completely dehalegonate PCE to ethene. However it was found that with the addition of nutrients, complete dehalogenation of PCE and TCE to ethene was possible under anaerobic conditions. In apparent contrast to the experiments carried out by many other researchers, the research found the addition of methanol to have a detrimental effect on the degradation of the contaminants however lactate and formate were able to degrade to ethene. The researchers postulated that methanogenic bacteria were not present in the sludge.

Jayaraj *et al* (2003) performed studies using ethyl lactate as an electron donor to a mixed anaerobic culture and a pure culture of *Dehalospirillium multivorans* in

the reductive dechlorination of tetrachloroethylene. Batch reactors were fed with 0.88µl/hr PCE and 1mM ethyl lactate every 12 hours at a rate of 2.5ml/min. PCE dechlorination was investigated by measuring chloride production using ion chromatography techniques. Simultaneous experiments using lactate and acetate were also performed. Chloride release measured from the reactors was found to be nearly ten times higher in the sample using ethyl lactate as an electron donor. The research concluded that ethyl lactate was able to stimulate the biodegradation of PCE to TCE under anaerobic conditions however the researchers did not investigate the further degradation of TCE to its daughter products.

2.2.5. *Field Studies of Bioremediation*

Harkness *et al* (1998) conducted studies at an industrial park contaminated with TCE (7700µg/L), 1,1,1-TCA, VC (56µg/L) and *cis*-DCE (830µg/L) and 1,1-DCE in a highly permeable groundwater aquifer. Soil samples were taken from the site and placed in 60cm length, 5cm internal diameter columns to which groundwater was pumped at an initial rate of 0.1ml/min. The groundwater was periodically spiked with TCE at a concentration of 5mg/L (38µM). Electron donors in the form of methanol (5.0mM) and sodium lactate (2.5mM initially then reduced to 1.0mM after 1 month) were added to the pumped groundwater. Dissolved oxygen measurements concluded that reducing conditions were achieved after 27 days and reducing potential finally reached -150 to -250mV indicating strongly reducing conditions. Degradation of TCE to cis-DCE was first observed at 18 days. By noting the height in the column that TCE transformation was complete, the researchers concluded that degradation to cis-DCE was taking approximately 3 hours. After 50 days no cis-DCE was detected in pore water samples and by day 81 VC and ethene were first detected however this coincided with a reduction in groundwater flowrate to 0.5ml/min. After 173 days complete transformation of TCE to ethene was observed by the lowest sampling port in the column and by 208 days ethene had been further reduced to ethane. Methanol and sodium lactate were found to have degraded to acetate, propionate, hydrogen, methane, and CO_2 by day 27. Acetate and propionate further degraded to methane and CO_2 in good agreement with the observations of Fennell and

Gossett (1989). An increase in TCE feed concentration from 4mg/L to 180mg/L at between days 208 and 404 resulted in continued dechlorination to ethene or ethane by the microbes however at day 321 sodium lactate addition was ceased, resulting in VC and cis-DCE appearing in column effluent samples. This phenomenon indicated the dependence of at least part of the microbial community on sodium lactate as an electron donor. The research concluded that the remediation of relatively high concentrations of TCE was possible given that an appropriate microbial community is present in the subsurface and an appropriate electron donor is added to stimulate dechlorination. The highest concentration of TCE added to the test column (180mg/L or 1400µM) is similar to the concentration of TCE found in the NAPL zones of contaminated aquifers, indicating the potential of enhanced in situ bioremediation to successfully dechlorinate source zones of contaminated aquifers. Table 2.3 summarises the key findings of the aforementioned research into the addition of electron donors to stimulate bioremediation of chlorinated solvents.

TABLE 2.3. SUMMARY OF RESEARCH INTO ADDITION OF ELECTRON DONORS TO STIMULATE BIOREMEDIATION OF CHLORINATED SOLVENTS.

Researchers (Year)	*Contaminants*	*Electron donors*	*Comments*
Freedman and Gossett (1989)	PCE, TCE	Methanol, glucose, formate, acetate, hydrogen	Successful dechlorination to ethene. Dechlorination acceleration with electron donor addition. Methanol most successful electron donor.
DiStefano *et al* (1992)	PCE	H_2, methanol	H_2 found to act as direct electron donor to dechlorinate PCE. Methanol ferments to provide H_2.
Gibson and Sewell (1992)	PCE	Acetate, lactate, propionate, butyrate, crotonate, methanol, ethanol, and isopropanol	Ethanol and lactate initiated degradation to TCE . Butyrate, crotonate and propionate also degraded PCE however at a slower rate. Methanol, acetate and isopropanol did not stimulate degradation.
De Bruin *et al* (1992)	PCE	Lactate	PCE successfully degraded to ethane.
Maymó-Gatell *et al* (1997)	PCE	H_2	PCE completely degraded to ethene using a single strain of bacterium, *Dehalococcoides ethenogenes.*
Fennell and Gossett (1997)	PCE	Ethanol, lactic acid, butyric acid, propionic acid.	Ethanol and lactic found to degrade quickly then slow rapidly. Butyric acid and propionic acid found to degrade more slowly however without sudden decrease.
Gerritse *et al* (1997)	PCE	Methanol, formate, acetate and glucose	Formate, acetate and glucose found to be more successful electron donors than methanol.
Harkness *et al* (1998)	TCE, 1,1,1-TCA, VC, *cis*-DCE, 1,1-DCE	Methanol, sodium lactate	Methanol and sodium lactate successful electron donors.
Jayaraj *et al* (2003)	PCE	Ethyl lactate, lactate, acetate	Ethyl lactate found to stimulate PCE dechlorination to TCE.

2.3. *In Situ Air Sparging and Transport of Gas in the Subsurface*

In situ air sparging (IAS) involves the injection of compressed air into the saturated zone of the subsurface to promote volatilization and physical removal and/or aerobic degradation of a dissolved contaminant (Hinchee, 1994, Roosevelt

et al, 1998, Elder *et al*, 1999). The technique was pioneered as an innovative technology in Germany in the mid 1980's to aid the in situ remediation of chlorinated solvents, as reported by Gudemann *et al* (1988). Since its implementation, sparging has been used extensively for the in situ remediation of both chlorinated solvents and petroleum hydrocarbons. A review of in situ air sparging is pertinent to the scope of this thesis as the technical factors influencing this technique will be crucial to understanding the injection of an anaerobic carrier gas into the subsurface to transport the atomised carbon substrates to the contaminated aquifer.

2.3.1. *Principle of Operation*

2.3.1.1. *IAS for Volatilisation*

The principle of using IAS for volatilization is to strip the contaminant from the soil/water matrix and transfer it to the gaseous phase. The gaseous contaminant will then be transported to the vadose zone where it may be collected using soil vapour extraction techniques for further treatment. The volatilization and transport of contaminants in the subsurface may cause problems if the vapours are not properly controlled. Transfer of the contaminant to the gas phase is a diffusion process that will be limited by the surface area and time of contact at the gas/contaminant interface (Baker and Benson, 1996). Figure 2.6 illustrates the volatilization of NAPL during IAS at the pore scale.

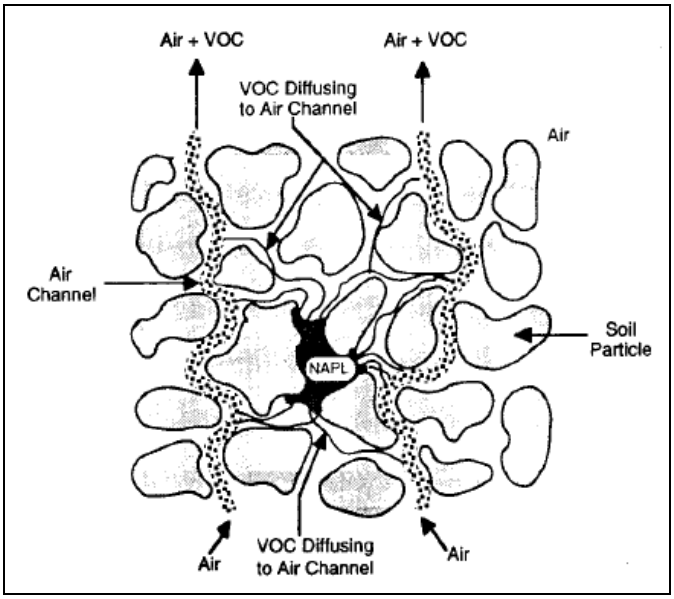

FIGURE 2.6. PORE SCALE VOLATILIZATION OF NAPL DURING IAS (Baker and Benson, 1996).

The proportion of NAPL mass removed will also be dependant on the Henry's constant of the NAPL and to a lesser degree, the tortuosity of the gas channels. Analytical modelling carried out by Elder et al (1996) sought to quantify the effect of several factors on the mass removal of contaminant from an aquifer. It was proposed that Henry's constant has the greatest influence on mass removal while tortuosity has the least influence.

2.3.1.2. *IAS for Bioremediation*

In situ air sparging may also be used to increase the dissolved oxygen content of the contaminated aquifer and therefore promote aerobic oxidation of chlorinated solvents by indigenous microbes as discussed in Chapter 2.2. Biodegradation of contaminant is more likely to occur toward the end of the clean up situation when volatilization has removed the majority of the contaminant. It has been proposed that in a typical IAS installation, biodegradation will account for around 15% of contaminant removal with volatilization accounting for the remaining 85% (Boersma, 1993). The low solubility of oxygen in water, around 10mg/l, limits the use of air sparging for this application however in zones where aerobic biological activity is already high, IAS can be used to replenish the oxygen that is constantly being consumed by the microbes and IAS is generally a cheaper

alternative to injection of hydrogen peroxide. Because IAS can be capable of delivering large volumes of oxygen to the subsurface. In situ sparging is not limited to injection of air. Gases such as O_2, H_2, CH_4, NH_3, and CO_2 may also be injected to promote aerobic or anaerobic degradation of chlorinated solvents.

In situ air sparging requires the injection of pressurised gas down a well, through a subsurface injection filter. A large surface compressor is typically used to create sufficient pressure to overcome capillary and hydrostatic forces. Figure 2.7 shows an idealised schematic of an in situ sparging installation.

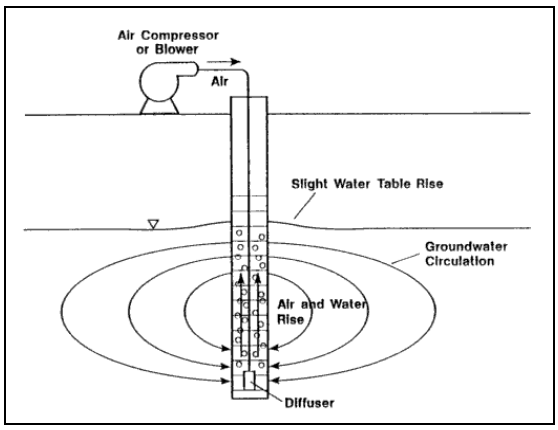

FIGURE 2.7. IDEALISED AIR SPARGING INSTALLATION (Hinchee, 1994).

In situ air sparging is a complex multi-phase fluid dynamic situation. Gas injected into the fully-saturated subsurface is transported laterally by driving pressure and vertically by buoyancy forces (Elder *et al*, 1999). The gas can be injected continuously or in a pulsed manner. Pulsing the gas flow can help to form new gas channels and therefore increase the distribution of gas channels in the subsurface (Boelsma *et al*, 2000). The migration of the air will be determined by the hydrogeological properties of the aquifer, particularly the height of the water table above the injection filter and the capillary pressure which is inversely proportional to the diameter of the pore spaces in the soil matrix. Knowledge of these factors can be used to calculate a zone of influence for a sparging well. In addition, the potential of IAS to be installed as a remediation method will be dependant on the physical characteristics of the contaminant and/or the biological activity in the subsurface.

Figure 2.8 illustrates the typical desaturation and subsequent resaturation of an aquifer during IAS. The period of air injection was 20 minutes.

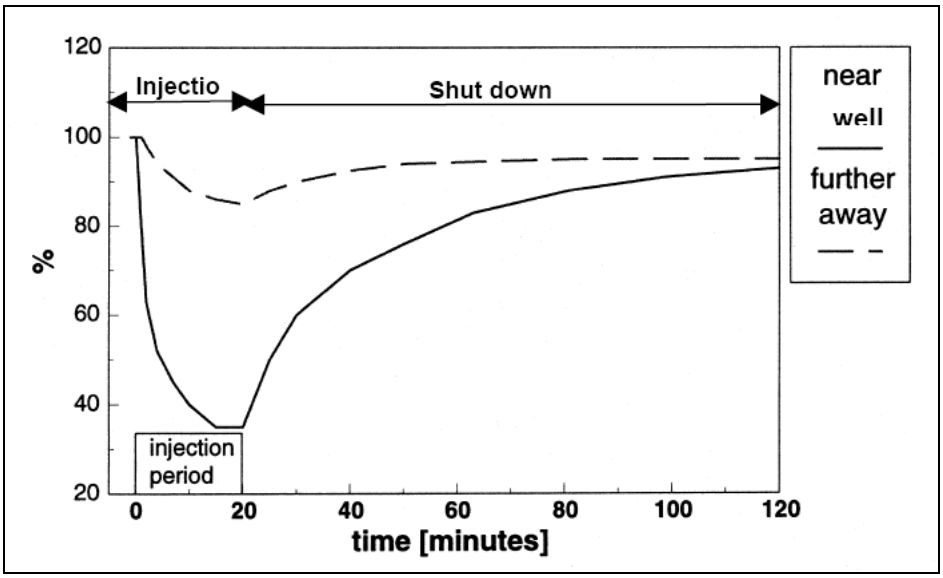

FIGURE 2.8. INFLUENCE OF IAS ON DEGREE OF SATURATION OF A GROUNDWATER AQUIFER (Boelsma *et al*, 2000).

Air sparging in homogeneous media can be characterised into 4 stages:

1. Initial injection of air leads to substantial dewatering in the region directly surrounding the injection point. This phenomenon has been observed in the field by Lesson *et al* (1995) who found that the majority of air was contained within 0.3 to 0.6m of the injection point. Lundegard *et al* (1998) found air saturation in this zone to be a maximum of 20-40%. This is due to the air pressure in this region being significantly greater than hydrostatic pressure. The air/water interface is likely to be spherical during this initial growth period.
2. Buoyancy forces transport the majority of the airflow vertically although a limited amount of lateral migration persists. Individual channels may be created that transport air away from the air zone.
3. Vertically transported air penetrates the vadose zone. Air pressure drops due to increased airflow into the vadose zone resulting in a reduction in the air volume.
4. Air volume reaches steady state. Individual channels may remain in the soil mass.

When a steady stage is reached the radius of influence will no longer increase in size. The radius of influence is the conceptual boundary at the base of the vadose zone outside which gas concentration is not high enough to be of benefit to volatilization or aerobic degradation. The term radius should be used with care as an air plume is rarely circular in nature due to subsurface heterogeneities. Because of this it is often desirable to pulse the gas injection so that a steady stage is not reached, thus maximising the radius of influence. It should be noted that not all air channels will breakthrough to the vadose zone. These are known as dead-end pores and are mostly located toward the fringe of the air plume where pressure is relatively low and may not be enough to locally displace pore water.

The effectiveness of any in situ air sparging technique will largely depend on the channel density and radius of influence of the gas plume. An increase in pressure may lead to an increase in channel density and radius of influence but there is a maximum pressure that must not be exceeded if liquefaction of the soil is to be avoided.

2.3.2. *Governing Parameters*

As the air migrates through the soil volatile pollutants diffuse into the gaseous phase and are carried into the vadose zone. The gaseous phase pollutants are consequently removed from the vadose zone using soil vapour extraction (SVE) techniques.. The airflow pattern will resemble a parabolic shape when injected into homogenous media as demonstrated in qualitative laboratory experiments by Ji *et al* (1993). Individual air channel characteristics are governed by the physical properties of the soil, particularly pore size, and the injection flow rates and pressures. For flow of gas to occur, air entry pressure must be exceeded at the point of injection. Air entry pressure, P_a can be given by:

$$P_a = P_1 - P_{hyd} \qquad \text{(EQN 2.1)}$$

Minimum injection pressure, $(P_{inj})_{\min}$ is given by the sum of hydrostatic pressure, P_{hyd} and capillary pressure, P_{cap}:

$$(P_{inj})_{\min} = P_{hyd} + P_{cap} = \rho_{pf} g h_{wt} + \frac{4(\sigma_{g/pf})\cos\theta}{D} \qquad \text{(EQN 2.2)}$$

ρ_{pf} = pore fluid density
g = gravitational acceleration
h_{wt} = height of water table above injection point
$\sigma_{g/pf}$ = interfacial tension between gaseous and liquid phase
θ = contact angle (assumed to be 0º for complete wetting)
D = average pore size diameter

In order to avoid fluidisation of the porous media, maximum injection pressure, $(P_{inj})_{\max}$ must not exceed the minimum in situ effective stress, σ':

$$(P_{inj})_{max} = min(\sigma'_{vertical}, \sigma'_{horizontal}) \qquad \text{(EQN 2.3)}$$

where:

$$\sigma'_{vertical} = (\rho_{sat} h_s - \rho_{pf} h_{wt}) g$$

$$\sigma'_{horizontal} = K_0 \sigma'_{vertical}$$

ρ_{sat} = saturated density of soil
h_s = height of soil above sparge point
$K_0 = 1 - \sin\varphi'$

Modified Bond number, N_B^*, defines whether capillary forces or buoyancy forces will dominate gaseous flow through porous media (Krauss et al, 2003):

$$N_B^* = \frac{\Delta\rho g r^2}{\sigma\alpha} \qquad \text{(EQN 2.4)}$$

σ = difference in surface tension between gaseous and liquid phase;
α = ratio of pore neck size to pore body size.

For N_B^*<1 capillary forces will dominate and for N_B^*>1 buoyancy forces will dominate (Krauss et al, 2003). In granular soils, buoyancy forces will dominate.

Figure 2.9 shows the effect of gas channel spacing on the clean up time for TCE. The graph shows that in theory clean up can proceed at three orders of magnitude faster if air channel spacing is reduced from 480mm to 20mm.

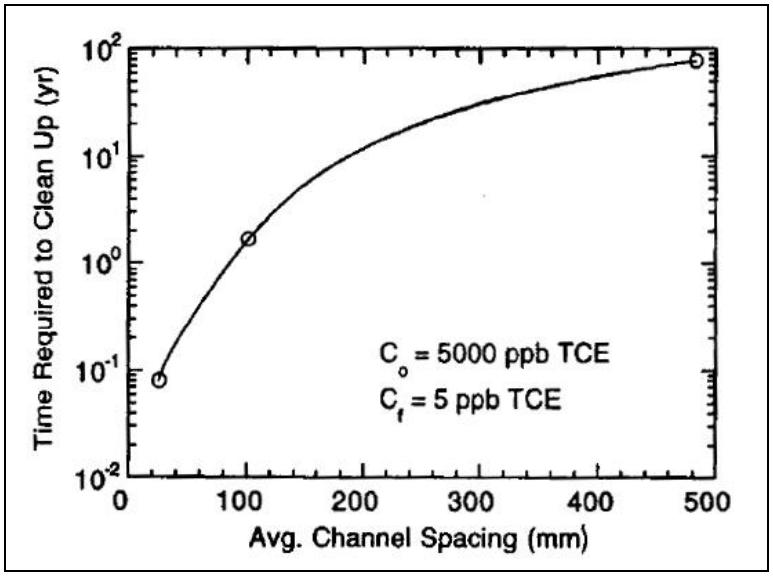

FIGURE 2.9. RELATIONSHIP BETWEEN GAS CHANNEL SPACING AND TCE CLEAN UP TIME (Ahlfield *et al*, 1994).

It could be inferred from this data that average channel spacing could have a similar effect on the efficiency of delivering fine droplets to the subsurface. If gas channels are spaced too far apart, droplets will likely not be able to reach all parts of the contaminated groundwater, thus reducing the stimulation of the biodegradation process and increasing the time taken to reduce the aqueous concentration of the chlorinated solvents to an acceptable level. One solution to effectively increase the average channel spacing is too pulse the injection of the carrier gas as discussed in Chapter 2.3.1.2. The advantage of pulsing carrier gas injection over continuous injection may be twofold. New air channels may be formed during each injection cycle, increasing the air channel density when considered over the long-term installation of the system. In addition the reintroduction of water into desaturated pores may disturb recalcitrant contaminant thereby increasing the effectiveness of the next injection cycle. This phenomenon has been observed during laboratory experiments into the volatilisation of contaminants using in situ air sparging by Baker (1996).

Average air saturation is considered to be a good measure of air channel density. Experiments carried out by Acomb *et al* (1995) and Baker (1995) appeared to show that an increase in gas flow rate or pressure increases the average air saturation briefly however a maximum is quickly reached whereby increase in flow rate or pressure no longer increases average air saturation as shown in Figures 2.10 and 2.11 respectively. Local air pressure increases until the air entry pressure has been reached. At this point a large proportion of water is expelled from the pore which is represented by the steep section of each graph. Once this has been achieved, any further increase in flow rate and/or pressure results in very little or no increase in air saturation. Field experiments carried out by Lundegard and LaBrecque (1995) showed that the average air saturation of an aquifer undergoing continuous air injection was approximately 42%.

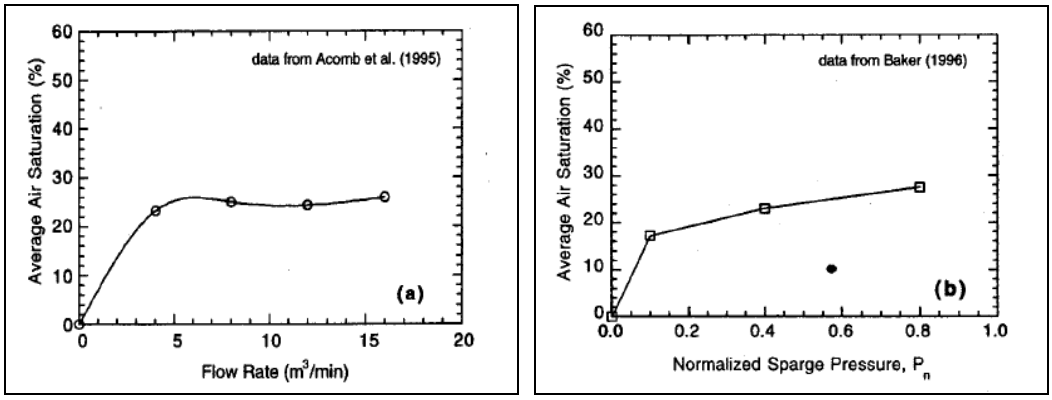

FIGURES 2.10 AND 2.11. RELATIONSHIP BETWEEN FLOW RATE AND PRESSURE RESPECTIVELY AND AVERAGE AIR SATURATION (Acomb *et al*, 1994 and Baker, 1995).

A similar relationship can be seen when relating the gas injection flow rate and pressure to the observed radius of influence. Experiments carried out by Acomb (1994) and Baker (1996) show that an increase in radius of influence is initially observed as flow rate or pressure is increased however after a certain critical value is reached the rate of increase lessens significantly. Again this raises interesting implications for the injection of a carrier gas into the subsurface to transport droplets as there appears to be a limit on the effectiveness of increasing gas flow rate or pressure. Radius of influence is notoriously difficult to measure in the field. Estimations using techniques such as ERT, mound observation, dissolved oxygen measurement, tracer measurement and vadose zone gas pressure measurement often yield significantly different results. Laboratory

experiments are therefore probably more reliable. Once air entry pressure has been exceeded any additional increase in gas injection flow rate and/or pressure will result in increased flow rate and pressure along existing gas channels as these represent least resistance. Figures 2.12 and 2.13 illustrate the relationship between observed radius of influence and air injection flow rate and air injection pressure respectively.

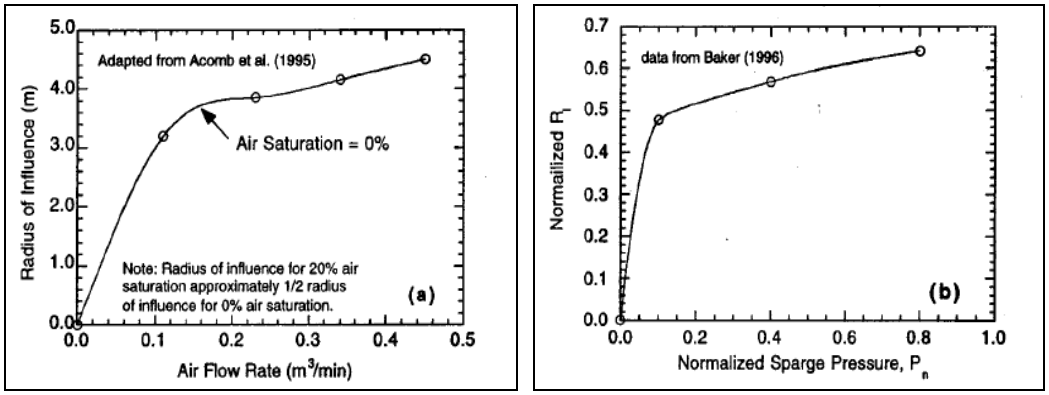

FIGURES 2.12. AND 2.13. RELATIONSHIP BETWEEN OBSERVED RADIUS OF INFLUENCE AND AIR INJECTION FLOW RATE AND AIR INJECTION PRESSURE RESPECTIVELY
(Acomb *et al*, 1994 and Baker, 1996).

The particle size of the porous medium into which the gas is injected will also have a marked effect on average air saturation. Generally, as particle size increases, mean pore size increases proportionally provided that there is not also a high proportion of fine material present to fill the voids. This allows increased air saturation due to relatively low capillary pressures. Experiments carried out by Baker (1996) using coarse and medium ballotini showed that increase in particle size increases the air saturation and therefore the air channel density as illustrated in Figure 2.14.

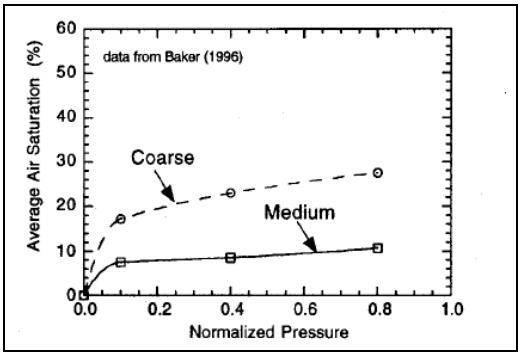

FIGURE 2.14. COMPARISON OF AVERAGE AIR SATURATION AS A FUNCTION OF INJECTION PRESSURE FOR COARSE AND MEDIUM GRAINED SOIL (Baker, 1996).

2.3.3. *Laboratory Studies into Gas Channel and Bubble Migration in Porous Media*

Wheeler (1988) proposed that unsaturated soil could be divided into three categories:

1. Gas phase continuous, liquid phase discontinuous (low saturation);
2. Both gas and liquid phase continuous (intermediate saturation);
3. Liquid phase continuous, gas phase discontinuous (high saturation).

Gas contained in soils will be in the form of discrete bubbles if the degree of saturation is greater than approximately 0.85. For bubbles with smaller diameter than the average pore size bubble radius will be equal to the radius of curvature of the gas-water interface which is determined by surface tension… A more complicated scenario is apparent for larger bubbles as bubble radius may be defined by several intergranular menisci. Gas transfer between large bubbles is possible by diffusion.

Wheeler (1990) also conducted studies into the movement of large gas bubbles in unsaturated soils. The work proposed buoyancy as a transport mechanism for discrete bubbles and that bubbles with diameter above some critical value should be able to move upward through the soil matrix under this force. The critical bubble radius will be proportional to the shear strength of the soil. Bubbles take different form depending on the pore size of the soil. In coarse-grained soils bubbles are likely to be interconnected and therefore not significantly affect the

soil structure however in fine-grained media bubbles are discrete and can deform the soil structure, forming cavities.

Gas movement in fine-grained media can be described by four separate mechanisms:

1. gas is dissolved in pore water and therefore transported by groundwater flow;
2. gas is dissolved in pore water however is transported due to gas concentration gradient;
3. gas is undissolved in the form of small bubbles. Bubbles are transported by buoyancy or groundwater flow.
4. gas is undissolved in the form of large bubbles. Bubbles are transported by buoyancy forces.

Wheeler suggested that large gas bubbles transported by buoyancy forces move by failing the soil directly surrounding the bubble. The vertical buoyancy force P_1 acting on an individual bubble is proportional to bubble radius a and can be calculated from the expression:

$$P_1 = \frac{4\pi a^3}{3}\left(\gamma_m - \gamma_g\right) \qquad \text{(EQN 2.5)}$$

γ_m = unit weight of soil matrix
γ_g = unit weight of gas

It can be seen that buoyancy force is dependant only on the volume of the bubble and the difference in unit weight between the liquid and gaseous phase however a resisting force P_2 will inhibit vertical bubble transportation. For most cases γ_g is so small compared to γ_m that P_2 is dependant on bubble radius a and the undrained shear strength of the infinite soil matrix S_m:

$$P_2 = 10\pi a^2 S_m \qquad \text{(EQN 2.6)}$$

The critical bubble radius a_c can then be defined by equating equations 2.5 and 2.6:

$$a_c = \frac{7.5 S_m}{\gamma_m - \gamma_g} \qquad \text{(EQN 2.7)}$$

Bubbles of radius greater than a_c will rise vertically through the soil matrix with rise velocity governed by viscous effects. Values of a_c predicted by equation 2.7 under static loading conditions would have to be very large to induce bubble transportation by buoyancy phases alone. These predictions are inconsistent with laboratory observations which suggest movement of bubbles of less than 1cm in diameter.

Ji *et al* (1993) conducted important experimental work into the qualitative analysis of airflow pathways in artificial soils. Glass beads (4.0, 2.0, 0.75, 0.4, 0.3 and 0.2mm diameter) were used to simulate soil particles to aid the visualisation of air channels. Although the glass beads have different surface characteristics than soil particles the major factors influencing air transport remain the same. The work concluded that two distinct airflow patterns were observed at different grain sizes. For a uniform sample of 4.0mm diameter glass beads at an injection flow rate of 0.6l/min, vertical "bubbly" flow was observed with air bubbles having a diameter of 1-3 bead diameters. An increase in airflow to 4.5l/min resulted in an increase in lateral transportation. At high airflow of 10l/min further increase in lateral transportation was negligible however a periodic oscillation of the bubble stream was observed. For a uniform sample of 0.75mm diameter beads (n ≈ 0.35) the airflow patterns were observed to be of a different regime. At 0.6l/min transported air was observed to be in the form of thin, continuous, largely vertical channels. Increase in airflow rate resulted in a significant increase in the number of air channels however individual channels remained similar in size. Further increases in airflow rate resulted in a further increase in plume size as well as an increase in channel density. The total volume of air contained within the steady plume was calculated to be 17.5% of the bulk plume volume. An intermediate bead size of 2.0mm diameter was used to investigate the transition form the two flow regimes described above. At an airflow rate of 3.0l/min a transitional airflow pattern was observed whereby bubbles coalesced to form a continuous air mass with extending channels. It was concluded that a 2.0mm bead size corresponded to the transitional airflow regime

from bubbly flow to channel flow. Ji *et al* also conducted experiments into the influence of porous medium heterogeneity on airflow by using mixtures of the glass beads. Meso-scale and macro-scale heterogeneities were introduced into the samples. Non-symmetrical airflow was recorded for bead mixtures.

Figure 2.15 shows gas injection into 0.75-1.00mm ballotini and the corresponding air entry pressures. It can be seen that entry pressure increases linearly until breakthrough of gas occurs approximately 10mbar above hydrostatic pressure. Subsequent peaks in entry pressure can then be seen where new air channels are formed before a steady state is eventually reached.

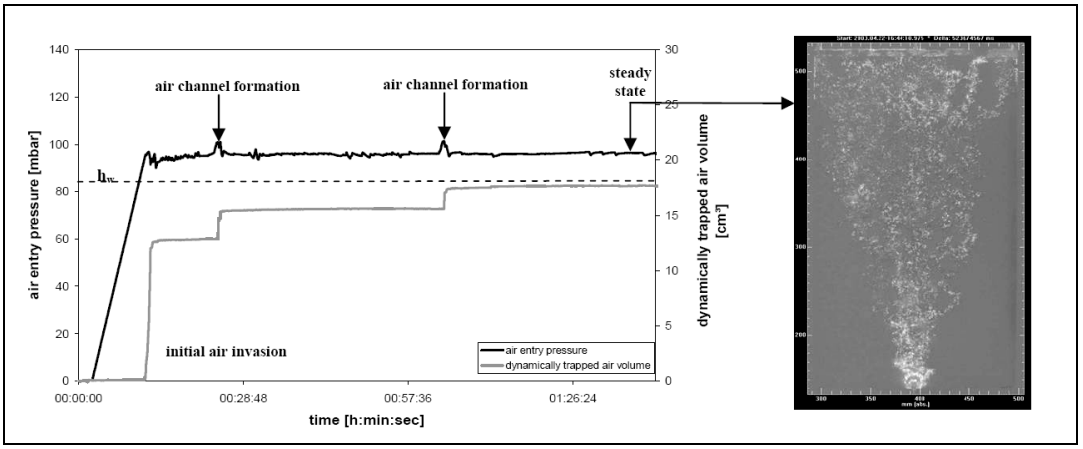

FIGURE 2.15. GAS INJECTION INTO 0.75-1.00MM BALLOTINI (Krauss *et al*, 2003).

Semer *et al* (1998) conducted observational experiments using sands and gravels under fully saturated conditions. The authors claimed that using glass beads to simulate porous media does not accurately reflect field soil characteristics, as insinuated by Ji *et al* (1993). A more complex experimental setup was designed to investigate airflow patterns during air sparging and extraction. Observations were carried out with extraction and without extraction. The research concluded that there was a fundamental difference between airflow in sans and airflow in gravel. In sand air can only be transported in the form of channels however in gravel air can be transported in the form of discrete bubbles. This is in good agreement with Ji *et al* (1993). Air channels formed during sparging in sand can be maintained if injection pressure is reduced from the initial breakthrough

pressure. There is however a threshold injection pressure, below which air channels collapse, will occur.

Roosevelt and Corapcioglu (1998) conducted quantitative experiments into the migration of air bubbles through porous media consisting of 4mm glass beads. The work measured the vertical rise velocity of the bubbles through the beads relative to the rise velocity of bubbles through a water-filled column using video capturing software. Changes in bubble radius during vertical displacement were also quantified using the same technique. Changes in bubble volume can be calculated by the change in bubble pressure from the bottom to the top of the column using the ideal gas law:

$$V_f = \frac{P_i V_i}{P_f} \qquad \text{(EQN 2.8)}$$

V_f = final bubble volume
V_i = initial bubble volume
P_i = initial bubble pressure
P_f = final bubble pressure

P_i and P_f can be determined from the following expressions:

$$P_i = P_0 + \rho_f g h + \left(\frac{2\sigma}{r_i}\right) \qquad \text{(EQN 2.9)}$$

$$P_f = P_0 - P_V + \left(\frac{2\sigma}{r_f}\right) \qquad \text{(EQN 2.10)}$$

P_0 = air pressure at top of column
P_V = vapour pressure of liquid
h = vertical column distance

Bubbles of identical radius were found to have the same rise velocity regardless of vertical position in the column so velocity during vertical displacement remained constant. The effect of migration through the porous media was observed to be a reduction in rise velocity by approximately 4cm/s. This corresponds to a reduction in bubble velocity of approximately 17.4-27.4%.

Elder *et al* (1999) performed macroscopic investigations into the size, spacing and tortuosity of air channels in coarse and fine glass beads under saturated conditions. Their observations were similar to those made by Ji *et al* (1993) in that the parabolic nature of the air plume was observed. Air channel diameter D_c, air channel spacing S_c and tortuosity factor τ were measured for each air channel. Mean air channel diameter was found to be between 2.8 and 8.1mm diameter and mean air channel spacing was found to be between 8.3 and 19.4mm. Mean tortuosity factor was in the range 0.81-0.97. The ratio of D_c to d_{50} was calculated for each media. D_c for fine beads was calculated to be 38. D_c for coarse beads was calculated to be 1.7. D_c for mixed beads was calculated to be 4.7. Sparging injection pressure was found to have negligible influence on D_c, S_c or tortuosity. Macroscopic channels, thought to be formed in coarse grained media such as gravel are often found to have wide spacing. This spacing can lead to gaseous flow bypassing considerable regions of the soil/groundwater matrix. Conversely, pore scale channelling may be in the region of ≥1 particle diameter. This phenomenon is reported in finer grained media such as sand.

Reddy *et al* (2001) investigated the influence of soil heterogeneity on airflow patterns in sands and gravels. A coarse uniform sand (D_{50} = 0.52, $k = 4.64\times10^{-2}$, n = 0.45) was injected with air and the resulting airflow pattern was scrutinised visually. It was recorded that air channels were visible in the sample at pore-scale forming a parabolic pattern as shown in Figure 2.16.

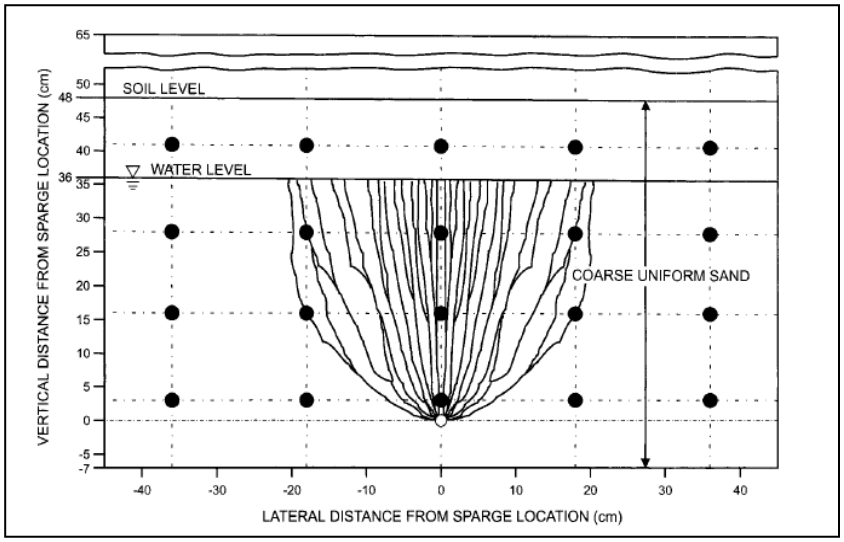

FIGURE 2.16. AIRFLOW PATTERN IN A COARSE UNIFORM SAND (Reddy *et al*, 2001).

Injection of air into a well-graded sand (D_{50} = 0.66, k = 1.30×10^{-2}, n = 0.35) resulted in the airflow pattern shown in Figure 2.17.

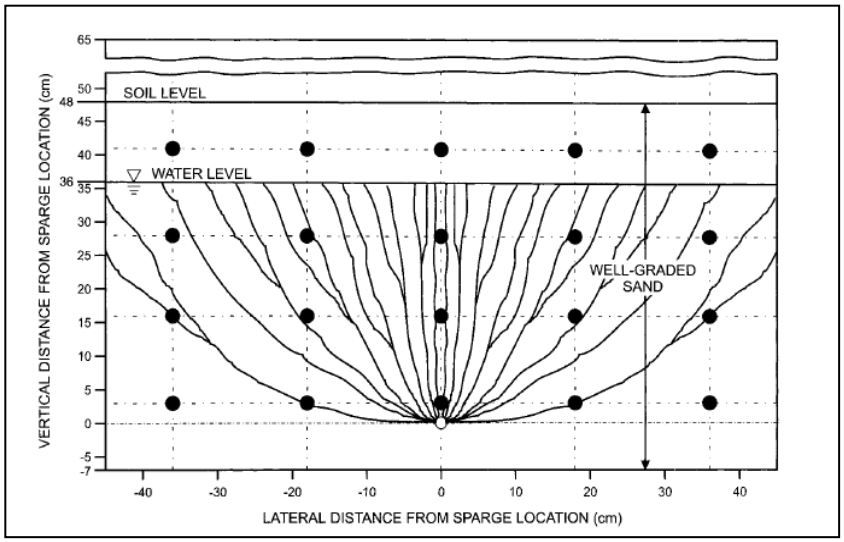

FIGURE 2.17. AIRFLOW PATTERN IN A WELL-GRADED SAND (Reddy *et al*, 2001).

Lateral distribution of air channels was much greater for this sample which was attributed to a decrease in permeability, porosity and subsequent increase in tortuosity. Overall air channel density in the well-graded sand was found to be lower than for the uniform sand injected at the same flow rate.

2.4. *Medical Jet Nebulisers*

The following section discusses the principle of operation of medical jet nebulisers for use in pulmonary therapy. These nebulisers are of particular interest to the research as they create a particularly fine droplet size at a relatively low cost. Two commercially available medical nebulisers manufactured by Intersurgical are presented, the Cirrus™ nebuliser and the Microcirrus™ nebuliser.

2.4.1. *Application of Medical Jet Nebulisers*

Medical nebulisers are designed to atomise a wide range of liquid drug solutions for delivery to the lower respiratory tract of the human lung (Hess, 2000). They are commonly used in the treatment and diagnosis of conditions such as asthma

and cystic fibrosis (Muers, 1997). The devices are an alternative to the more commonly used pressurised metered dose inhalers (pMDI's) and dry powder inhalers when the desired drug is only available in the form of a solution (Hess, 2000). Medical jet nebulisers also offer the advantage of requiring no propellant and they are capable of being used during patient's normal tidal breathing (MacCallion *et al*, 1995). Most importantly, delivery of drugs to the lung in the form of an aerosol allows specific regions of the lung to be targeted, increasing the efficacy of the administered drug as well as inhibiting unwanted side effects (Ledermuller *et al*, 2003).

2.4.2. *Medical Jet Nebuliser Principle of Operation*

Medical jet nebulisers achieve liquid atomisation by using high velocity gas to initiate shear break up of bulk liquid. The liquid is stored in a small reservoir. To achieve atomisation, compressed gas is forced through a narrow aperture known as a Venturi, the diameter of which is typically 0.3-0.7mm. At the Venturi gas velocity increases resulting in a subsequent loss in pressure. This drop in pressure causes liquid to be drawn from the liquid reservoir into the expanding gas stream via a tube (otherwise known as an external mixing chamber) concentric feed (internal mixing chamber) system as illustrated in Figure 2.18.

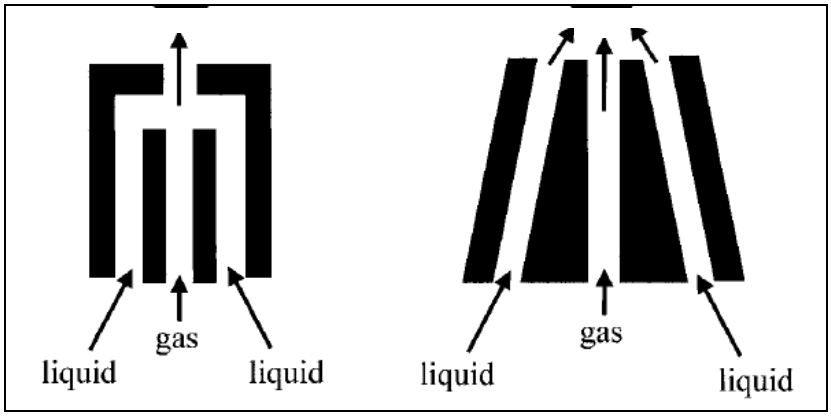

FIGURE 2.18. CROSS-SECTION THROUGH A CONCENTRIC LIQUID FEED SYSTEM.

Primary atomisation is initiated in this mixing zone. The liquid sheet delivered through the concentric feed disintegrates in the gas stream into ligaments which then form droplets. The size distribution of droplets created by this process is

typically 15-500µm diameter (Nerbrink *et al*, 1994) with mean droplet size being inversely proportional to gas pressure. A baffle placed directly above the Venturi acts to further reduce droplet size by inertial impaction. The baffle also forces relatively large droplets (>10µm) to return to the liquid reservoir where they are recycled. The size distribution of droplets released from the device is reduced to approximately 1-10µm however 93-99% of the droplets created by primary atomisation are returned to the liquid reservoir (Nerbrink *et al*, 1994). Several jet nebulisers are capable of producing a maximum droplet size of approximately 3µm by using a larger diameter baffle. Figure 2.19 illustrates the principle of atomisation by medical jet nebulisers in the context of drug delivery.

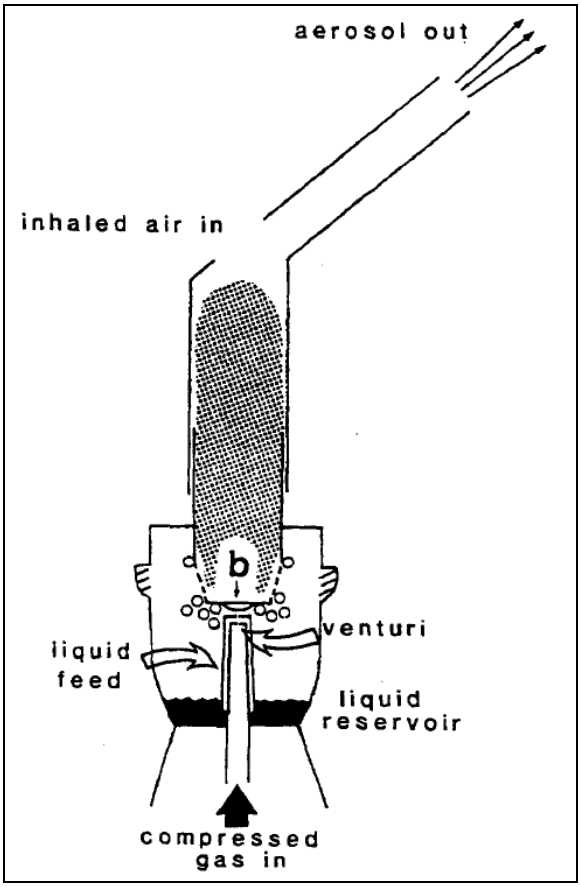

FIGURE 2.19. CONVENTIONAL MEDICAL JET NEBULISER DESIGN AND OPERATION (O'Callaghan *et al*, 1996).

Steckel and Eskandar (2003) considered the factors affecting medical jet nebuliser performance, in particular the effect of temperature and solution concentration change during nebulisation. The research measure the change in temperature and concentration of a liquid drug solution, reconstituted with 0.9%

NaCl and subsequent changes in viscosity and surface tension over a ten minute nebulisation period in a Pari Boy medical jet nebuliser. The research found the temperature in the liquid reservoir to drop from 24°C to 17°C over the first two minutes of nebulisation followed by a much smaller, 0.6°C decrease over the following eight minutes. This drop in temperature resulted in an increase in solution viscosity of 0.16mPas in the first two minutes followed by a further 0.1mPas increase for the remaining eight minutes. This drop in temperature was attributed to latent heat loss caused by evaporation of the solution in the liquid reservoir. Over the same ten minute period, the concentration of the solution was found to increase by approximately 13%, resulting in an approximate 9.5mN/m decrease in surface tension over the ten minute period. The volume median diameter (VMD) of the released spray was measured using a laser diffraction particle sizer. Over the ten minute period, VMD increased by 1.26µm over the first two minutes as a result of viscosity increase due to temperature decrease. The volume median diameter subsequently dropped over the remaining eight minutes by 2.38µm due to a despite a further increase in viscosity. The research raises interesting implications for the use of medical jet nebulisers to deliver droplets to the subsurface. An increase in median droplet diameter over a two minute period could be detrimental to the distribution of substrates in a porous media, particularly if the injection period was short.

2.4.3. *Cirrus™ and Microcirrus™ Nebulisers*

The Cirrus™ nebuliser, manufactured by Intersurgical® is designed to atomise liquid solutions to a droplet size distribution suitable for deposition in the tracheobronchial airways of the human lung. Figure 2.20 shows a photograph of the Cirrus™ nebuliser and droplet size distribution of aerosol released by the device (Intersurgical, 2003).

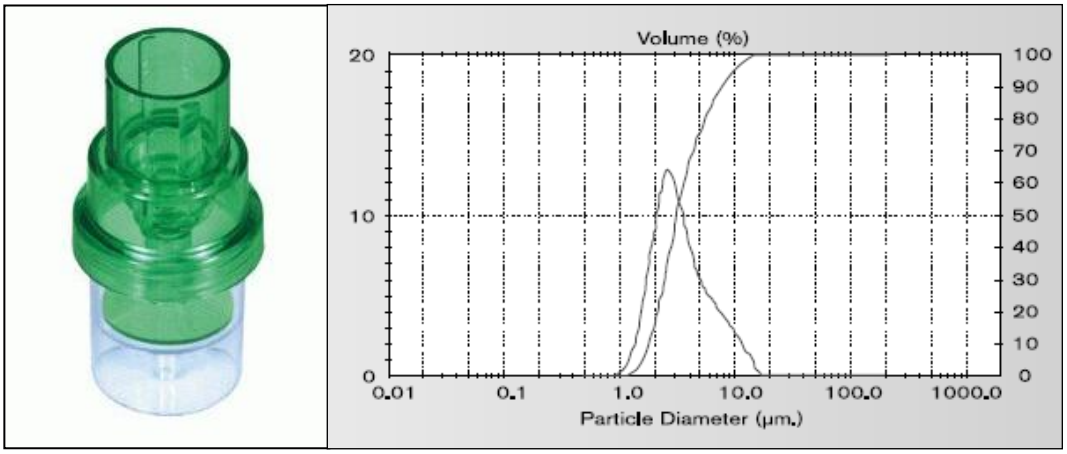

FIGURE 2.20. CIRRUS™ NEBULISER AND DROPLET SIZE DISTRIBUTION (Intersurgical, 2003).

The Microcirrus™ nebuliser is designed to atomise liquid solutions to a droplet size distribution suitable for deposition in the alveolar region of the human lung. Figure 2.21 shows a photograph of the Microcirrus™ nebuliser as well droplet size and cumulative droplet size distributions for this nebuliser.

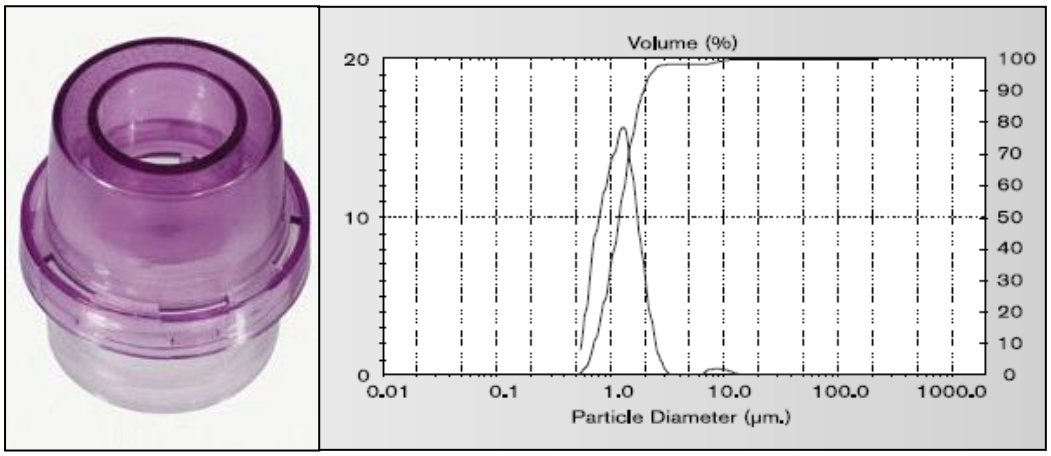

FIGURE 2.21. MICROCIRRUS™ NEBULISER AND DROPLET SIZE DISTRIBUTION (Intersurgical, 2003).

2.5. *Particle Transportation and Deposition in the Human Lung*

A considerable volume of research has been committed to the study of particle deposition in the human lung for a number of scientific disciplines, particularly the delivery of drug solutions. This research is pertinent to the scope of the thesis as the motion of droplets in granular soil can be closely related to particle transportation and deposition in the human lung, particularly the alveolar regions which are typically 250µm in diameter in adults.

2.5.1. *Basic Human Lung Morphology*

The human lung can be considered as two distinct respiratory systems; the upper respiratory tract and the lower respiratory tract. The upper respiratory tract consists of the nasal and paranasal passages including the trachea, which connects the upper and lower tracts. The trachea can be considered as the first airway in the lung and has a mean diameter of 18mm.

Weibel (1963) presented a model of the lower respiratory tract consisting of a 23-generation bifurcating architecture. The total number of alveoli in Weibel's model was therefore equal to $2^{23} = 8.39 \times 10^7$ however laboratory studies have shown the real number to be between 2.0×10^8 and 6.0×10^8. Each alveolus has an typical average diameter of 250μm in adults.

Quantifying fluid flow in the human lung is particularly complicated due to its inherent bifurcating structure. The combination of airway resistance as well as reducing airway diameter towards the alveoli results in airway velocity decreasing proportionally with lung depth. Inspired air velocity in the main bronchi is estimated to be 100 times that of the air velocity in the terminal bronchioles. Understanding the factors influencing deposition allows the particle diameter required to penetrate certain areas of the human lung to be estimated.

The general fate of inhaled particles is summarized in Table 2.4.

TABLE 2.4. FATE OF INHALED PARTICLES IN THE HUMAN LUNG (Intersurgical, 2003).

Particle MMD	Fate
>5μm	Deposit in pharynx, larynx and upper respiratory airways.
2-5μm	Deposit in tracheobronchial airways.
0.5-2μm	Deposit in alveoli.
<0.5μm	Exhaled

Three mechanisms govern the transportation and deposition of particles in the human lung (Schulz, 1998), namely:

1. inertial impaction;
2. gravitational sedimentation;
3. Brownian diffusion.

The aforementioned mechanisms however influence different particle sizes to different extents. Figure 2.22 gives a broad overview of the relationship between mode of particle deposition and particle diameter. Analytical and experimental verification of this data is discussed in more detail in Chapter 2.5.2.

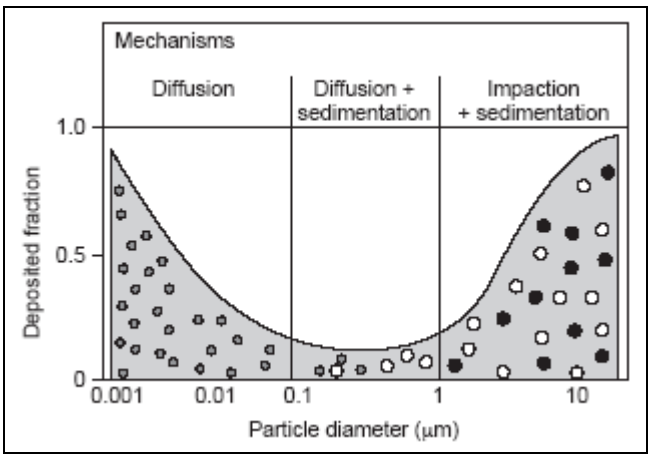

FIGURE 2.22. RELATIONSHIP BETWEEN MODE OF PARTICLE DEPOSITION AND PARTICLE DIAMETER IN THE HUMAN LUNG (Schulz, 1998).

Inertial impaction is the predominant deposition mechanism for particles >2μm. Inertia can be defined as the distance a particular particle will travel in the absence of external forces having been given an initial velocity. Deposition by this mechanism is greatest in the relatively high velocity, shallow regions of the human lung (Schulz, 1998).

Gravitational sedimentation is governed by the settling velocity for a particular particle diameter and the residence time of that particle in a system. Settling velocity is proportional to particle mass, which will be proportional to particle diameter, assuming uniform density and shape. Gravitational sedimentation is negligible for particle diameters <0.5μm explaining why most particles below

this diameter exit the lung upon expiration. Deposition by this mechanism is greatest in the alveolar region due to the relatively long residence times in this zone of the lung (Schulz, 1998).

Brownian diffusion only significantly affects particles of diameter <0.5μm. Relatively long residence times due to low particle velocity means deposition by this mechanism is highest in the alveolar region of the lung (Schulz, 1998).

Velocity will also have a significant effect on deposition mechanism. Impaction will be the dominant deposition mechanism at higher velocities. At lower velocities sedimentation and diffusion will become increasingly dominant as particle residence time rises (Schulz, 1998). The velocities at which each mechanism dominates will be dependant on particle size and airway size.

2.5.2. *Analytical and Experimental Studies into Particle Deposition in the Human Lung*

Davies *et al* 1972 conducted experimental studies with 0.5μm particles with a geometric standard deviation of 1.15. Tests in artificial media with a uniform particle size of 4.5mm, somewhat similar to that of a fine gravel, resulted in a deposition rate of 0.434 ± 0.016 averaged over 20 measurements. Further experiments in human patients revealed a deposition rate of approximately 0.13 when breathing normally at a tidal volume of 600-800cm^3. Interestingly, the researchers also found that deposition of particles did not occur during one single breath, instead it took a number of breaths for total aerosol deposition to be achieved. Particles were found to remain airborne in the lung over several breaths before finally depositing. This raises interesting issues about the pulsed injection of gas and droplets into porous media. Injected droplets may not deposit immediately following injection but may remain in the desaturated pore spaces for several cycles.

Taulbee and Yu (1975) presented a mathematical theory of aerosol deposition in the human respiratory tract. The researchers used the geometric models of the human lung proposed by Scherer *et al* (1972) and Weibel (1963) and assumed

that deposition of particles was governed by Brownian diffusion, impaction and sedimentation. Analytical models were then compared with established experimental data. The research concluded that the optimum particle diameter for minimum deposition is approximately 0.3µm, smaller than this resulting in increased deposition by Brownian diffusion and larger resulting in increased deposition by gravitational sedimentation. This hypothesis compared well with established experimental data.

Darquenne and Pavia (1994) used numerical modelling to compare particle deposition in three, one-dimensional models of the human lung, based on the 23 generation structure proposed by Weibel (1963). The investigation used a tidal volume of 500ml and a flowrate of 0.25l/s. Their findings were subsequently compared with the work of Heyder *et al* (1986) Taulbee and Yu (1975) as shown in Figure 2.23.

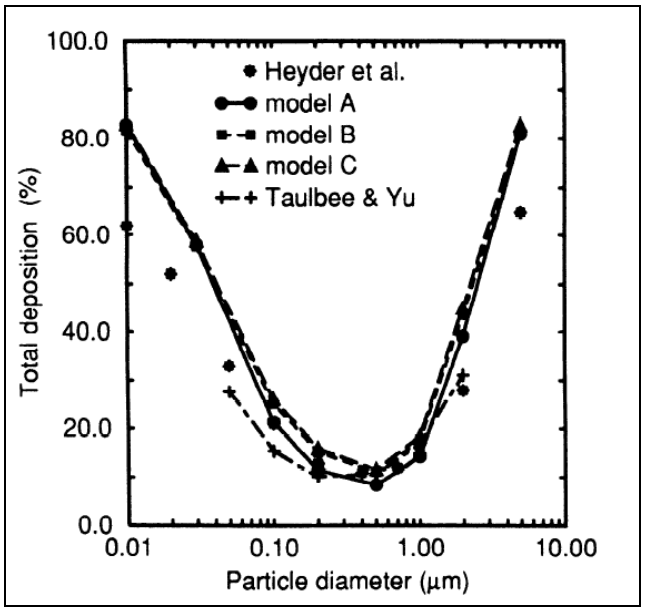

FIGURE 2.23. TOTAL DEPOSITION VS. PARTICLE DIAMETER COMPUTED WITH MODELS A, B, AND C COMPARED TO RESEARCH OF HEYDER *ET AL* (1986) AND TAULBEE AND YU (1972) (Darquenne and Pavia, 1994).

The results show good agreement between the three models, with the optimum particle diameter for minimum deposition lying between 0.3 and 0.5µm. Darquenne and Pavia (1996) extended their one-dimensional investigation to conduct two and three-dimensional studies into the deposition of particles in

four-generational, branching alveolated ducts, again using numerical modelling. Particle diameters of 0.01, 0.5 and 5µm were simulated flowing through the ducts as shown in Figure 2.24.

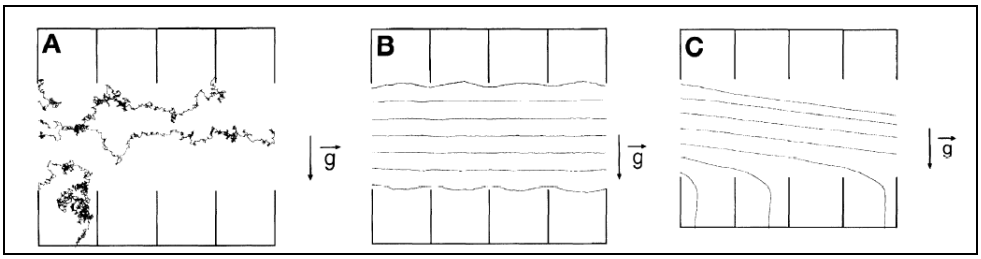

FIGURE 2.24. PARTICLE TRAJECTORIES IN A HORIZONTAL ALVEOLATED DUCT FOR PARTICLE DIAMETERS 0.01µm (A), 0.5µm (B), AND 5.0µm (C) (Darquenne and Pavia, 1996).

It can be seen that the particle trajectories shown in Figure 2.24 (A) indicate that Brownian diffusion is governing the motion of the 0.01µm particles, leading to sporadic deposition in the ducts. The particle trajectories shown in Figure 2.24 (C) appear to indicate that gravitational sedimentation governs particles of 5µm diameter, resulting in relatively high levels of deposition. The particle trajectories shown in Figure 2.24 (B) appear to show that Brownian diffusion and gravitational sedimentation do not significantly influence particles of this diameter, resulting in a relatively low rate of deposition. Three-dimensional studies exhibited similar results. In a single duct model, particle deposition was found to be 70.22%, 5.22% and 38.79% for 0.01µm, 0.5µm and 5µm diameters respectively. The research concluded that previous one-dimensional studies had overestimated the deposition of particles due to an underestimation of carrier gas penetration into the models.

Darquenne (2002) investigated the deposition of 0.5-5µm particles in a six-generation model of the human acinus using a computational fluid dynamics program. Particle sizes of 0.5, 1, 2, 3 and 5µm were transported into the model at a flowrate of 500ml/s for 2 seconds inspiration followed by 2 seconds expiration. The research found that the percentage deposition of particles increased from just 2% (0.5µm) to 6% (1µm) to 68% (2µm) to 93% (3µm) and finally to 100% at 5µm and in general the percentage deposition increased as the generation number increased. It was found that the small particles (0.5µm and 1µm) only deposited

during expiration, indicating that they remain airborne for longer than the larger particles (2µm, 3µm and 5µm) which were typically deposited during inhalation. The orientation of the alveoli relative to particle trajectory was also found to considerably influence deposition, particularly for particle diameters of 2µm and 3µm. This is in agreement with investigations carried out by Balashazy *et al* (2000), who used numerical modelling to show that the orientation of alveoli greatly affected the proportional deposition of particles larger than 0.1µm diameter. Above 1µm diameter, particle deposition was shown to vary from 0 - 100% depending on alveolar orientation. The relatively low percentage deposition of small particles in Darquenne's (2002) studies was attributed to the phenomenon by which these particles are not significantly affected by gravitational sedimentation or Brownian diffusion and therefore closely follow the flow of the carrier gas. As particle size increases, the influence of sedimentation increases, resulting in much higher percentage particle deposition. This phenomenon also results in the significant depositional differences caused by alveolar orientation. Figure 2.25 summarises the general relationship between particle diameter and total percentage deposition in Darquenne's model.

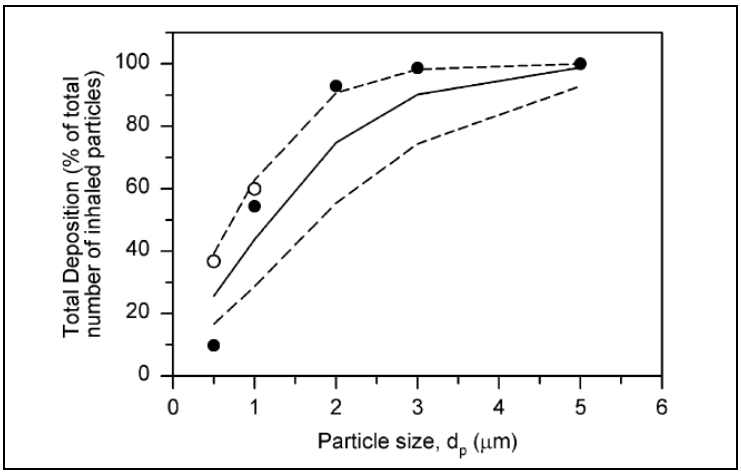

FIGURE 2.25. GENERAL RELATIONSHIP BETWEEN PARTICLE DIAMETER AND TOTAL PARTICLE DEPOSITION (Darquenne, 2002).

2.5.3. *Similarities between the Human Lung and Porous Media*

The human lung contains a tortuous set of airways that terminate in very small *voids*. Likewise a porous media could be described as containing pore spaces with sizes similar to those of the terminal regions of the lung, linked by tortuous

flow paths. Table 2.5 shows the pore radius and waist radius of a group of spheres of identical radius, *r* for both cubical and rhombohedral packing arrangements (Coulson and Richardson, 1962).

TABLE 2.5. RELATIONSHIP BETWEEN PACKING ARRANGEMENT AND PORE AND WAIST RADIUS (Coulson and Richardson, 1962).

Packing Arrangement	*Porosity*	*Pore radius*	*Waist radius*
Cubical	47.6	0.700*r*	0.414*r*
Rhombohedral	25.9	0.288*r*	0.155*r*

A homogeneous soil of particle diameter 600μm (medium sand) would have a pore diameter of 420μm and waist diameter of 249μm if packed in a *cubical* arrangement and a pore diameter of 173μm and waist diameter of 93μm if packed in a *rhombohedral* arrangement. These dimensions are similar to those of a typical alveolus.

2.6. *The LINER® Technique*

The LINER® (Liquid Nitrogen Enhanced Remediation) system was implemented by Tauw in 2001. The system involves the atomisation and delivery of a carbon substrate to the subsurface using nitrogen as an anaerobic sparging gas. The system was initially piloted at a metal-working factory in the town of Zwolle, The Netherlands. The use of tetrachloroethylene as a degreaser in the cleaning process had led to contamination of the subsurface beneath the factory. Because of the surface infrastructure only an in situ remediation technique was appropriate.

2.6.1. *LINER® System Principle of Operation*

Figure 2.26 shows the operating principle of the LINER® system. Ethyl lactate is atomised using a Spray Systems air-assist atomiser at the subsurface using nitrogen gas. An additional source of nitrogen gas is then used to transport the droplets to the subsurface. Nitrogen is used as a carrier gas to maintain anaerobic conditions in the subsurface.

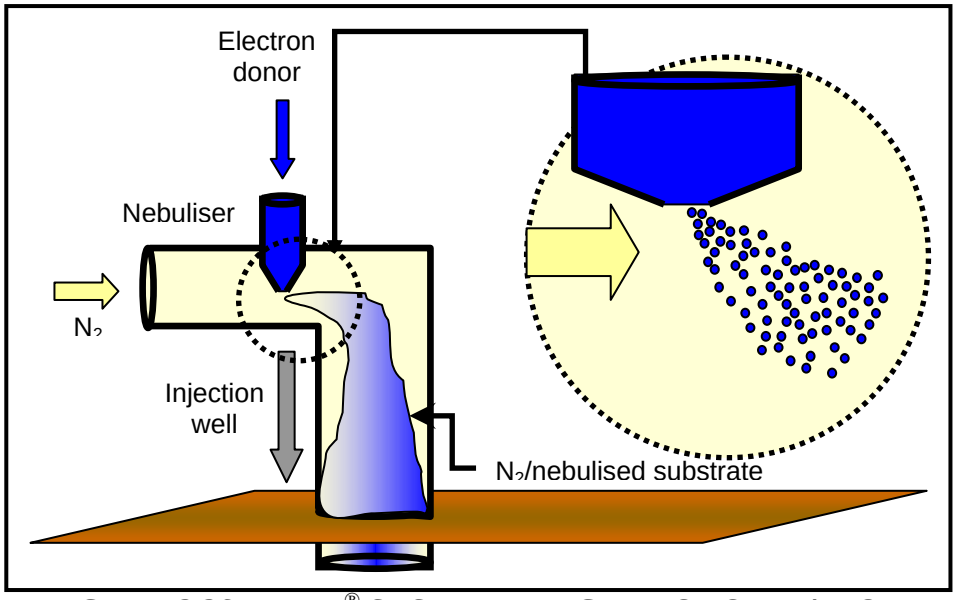

FIGURE 2.26. LINER® SYSTEM PRINCIPLE OF OPERATION.

The injection system consisted an array of injection filters at depths of 24-25m and 44-45m. A total of 500ml of ethyl lactate was injected per day however the injection time was limited to 3 minutes to prevent volatilization and transportation of the contaminant into the vadose zone which would have presented a risk to human health. An array of monitoring wells were placed at depths of 4-5m, 9-10m, 14-15m, 24-25m, 34-35m, 39-40m and 44-45m. Table 2.5 summarises the injection data for the LINER® system at Zwolle.

TABLE 2.5. INJECTION DATA FOR LINER® SYSTEM AT ZWOLLE.

Volume of injected substrate (ethyl lactate)	500ml
Duration of injection	3mins
Frequency of injection	Daily
Injection gas flow rate	50-65 Nm^3/hr
Injection gas pressure at 25m depth	350-370kPa
Injection gas pressure at 45m depth	620-650kPa
Jet nebuliser gas pressure	900kPa

Figure 2.27 shows a photograph of the LINER® system at Zwolle, The Netherlands.

FIGURE 2.27. LINER® SYSTEM AT ZWOLLE.

Figure 2.28 shows a photograph of the injection system control panel.

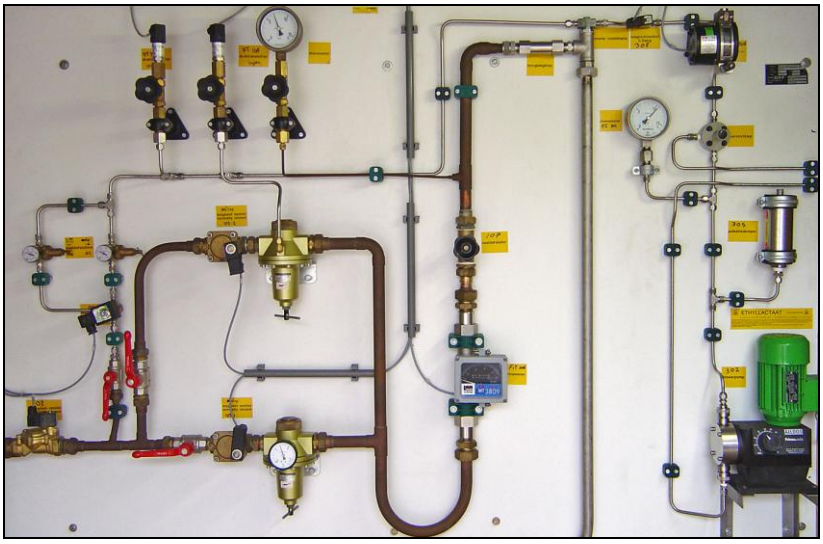

FIGURE 2.28. INJECTION SYSTEM CONTROL PANEL.

2.6.2 *Pilot Study Results*

The pilot study at Zwolle ran for a total of 59 weeks. Figure 2.29 shows the molar concentration of PCE, TCE, cis-DCE, VC, ethene and ethane in monitoring well 906 at a depth of 14-15m over the 59 week period.

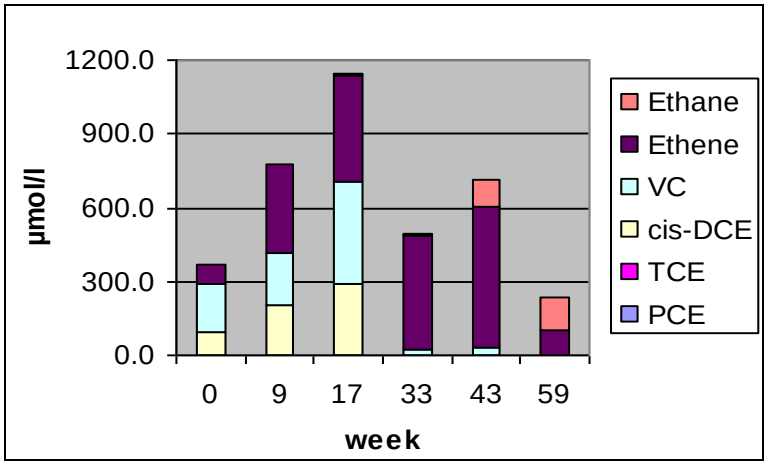

FIGURE 2.29. MOLAR CONCENTRATION OF PCE, TCE, CIS-DCE, VC, ETHENE AND ETHANE IN MONITORING WELL 906 AT A DEPTH OF 14-15M OVER A PERIOD OF 59 WEEKS.

It can be seen that the molar concentration of chlorinated solvents is reduced to zero after 59 weeks. Figure 2.30 shows the molar concentration of PCE, TCE, cis-DCE, VC, ethene and ethane in monitoring well 909 at a depth of 24-25m over a period of 59 weeks.

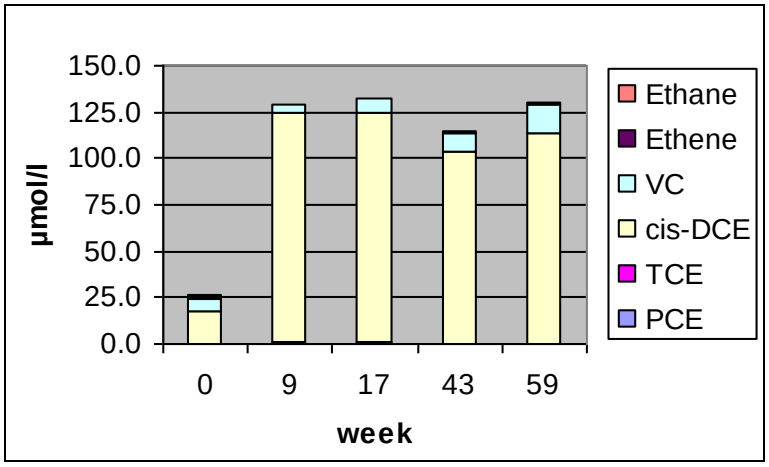

FIGURE 2.30. MOLAR CONCENTRATION OF PCE, TCE, CIS-DCE, VC, ETHENE AND ETHANE IN MONITORING WELL 909 AT A DEPTH OF 24-25M OVER A PERIOD OF 59 WEEKS.

It can be seen that the concentration of cis-DCE rises significantly after week 9 and is subsequently not reduced by week 59. This suggests that although remediation of the chlorinated solvents began to take place, the dehalogenation process had not progressed past *cis*-DCE and VC, both of which present a risk to human health.

Figure 2.31 shows a diagram detailing the overall quality of biostimulation achieved the LINER® system pilot study at Zwolle, inferred from contaminant molar concentration data.

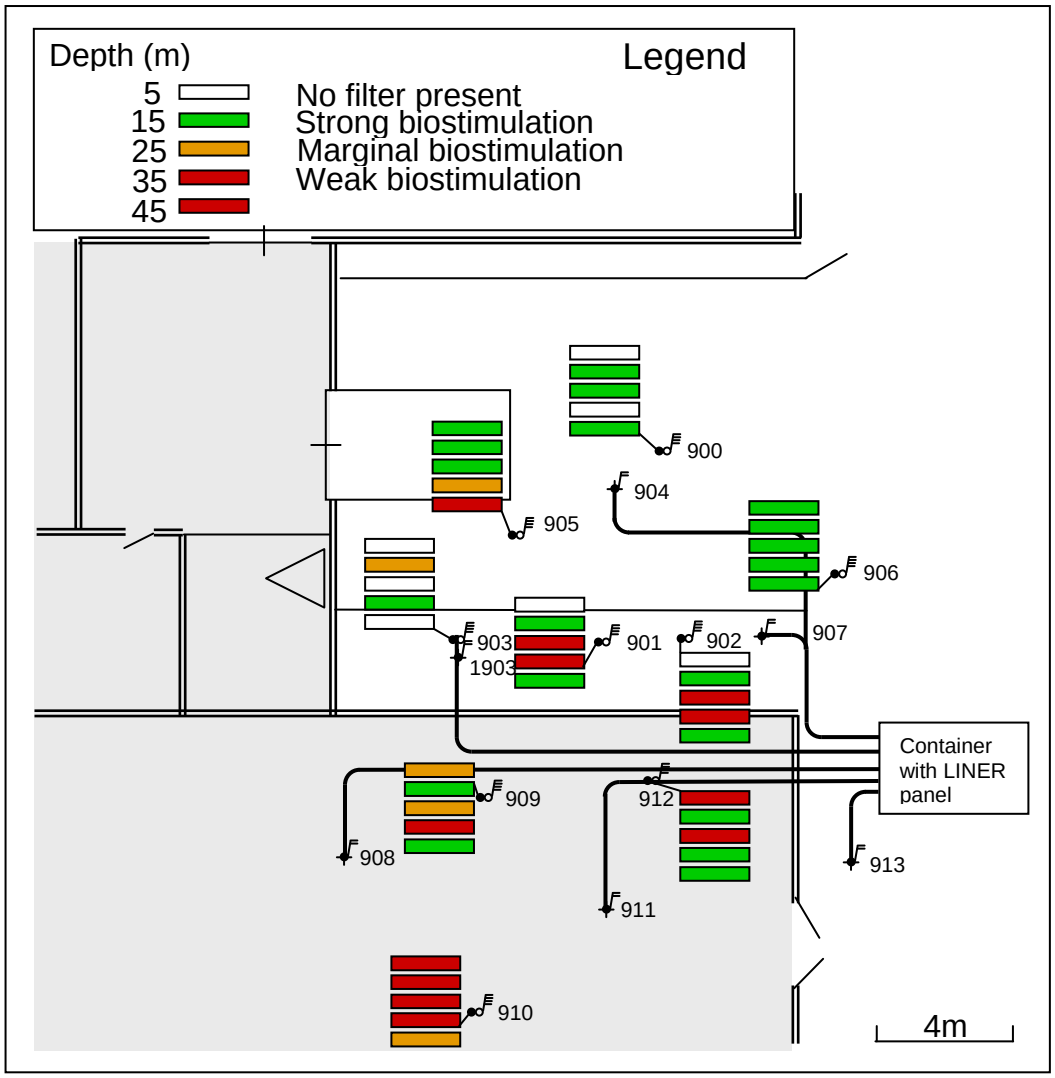

FIGURE 2.31. REPRESENTATION OF QUALITY OF BIOSTIMULATION AFTER COMPLETION OF LINER® PILOT STUDY AT ZWOLLE.

It can be seen that the monitoring wells in close proximity to the injection wells show strong to weak biostimulation however monitoring wells further away from injection filters show weak to marginal biostimulation. This infers that droplet transportation may have been restricted to the regions directly surrounding the injection filters, resulting in relatively small radii of influence.

2.7. *Summary*

The theoretical processes of in situ bioremediation as well as the conclusions of several laboratory and field studies have been described in detail. It is evident that under the correct conditions, in situ bioremediation provides an effective, rapid and relatively cheap technique for the remediation of chlorinated solvents in the subsurface.

This chapter has described the principles and governing parameters of in situ air sparging. It has been shown that the injection of compressed gas into the subsurface causes a local displacement of pore water which could be adapted to transport atomised substrates. The principles of in situ air sparging should be adaptable to delivering atomised substrates to the subsurface using an anaerobic carrier gas. In fact this particular technique has recently been pioneered by the Dutch environmental consultancy Tauw in the form of the LINER® system.

The possibility of adapting technology from the pulmonary therapy field to transport aerosol through fine gravels and coarse sands is evident. The technology employed in medical jet nebulisers is ideal for producing a fine, near monodisperse aerosol that could be well suited to penetrating porous media with particle size $\geq 600\mu m$.

The results of the LINER pilot study at Zwolle have shown the potential for delivering substrates to the subsurface in the form of fine droplets for in situ bioremediation of chlorinated solvents. Strong biostimulation in monitoring wells surrounding injection filters indicates that ethyl lactate was successfully delivered to these regions. It is apparent however that atomised substrate was not successfully delivered to those regions not in close proximity to an injection filter. This was attributed to the droplet size of the atomised substrate being insufficiently small and local variations in stratigraphy.

It is apparent that if the droplet size of the atomised substrate can be reduced by using a different atomiser then the distribution of the substrates injected in the subsurface should be much improved.

CHAPTER 3. THEORETICAL BACKGROUND

3.1. *Chapter Synopsis*

The following chapter discusses the theory behind the processes and governing parameters influencing the atomisation and transportation of liquid droplets into a saturated porous medium. In addition, data is presented on the physiochemical properties of chlorinated solvent pollutants as well as commonly used droplet sizing techniques.

3.2. *Physiochemical Properties of Common Chlorinated Solvents*

Many chlorinated solvents used in commercial and industrial applications pose a serious risk to the environment and human health. This chapter lists some of the most commonly encountered chlorinated solvent contaminants and their respective toxicity details.

3.2.1. *Tetrachloroethylene*

Tetrachloroethylene is a clear, colourless, non-flammable liquid at room temperature with a sweet odour. Table 3.1 lists the physiochemical properties of tetrachloroethylene at 20°C.

TABLE 3.1. PHYSIOCHEMICAL PROPERTIES OF TETRACHLOROETHYLENE.

Synonyms	perchloroethylene, PCE, perc
Applications	metal degreasing, dry cleaning of textiles
Molecular formula	C_2Cl_4
Molecular weight	165.8g mol^{-1}
Density	1.622g cm^{-3}
Vapour pressure	18.47mm Hg
Solubility in water	0.15g/L

Figure 3.1. shows the chemical structure of tetrachloroethylene. It comprises of a carbon double bond with 4 chlorine atoms.

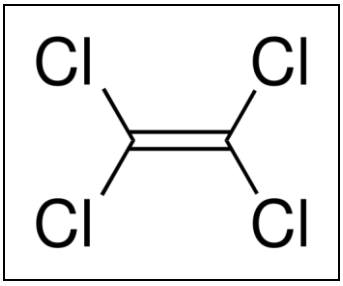

FIGURE 3.1. CHEMICAL STRUCTURE OF TETRACHLOROETHYLENE.

Table 3.2 lists the acute and chronic toxicity details for tetrachloroethylene ingested by humans.

TABLE 3.2. TOXICITY DATA FOR TETRACHLOROETHYLENE.

Acute	Irritation of upper respiratory tract and eyes, kidney dysfunction, neurological effects.
Chronic	Headaches, cognitive impairments, colour vision decrements, cardiac arrhythmia, liver damage, and kidney effects. Category 3 human carcinogen.

Table 3.3 lists the relevant UK occupational standards and public health guidelines for human exposure to tetrachloroethylene (Health Protection Agency, 2007).

TABLE 3.3. EXPOSURE STANDARDS AND GUIDELINES FOR TETRACHLOROETHYLENE.

Workplace Exposure Limit	LTEL: 50ppm (345mg/m^3)
	STEL: 100ppm (689mg/m^3)
Drinking Water Quality Guideline	0.04mg/L
Air Quality Guideline	0.25mg/m^3
Soil Guideline Value and Health Criteria Values	*Tolerable Daily Intake* (oral) 14µg/kg/bw/day
	Mean Daily Intake (oral) 8.4µg/day
	Tolerable Daily Soil Intake (oral) Adult: 14µg/kg/bw/day Child: 14µg/kg/bw/day
	Tolerable Daily Intake (inhalation) 71µg/kg/bw/day
	Mean Daily Intake (inhalation) 200µg/kg/bw/day
	Tolerable Daily Soil Intake (inhalation) Adult: 68µg/kg/bw/day Child: 66µg/kg/bw/day

3.2.2. *Trichloroethylene*

Trichloroethylene is a clear colourless liquid with at room temperature a sweet odour. It is commonly used for metal cleaning, grease and fat extraction, paint stripping and as a refrigerant. Table 3.4 lists the physiochemical properties of trichloroethylene at 20°C.

TABLE 3.4. PHYSIOCHEMICAL PROPERTIES OF TRICHLOROETHYLENE.

Synonyms	TCE
Molecular formula	C_2HCl_3
Molecular weight	131.4g/mol
Density	1.460g/cm^3
Vapour pressure	74mm Hg
Solubility in water	1.00g/L

Figure 3.2 shows the chemical structure of trichloroethylene comprising of a carbon double bond, three chlorine atoms and one hydrogen atom.

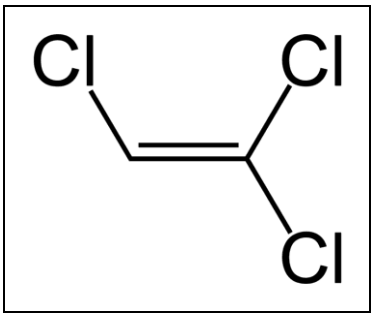

FIGURE 3.2. CHEMICAL STRUCTURE OF TRICHLOROETHYLENE.

Table 3.5 lists the acute and chronic toxicity details for trichloroethylene ingested by humans.

TABLE 3.5. TOXICITY DATA FOR TRICHLOROETHYLENE.

Acute	Irritation of upper respiratory tract and eyes, kidney dysfunction, neurological effects. Causes skin blistering
Chronic	Liver, kidney, central nervous system, and peripheral nervous system effects. Category 3 carcinogen.

Table 3.6 lists the relevant UK occupational standards and public health guidelines for human exposure to trichloroethylene (Health Protection Agency, 2007).

TABLE 3.6. EXPOSURE STANDARDS AND GUIDELINES FOR TRICHLOROETHYLENE.

Workplace Exposure Limit	LTEL: 100ppm (550mg/m^3)
	STEL: 150ppm (820mg/m^3)
Drinking Water Quality Guideline	0.02mg/L
Air Quality Guideline	10^{-6} risk at 2.3µg/m^3
Soil Guideline Value and Health Criteria Values	*Index dose* (oral) 5.2µg/kg/bw/day
	Index dose (inhalation) 5.2µg/kg/bw/day

3.2.3. *Dichloroethylene*

Dichloroethylene is colourless, highly flammable liquid at room temperature with a harsh odour. Dichloroethylene has two geometric isomers, *cis*-dichloroethylene and *trans*-dichloroethylene, dependant on the location of the chlorine atoms around the carbon double bond. It is commonly used a solvent in waxes, resins, polymers, fats and lacquers. Dichloroethylene is an intermediate in the sequential dehalogenation of tetrachloroethylene to ethene. Table 3.7 physiochemical properties of trichloroethylene at 20°C.

TABLE 3.7. PHYSIOCHEMICAL PROPERTIES OF DICHLOROETHYLENE.

Synonyms	DCE	
Molecular formula	$C_2H_2Cl_2$	
Molecular weight	96.95g/mol	
Density	*cis*: 1.23g/cm^3	*trans*: 1.26g/cm^3
Vapour pressure	273mm Hg	395mm Hg
Solubility in water	3.5g/L	6.3g/L

Figure 3.3 shows the chemical structure of *cis*-dichloroethylene and *trans*-dichloroethylene. Table 3.8 lists the acute and chronic toxicity details for dichloroethylene ingested by humans.

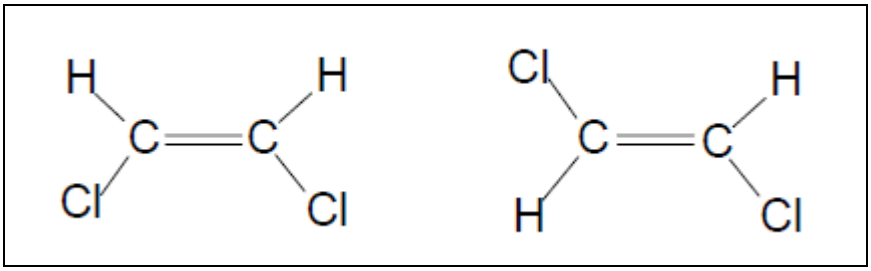

FIGURE 3.3. CHEMICAL STRUCTURE OF *CIS*-DICHLOROETHYLENE AND *TRANS*-DICHLOROETHYLENE

TABLE 3.8. TOXICITY DATA FOR DICHLOROETHYLENE.

Acute	Harmful if ingested, inhaled or absorbed through the skin. May cause systemic effects if inhaled. May cause reproductive damage.
Chronic	Possible carcinogen, tumorigen, neoplastigen and teratogen

Table 3.9 lists the relevant UK occupational standards and public health guidelines for human exposure to trichloroethylene (Health Protection Agency, 2007).

TABLE 3.9. EXPOSURE STANDARDS AND GUIDELINES FOR DICHLOROETHYLENE.

Workplace Exposure Limit	LTEL: ppm (550mg/m^3)
	STEL: ppm (820mg/m^3)
Drinking Water Quality Guideline	mg/L
Air Quality Guideline	10^{-6} risk at µg/m^3
Soil Guideline Value and Health Criteria Values	*Index dose* (oral) µg/kg/bw/day
	Index dose (inhalation) µg/kg/bw/day

3.2.4. *Vinyl chloride*

Vinyl chloride is a colourless, flammable gas at room temperature with a sweet odour. It is commonly used in the manufacture of polyvinyl chloride and as a refrigerant. Table 3.10 lists the physiochemical properties of vinyl chloride at 20°C.

TABLE 3.10. PHYSIOCHEMICAL PROPERTIES OF VINYL CHLORIDE.

Synonyms	VC, chloroethene
Applications	Plastic manufacture, refrigerant
Molecular formula	C_2H_3Cl
Molecular weight	62.5g/mol
Density	g/cm^3
Vapour pressure	2600mm Hg
Solubility in water	2.8g/L

Figure 3.4 shows the chemical structure of vinyl chloride. It consists of a carbon double bond surrounded by one chlorine atom and three hydrogen atoms.

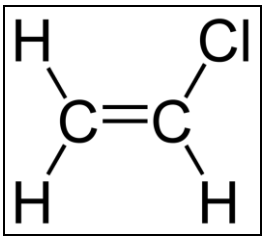

FIGURE 3.4. CHEMICAL STRUCTURE OF VINYL CHLORIDE.

Table 3.11 lists the acute and chronic toxicity details for vinyl chloride ingested by humans.

TABLE 3.11. TOXICITY DATA FOR VINYL CHLORIDE .

Acute	Causes irritation of upper respiratory tract and eyes, headaches, nausea, vomiting and burns. Rapid evaporation can cause frostbite.
Chronic	Category 1 carcinogen.

Table 3.12 lists the relevant UK occupational standards and public health guidelines for human exposure to vinyl chloride (Health Protection Agency, 2007).

TABLE 3.12. EXPOSURE STANDARDS AND GUIDELINES FOR VINYL CHLORIDE.

Workplace Exposure Limit	LTEL: 3ppm (7.3mg/m^3)
	STEL: Not Specified
Drinking Water Quality Guideline	0.5µg/L
Air Quality Guideline	10^{-6} risk at 0.21mg/m^3
Soil Guideline Value and Health Criteria Values	*Index dose* (oral) 0.014µg/kg/bw/day
	Index dose (inhalation) 0.3µg/kg/bw/day

3.3. *Behaviour and Transport of Chlorinated Solvents in the Subsurface*

3.3.1. *Transport of Chlorinated Solvents to the Subsurface*

The majority of chlorinated solvents are released to the environment as a bulk organic liquid known as NAPL (non-aqueous phase liquid) (USEPA, 2000). The

fate of the NAPL in the subsurface is determined by its physiochemical characteristics, particularly density, aqueous solubility, hydrophobicity and vapour pressure. The solvents may remain in NAPL form, dissolve in the groundwater, adsorb to soil particles or volatilize to a gas. NAPL density will determine whether the NAPL floats or sinks in the subsurface aquifer. Aqueous solubility and hydrophobicity will determine whether the NAPL dissolves into the groundwater or sorbs to soil particles. Vapour pressure will determine whether the NAPL volatilizes to a gas or remains in NAPL form. Ultimately the NAPL may undergo any of these transformations until an equilibrium is attained. Figure 3.5 illustrates the phase equilibrium mechanism diagram for NAPL's in the subsurface.

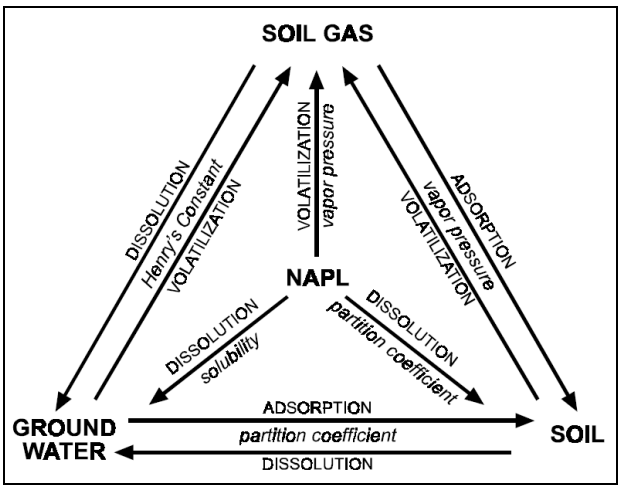

FIGURE 3.5. PHASE EQUILIBRIUM MECHANISMS FOR NAPL'S IN THE SUBSURFACE (USEPA, 2000).

NAPL can be further divided into two sub categories. LNAPL's (light non-aqueous phase liquids) have densities less than water and therefore tend to float on the phreatic surface. DNAPL's (dense non-aqueous phase liquids) have densities greater than water and therefore tend to sink through the groundwater until a confining layer is reached. The majority of chlorinated solvents are in DNAPL form at room temperature, having densities in the range 1.1-1.6g/cm^3 (Kueper *et al*, 2003). The exceptions to this are VC, chloroethane and chloromethane which are in the gaseous phase in pure form (USEPA, 2000). Figure 3.6 illustrates potential DNAPL transportation in the subsurface.

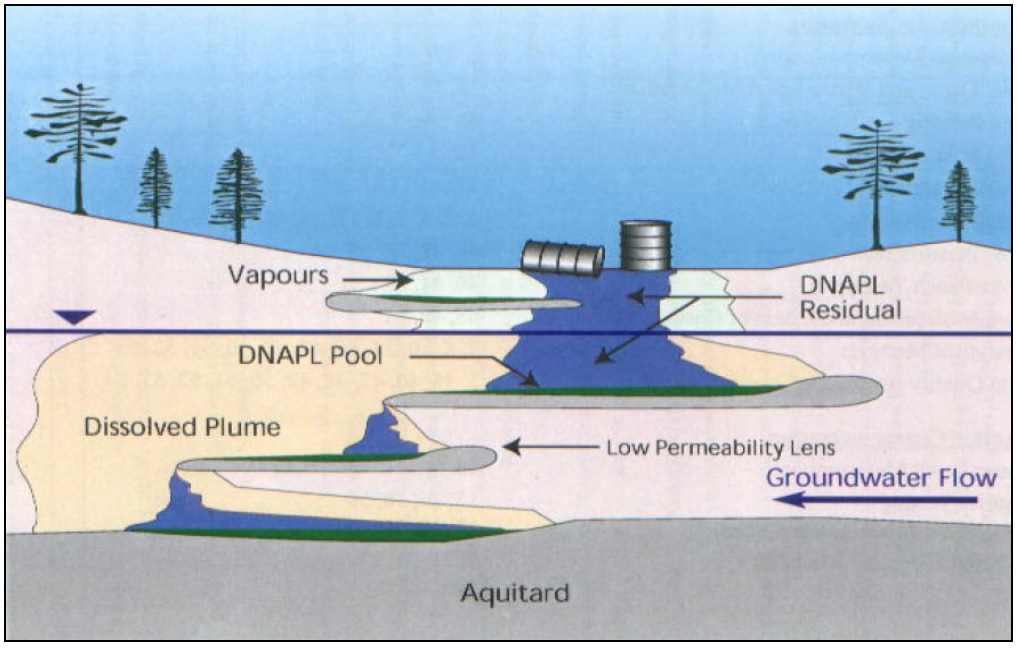

FIGURE 3.6. DNAPL TRANSPORTATION IN THE SUBSURFACE (USEPA, 2004).

3.3.2. *Transport of Chlorinated Solvents in the Subsurface*

The transportation of DNAPL in the subsurface is governed by the following factors:

- advection;
- dispersion;
- diffusion;
- dilution;
- retardation;
- decay.

Advection is the process whereby dissolved solvent is transported by the solute, the subsurface groundwater. Most DNAPL's have relatively low solubility water and therefore their transport in the subsurface is largely governed by gravity and underlying stratigraphy and not groundwater flow (USEPA, 2004). Dispersion is the spreading of the molecules due to advection and will be governed by Fick's first law however the tortuous nature of the saturated pore spaces will restrict this phenomenon. Although dispersion will occur in three dimensions, it will typically be greatest in the direction of groundwater flow. Molecular diffusion

arises from the concentration gradient of the contaminant in the subsurface and is typically a slow process. Retardation is caused by the sorption of the solvent onto soil particles. Sorption is influenced by the chemical composition of the solvent, the mineralogy of the aquifer and the amount of organic matter in the soil matrix. The retardation of a contaminant is described by the ratio of groundwater flow to the rate of contaminant transport, with retardation values generally less than 10 (Balazova and Slodika, 2005). Figure 3.7 illustrates an idealised view of DNAPL trapped in a saturated soil matrix.

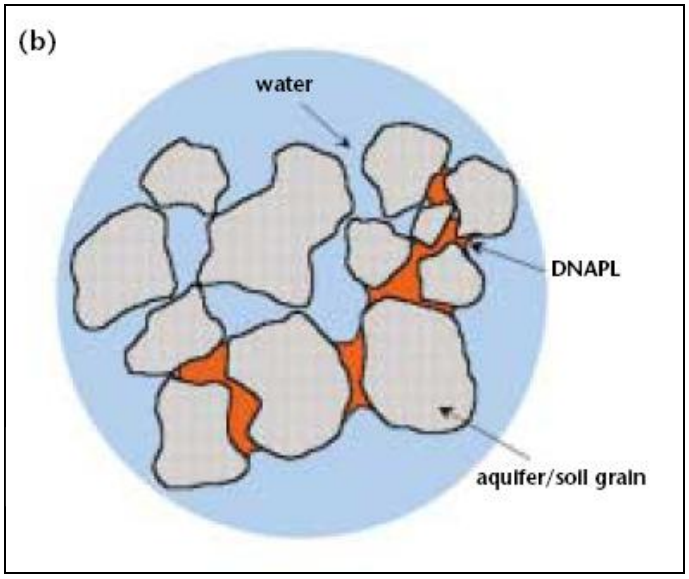

FIGURE 3.7. RESIDUAL DNAPL IN SATURATED POROUS MEDIA (Kueper *et al*, 2003).

The behaviour and transport of chlorinated solvents in the subsurface is highly complex and dependant on many factors. It is apparent that the in situ remediation of chlorinated solvents in the saturated zone is made difficult due to the inherent low solubility of these pollutants in groundwater.

3.4. *Established In situ Remediation Techniques*

Over the past three decades an extensive range of techniques have been researched and developed for in situ remediation of chlorinated solvents in the subsurface. These treatments may be physical, chemical, biological or a combination of these. This section describes some of the most common techniques developed in recent years for the in situ remediation of chlorinated

solvents. The objective of any remediation project is to reduce or remove the risk to human health or to the environment posed by the contaminant. This is generally accomplished by aquifer restoration or plume interception.

In most circumstances it is unlikely that total remediation of an aquifer will be achievable due to the fact that complete desorption of chlorinated solvent DNAPL from soil particles may take a prohibitive length of time to complete (Kueper *et al*, 2003). The goal of a remediation project may therefore be to reduce the aqueous concentration of the chlorinated solvents to a level that is deemed acceptable by the relevant health regulations for that particular country.

If the contaminant source is located in an area that is not deemed a risk to human health it may be more desirable and cost effective to retain the subsurface contaminant in this zone, therefore removing the pathway to human receptors. Reduction of contaminant concentration or total removal of the contaminant in the direction of groundwater flow from the chlorinated solvent source has previously been achieved using technology such as "pump and treat" and permeable reactive barriers (PRB's) or the positioning of physical barriers to control groundwater migration.

3.4.1. *Pump-and-Treat*

Pump-and-treat technology involves the removal of contaminated groundwater from an aquifer for treatment at the surface. The contaminated groundwater may be treated using chemical or biological techniques. The treated groundwater is subsequently discharged either into the local sewerage system or reinjected into the groundwater aquifer. Figure 3.8 shows and idealised schematic of a pump-and-treat system.

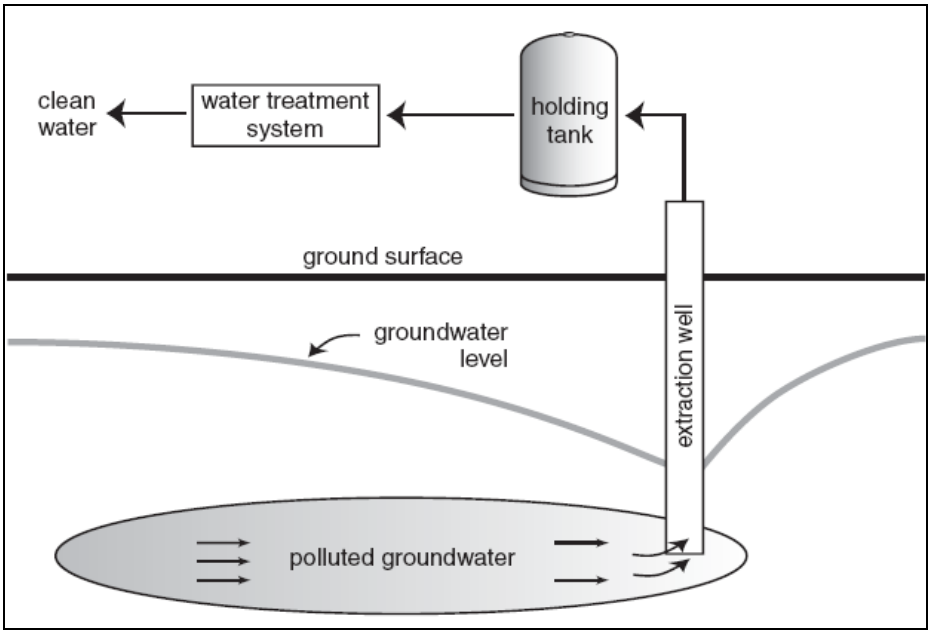

FIGURE 3.8. IDEALISED PUMP AND TREAT SCHEMATIC (USEPA, 2001).

Pump-and-treat installations can be hampered by the length of time taken to completely desorb the contaminant from the soil matrix, which is in turn influenced by hydrogeological conditions and the nature and depth of the contaminant. As discussed previously, most chlorinated solvents have solubility in water <5g/L so only relatively small amounts of contaminant are removed per unit volume of water pumped to the surface. Some installations may operate for decades before an acceptable aqueous concentration is attained (Kueper *et al*, 2003). Relatively high costs may be incurred if large volumes of groundwater must be extracted from the subsurface aquifer. If the contaminant is located at depth, large and relatively expensive pumping equipment may be required to extract the groundwater. In addition, pump-and-treat technologies often result in aquifer drawdown and may only be able to extract groundwater along preferential subsurface pathways, resulting in contamination persisting in zones of low permeability (Allmon *et al*, 1999). Extraction wells may silt up over extended periods of time resulting in groundwater becoming increasingly difficult to extract. Treatment costs at the surface may also be considerable if the contamination concentration is relatively high. From a legislative point of view, additional licences will likely be required to discharge the treated water back into the local water system.

3.4.2. *Groundwater Circulating Well Technology*

Groundwater circulating well technology (GCW) is an adaptation of the pump-and-treat system. Pumping systems are used to draw contaminated groundwater towards subsurface wells in the aquifer however the groundwater is not extracted to the surface. Instead the contaminated groundwater is treated in the well by activated carbon, air stripping, adsorption, in-well bioreactors or a combination of one or more of these techniques. Air-pumping may be used to increase groundwater circulation and may be in the up-well or down-well configuration (USEPA, 1998). Soil vapour extraction (SVE) may be required if the contaminant is transferred from the aqueous phase to the gaseous phase to inhibit contaminant vapours from reaching the atmosphere. Figure 3.9 illustrates an idealised schematic of a GCW system.

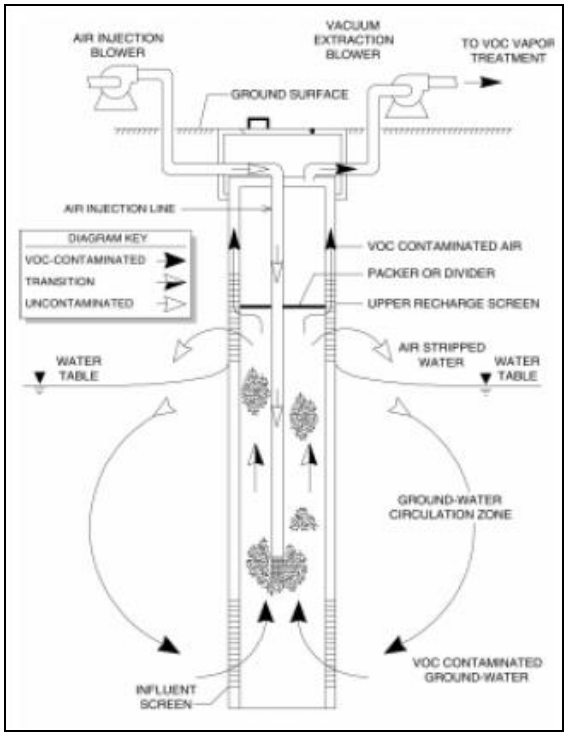

FIGURE 3.9. IDEALISED GCW SYSTEM SCHEMATIC (USEPA, 1998).

Groundwater circulating wells reduce costs when compared to conventional pump-and-treat techniques as groundwater does not have to be extracted to the surface, requiring less powerful pumping equipment. Also, because groundwater is not removed from the aquifer additional licensing may not be required for

subsequent discharge. GCW promotes improved subsurface groundwater flow in both horizontal and vertical directions resulting in improved contaminant removal from the aquifer. If the contaminant is present in both LNAPL and DNAPL forms then aforementioned soil vapour extraction can be used to treat the contaminant in the vadose zone.

The effectiveness of GCW can be limited by the hydrogeological characteristics of the contaminated aquifer and the nature of the contaminant in question. Similarly to pump-and-treat systems, treatment by GCW may take many years if subsurface conditions are not conducive to good groundwater circulation. Hydrogeological conditions may significantly restrict groundwater flow and the radius of influence of the circulating wells resulting in GCW being prohibited at some sites. The introduction of dissolved oxygen into the aquifer during air-pumping may result in iron or manganese oxides being formed which may consequently inhibit microbial growth in the subsurface and/or clog circulating wells (USEPA, 1998).

3.4.3. *Permeable Reactive Barriers*

Permeable reactive barriers (PRB's) are installed in the subsurface to intercept and remediate contaminated groundwater which flows through the barrier under natural hydraulic gradient (USEPA, 1998 and 2002). In this way the contaminated groundwater is contained upstream of the barrier ensuring that contaminants do not reach a receptor. Because PRB's are a form of passive remediation, the contaminant plume is not directly treated and some systems may be required to be installed permanently. PRB's may use the following chemical or biological techniques to treat the contaminated groundwater:

- sorption of contaminant onto barrier;
- precipitation;
- chemical transformation using materials such as zero-valent iron;
- bioremediation using microbes.

Figure 3.10 shows an idealised schematic of a permeable reactive barrier.

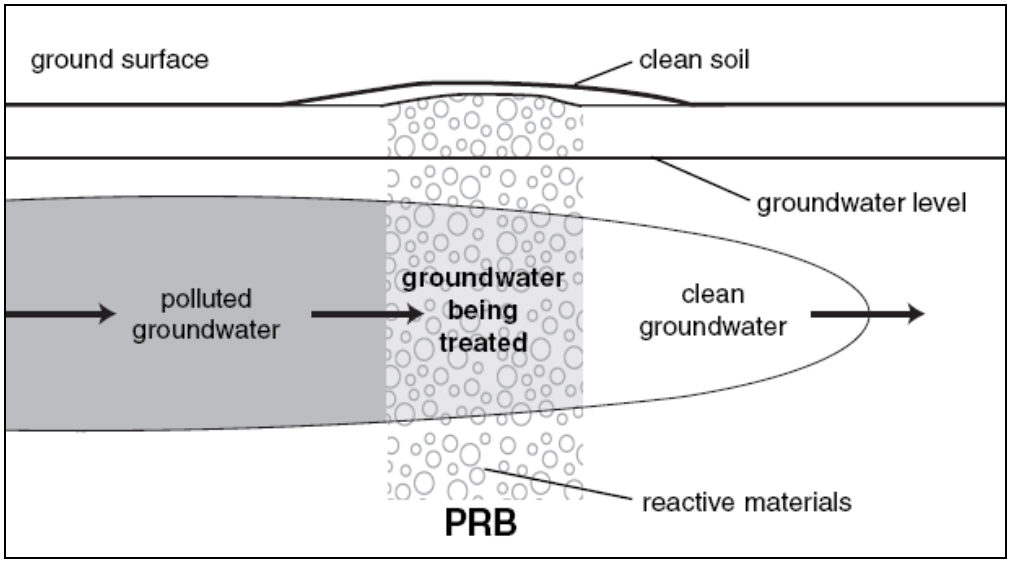

FIGURE 3.10. IDEALISED SCHEMATIC OF A PERMEABLE REACTIVE BARRIER (USEPA, 2001).

The majority of PRB's use zero-valent iron to immobilise or dehalegonate the chlorinated solvents. PRB's may form a continuous linear trench or employ a "funnel and gate" system to direct the groundwater into the reactive zone. Continuous trench systems consist of a straight line reactive barrier designed to be sufficiently wide to intercept the entire width of the contaminant plume. The funnel and gate system uses impermeable walls, constructed from sheet piles or slurry walls, to direct groundwater to flow through the reactive section of the barrier. Groundwater flow velocity will increase as it is funnelled through the barrier which may require that the thickness of the reactive zone be increased. Figure 3.11 shows the principle of the "funnel and gate" system.

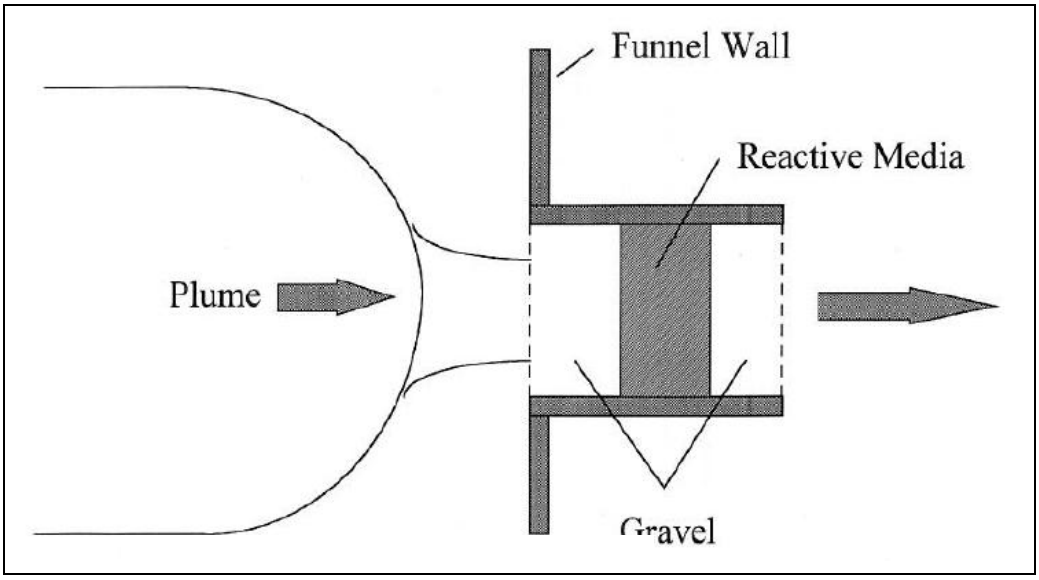

FIGURE 3.11. "FUNNEL AND GATE" PRINCIPLE (ITRC, 1999).

PRB's have the advantage that after construction, very little infrastructure is required above the ground surface. Running and maintenance costs are relatively low for periods of up to ten years. In addition, the flow of groundwater is considerably less disturbed than during pump-and-treat operations. (USEPA, 2002).

The most obvious drawback to PRB installations is that in most situations only relatively shallow contaminant plumes, to a maximum depth of approximately 50-70 feet, can be treated. This may result in PRB techniques being precluded at many contaminated sites. In addition, PRB installations may not be suitable where significant surface infrastructure or subsurface utilities are already present. PRB's may also take many years to sufficiently remediate a contaminated aquifer depending on the groundwater flow velocity and nature and concentration of the contaminant. Long-term precipitation may reduce the permeability of the barrier. In some climates PRB's may also be sensitive to seasonal variations.

3.5. *Atomisation of Bulk Liquids*

The transformation of bulk liquids into sprays has been desirable for many commercial and industrial applications for many decades. A wide range of commercial industries require the atomisation of liquids, for example the automotive industry requires petrol and diesel to be finely atomised before

entering the engine cylinders in order to maximise the ignition of the fuel. In pulmonary therapy, medical nebulisers are employed to create fine droplets for delivery of drug solutions to targeted regions of the human lung. Each particular atomisation application requires a specific droplet size distribution or a specific volume of droplets and consequently the spray industry and the range of commercially available atomisers is extensive. This section describes the fundamental processes involved in the atomisation of bulk liquids as well as some of the atomisers commercially available.

3.5.1. *Atomisation Definitions*

Atomisation can be defined as the transformation of bulk liquid into sprays and other physical dispersions of small particles in a gaseous atmosphere (Lefebvre, 1989).

An aerosol or spray can be defined as "a stable suspension of solid or liquid particles in a gas phase such as air" (Taylor and Gumbleton, 2004). A spray is just one type of two-phase flow. The droplets are known as the dispersed or discrete phase and the gas is known as the continuous phase.

A drop or droplet can be defined as a small spherical mass of any liquid that is bound completely or almost completely by free surfaces. A drop becomes a droplet at a notional diameter of less than 200μm (Lefebvre, 1989).

Figure 3.12 illustrates the range of droplet sizes found in nature and atomised liquids.

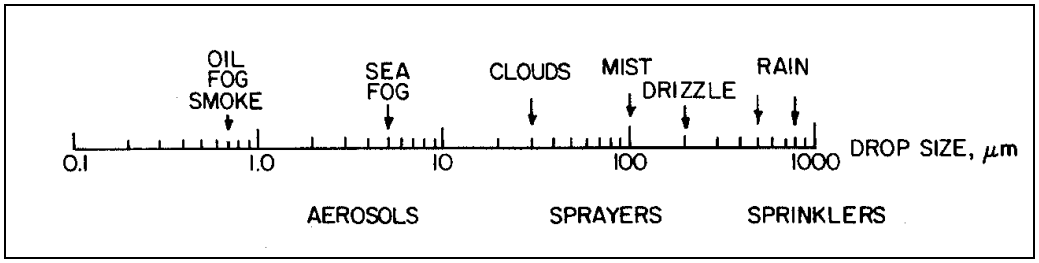

FIGURE 3.12. RANGE OF DROPLET SIZES IN ATOMISED LIQUIDS AND NATURAL PROCESSES (Lefebvre, 1989).

In most practical situations a spray will consist of a large number of droplets with many different sizes, transported in very close proximity to each other. In this way the individual motion of any droplet will be strongly influenced by the surrounding droplets in the bulk spray (Sirignano, 1999).

The creation and transportation of droplets in a gaseous medium is extremely complex as macro-scale transport processes are strongly coupled to micro-scale phenomena such as local velocity profile, droplet disintegration, drag, evaporation, collisions and coalescence (Sirignano, 1999). A great deal of research has been carried out into the factors influencing droplet formation and transportation in a gaseous atmosphere.

3.5.2. *Factors Governing Atomisation of Liquids*

The atomisation of a liquid released into a vacuum is governed by three liquid properties namely density, viscosity and surface tension. The density of a liquid affects the mass flow rate through a nebuliser. In practice, the density of most liquids does not vary widely and therefore the influence of this liquid property is relatively small.

Viscosity is the phenomenon of all real fluids to internally resist deformation under shear stress. This can be thought of as a resistance to one fluid "layer" to move relative to another fluid layer. Viscosity arises due to attractive intermolecular forces as well as transfer of momentum between fluid layers caused by random molecular motion between these layers. These forces tend to resist any differences in velocity between one layer and another. This explains how gases can have appreciable levels of viscosity regardless of the fact that intermolecular distances are relatively large. The viscosity of fluids ranges widely. Under laminar flow conditions the viscosity of a liquid can be defined by Newton's formula.

$$\tau = \mu \frac{dV}{dy} \qquad \text{(EQN 3.1)}$$

τ = shear stress

μ = dynamic viscosity ($kgm^{-1}s^{-1}$)

$\frac{dV}{dy}$ = liquid velocity gradient

An increase in pressure causes a small proportional increase in viscosity however this can be largely ignored for most situations. Temperature, however has a much more pronounced, inversely proportional relationship with viscosity.

Increase in viscosity has an adverse effect on liquid atomisation. Viscous forces prohibit the build up of disturbance waves on the surface of a liquid that are essential for liquid disintegration when using pressure or pneumatic atomisers. Higher viscosity liquids result in atomisation occurring further away from the atomiser orifice, leading to larger droplets being formed (Lefebvre, 1989).

Figure 3.13 illustrates the influence of liquid viscosity on the disintegration of various liquid jets.

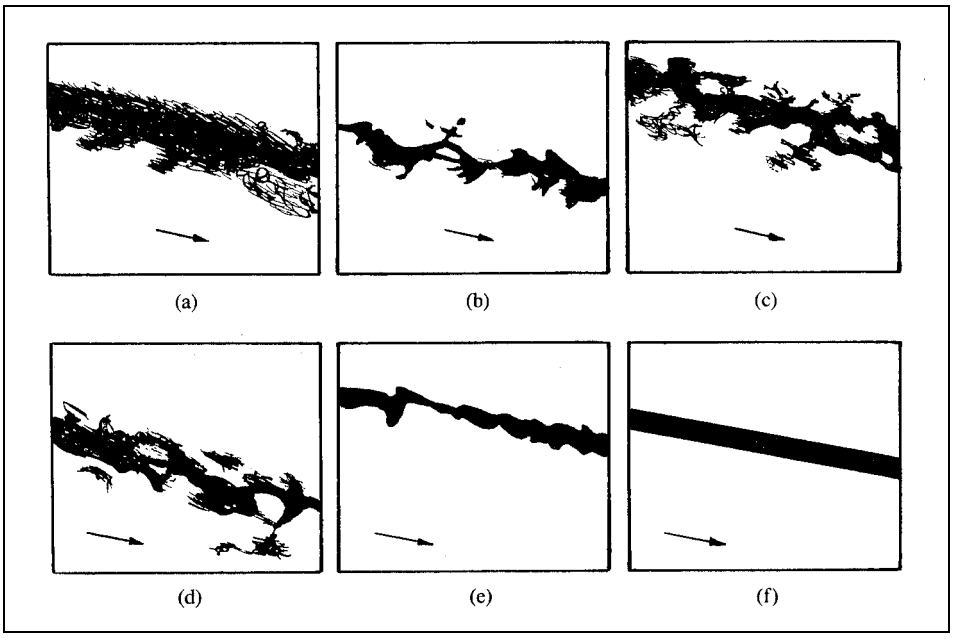

FIGURE 3.13. DISINTEGRATION OF LIQUID JETS WITH INCREASING VISCOSITIES. (A) PETROL, (B) WATER, (C) ETHANOL, (D) LIGHT DIESEL OIL, (E) HEAVY DIESEL OIL AND (F) LUBRICATING OIL (BAYVEL *et al*, 1993).

Reynolds number, Re, is the ratio of inertia forces to viscous forces.

$$\mathrm{Re} = \frac{\rho \bar{u} d}{\mu} \qquad \text{(EQN 3.2)}$$

In line with the above theory, there will typically be an inverse relationship between Reynolds number and droplet size.

Surface tension, σ (N/m) is the force in liquid that resists increase in surface area. Droplets tend towards a spherical shape as this shape has the minimum surface area for a given volume. To overcome this force and increase the surface area (ΔA) of the liquid and therefore create droplets, sufficient kinetic energy must be transferred to the liquid. The minimum kinetic energy required to increase the surface area of a liquid must be equal to the *surface energy* of the liquid (Lefebvre, 1989):

$$\textit{surface energy} = \sigma \times \Delta A \qquad \text{(EQN 3.3)}$$

Weber number, *We*, is the ratio of inertia forces to surface tension forces:

$$We = \frac{\rho u^2 l^2}{\sigma l} = \frac{\rho u^2 l}{\sigma} \qquad \text{(EQN 3.4)}$$

There will therefore typically be an inverse relationship between Weber number and droplet size.

3.5.3. *Atomisation Pathways*

Atomisation is typically achieved by one of two pathways (Azzopardi, 2003):

1. liquid sheet ⟶ ligaments ⟶ droplets;
2. liquid jet ⟶ primary droplets ⟶ secondary droplets.

Sheet break up occurs when liquid exits an orifice as a thin sheet. Disturbance waves along the sheet are caused by the competition between gaseous aerodynamic forces and liquid surface tension. Ligaments are created when surface tension is overcome. These ligaments are unstable and quickly disintegrate into droplets. The size of both the ligaments and the final stable droplets are governed by the surface tension of the liquid and the relative velocity between the sheet and the gaseous atmosphere. Figure 3.14 illustrates droplet formation by sheet break up.

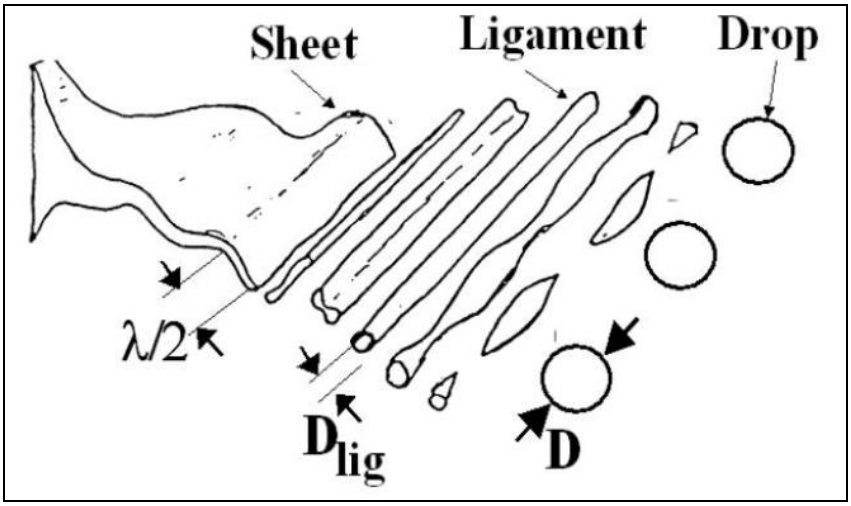

FIGURE 3.14: LIQUID DISINTEGRATION OF A LIQUID SHEET.

In comparison, liquid jet break up is caused when a bulk liquid exits a circular orifice as a cylindrical jet. Again, instabilities occur due to the competition between gaseous aerodynamic forces and liquid surface tension.

3.5.4. *Instability of Liquid Jets*

The disintegration of a liquid forced through an orifice under pressure was investigated experimentally as early as 1829 by Bidone. In it's simplest form liquid jet disintegration arises from instability waves created as the liquid jet exits the orifice. Under laminar conditions these disruptive forces will amplify until a critical wavelength is reached and surface tension is no longer able to hold the liquid together. The disintegration of a liquid forced under pressure through a circular orifice with diameter d_o is illustrated in Figure 3.15.

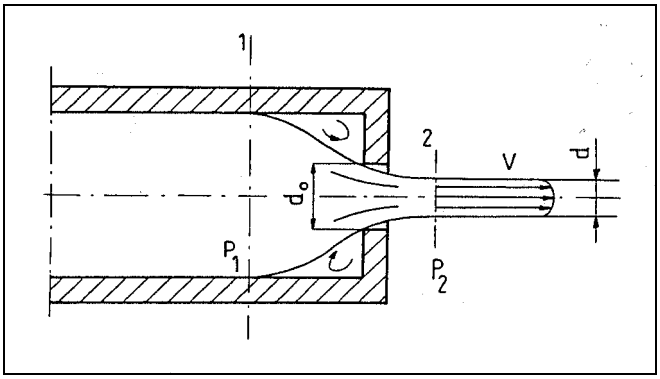

FIGURE 3.15. DISCHARGE OF A LIQUID JET THROUGH A CIRCULAR ORIFICE (Bayvel *et al*, 1993).

Rayleigh (1878) described the disintegration of a nonviscous liquid jet released into a vacuum through a cylindrical orifice, considering only the effect of surface tension to create instabilities on the surface of the jet. Rayleigh proposed that a non-rotational cylindrical liquid jet will disintegrate when the wavelength of an axisymmetric wave becomes greater than the cross-sectional circumference of the jet itself and calculated the optimal value of λ to be 9.02 times the diameter of the jet orifice. At this optimum disturbance wavelength the radius of the droplets produced from a cylindrical liquid jet will be nearly twice the radius of the orifice from which the jet is released. Figure 3.16 illustrates an idealised view of liquid jet disintegration and actual liquid jet disintegration recorded experimentally using high-speed photography. Note the presence of smaller satellite droplets created as the jet "pinches".

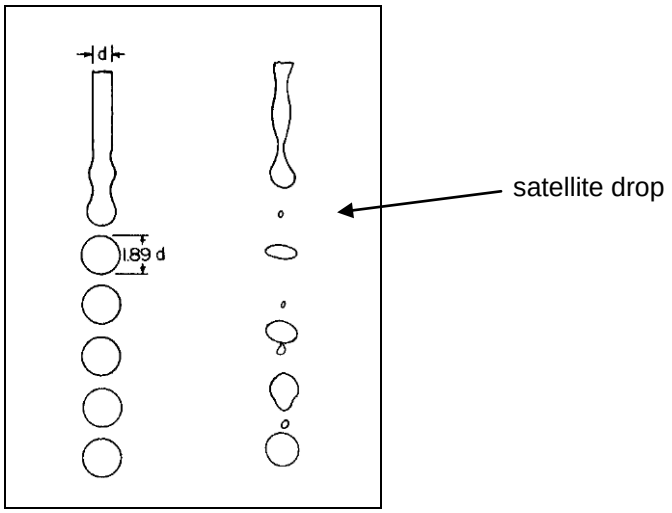

FIGURE 3.16. IDEAL AND ACTUAL LIQUID JET DISINTEGRATION (Lefebvre, 1989).

3.5.5. *Instability of a Liquid Sheet*

Similarly to the disintegration of a liquid jet, liquid sheet atomisation requires the formation of instability waves to initiate droplet formation. When the instability waves reach a critical amplitude liquid break up begins however the process is somewhat different to liquid jet break up.

When the liquid sheet enters a gaseous medium, a decease in aerodynamic static pressure is created in the region of the liquid. This local pressure decrease results in an increase in local gas velocity which causes the liquid sheet to deform. Surface tension forces attempt to return the liquid to its original form and this process creates instability waves. Figure 3.17 illustrates this phenomenon.

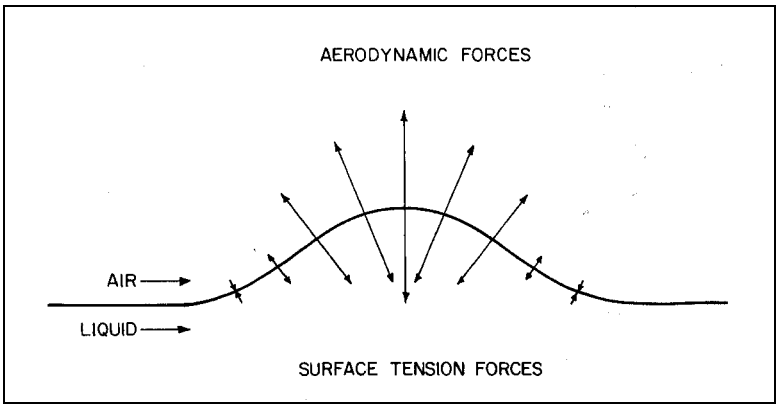

FIGURE 3.17. FORCES ACTING ON A LIQUID SHEET (Lefebvre, 1989).

The balance of forces at the liquid-gas interface can be described by:

$$p_L - p_G = -\sigma \frac{d^2 h}{dx^2} \qquad \text{(EQN 3.5)}$$

Hagerty and Shea (1955) performed a series of experiments using high speed photography to investigate the build up of instability waves on uniform thickness liquid sheets. Two types of instability wave were found to build up on the sheet:

1. *sinuous waves* – instability waves are in phase;
2. *dilational waves* – instability waves are out of phase.

Hagerty and Shea assumed that the liquid sheet disintegrated directly to droplets with diameter equal to the amplitude instability wave due to surface tension and aerodynamic pressure. They proposed that optimum liquid disintegration was caused by sinuous waves and the minimum mean droplet size created by liquid sheet disintegration was found to be approximately 40-60μm.

The work of Hagerty and Shea was further explored by Fraser *et al* (1962) who proposed that a liquid sheet would initially disintegrate into ligaments which are unstable and pinch under surface tension forces in the same manner proposed by Rayleigh to form droplets with diameter 1.89 times the size of the sheet orifice. These expressions have been found to be in good agreement with experimental observations.

3.5.6. *Secondary Droplet Disintegration*

Atomisation processes often require more than one stage to achieve a stable aerosol. The final stages of liquid break up will occur when relatively large droplets disintegrate into smaller ones. Droplet disintegration is initiated by an uneven pressure distribution around the droplet, causing deformation. Surface tension will act to force the droplet back to a spherical shape, however if droplet diameter is insufficiently small, or aerodynamic forces are relatively large then droplet break-up will occur (Lefebvre, 1989).

Figure 3.18 shows and idealised cross-sectional view of a primary droplet disintegrating to two identically sized smaller droplets in a steady gas stream.

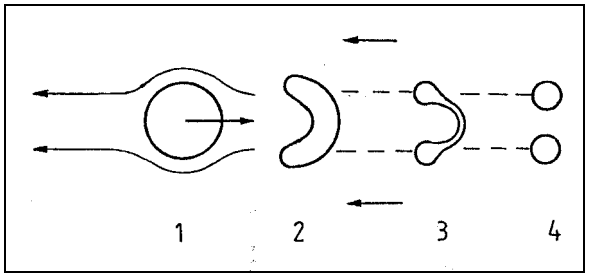

FIGURE 3.18. PRIMARY DROPLET DISINTEGRATION
(Bayvel *et al*, 1993).

Figures 3.19 shows an idealised image of a droplet disintegrating in a steady gas stream due to parachute disintegration.

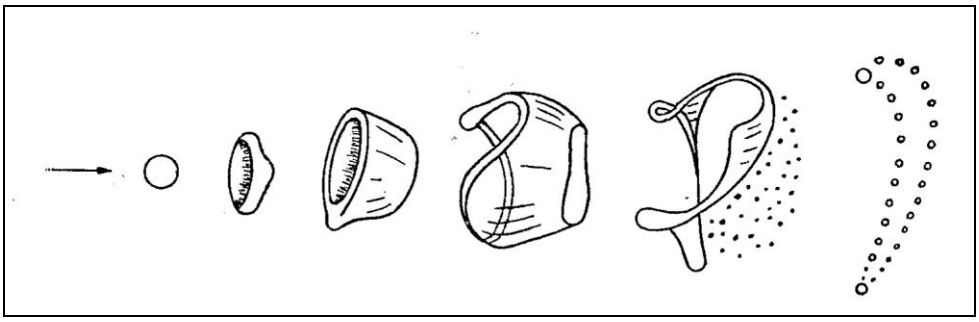

FIGURE 3.19. "PARACHUTE" OR "BAG" TYPE SECONDARY DROPLET DISINTEGRATION (Bayvel *et al*, 1993).

Droplets disintegrating due to aerodynamic forces will generally break-up in one of three ways depending on the flow of the continuous medium in which the droplets are dispersed, as described below.

1. *Lenticular* deformation describes the process whereby an individual droplet is initially "flattened" to an oblate ellipsoid and then to a torus that disintegrates under stretching. This type of droplet break-up is typical of laminar flow conditions.
2. *Cigar-shaped* deformation describes the process whereby an individual droplet disintegrates having been stretched to resemble a ligament. This type of droplet break-up is typical of plane hyperbolic flow.
3. *Bulgy* deformation describes the process whereby irregular flow in the continuous medium causes small bulges to form on the surface of a droplet that may detach. This type of droplet break-up is typical of turbulent flow conditions.

Figure 3.20 illustrates lenticular, cigar-shaped and bulgy deformation respectively (Lefebvre, 1989).

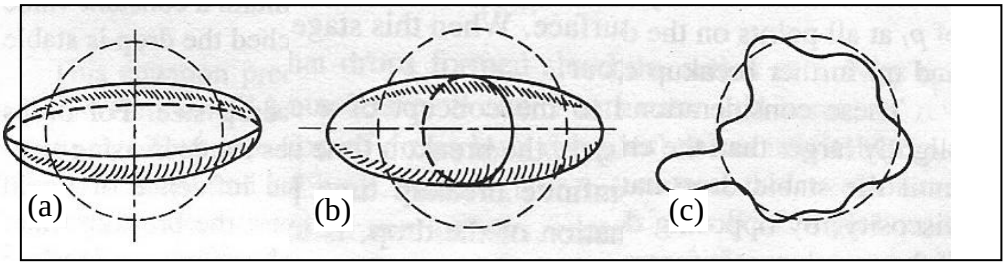

FIGURE 3.20. LENTICULAR (A), CIGAR-SHAPED (B) AND BULGY DEFORMATION (C) OF DROPLETS (Lefebvre, 1989).

It is clear that droplet disintegration is greatly influenced by the physical properties of the liquid and gaseous media (Lefebvre, 1989).

3.6. *Droplet Coalescence and Separation*

The motion of a droplet or group of droplets through a gaseous medium is a complex situation. Each droplet is surrounded by a gas film. Drag and lift forces act on individual droplets as they move through the gas, causing them to deform and potentially undergo secondary disintegration. Droplets may also evaporate and collide. In polydisperse sprays the motion of the droplet group is complicated by different sized droplets travelling at different velocities within the global spray. In essence, there are three degrees of droplet interaction (Sirignano, 1999):

1. droplets are sufficiently far apart that they only experience the slight effects in ambient gas pressure caused by neighbouring droplets. The forces acting on a droplet can be considered as if the droplet is an individual. This can be called a droplet array;
2. droplets are sufficiently close that changes in ambient gas pressure significantly affect the drag and lift of neighbouring droplets. Depending on the characteristics of the gas and the liquid droplets this influence may affect droplets within a few radii of each other. This may be called a droplet group;
3. droplets are sufficiently close that collisions occur. This may be called a spray.

3.6.1. *Droplet Collisions*

Collisions between droplets may be frequent when sprays are released into environments of limited volume. Qian *et al* (1996) conducted empirical experiments using high speed photography and found five possible outcomes of binary droplet collision:

1. coalescence after minor deformation;
2. bouncing;
3. coalescence after substantial deformation;
4. coalescence followed by separation for near head-on collisions;
5. coalescence followed by separation for off-centre collisions.

For water droplets colliding in a continuous medium of pressure 1-atmosphere regimes 2 and 3 can be disregarded (Qian et al, 1996). Regime 2 is not possible at atmospheric pressure for water droplets due to their relatively high surface tension and low viscosity that favours coalescence.

As two droplets approach each other due to Brownian motion or electrostatic attraction, the pressure in continuous medium increases in the immediate region between the two drops. Since gas absorption during a collision is very low, this continuous medium must be expelled in order that the droplets can reach Å, the proximity needed for molecular interaction and hence coalescence.

The pressure build-up tends to cause the droplets to "flatten" thereby converting a proportion of the kinetic energy into surface tension energy. The inertia of the gaseous film between the two droplets is proportional to the density of the gas so the influence on collision regime depends on the physical properties of the gaseous medium.

3.7. *Droplet Size Distribution Measurement*

The precise sizing of a global spray can be problematic. A spray will usually contain a very large number of droplets with varying trajectories and velocities.

Apart from very specialist atomisers, the range of droplet sizes in a spray can be very wide and droplets may coalesce or evaporate during the sizing measurement. Ideally a sizing technique would have the following attributes:

1. be non-intrusive – the technique does not influence the flow or size of the droplets in the spray;
2. have a wide size range capability;
3. be able to account for size changes over time;
4. be able to size a large number of droplets;
5. be able to size a spray quickly.

Common sizing techniques fall into 1 of 3 methods described hereafter.

3.7.1. *Mechanical Sizing Techniques*

Mechanical techniques are typically used to physically collect droplets so that they can be photographed and sized with a microscope. A coated glass plate is usually used to collect the droplets. Droplet sizes as small as 3µm are capable of being measured using this technique. Obtaining a representative sample using this technique can be problematic as large numbers of droplets can lead to coalescence on the plate and long measurement times. Another problem is collecting relatively small droplets on the plate as they tend to be carried by the gas flow and do not intercept it leading to droplet size being overestimated. In addition, as the droplets tend to flatten on the coated glass, a correction factor must be applied to calculate the original diameter of the spherical droplet. This is highly dependant on the physical properties of the liquid and the glass coating and can lead to significant errors.

Another mechanical sizing technique is the substitution of a molten wax such as paraffin to the desired liquid to be atomised. The molten wax rapidly cools and solidifies after atomisation and can be collected. The solid particles can then be sieved to ascertain the droplet size distribution. This technique has the advantage of measuring a large number of droplets and therefore a representative sample however the physical properties of the wax are unlikely to be identical to the

desired liquid and therefore correction factors must be applied which will lead to errors.

A similar technique involves the rapid freezing of droplets using nitrogen gas as soon as they leave the atomiser. The droplets can then be immediately sieved. As with the molten wax technique errors can occur due to the correction factor applied to calculate the size of the liquid droplet from the size of the solid droplet.

3.7.2. *Electrical Sizing Techniques*

Electrical techniques measure the disturbances caused by liquid droplets passing an electrical current. The contact electrode method investigated by Wicks and Dukler (1966) measures the electrical pulses caused by droplets passing between two thin electrodes across which there is a potential difference. Droplets with a diameter larger than the separation distance of the electrodes short circuit the instrument and create a pulse. Each pulse is counted and by varying the separation distance between the electrodes each droplet can be placed into a size class. Problems arise from the very low voltages that must be used to avoid short circuiting without droplet contact and hence background noise and the phenomenon whereby the electrical resistance of the droplet is influenced by its velocity and immersion depth on the electrodes.

The charged wire technique involves the measurement of charge drop when a droplet comes into contact with a conducting wire. Larger droplets cause a larger charge transfer. This technique is unsuitable for high conductivity liquids however as they tend to cause longer periods of charge drop and therefore successive droplet contacts with the wire may be difficult to distinguish.

A similar technique involves measuring the reduction in electrical resistance caused by cool droplets contacting a hot wire. Resistance reduction is directly proportional to droplet size. This technique is extremely rapid, taking approximately 2ms however it is an intrusive technique as droplets must come into physical contact with the wire. This may lead to droplet break up if flow

velocity is not sufficiently small therefore adversely affecting droplet size distribution.

3.7.3. *Optical Sizing Techniques*

Optical techniques may be classes as imaging or nonimaging. Imaging techniques typically employ high-speed photography or holography so that image data of the global spray can be captured and used for sizing. Nonimaging techniques use light to count of size droplets.

Dombrowski and others pioneered early high-speed photography measurement techniques from the 1950's. Laser pulse flashes can be emitted in the order of nanoseconds to capture an image of the global spray. The resulting photographs must then be analysed manually to measure the sizes of individual droplets. If a very rapid double flash is emitted then the trajectory and velocity of a single droplet can be calculated by measuring the distance travelled between exposures. This technique has the advantage of being non-intrusive and is relatively inexpensive however the human element of processing the photographs can be laborious and lead to errors. The technique may be better suited to low density sprays where the possibility of droplet overlapping is reduced

Holography uses a similar principle to high-speed photography. A collimator is used to produce a cylindrical laser beam with wide diameter and duration of approximately 20ns. This allows a three-dimensional image to be produced with droplet sizes as small as 2μm theoretically visible depending on the wavelength of the light source. As with high-speed photography however the technique is limited to sprays of low number density.

Light scattering techniques use the phenomenon of light scattering due to liquid refractive index to ascertain droplet size distribution. Dobbins *et al* (1963) were the first to suggest that droplet size could be measured by scattering due to refractive index. It was proposed that the radiant intensity of a scattered monochromatic laser beam can be used to calculate droplet size distribution of a spray if the refractive index of the liquid and wavelength of the laser is known.

3.7.3.1. *Fraunhofer Theory*

The size of an opaque disc can be calculated by the scattering caused when a monochromatic parallel beam is diffracted by the object. A monodisperse spray would create a diffraction pattern of light and dark rings, with droplet size being inversely proportional to the spacing of the rings. In reality most sprays are polydisperse so a large number of diffraction patterns are produced. Fraunhofer theory is clearly not suitable for measuring droplet sizes of transparent liquids as it does not take into account the transmission of light through the particles.

3.7.3.2. *Mie Theory*

Unlike Fraunhofer diffraction theory, Mie theory takes into account the transmission and adsorption of light through the droplets. The complex refractive index which is the sum of the of the real refractive index and the imaginary refractive index liquid droplets must be known.

3.7.4. *Malvern Particle Sizer*

The Malvern particle sizer is one of the most commonly used non-intrusive droplet sizing methods available (Lefebvre, 1989). The instrument's popularity stems from it's ease of use and ability to quickly characterise a global spray. Figure 3.21 shows the Mastersizer S.

FIGURE 3.21. MALVERN MASTERSIZER S (Malvern Instruments ltd).

A 2mW, 633nm wavelength He-Ne laser is expanded to create a parallel, monochromatic light beam. As a spray passes through the beam the laser is diffracted due to the refractive index of the liquid. The scattered light is focussed using a 300m Fourier transform lens onto a detector comprised of 45 photo-diodes arranged in a radial pattern. A diffraction pattern consisting of light and dark concentric rings on the detector is created with the width of the rings directly proportional to droplet size. As a polydisperse spray passes through the beam a series of overlapping diffraction patterns are created. Figure 3.22 shows the setup of a Malvern Mastersizer S.

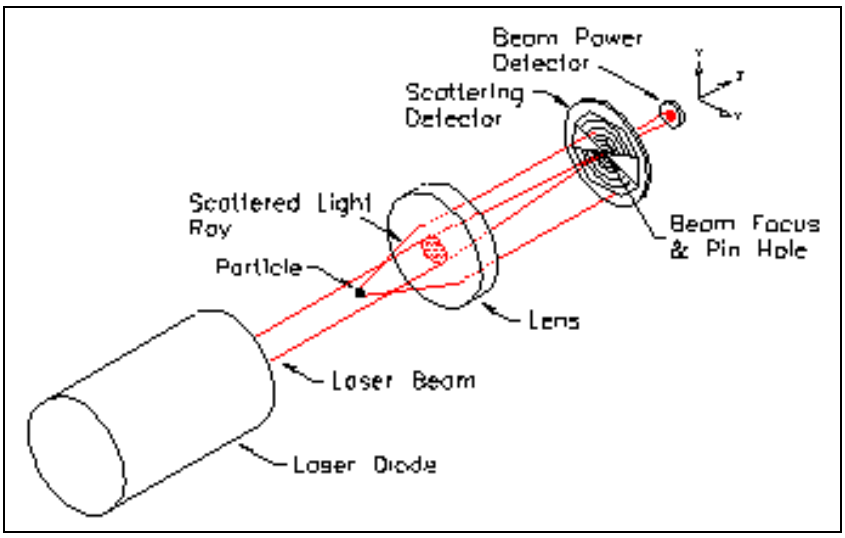

FIGURE 3.22. MEASUREMENT OF LIGHT SCATTERING (Malvern USA).

Using a 300mm lens, the Mastersizer can measure droplet sizes in the range 0.5-900µm. Once the light scattering data has been collected Mie theory can be applied and the droplet size distribution of the spray can be presented. This technique has the advantage that droplet size distribution can be modified after the measurement has been completed if the liquid refractive index data is found to be inaccurate. As well as droplet size distribution, cumulative droplet size distribution can also be presented. Figure 3.23 shows an idealised view of droplet size distribution data produced by the Mastersizer S.

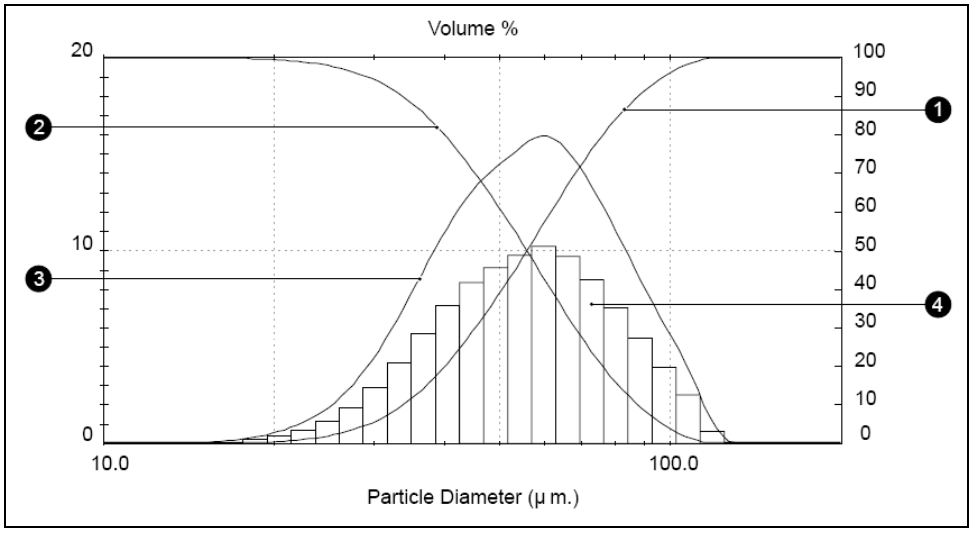

FIGURE 3.23. IDEALISED DATA OUTPUT (Malvern Instruments ltd).

The Malvern Mastersizer however is expensive and requires regular calibration by a certified engineer meaning running costs are relatively high. Multiple scattering from relatively dense sprays occurs when scattered light from a droplet is further scattered by subsequent droplets. The instrument is unable to detect this secondary scattering and processes the data as if it had been scattered only once. This phenomenon can be countered by measuring the obscuration of the beam caused by the spray by measuring the light intensity at the very centre of the beam. As this light will not have been scattered it is possible to determine the amount of light scattering that has taken place. If the value of obscuration falls outside of certain limits 5-50% then the results should be disregarded and the position of the spray must be moved to bring the obscuration value between these limits.

Another problem is that scattering of the laser beam is inversely proportional to droplet size therefore very small droplets have higher scattering angles. If the scattering angle is too high the Fourier lens may not be able to focus the light onto the detector and data will be lost. As the lost data will usually be from relatively small droplets the droplet size distribution will be skewed to larger sizes. This phenomenon is known as vignetting and can be remedied by moving the spray closer to the lens but this increases the possibility of droplets impacting on the lens and creating a false reading. The maximum allowable distance can be expressed as:

$$x = f\left(\frac{d_l - d_b}{d_d}\right) \qquad \text{(EQN 3.6)}$$

For a 300mm lens the cut off distance is equivalent to approximately 84mm. Care must be taken to extract the spray when working so close to the lens so as to avoid droplet impaction.

Beam steering is the phenomenon by which the laser beam can be affected by slight fluctuations in thermal gradient in the ambient atmosphere. These fluctuations can be even higher in the presence of a spray. Beam steering mostly affects the innermost detectors as this is where beam intensity is highest and can result in abnormally high results for these detectors. Beam steering can be remedied with some human judgement. If it is expected that droplet size distribution will fall into the relatively small end of the lens range any spurious results on the large end can be ignored or "killed" through the instrument's software. Although care must be taken with this procedure, checks can be made to ensure that errors are not introduced.

3.8. *Droplet Size Representation*

In practice a monodisperse spray can not be created. Under certain conditions some rotary atomisers are capable of producing sprays which are considered to be monodisperse as they have a geometric standard deviation of less than 1.2, however in reality most atomisers will produce a spray with a relatively large range of droplet sizes. There are many potential parameters to describe the size characteristics of a polydisperse spray and the most relevant will often depend on the spray application under consideration. Often, establishing a mean value for droplet size is inadequate as this does not take into account the possible range of droplet sizes in the spray and it may be more beneficial to establish values such as minimum or maximum diameter.

3.8.1. *Graphical Methods of Droplet Size Distribution*

Droplet size distribution data gathered from a sizing procedure can be plotted as a simple histogram with determined class width. Figure 3.24 shows an example of droplet size plotted against frequency with a class width of 17μm.

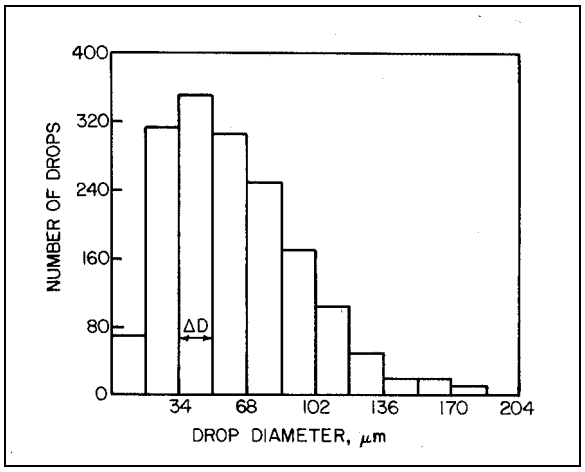

FIGURE 3.24. DROPLET SIZE FREQUENCY DISTRIBUTION (Lefebvre, 1989).

In practice it is usually more beneficial to plot the *surface area* or *volume* of droplets that fall into determined size classes. This will obviously result in the positive skewing of the frequency distribution as larger droplets have a larger volume. Figure 3.25 shows this positive skewing effect.

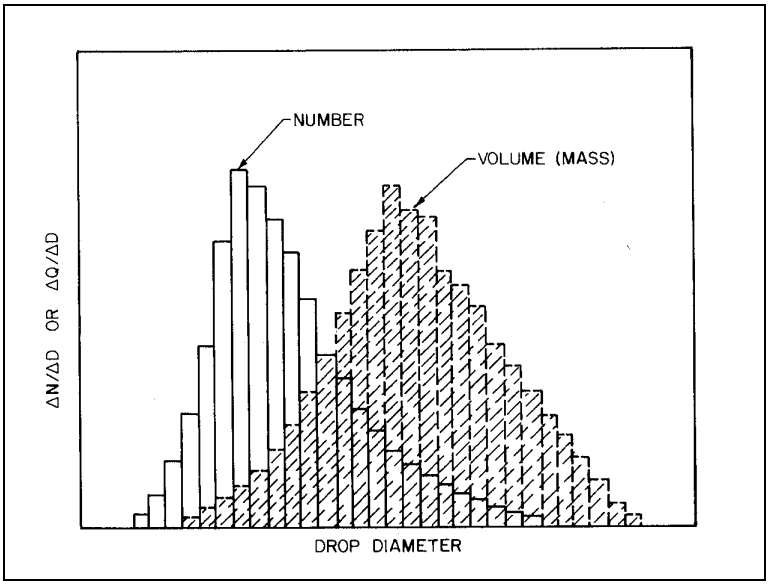

FIGURE 3.25. SKEWING OF FREQUENCY DATA WHEN DROPLET VOLUME IS TAKEN INTO ACCOUNT (Lefebvre, 1989).

In addition it is possible to plot cumulative frequency distributions and cumulative volume distributions. From these graphs it is possible to determine parameters such as volume median diameter dv50 or any other arbitrary percentage below or above which a certain volume of droplets lie.

3.8.2. *Representative Diameters*

A distinction should be made between mean diameters and representative diameters as some terms can be misleading. Mean values represent some average dimension such as diameter, surface area or volume. A mean diameter is typically of the form d_{ab} where a and b represent the dimensions under consideration. For example Arithmetic Mean Diameter is denoted d_{10} and Volume Mean Diameter is denoted d_{30}. Figure 3.26 shows a group of droplets of various sizes and a group of droplets with identical diameter equivalent to the poly disperse group.

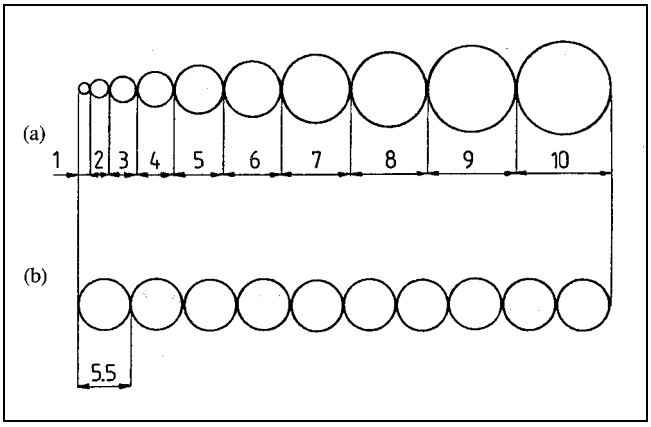

FIGURE 3.26. EQUIVALENT DROPLET DIAMETERS
(Bayvel *et al*, 1993).

Sauter mean diameter is the size of the droplet with an identical surface area to volume ratio as the entire aerosol (Lefebvre, 1989). In line with the above rule, SMD is denoted d_{32}. A low SMD value indicates a large total droplet surface area and hence a relatively fine aerosol.

$$\text{SMD} = \frac{\sum N_i d_i^3}{\sum N_i d_i^2} \qquad \text{(EQN 3.7)}$$

Representative diameters are those droplet diameters which indicate some particular volume boundary, for example $d_{0.1}$ is the diameter below which 10% of the total volume of a given aerosol will be. A representative diameter is usually denoted d_a where a represents the fraction to which the diameter corresponds (Lefebvre, 1989).

Mass median diameter, MMD is the diameter below which 50% of the total aerosol volume will be found. In line with the above statement, MMD is denoted $d_{0.5}$. MMD is an often quoted diameter for medical jet nebulisers, however the optimum mean or representative diameter may depend on the application in question. No single mean or representative diameter can totally describe the size distribution of an aerosol (Lefebvre, 1989).

3.9.4. *Droplet Size Dispersion*

The range of droplet sizes in a global spray may be more relevant than a particular mean or representative diameter. Two functions for describing droplet size dispersion are particularly useful.

Droplet Uniformity Index, *UI* is a measure of the dispersion of droplet sizes about the mass or volume median diameter, $d_{0.5}$. It is expressed as:

$$UI = \frac{\sum_i V_i (d_{0.5} - d_i)}{d_{0.5}} \qquad \text{(EQN 3.8)}$$

It can be seen from equation 3.20 that a monodisperse spray would have a droplet uniformity index equal to zero.

Relative Span Factor, Δ is another measure of droplet size dispersion about the mass or volume median diameter, $d_{0.5}$. It can be expressed as:

$$\Delta = \frac{d_{0.9} - d_{0.1}}{d_{0.5}} \qquad \text{(EQN 3.9)}$$

It can be seen from equation 3.21 that a monodisperse spray would have a relative span factor tending towards unity.

3.9. Summary and Implications for Test Programme

This chapter has discussed the technical parameters and obstacles surrounding the atomisation and delivery of liquids to the subsurface. It is clear that the creation of a relatively monodisperse spray with minimum achievable droplet size will be desirable if the test programme is to be successful. While this is difficult to achieve in practice, medical jet nebulisers appear to offer the best solution whilst being cost efficient. Significant experimental research will be needed into the effect of passing sprays from medical jet nebulisers through granular soils, on both droplet size and droplet size distribution. This will help ascertain the effectiveness of using these devices to deliver carbon substrates to the subsurface for in situ bioremediation of chlorinated solvents.

CHAPTER 4. TEST PROGRAMME AND METHODOLOGY

4.1. *Chapter Synopsis*

The following chapter discusses the methods and materials used to perform experiments in order to investigate the possibility of adapting medical nebulisers for delivering atomised carbon substrates to the subsurface for in situ bioremediation of chlorinated solvents.

4.2. *Transportation of Atomised Carbon Substrates through Various Granular Media*

Two types of medical nebuliser, the Cirrus™ and Microcirrus™, both manufactured by *Intersurgical* were used with two types of carbon substrate, methanol and ethyl lactate, commonly used in practice for in situ bioremediation of chlorinated solvents. The atomised carbon substrates were injected into a variety of different coarse and medium-grained soils. Initial tests were carried out using ballotini with uniform particle diameters of 4mm, 3mm and 2mm as a substitute for natural soil. The ballotini were held in Perspex tubing in lengths of 100mm, 200mm and 400mm. A small piece of wire mesh was placed at the base of the tubing, just above the nebuliser output, to support the ballotini. It was important to control the speed at which the ballotini were poured into the tubes to ensure that the packing arrangement remained as constant as possible throughout the length of the tube. If the pouring speed was too fast the ballotini tended to arrange themselves in a cubical rather than rhombohedral packing arrangement, resulting in the pore spaces in the column becoming relatively large. Tests were carried out under both dry and field capacity conditions. Field capacity is defined here as the amount of moisture left in a medium after all excess water has drained away under gravity. It is therefore the water that is held in the medium by surface tension.

Having measured the droplet size distribution of atomised substrates transported through ballotini, further tests were carried out to measure the droplet size distribution of atomised substrates transported through two soil types; a fine-

grained gravel and a coarse-grained sand. All tests were performed in triplicate to ensure consistency. Upon analysis, the test with the best obscuration value was selected as the most accurate result for that particular test. The obscuration values gives an indication of the percentage of the laser beam that has been obscured by the spray. Malvern instruments recommends that the ideal obscuration value range is 10-30% (Malvern Instruments Ltd ,1997). In general the obscuration values for each test were repeatable. If the obscuration value fell outside of the aforementioned range the test was repeated until an acceptable value was attained.

A laser diffraction particle sizer was used to measure the droplet size distribution of atomised carbon substrates both released directly to atmosphere and after transportation through the ballotini or natural soil. A Malvern Mastersizer S was selected due to its large measurement range and ability to quickly measure droplet size distribution without interfering with the flow of the spray. As discussed in Chapter 3.8.4, the instrument determines droplet size distribution by measuring the light scattering caused by individual droplet diffraction which is dependant on the diameter of the droplet and the complex refractive index of the atomised liquid.

The layout of the Mastersizer was rearranged to focus on droplets emitted from the top of a soil column by constructing a rig that permitted the Mastersizer S to be rotated 90° about it's longitudinal axis, allowing columns of up to 1m to be positioned in line of the laser beam. Malvern Instruments were consulted prior to this procedure to ensure that the instrument would not be adversely affected in this position. The experimental set up is shown in Figures 4.1 and 4.2..

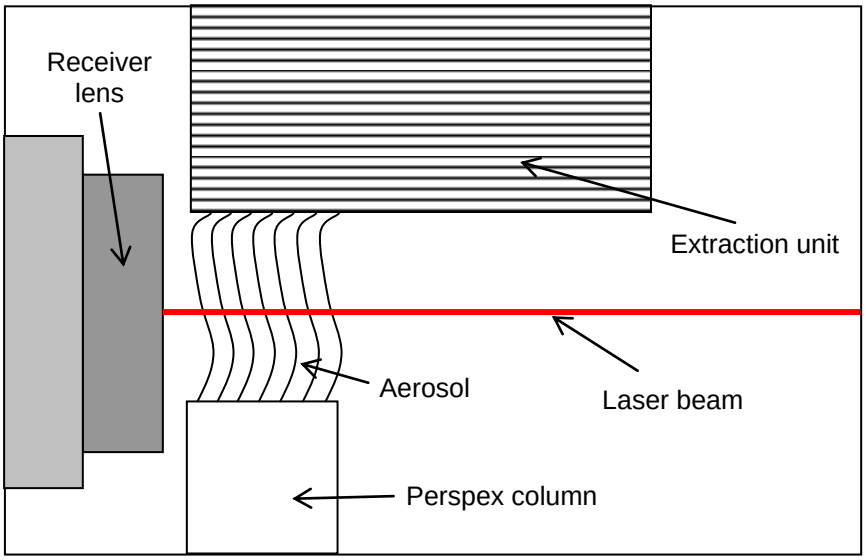

FIGURE 4.1. DROPLET SIZE DISTRIBUTION MEASUREMENT EXPERIMENTAL SETUP.

After sample preparation, the column was fixed in position using a clamp stand so that the exiting droplets would intercept the laser beam as close as possible to the receiver lens. An extraction system allowed the column to be placed in close proximity to the receiver lens without droplets impacting on the lens as this would produce inaccurate results. It was assumed that the flowrate of the extraction system was insufficient to significantly influence the flow of droplets through the column during testing. Each nebuliser was filled in turn with liquid substrate and attached to the base of the column, creating an airtight seal. When atomised substrate could be seen exiting the top of the column, the histogram on the Mastersizer software screen was checked to ensure that the data was steady. The measurement was then taken.

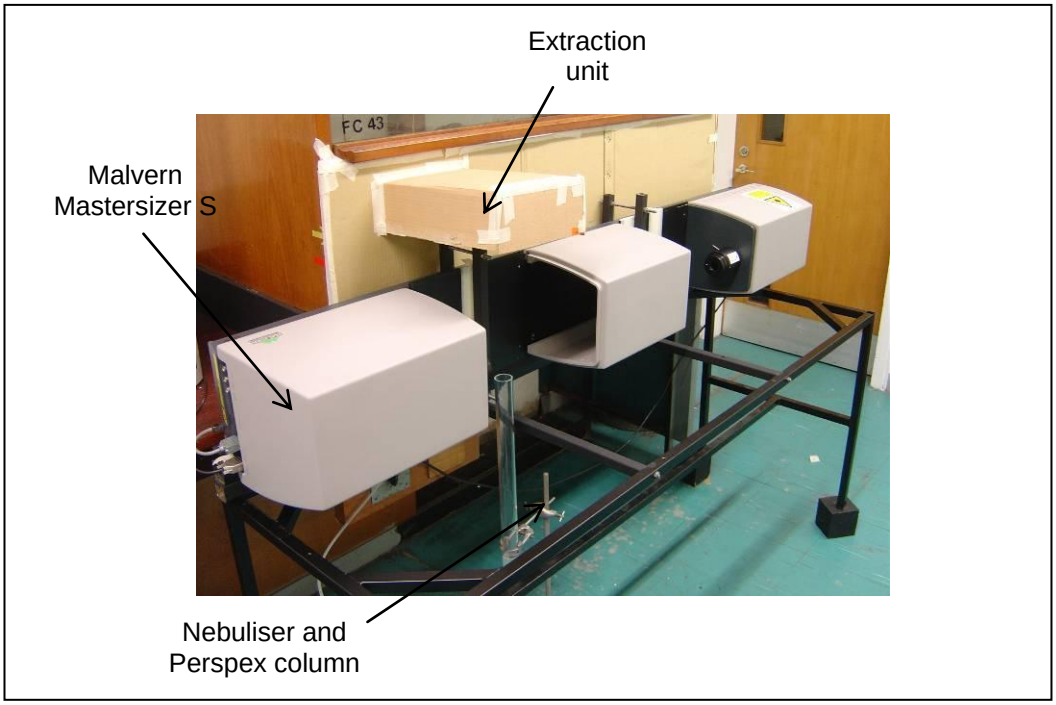

FIGURE 4.2. DROPLET SIZE DISTRIBUTION MEASUREMENT EXPERIMENTAL RIG SETUP.

Figure 4.3 shows atomised methanol exiting a 100mm column packed with fine gravel under dry conditions intercepting the laser beam of the Mastersizer S.

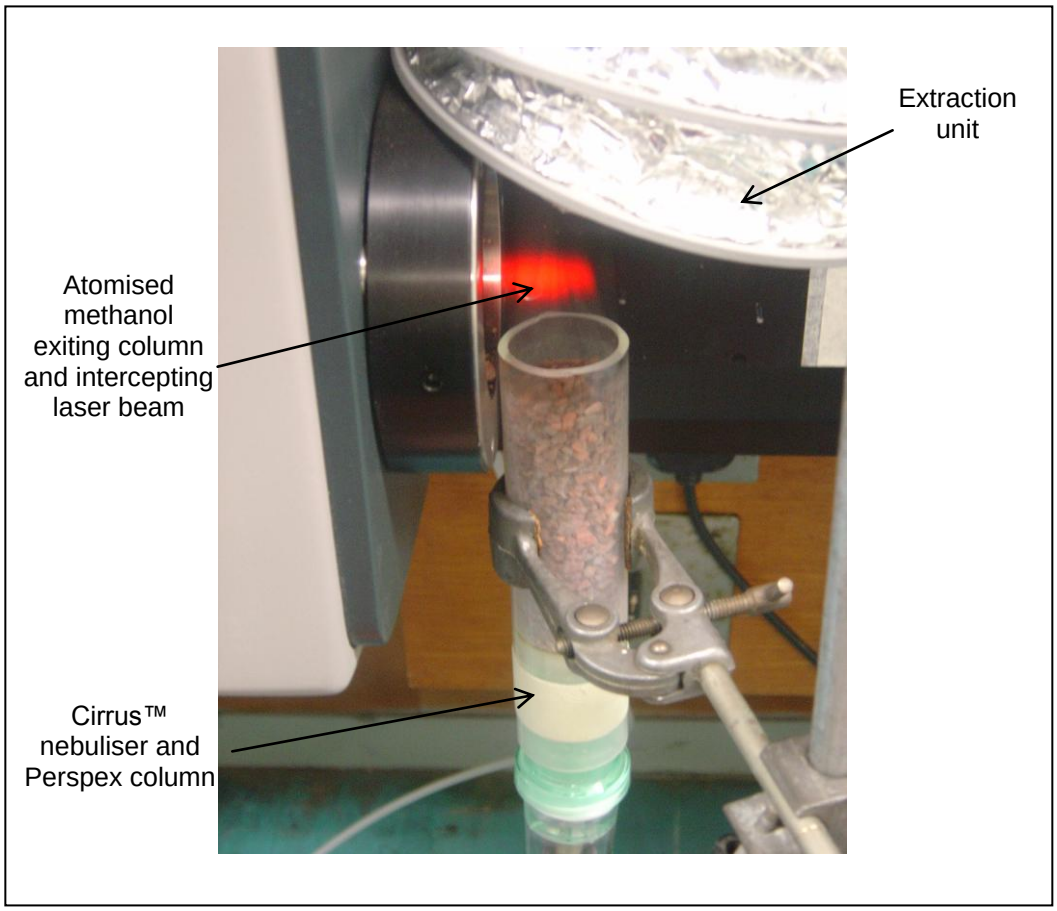

FIGURE 4.3. ATOMISED METHANOL EXITING 1OOMM FINE GRAVEL COLUMN UNDER DRY CONDITIONS.

It was of critical importance to ensure the correct set up of the Mastersizer S software and hardware so that light scattering caused by the substrate droplets was accurately measured and interpreted by the instrument. The *Range* option in the software allowed the appropriate lens to be selected for the droplet size measurement application. Table 4.1 shows that the appropriate lens for measuring the droplet size distribution of atomised liquids released by medical nebulisers is the 300mm Fourier lens. This lens allows measurement of particles in the size range 0.5-880µm. Although a 300mm Reverse Fourier lens, capable of measuring droplet sizes in the range 0.05-900µm is available, this technique is not appropriate for measuring the droplet size distribution of atomised liquids. It was clear that a proportion of droplets, particularly those released from the Micro-cirrus nebuliser, may be smaller than 0.5µm in diameter. This would inevitably result in data being lost from the droplet size distribution presentations.

TABLE 4.1. MASTERSIZER S LENSES AND APPROXIMATE DROPLET SIZE RANGES.

Lens	*Approximate size range*
300mm Fourier	0.5-880µm
1000mm Fourier	4.2-3489µm

In addition, an *Active Beam Length* option in the software had to be selected for the length of laser intersected by the aerosol droplets during measurement. In practice this is difficult to accurately establish as the size of the global aerosol varies over time. For all measurements the active beam length was set to slightly wider than the width of the column diameter at 40mm. The *Particle Density* for the nebulised liquid in bulk form was specified for a temperature controlled environment of 20°C.

The *Sweeps* option allowed the user to specify the number of sweeps or the length of time that light scattering measurements are taken. Each sweep takes 2ms to perform so a sample number of 250 equates to a sample time of 0.5s. Clearly the greater the number of sweeps the more the droplet size distribution will be averaged for temporal variations.

The results of the analysis were displayed in both graphical and tabular form as shown in Figure 4.3. The percentage volume of droplets in each size class is tabulated and a graph is drawn to show the frequency distribution of droplets in each size class. In addition, it was possible to display cumulative droplet size distribution data. The *Result - Analysis* screen also lists important mean and representative diameters such as SMD (Sauter mean diameter), $d_{0.5}$ (mass median diameter), $d_{0.1}$ (10% mass diameter), $d_{0.9}$ (90% mass diameter), Δ (relative span factor) and DUI (droplet uniformity index). The concentration and specific surface area of the spray can also be displayed however this requires that the active beam length be accurately known which was not possible during these experiments as discussed previously. Figure 4.4 shows a screenshot from the *Result Analysis* stage.

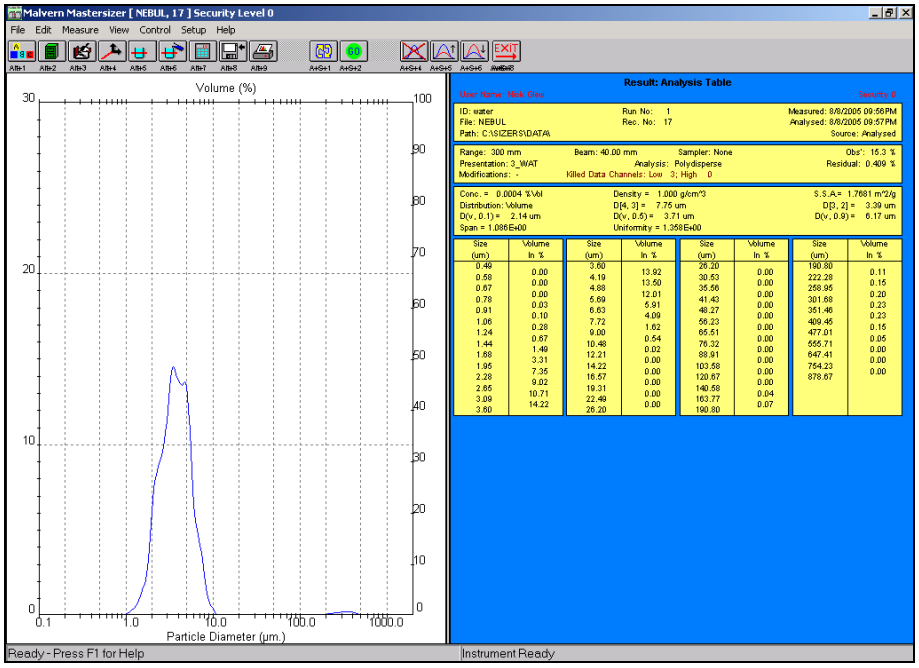

FIGURE 4.4. TYPICAL OUTPUT DATA FOR DROPLET SIZE MEASUREMENT.

3.3. *Medium-scale Column Tests with Rhodamine Water Tracer*

In addition to measuring the droplet size distribution of atomised carbon substrates, the distribution of liquid, atomised using Cirrus and Microcirrus nebulisers was measured in a medium-scale test column using the fluorescent tracer dye, rhodamine water tracer. The dye emits radiation at a lower wavelength than that of the radiation it absorbs, allowing detection at ng/l levels (Sabatini *et al*, 1991) using a handheld, portable fluorometer. The rhodamine WT molecule is comprised of two carboxyl groups with distinct sorption characteristics, which leads to a two-step column breakthrough curve. The mass ratio of the two isomers has been determined to be 50:50. Figure 4.5 illustrates the two RWT isomers. It is expected that the meta-isomer sorbs to an extent of 1 order of magnitude greater than the para-isomer. This is due to the meta-isomer exhibiting greater hydrophobic exclusion from aqueous solution and greater electrostatic attraction to oppositely charged solid surfaces than the para-isomer.

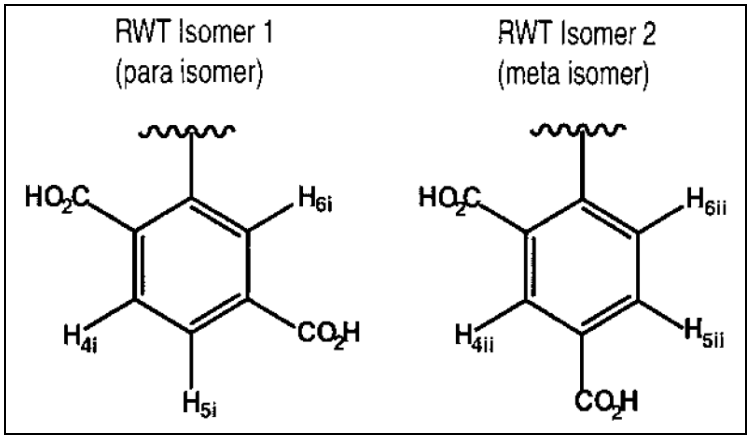

FIGURE 4.5. RHODAMINE WATER TRACER ISOMER 1 (PARA-ISOMER) AND ISOMER 2 (META-ISOMER) (Vasudevan *et al*, 2001).

A handheld fluorometer manufactured by Turner Designs was used to measure the fluorescence of rhodamine WT solutions. Figure 4.6 shows a photograph of the *Aquafluor*™ portable fluorometer. The instrument must be calibrated using a two point calibration procedure using a blank sample and standard sample. The fluorometer was calibrated at 300µg/l as this is the upper limit of linearity. Solutions were prepared at 50µg/l, 100µg/l, 150µg/l, 200µg/l, 250µg/l, 300µg/l, 350µg/l, 400µg/l, 500µg/l, 600µg/l, 800µg/l and 1000µg/l. The fluorescence of each solution was measured to ascertain the accuracy of the instrument.

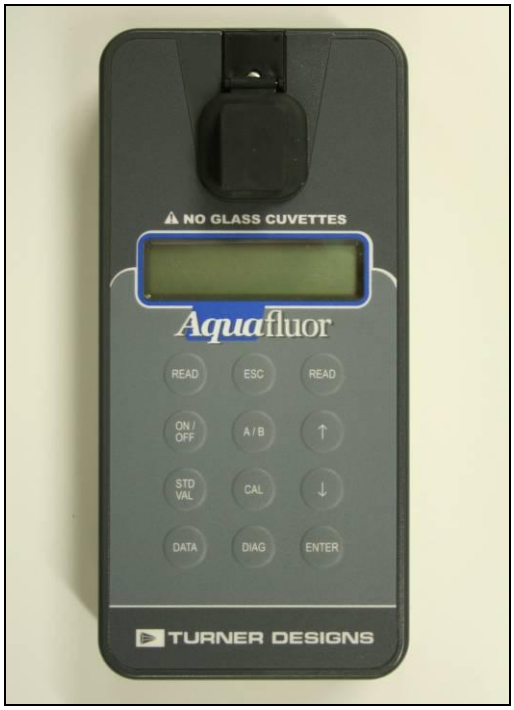

FIGURE 4.6. TURNER DESIGNS *AQUAFLUOR*™ FLUOROMETER.

Additional laboratory experiments were designed to measure the sorption characteristics of rhodamine WT transported through a sand column. A solution was prepared containing 250µg/l rhodamine WT and 5g/l NaCl. NaCl can be used to comparison as it does not sorp to the soil particles. Electrical conductivity can be used to measure NaCl concentration. The initial electrical conductivity was found to be 7.91mS/m and the true concentration of the solution was found to be 258.2µg/l. The solution was flushed through a sand column at approximately 12ml/min using a peristaltic pump. The time taken to flush one pore volume was measured to be 23 minutes. Conductivity and fluorescence measurements of the flushed solution were taken every 5 minutes. The experimental setup is shown in Figure 4.7.

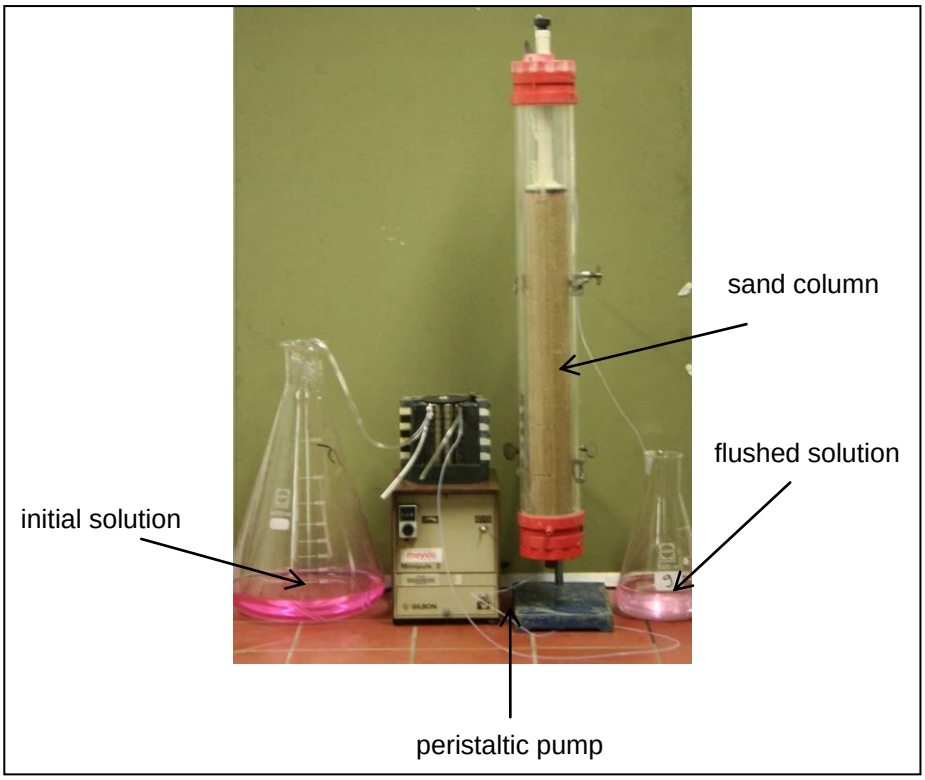

FIGURE 4.7. EXPERIMENTAL SETUP FOR RHODAMINE WATER TRACER RETARDATION MEASUREMENT.

The relationship determined between rhodamine WT concentration and measured fluorescence is shown in Figure 4.8. It can be seen that once the standard calibration value of 300µg/l has been exceeded, the accuracy of the instrument is adversely affected. The correlation coefficient, r^2 for solution concentrations ≤300µg/l was calculated to be 0.997. In addition Figure 4.9 shows the

breakthrough curves for NaCl and rhodamine WT through a sample of clean sand. C/C_0 refers to concentration/initial concentration, V/V_0 refers to volume/initial volume and therefore indicates the number of pore volumes flushed through the sample.

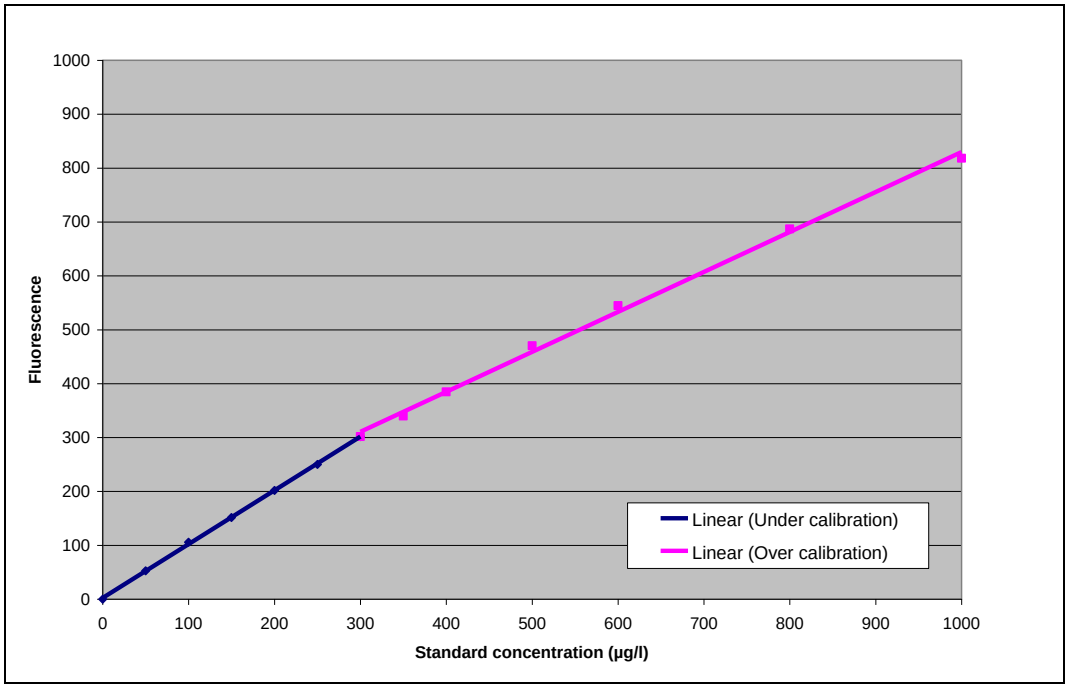

FIGURE 4.8. RELATIONSHIP BETWEEN RHODAMINE WATER TRACER CONCENTRATION AND FLUORESCENCE.

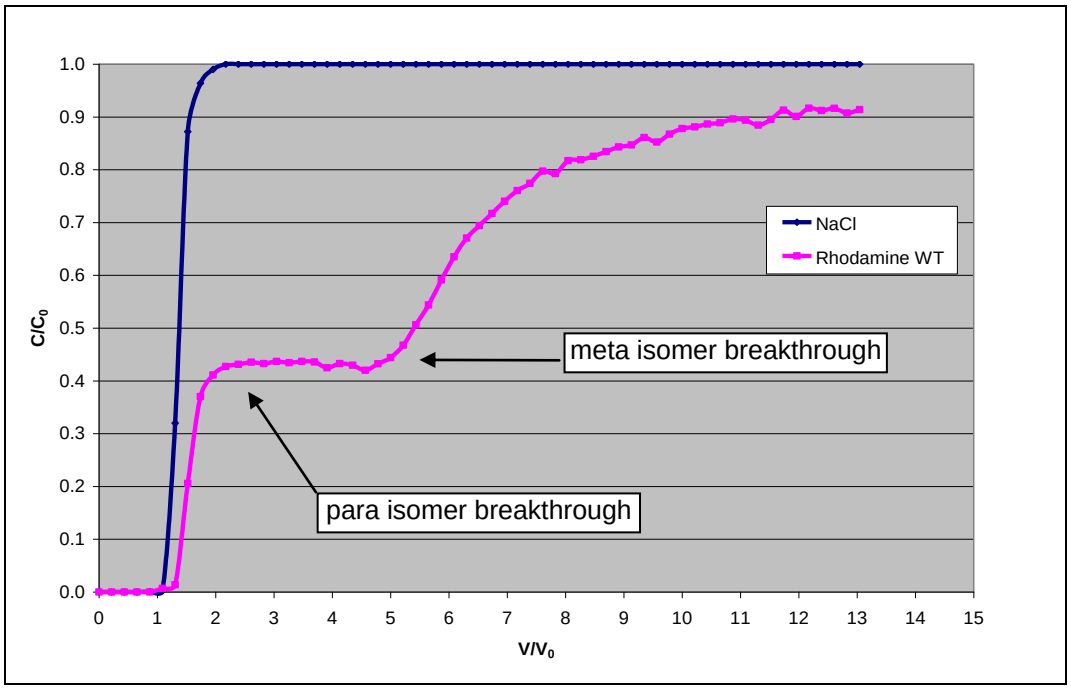

FIGURE 4.9. BREAKTHROUGH CURVE FOR NACL AND RHODAMINE WATER TRACER.

The tracer tests were initially used in a test column measuring 175mm diameter and 800mm length filled with fully-saturated medium grained sand. A Cirrus or Microcirrus nebuliser was situated at the base of the column with a control valve to allow flow of nebulised rhodamine WT solution into the sand. A peristaltic pump was used to ensure a continuous feed of rhodamine WT solution to the nebuliser. Rhodamine WT injection was either continuous, or pulsed for 15 minutes with 5 minute intervals. Five sample ports (A, B, C, D and E) were placed on the side of the column at 100mm spacing from the base of the column. Small (<3ml) samples of pore water were taken at 15 minute intervals from the sample ports and measured for fluorescence using an *Aquafluor* portable fluorometer. Background pore water fluorescence was measured prior to tracer injection and subtracted from all subsequent fluorescence readings. Figure 4.10 shows the experimental setup for injection of RWT solution into the column.

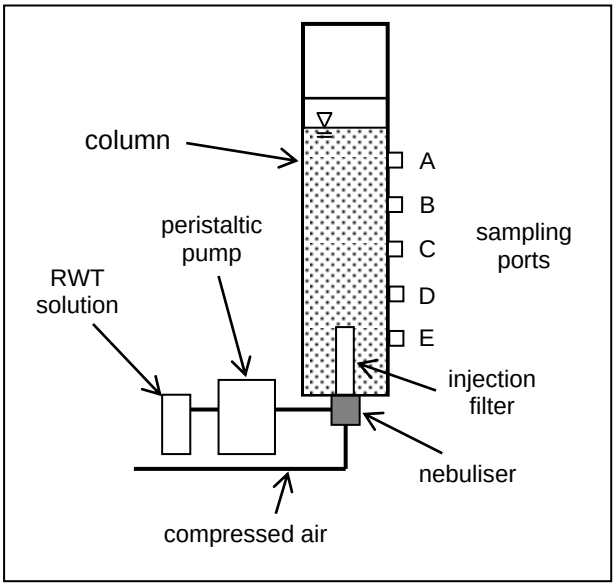

FIGURE 4.10. EXPERIMENTAL SETUP OF MEDIUM-SCALE TEST COLUMN.

4.4. *Large-scale Test Column*

A large-scale test column was constructed to more accurately simulate anticipated field conditions during the injection of atomised substrates into fully-saturated granular soils.. The column was initially manufactured by Alibert Buckhorn UK Ltd and was constructed from 16mm thickness high density polyethylene (HDPE) with an internal height of 2.0m and an internal diameter of

1.2m, giving the column an approximate internal volume of 2000litres. The column was manufactured using a helical winding system which requires no welding, ensuring that the possibility of fluid leakage was minimised. Figure 4.11 shows the initial design of the large-scale test column prior to modification.

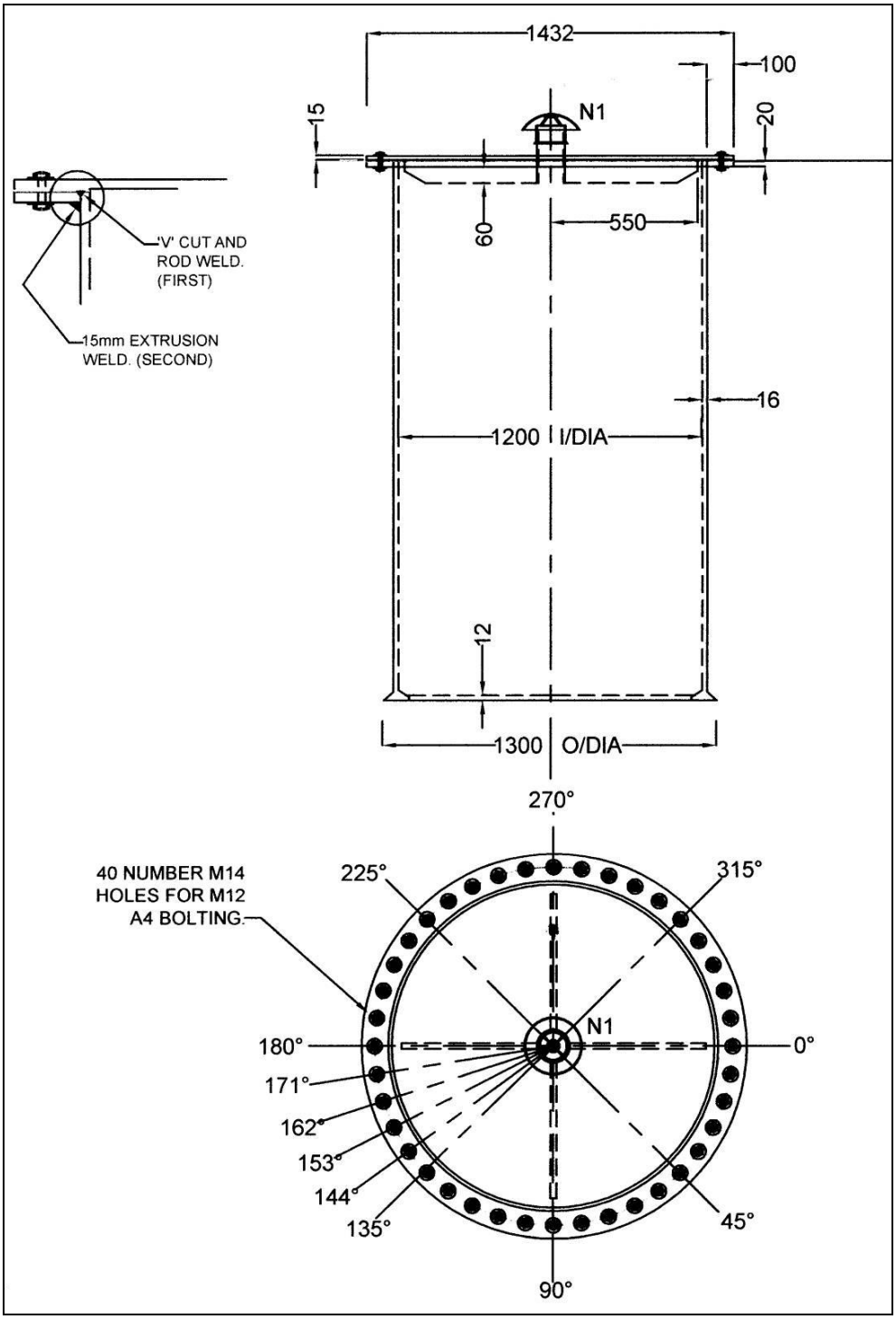

FIGURE 4.11. CROSS-SECTION AND PLAN VIEW OF LARGE-SCALE TEST COLUMN.

Although it is apparent that the tank would not entirely simulate anticipated field conditions it was selected as it represented the largest diameter column that could be safely commissioned and filled with saturated granular soil under laboratory conditions. To this end a concrete base was constructed for the column to provide support and also to ensure that the column was level. In the field it would be likely that injection filters would be situated at greater depths and more importantly the flow of gas and droplets into the subsurface would not be constricted by the lateral boundaries of the column. It is likely therefore that the lateral transport of atomised rhodamine WT in the large-scale column will have been somewhat restricted by the internal wall of the tank. Under field conditions it could be reasonably expected that lateral transportation, of the sparging gas at least, would be significantly improved when compared with the large-scale column. This in turn could have led to the overall effectiveness of the atomisation system to transport droplets being underestimated.

A series of modifications were necessarily made to the column in order to commission it for measuring the distribution of atomised rhodamine WT. A water inlet was situated at the base of the column to allow filling of the tank during sand placement and between tests. In addition a 2m length of Perspex pipe was attached vertically to the side of the column with connections at the base and the top of the column. This allowed for the water level inside the column to be determined during filling and testing.

A mobile platform was needed to fill the column with sand. Sand was placed into the column one 10 litre bucket at a time. The water level was maintained approximately 20-30cm above the level of the sand during filling. This served two purposes. Firstly the procedure prevented the trapping of air bubbles in the pore spaces of the sand and ensured that the medium was fully saturated. Secondly it allowed the sand to settle relatively slowly which prevented damage to the sampling array. Every five buckets the sand in the column was spread using a rake and tamped using a long rod to ensure proper settlement. The sand level was brought to 1.75m and levelled. A layer of mesh was then placed on top of the sand. The remaining 0.25m was filled with a coarse gravel to provide ballast whilst not adversely affecting the flow of gas through the column.

4.4.1. *Injection of Atomised Rhodamine WT*

The rhodamine WT injection system consisted of four Cirrus™ nebulisers fixed into a 400mm section of 80mm diameter Perspex tubing using Araldite. An auxiliary gas line was attached to the end of the pipe to control the injection of the aerosol into the column. A peristaltic pump was used to supply rhodamine WT solution to the nebulisers by means of small diameter flexible pipes glued into the side of the nebulisers using Araldite. A regulator controlled the compressed gas entering the injection system. A pressure gauge was fitted to record the pressure to the nebulisers and two additional pressure gauges were fitted to record the auxiliary gas pressure and the total pressure entering the column. A flow meter was also used to record the flow rate of gas entering the column. A non return valve was used to ensure unidirectional flow of the injected gas and droplets. The injection system is illustrated in Figure 4.12 and Figure 4.13.

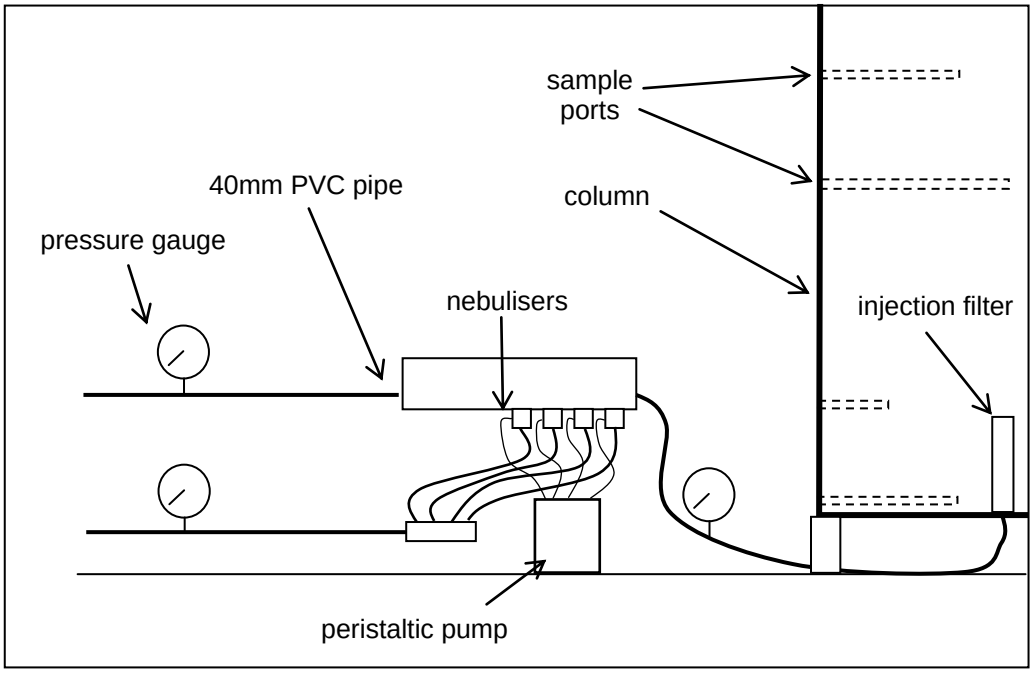

FIGURE 4.12. INJECTION SYSTEM EXPERIMENTAL SETUP.

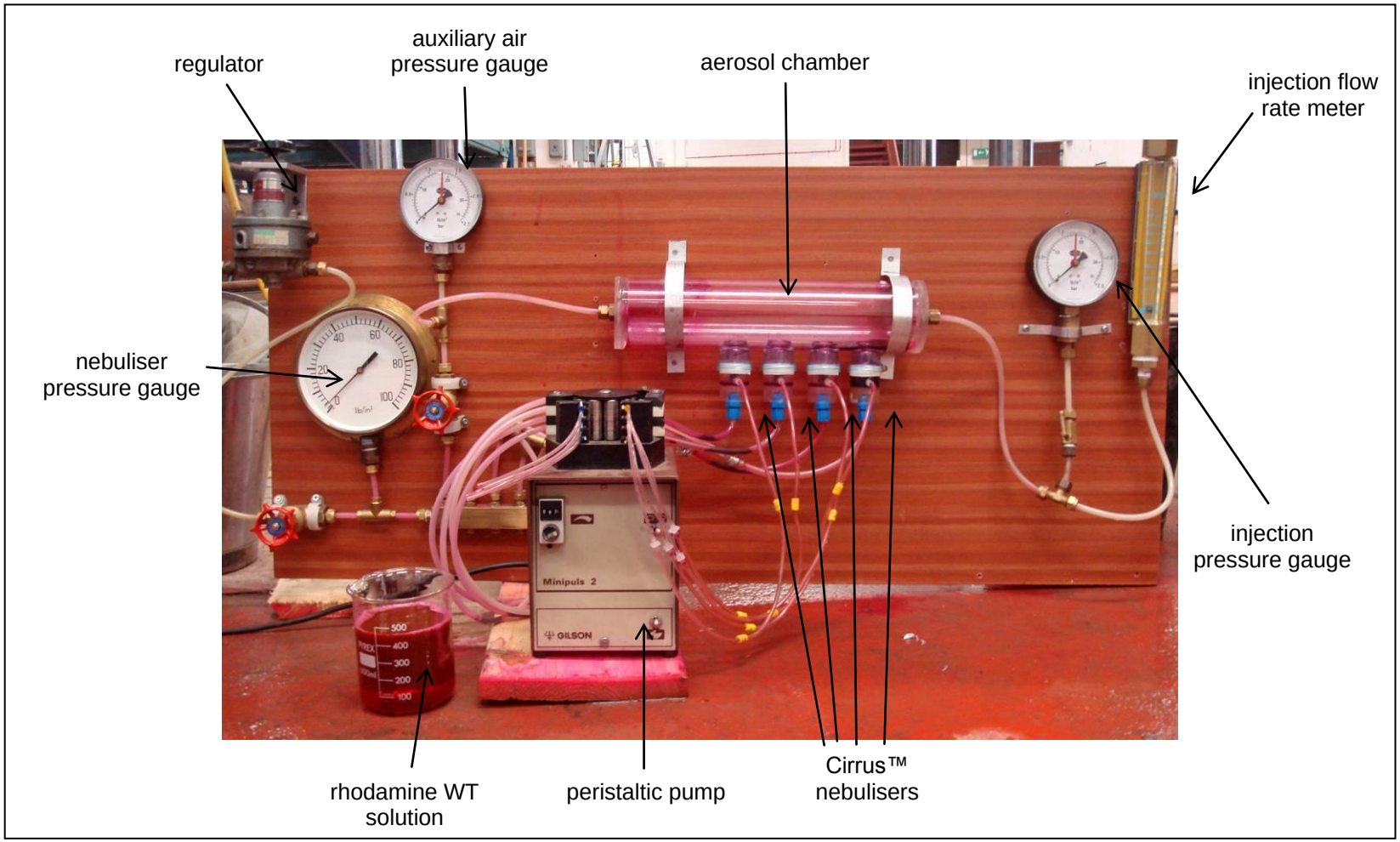

FIGURE 4.13. ATOMISED RHODAMINE WATER TRACER INJECTION SYSTEM SETUP.

An injection filter was constructed from 25mm diameter PVC tubing. 4mm holes were drilled at a vertical spacing of 15mm and a lateral spacing of 15mm. Wire mesh was glued to the exterior of the tube to prevent sand particles from entering the filter. Figure 4.14 illustrates the construction of the injection filter.

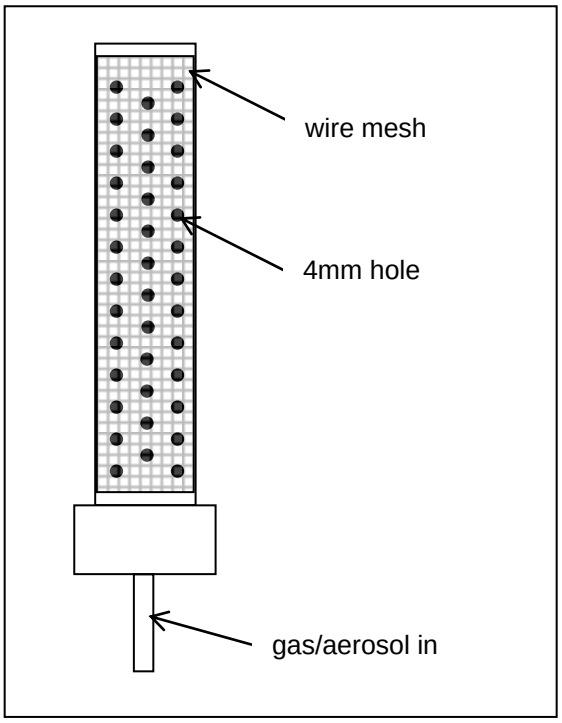

FIGURE 4.14. INJECTION FILTER CONSTRUCTION.

The injection pressure was limited by the construction of the Cirrus™ nebulisers and the necessity of not allowing the soil in the column to fluidise during injection. Under field conditions it is likely that injection pressures would have to be raised to overcome hydrostatic pressure at depth. It is therefore likely that the injection system would have o be made more robust to cope with this anticipated increase in pressure.

As the anticipated volume of injected RWT was relatively small, in the region of 100-200ml, it was decided that the total injection period was to be five hours. It was hoped that this would allow for reliable levels of rhodamine WT to be detected in all sample ports if the injection was successful. Although this duration of constant injection would

be unlikely in the field, due to the danger of volatilising contaminant and transporting it to the surface, the testing programme was attempting to establish the distribution of atomised substrates under steady-state conditions. In addition to constant injection, pulsed injection of the atomised RWT was also investigated to analyse the benefits of such an injection regime. In the same way as medium-scale tests, the injection period for pulsed injection was 15 minutes followed by 5 minutes cessation.

Injection of the tracer dye was initiated by opening the compressed air valve to the injection system. During the minute of injection the water level in the tank rose by approximately 10cm due to air entering the base of the column. The displaced water was collected using a number of buckets. The collected water was weighed so that the total volume of displaced water could be measured. This gave an indication of the maximum size of the air plume in the column.

The airflow through the nebulisers was sufficient to displace the pore water in the column. After approximately 5 seconds, air bubbles could be seen at the top of the column as shown in Figure 4.15.

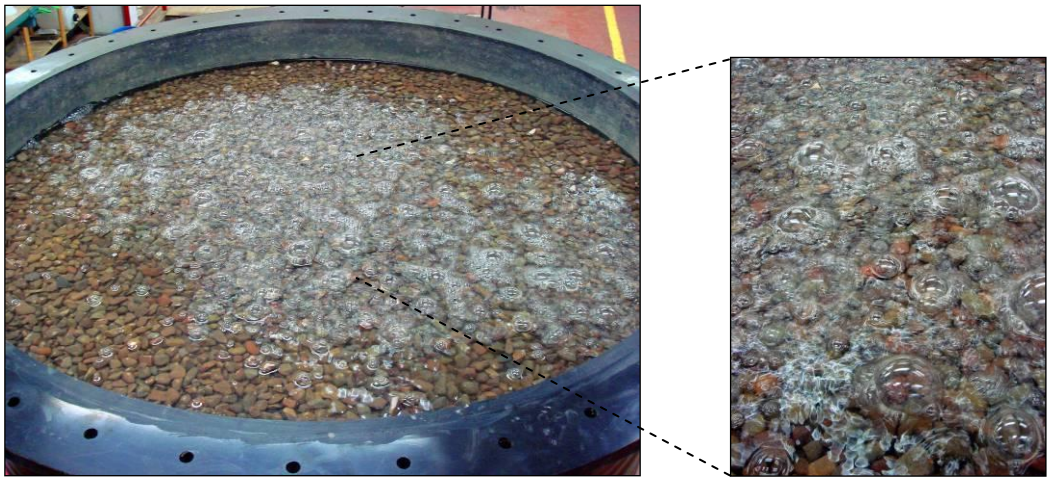

FIGURE 4.15. BUBBLES FROM AIR SPARGING ON SURFACE OF SAMPLE.

The bubbles were an indication that air was successfully overcoming hydrostatic pressure and displacing pore water in the column. After a period of five minutes the water level fell below the top layer of gravel so that air bubbles could no longer be seen. A steady reading on the pressure gauges and flow meters indicated that airflow through the column remained constant.

4.4.2. *Sampling of injected Rhodamine WT*

In order to quantify both the vertical and lateral distribution of the aerosol in the column a five level sampling array was designed with each level consisting of 4 sample ports that would protrude 0mm, 200mm, 400mm and 600mm respectively from the inside wall into the tank. This allowed for sampling from the centre of the column out to the no flow boundary. The sample ports were positioned so that the array was rotated through 90° at each consecutive level, as seen from the top of the column. This ensured that the location of the sample ports, particularly those of 0, 200 and 400mm length varied in the soil mass to compensate for any heterogeneities inside the column. The positions of the sample ports are illustrated in Figure 4.16 in plan view.

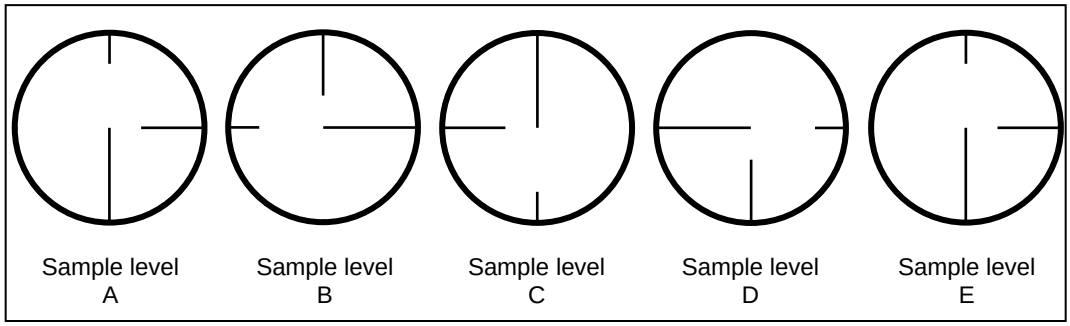

FIGURE 4.16. LOCATION OF SAMPLING PORTS AT LEVELS A, B, C, D AND E AS SEEN IN PLAN VIEW.

Each sample port consisted of a 13mm diameter Perspex pipe with a septum glued to the end. Each length of pipe was sheathed with 12.5mm PVC reinforced hosepipe to increase strength and resist crushing by the sand. The sampling pipes were fixed into the column in pre-drilled holes and glued with Araldite. The pipes were supported using

clamps during gluing however once in place no support was given to the pipes as this may have led to preferential pathways being created in the sand column.

Samples were taken from the ports by inserting a long needle down the internal pipes and piercing the septum at the end. Pore water was then removed by the column using a 10ml syringe. Figure 4.17 shows a pore water sample being taken using the syringe. The samples were then transferred directly to numbered curvettes for sampling using the fluorometer.

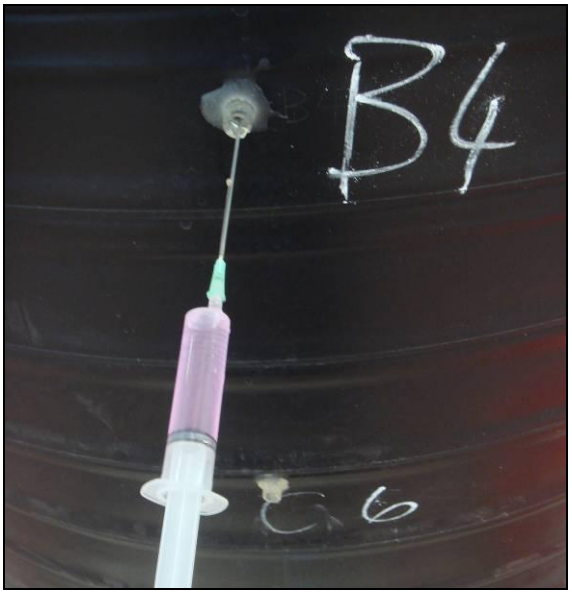

FIGURE 4.17. PORE WATER SAMPLING USING SYRINGE.

After a test was completed it was necessary to return the column to steady state before another injection period was commenced. To this end it was necessary to return the pore water to a state where no rhodamine WT could be detected. To achieve this an overflow pipe was situated at the top of the column to allow water to be flushed through the sand matrix. Flushing was carried out after each test, over a period of 24 hours to ensure that all RWT had been removed from the saturated medium. The Aquafluor portable fluorometer was used to analyse the flushed water as it flowed from the overflow pipe to estimate the relative RWT concentration in the column. When the concentration ceased

to drop further it was deemed that additional flushing would have no further impact and was therefore stopped. Although it was never possible to *exactly* replicate initial conditions for each test, the results are presented as the *difference* between initial concentration and final concentration so it was deemed that slight variations in initial concentrations were tolerable and would not effect overall conclusions.

CHAPTER 5. DROPLET SIZE DISTRIBUTION RESULTS

5.1 *Chapter Synopsis*

The following chapter presents the results from the droplet size distribution experiments carried out with a Malvern Mastersizer S as described in Chapter 4.2. The purpose of the experiments was to ascertain the feasibility of transporting carbon substrates, atomised by medical jet nebulisers, through small columns of granular material. Initial experiments used ballotini of constant diameter as a substitute for granular soil. Further experiments used fine gravel and coarse sand.

5.2. *Presentation of Results*

An initial series of column tests were carried as detailed in Tables 5.1 and 5.2. The term "field condition" refers to the maximum moisture content for soil in the vadose zone. The results show the distribution of droplet sizes for two types of carbon substrates, namely methanol and ethyl lactate, transported through a columns filled with single size ballotini, fine gravel or coarse sand according to BS5930. The results are presented with the droplet diameter plotted on the *x*-axis. A logarithmic scale is used due to the range of droplet sizes measured. A primary *y*-axis is used to plot the percentage of total droplets by volume in each size class, as recorded by the Mastersizer S. A secondary *y*-axis on the right hand side of the diagrams shows the cumulative percentage volume of droplets recorded by the Mastersizer S. In addition to a graphical representation, important mean diameters and representative diameters, as well as two measures of droplet size dispersion are tabulated. Each table lists $d_{0.1}$, $d_{0.5}$, $d_{0.9}$, and d_{32}, as defined in Chapter 3.9.3. The data are presented in Figures 5.1 to 5.44 and are listed in Tables 5.1, 5.2 and 5.3. The results demonstrate the feasibility of transporting atomised droplets of ethyl lactate and methanol of between 0.5 to 3.0μm through dry and fully wetted samples of gravel and sand size particles of soil and uniform diameter ballotini. The results bode

well for the use of medical nebulisers to transport similar size droplets of liquid chemicals or for that matter bacterium through the vadose zone.

5.3. *Droplet Size Distribution Results*

TABLE 5.1. DROPLET SIZE MEASUREMENT TESTS PERFORMED IN AIR WITH MICROCIRRUS™ AND CIRRUS™ NEBULISERS.

Figure No	Carbon Substrate	Medium	Condition	Nebuliser
5.1	Methanol	Air	n/a	Microcirrus
5.2	Ethyl Lactate	Air	n/a	Microcirrus
5.3	Methanol	Air	n/a	Cirrus
5.4	Ethyl Lactate	Air	n/a	Cirrus

TABLE 5.2. DROPLET SIZE MEASUREMENT TESTS PERFORMED THROUGH BALLOTINI WITH MICROCIRRUS™ AND CIRRUS™ NEBULISERS.

Figure No	Carbon Substrate	Medium	Condition	Nebuliser
5.5	Ethyl Lactate	4mm Ballotini	Dry	Microcirrus
5.6	Ethyl Lactate	4mm Ballotini	Field Condition	Microcirrus
5.7	Ethyl Lactate	3mm Ballotini	Dry	Microcirrus
5.8	Ethyl Lactate	3mm Ballotini	Field Condition	Microcirrus
5.9	Ethyl Lactate	2mm Ballotini	Dry	Microcirrus
5.10	Ethyl Lactate	2mm Ballotini	Field Condition	Microcirrus
5.11	Methanol	4mm Ballotini	Dry	Cirrus
5.12	Methanol	4mm Ballotini	Field Condition	Cirrus
5.13	Methanol	3mm Ballotini	Dry	Cirrus
5.14	Methanol	3mm Ballotini	Field Condition	Cirrus
5.15	Methanol	2mm Ballotini	Dry	Cirrus
5.16	Methanol	2mm Ballotini	Field Condition	Cirrus
5.17	Methanol	4mm Ballotini	Dry	Microcirrus
5.18	Methanol	4mm Ballotini	Field Condition	Microcirrus
5.19	Methanol	3mm Ballotini	Dry	Microcirrus
5.20	Methanol	3mm Ballotini	Field Condition	Microcirrus
5.21	Methanol	2mm Ballotini	Dry	Microcirrus
5.22	Methanol	2mm Ballotini	Field Condition	Microcirrus
5.23	Ethyl Lactate	4mm Ballotini	Dry	Cirrus
5.24	Ethyl Lactate	4mm Ballotini	Field Condition	Cirrus
5.25	Ethyl Lactate	3mm Ballotini	Dry	Cirrus
5.26	Ethyl Lactate	3mm Ballotini	Field Condition	Cirrus
5.27	Ethyl Lactate	2mm Ballotini	Dry	Cirrus
5.28	Ethyl Lactate	2mm Ballotini	Field Condition	Cirrus

TABLE 5.3. DROPLET SIZE MEASUREMENT TESTS PERFORMED THROUGH FINE GRAVEL AND COARSE SAND WITH MICROCIRRUS™ AND CIRRUS™ NEBULISERS.

Figure No	*Carbon Substrate*	*Granular Material*	*Condition*	*Nebuliser*
5.29	Methanol	Fine Gravel	Dry	Microcirrus
5.30	Methanol	Fine Gravel	Field Condition	Microcirrus
5.31	Methanol	Coarse Sand	Dry	Microcirrus
5.32	Methanol	Coarse Sand	Field Condition	Microcirrus
5.33	Ethyl Lactate	Fine Gravel	Dry	Microcirrus
5.34	Ethyl Lactate	Fine Gravel	Field Condition	Microcirrus
5.35	Ethyl Lactate	Coarse Sand	Dry	Microcirrus
5.36	Ethyl Lactate	Coarse Sand	Field Condition	Microcirrus
5.37	Methanol	Fine Gravel	Dry	Cirrus
5.38	Methanol	Fine Gravel	Field Condition	Cirrus
5.39	Methanol	Coarse Sand	Dry	Cirrus
5.40	Methanol	Coarse Sand	Field Condition	Cirrus
5.41	Ethyl Lactate	Fine Gravel	Dry	Cirrus
5.42	Ethyl Lactate	Fine Gravel	Field Condition	Cirrus
5.43	Ethyl Lactate	Coarse Sand	Dry	Cirrus
5.44	Ethyl Lactate	Coarse Sand	Field Condition	Cirrus

5.3.1. *Droplet Size Distribution Released to Atmosphere*

A number of comparisons can be made about the atomisation and transportation of droplets from the two medical jet nebulisers, Microcirrus™ and Cirrus™ in different media. The simplest comparison is the range of droplet sizes using the parameters $d_{0.1}$, (the diameter at which 10% of the total volume of the spray is below), $d_{0.5}$, (the diameter at which 50% of the total volume of the spray is below), $d_{0.9}$, (the diameter at which 90% of the total volume of the spray is below).

Figure 5.1 shows a comparison of droplet sizes released by the Microcirrus™ and Cirrus™ nebulisers to atmosphere and confirms that finer droplets were produced by Microcirrus™ nebuliser. Figures 5.2 to 5.5 show that the droplet sizes produced by Microcirrus™ nebuliser varied from 0.62 to 1.85µm; whereas the droplet size produced by Cirrus™ nebuliser varied from 0.72 to 4.75µm for $d_{0.1}$ and $d_{0.9}$ respectively. Furthermore the figures show that atomisation of ethyl lactate produced a marginally finer droplet distribution than for methanol, however the $d_{0.1}$ size is equivalent. The most

significant difference in droplet size is the type of nebuliser and not the substrate with the Microcirrus™ nebuliser producing the finer droplet size distribution.

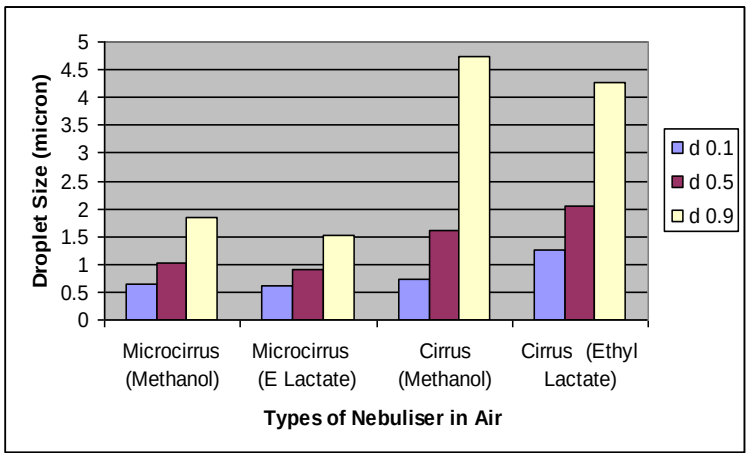

FIGURE 5.1. COMPARISON OF DROPLET SIZE DISTRIBUTION FOR ATOMISED OF ETHYL LACTATE AND METHANOL IN AIR.

Figures 5.2 to 5.5 present the droplet size distribution of atomised methanol and ethyl lactate released to atmosphere by the Cirrus™ and Microcirrus™ nebuliser.

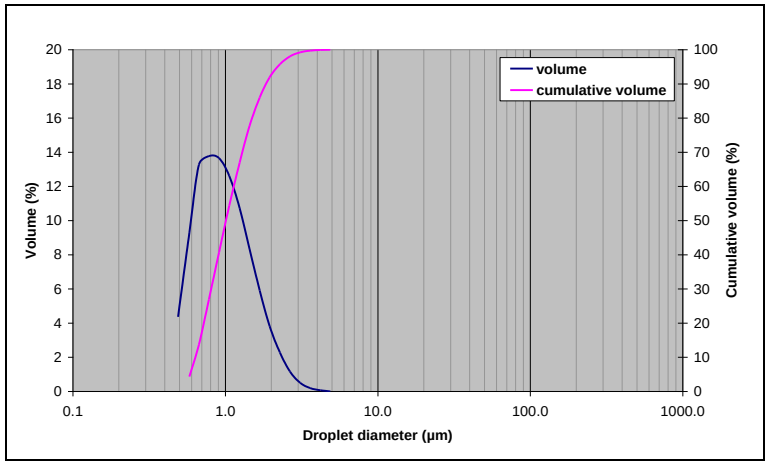

Parameter	*Value*
$d_{0.1}$	0.64
$d_{0.5}$	1.01
$d_{0.9}$	1.85
d_{32}	0.97
Δ	1.196
UI	0.379

FIGURE 5.2. DROPLET SIZE AND CUMULATIVE DROPLET SIZE DISTRIBUTION OF ATOMISED METHANOL RELEASED TO ATMOSPHERE BY THE MICROCIRRUS™ NEBULISER.

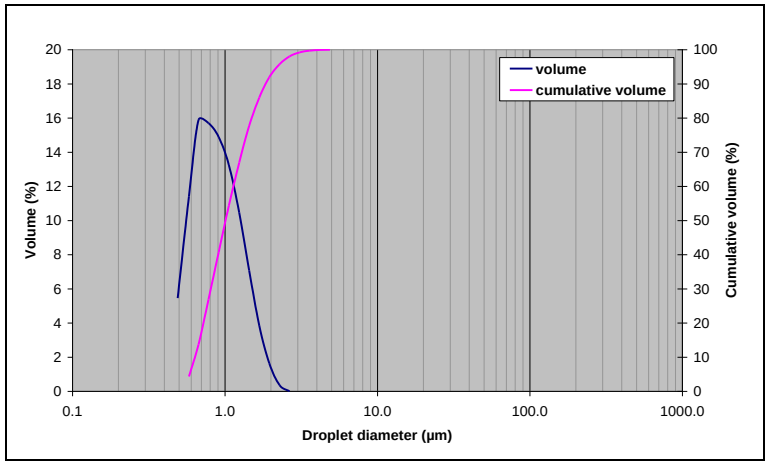

Parameter	*Value*
$d_{0.1}$	0.62
$d_{0.5}$	0.92
$d_{0.9}$	1.52
d_{32}	0.90
Δ	0.975
UI	0.308

FIGURE 5.3 DROPLET SIZE AND CUMULATIVE DROPLET SIZE DISTRIBUTION OF ATOMISED ETHYL LACTATE RELEASED TO ATMOSPHERE BY THE MICROCIRRUS™ NEBULISER.

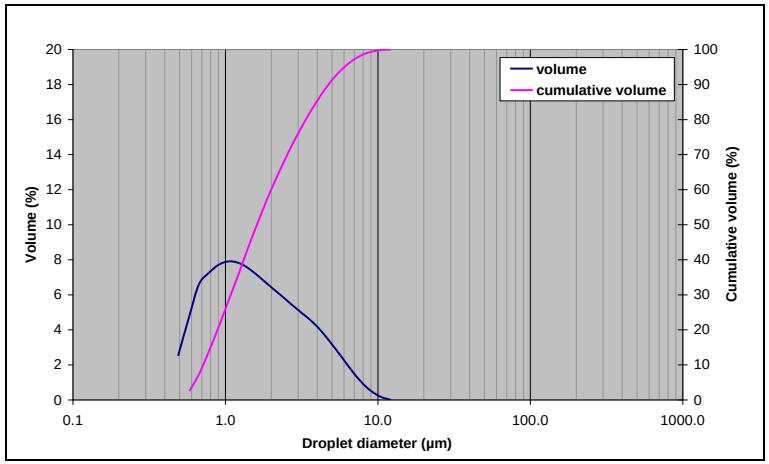

Parameter	*Value*
$d_{0.1}$	0.72
$d_{0.5}$	1.61
$d_{0.9}$	4.75
d_{32}	1.39
Δ	2.510
UI	0.768

FIGURE 5.4. DROPLET SIZE AND CUMULATIVE DROPLET SIZE DISTRIBUTION OF ATOMISED METHANOL RELEASED TO ATMOSPHERE BY THE CIRRUS™ NEBULISER.

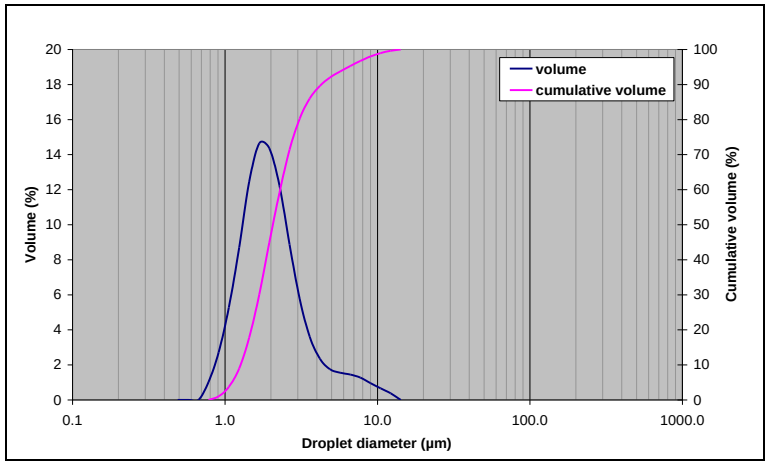

Parameter	*Value*
$d_{0.1}$	1.26
$d_{0.5}$	2.06
$d_{0.9}$	4.28
d_{32}	1.98
Δ	1.465
UI	0.498

FIGURE 5.5. DROPLET SIZE AND CUMULATIVE DROPLET SIZE DISTRIBUTION OF ATOMISED ETHYL LACTATE RELEASED TO ATMOSPHERE BY THE CIRRUS™ NEBULISER.

5.3.2. *Droplet Size Distribution following Transportation through Ballotini*

Following the comparison of droplet size distribution in air, it is interesting to examine the droplet size distributions measured for transportation through different sizes of ballotini when dry and when wetted to field condition. The results for the transportation of atomised methanol and ethyl lactate transported through ballotini are summarised in Figure 5.6. There are number of features that can be identified from Figure 5.6 in particular:

1. the $d_{0.9}$ value for droplets released to atmosphere is noticeably smaller when compared with atomised substrate transported through 3mm and 4mm ballotini, especially for ethyl lactate atomised by the Microcirrus nebuliser as shown in Figures 5.7, 5.8, 5.9 and 5.11. This phenomenon could indicate that the droplets collided when transported through the ballotini to coalesce and become larger;

2. in contrast the $d_{0.1}$ size appears to be fairly consistent when released to atmosphere and when transported through dry or wetted ballotini as supported by Figures 5.7 to 5.30;

3. wetting the ballotini to field capacity did not appear to have a consistent affect on droplet size distribution. In general the droplet size distributions of transported spray through these media do not appear significantly different if water is introduced into the medium. An exception is the transportation of methanol droplets through wetted 4mm ballotini where the $d_{0.9}$ size reduced markedly from 3.03 to 1.69µm as shown in Figures 5.19 and 5.20. In addition the $d_{0.9}$ size measured for transportation of methanol droplets through 2mm dry ballotini is noticeably low compared to similar measurements for transportation of atomised ethyl lactate through similar size ballotini.

These observations suggest that the main consequence of transporting atomised carbon substrate droplets through a coarse porous media is for droplets to coalesce into large size droplets and hence increase the $d_{0.9}$ size. Fully wetting the ballotini did not appear to significantly change the droplet size distribution except in one case (4mm, field ballotini). The results appear to confirm the feasibility of transporting a droplet size of 0.5 to 3.0µm through the pore spaces of coarse-grained sand.

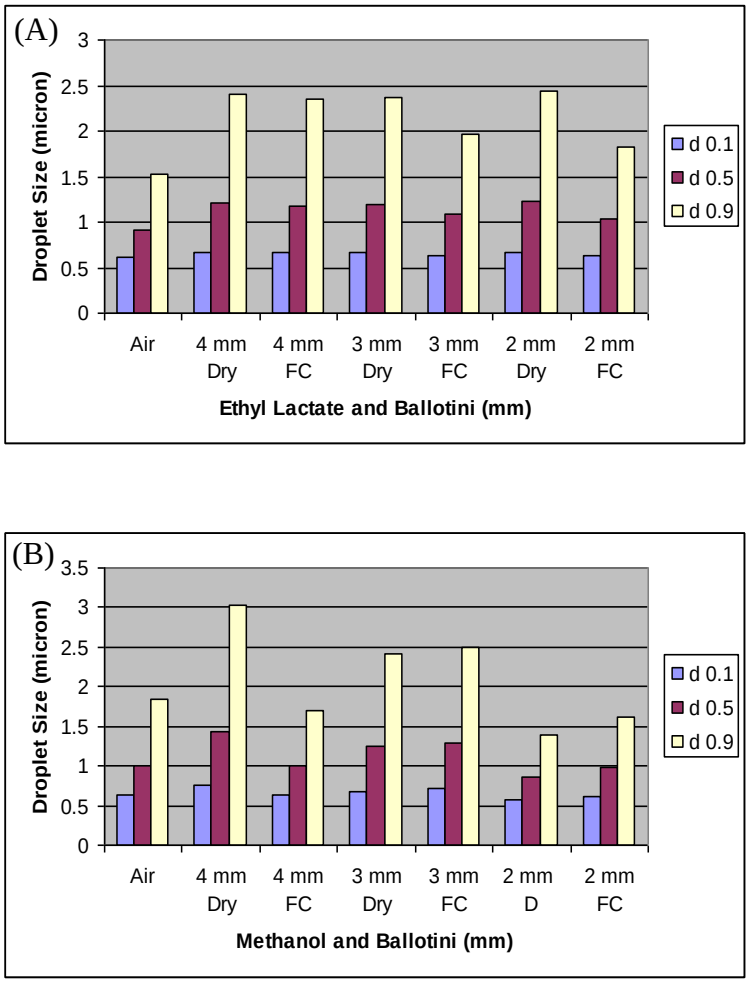

FIGURE 5.6. COMPARISON OF DROPLET SIZE DISTRIBUTION FOR TRANSPORTATION OF ATOMISED CARBON SUBSTRATE (A) ETHYL LACTATE (B) METHANOL WITH MICROCIRRUS™ THROUGH DRY (D) AND FIELD SATURATED CONDITION (FC) BALLOTINI.

Figures 5.7 to 5.30 present the droplet size distribution of atomised methanol and ethyl lactate released by the Cirrus™ and Microcirrus™ nebuliser and transported through ballotini under dry and field capacity conditions.

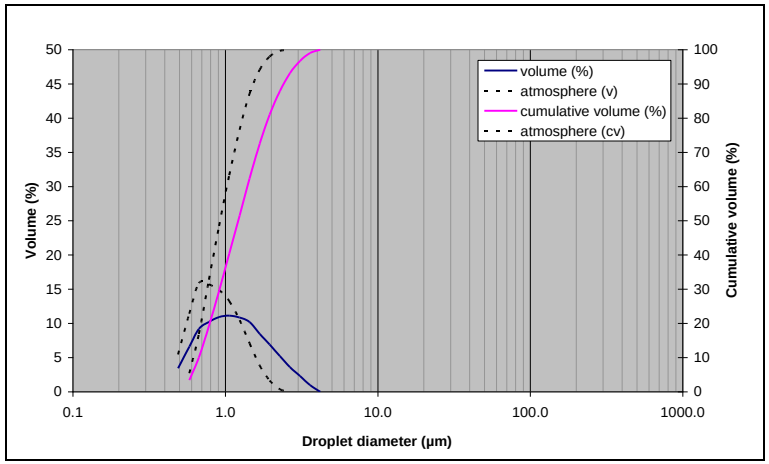

Parameter	Value
$d_{0.1}$	0.67
$d_{0.5}$	1.21
$d_{0.9}$	2.40
d_{32}	1.12
Δ	1.433
UI	0.444

FIGURE 5.7. DROPLET SIZE AND CUMULATIVE DROPLET SIZE DISTRIBUTION OF ATOMISED ETHYL LACTATE TRANSPORTED THROUGH 4MM BALLOTINI BY THE MICROCIRRUS™ NEBULISER UNDER DRY CONDITIONS.

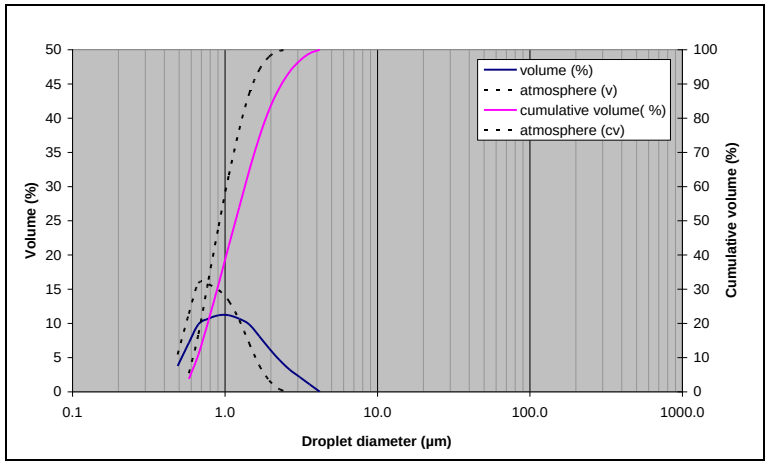

Parameter	Value
$d_{0.1}$	0.66
$d_{0.5}$	1.17
$d_{0.9}$	2.35
d_{32}	1.09
Δ	1.446
UI	0.447

FIGURE 5.8. DROPLET SIZE AND CUMULATIVE DROPLET SIZE DISTRIBUTION OF ATOMISED ETHYL LACTATE TRANSPORTED THROUGH 4MM BALLOTINI BY THE MICROCIRRUS™ NEBULISER UNDER FIELD CAPACITY CONDITIONS.

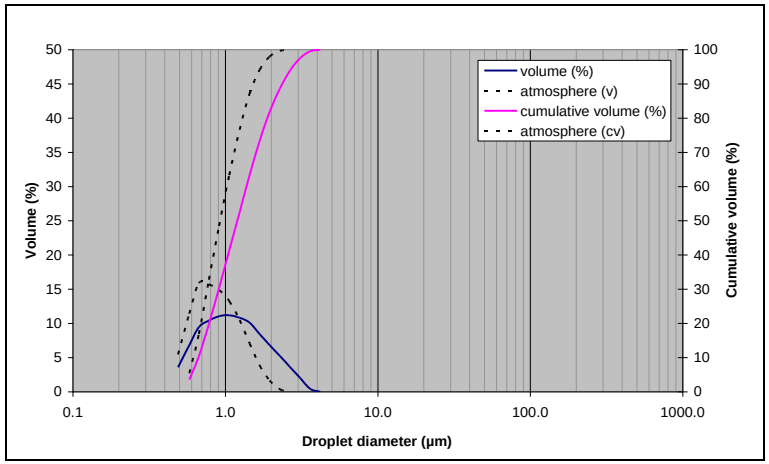

Parameter	Value
$d_{0.1}$	0.67
$d_{0.5}$	1.19
$d_{0.9}$	2.36
d_{32}	1.10
Δ	1.417
UI	0.436

FIGURE 5.9. DROPLET SIZE AND CUMULATIVE DROPLET SIZE DISTRIBUTION OF ATOMISED ETHYL LACTATE TRANSPORTED THROUGH 3MM BALLOTINI BY THE MICROCIRRUS™ NEBULISER UNDER DRY CONDITIONS.

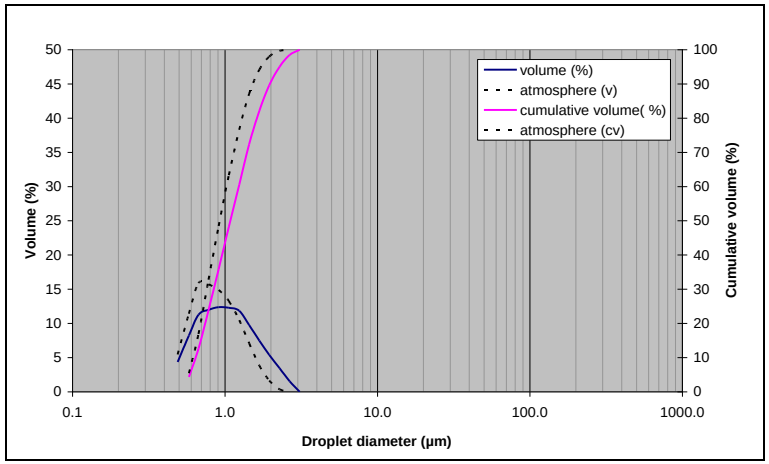

Parameter	Value
$d_{0.1}$	0.64
$d_{0.5}$	1.08
$d_{0.9}$	1.97
d_{32}	1.02
Δ	1.226
UI	0.379

FIGURE 5.10. DROPLET SIZE AND CUMULATIVE DROPLET SIZE DISTRIBUTION OF ATOMISED ETHYL LACTATE TRANSPORTED THROUGH 3MM BALLOTINI BY THE MICROCIRRUS™ NEBULISER UNDER FIELD CAPACITY SATURATION CONDITIONS.

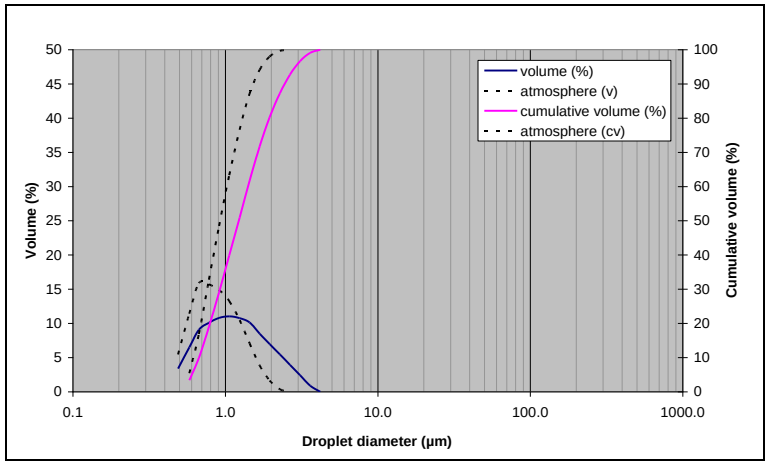

Parameter	Value
$d_{0.1}$	0.67
$d_{0.5}$	1.22
$d_{0.9}$	2.44
d_{32}	1.12
Δ	1.453
UI	0.447

FIGURE 5.11. DROPLET SIZE AND CUMULATIVE DROPLET SIZE DISTRIBUTION OF ATOMISED ETHYL LACTATE TRANSPORTED THROUGH 2MM BALLOTINI BY THE MICROCIRRUS™ NEBULISER UNDER DRY CONDITIONS.

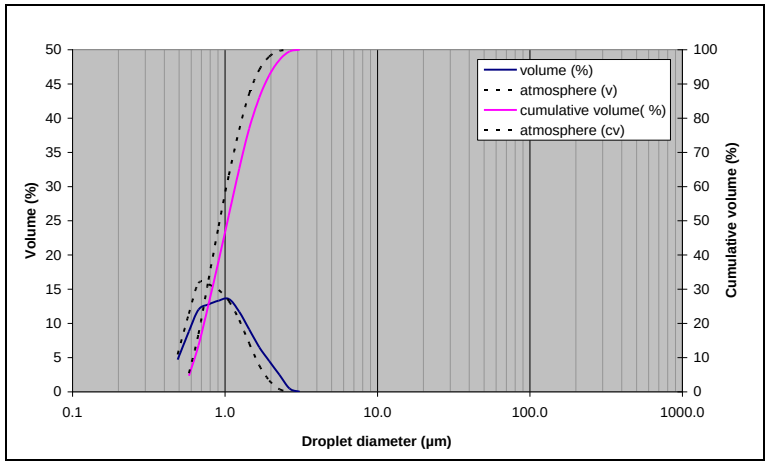

Parameter	Value
$d_{0.1}$	0.64
$d_{0.5}$	1.04
$d_{0.9}$	1.83
d_{32}	0.98
Δ	1.144
UI	0.354

FIGURE 5.12. DROPLET SIZE AND CUMULATIVE DROPLET SIZE DISTRIBUTION OF ATOMISED ETHYL LACTATE TRANSPORTED THROUGH 2MM BALLOTINI BY THE MICROCIRRUS™ NEBULISER UNDER FIELD CAPACITY SATURATION CONDITIONS.

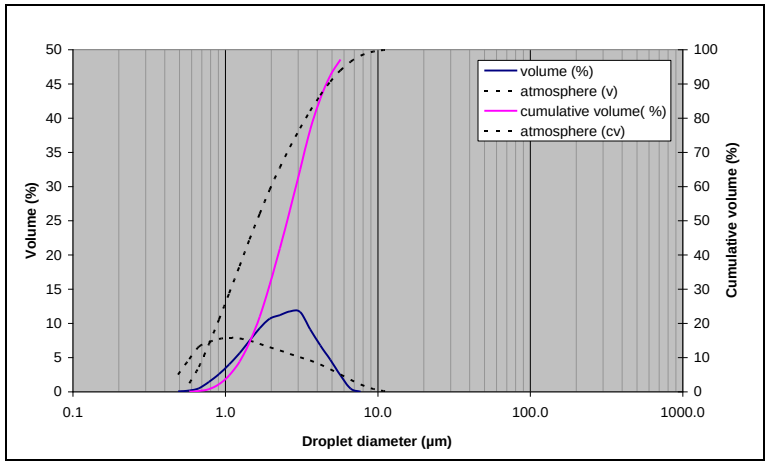

Parameter	*Value*
$d_{0.1}$	1.28
$d_{0.5}$	2.54
$d_{0.9}$	4.60
d_{32}	2.19
Δ	1.304
UI	0.403

FIGURE 5.13 DROPLET SIZE AND CUMULATIVE DROPLET SIZE DISTRIBUTION OF ATOMISED METHANOL TRANSPORTED THROUGH 4MM BALLOTINI BY THE CIRRUS™ NEBULISER UNDER DRY CONDITIONS.

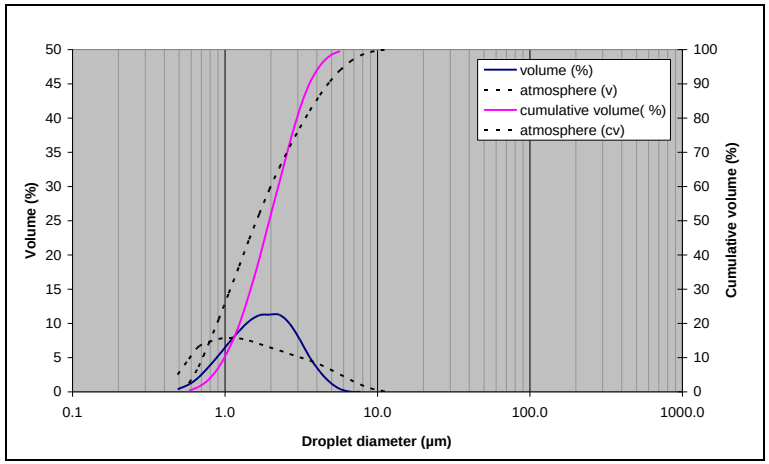

Parameter	*Value*
$d_{0.1}$	0.99
$d_{0.5}$	1.95
$d_{0.9}$	3.58
d_{32}	1.70
Δ	1.326
UI	0.418

FIGURE 5.14. DROPLET SIZE AND CUMULATIVE DROPLET SIZE DISTRIBUTION OF ATOMISED METHANOL TRANSPORTED THROUGH 4MM BALLOTINI BY THE CIRRUS™ NEBULISER UNDER FIELD CAPACITY SATURATION CONDITIONS.

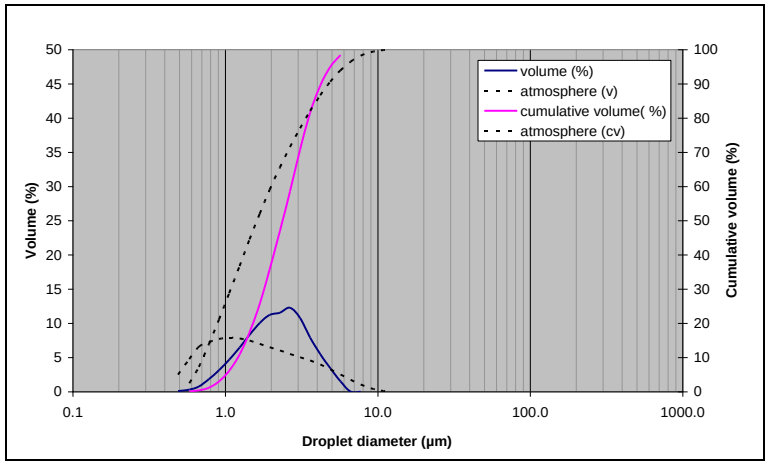

Parameter	Value
$d_{0.1}$	1.20
$d_{0.5}$	2.37
$d_{0.9}$	4.24
d_{32}	2.57
Δ	1.281
UI	0.397

FIGURE 5.15. DROPLET SIZE AND CUMULATIVE DROPLET SIZE DISTRIBUTION OF ATOMISED METHANOL TRANSPORTED THROUGH 3MM BALLOTINI BY THE CIRRUS™ NEBULISER UNDER DRY CONDITIONS.

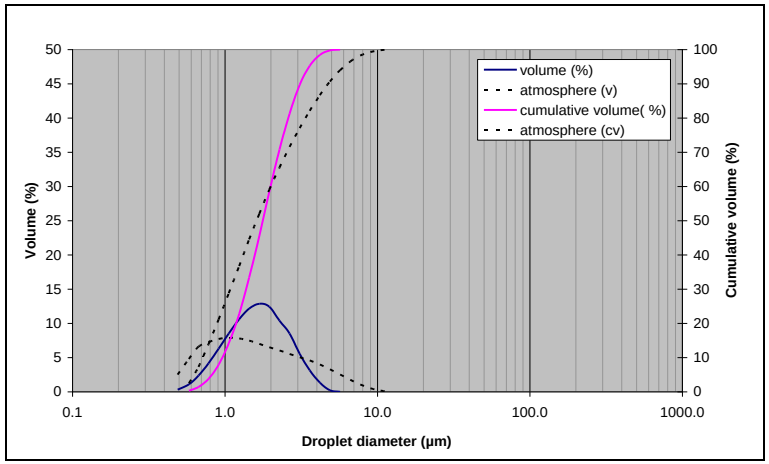

Parameter	Value
$d_{0.1}$	0.96
$d_{0.5}$	1.77
$d_{0.9}$	3.11
d_{32}	1.58
Δ	1.213
UI	0.376

FIGURE 5.16. DROPLET SIZE AND CUMULATIVE DROPLET SIZE DISTRIBUTION OF ATOMISED METHANOL TRANSPORTED THROUGH 3MM BALLOTINI BY THE CIRRUS™ NEBULISER UNDER FIELD CAPACITY SATURATION CONDITIONS.

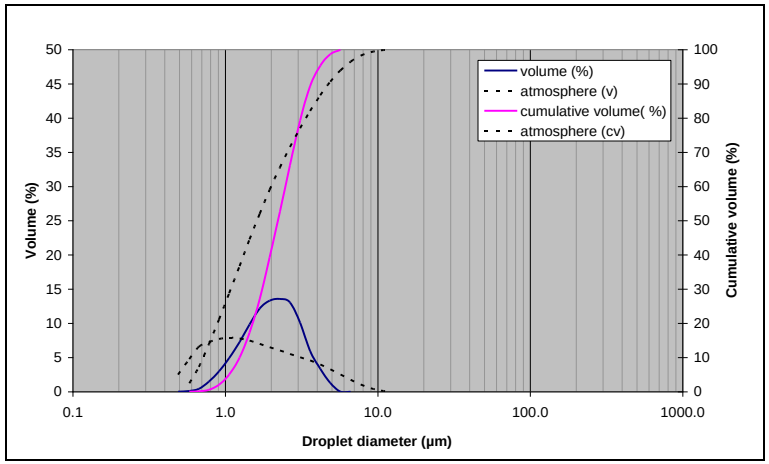

Parameter	*Value*
$d_{0.1}$	1.23
$d_{0.5}$	2.21
$d_{0.9}$	3.64
d_{32}	1.98
Δ	1.091
UI	0.343

FIGURE 5.17. DROPLET SIZE AND CUMULATIVE DROPLET SIZE DISTRIBUTION OF ATOMISED METHANOL TRANSPORTED THROUGH 2MM BALLOTINI BY THE CIRRUS™ NEBULISER UNDER DRY CONDITIONS.

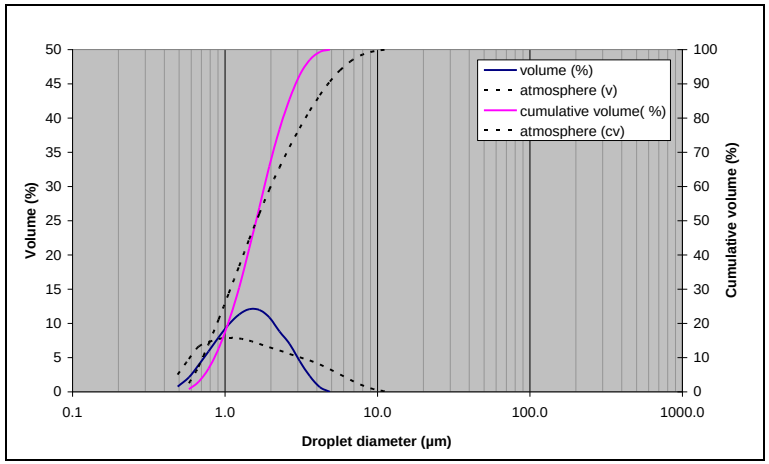

Parameter	*Value*
$d_{0.1}$	0.85
$d_{0.5}$	1.60
$d_{0.9}$	2.91
d_{32}	1.43
Δ	1.285
UI	0.399

FIGURE 5.18. DROPLET SIZE AND CUMULATIVE DROPLET SIZE DISTRIBUTION OF ATOMISED METHANOL TRANSPORTED THROUGH 2MM BALLOTINI BY THE CIRRUS™ NEBULISER UNDER FIELD CAPACITY SATURATION CONDITIONS.

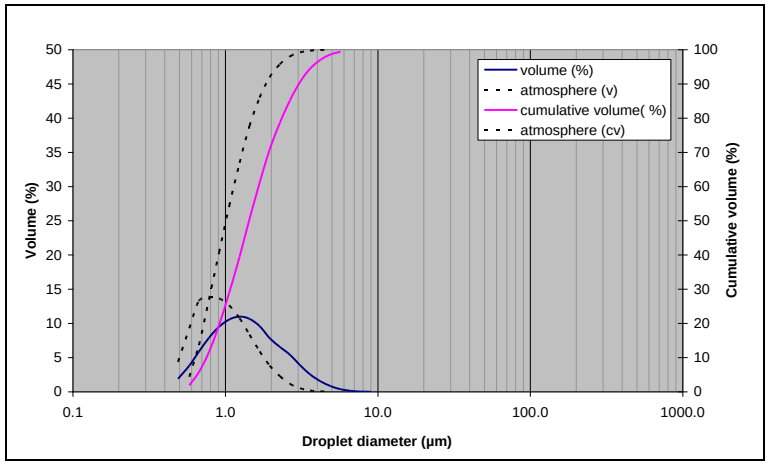

Parameter	*Value*
$d_{0.1}$	0.75
$d_{0.5}$	1.43
$d_{0.9}$	3.03
d_{32}	1.30
Δ	1.595
UI	0.499

FIGURE 5.19. DROPLET SIZE AND CUMULATIVE DROPLET SIZE DISTRIBUTION OF ATOMISED METHANOL TRANSPORTED THROUGH 4MM BALLOTINI BY THE MICROCIRRUS™ NEBULISER UNDER DRY CONDITIONS.

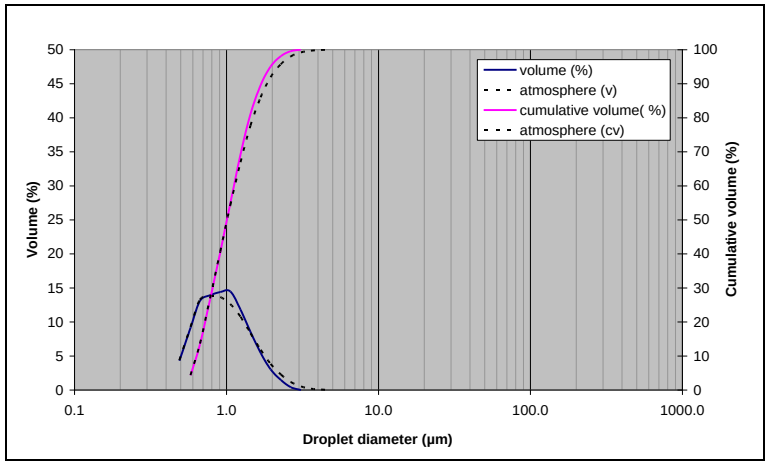

Parameter	*Value*
$d_{0.1}$	0.64
$d_{0.5}$	1.01
$d_{0.9}$	1.69
d_{32}	0.96
Δ	1.043
UI	0.327

FIGURE 5.20. DROPLET SIZE AND CUMULATIVE DROPLET SIZE DISTRIBUTION OF ATOMISED METHANOL TRANSPORTED THROUGH 4MM BALLOTINI BY THE MICROCIRRUS™ NEBULISER UNDER FIELD CAPACITY SATURATION CONDITIONS.

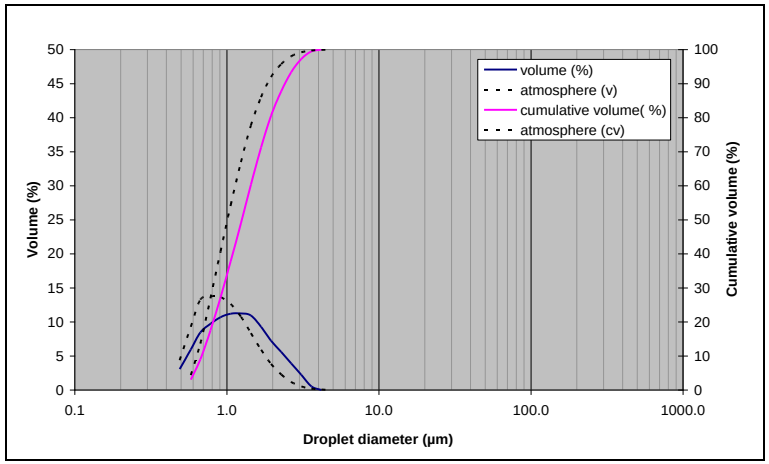

Parameter	Value
$d_{0.1}$	0.68
$d_{0.5}$	1.25
$d_{0.9}$	2.41
d_{32}	1.14
Δ	1.377
UI	0.424

FIGURE 5.21. DROPLET SIZE AND CUMULATIVE DROPLET SIZE DISTRIBUTION OF ATOMISED METHANOL TRANSPORTED THROUGH 3MM BALLOTINI BY THE MICROCIRRUS™ NEBULISER UNDER DRY CONDITIONS.

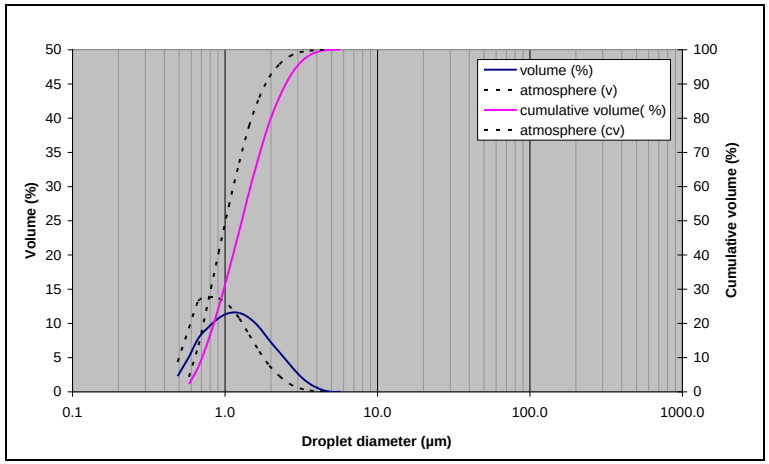

Parameter	Value
$d_{0.1}$	0.71
$d_{0.5}$	1.29
$d_{0.9}$	2.50
d_{32}	1.18
Δ	1.394
UI	0.432

FIGURE 5.22. DROPLET SIZE AND CUMULATIVE DROPLET SIZE DISTRIBUTION OF ATOMISED METHANOL TRANSPORTED THROUGH 3MM BALLOTINI BY THE MICROCIRRUS™ NEBULISER UNDER FIELD CAPACITY SATURATION CONDITIONS.

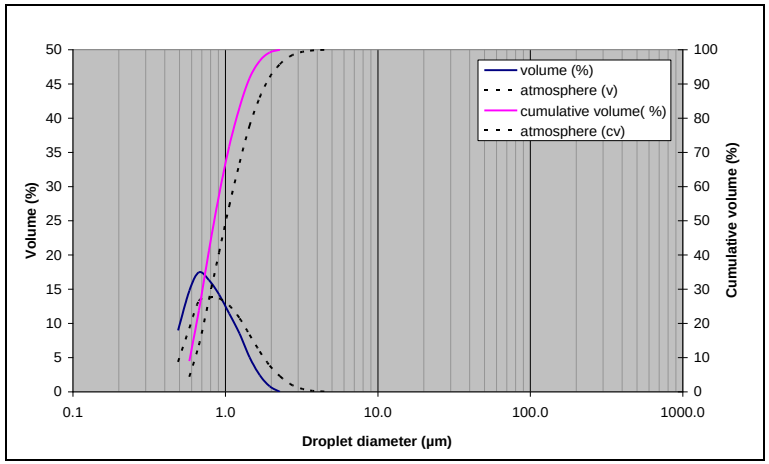

Parameter	*Value*
$d_{0.1}$	0.58
$d_{0.5}$	0.85
$d_{0.9}$	1.39
d_{32}	0.83
Δ	0.951
UI	0.292

FIGURE 5.23. DROPLET SIZE AND CUMULATIVE DROPLET SIZE DISTRIBUTION OF ATOMISED METHANOL TRANSPORTED THROUGH 2MM BALLOTINI BY THE MICROCIRRUS™ NEBULISER UNDER DRY CONDITIONS.

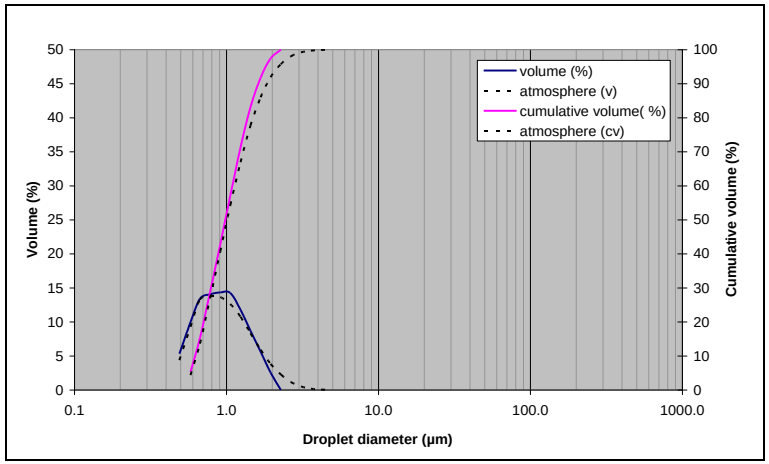

Parameter	*Value*
$d_{0.1}$	0.62
$d_{0.5}$	0.98
$d_{0.9}$	1.62
d_{32}	0.93
Δ	1.008
UI	0.309

FIGURE 5.24. DROPLET SIZE AND CUMULATIVE DROPLET SIZE DISTRIBUTION OF ATOMISED METHANOL TRANSPORTED THROUGH 2MM BALLOTINI BY THE MICROCIRRUS™ NEBULISER UNDER FIELD CAPACITY SATURATION CONDITIONS.

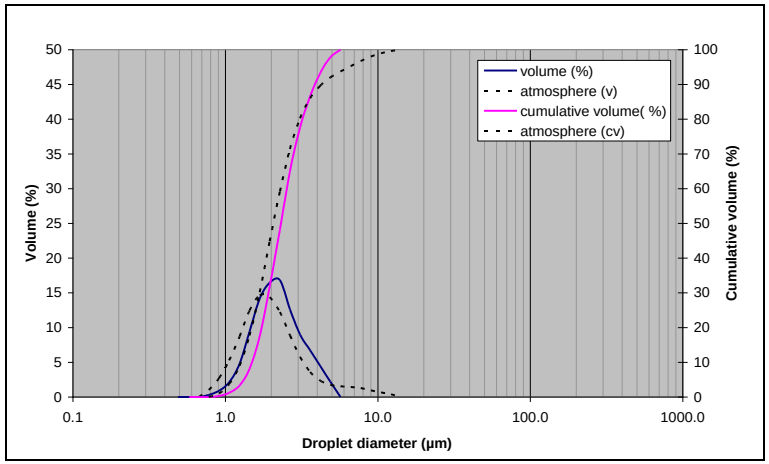

Parameter	Value
$d_{0.1}$	1.49
$d_{0.5}$	2.31
$d_{0.9}$	3.86
d_{32}	2.20
Δ	1.024
UI	0.311

FIGURE 5.25. DROPLET SIZE AND CUMULATIVE DROPLET SIZE DISTRIBUTION OF ATOMISED ETHYL LACTATE TRANSPORTED THROUGH 4MM BALLOTINI BY THE CIRRUS™ NEBULISER UNDER DRY CONDITIONS.

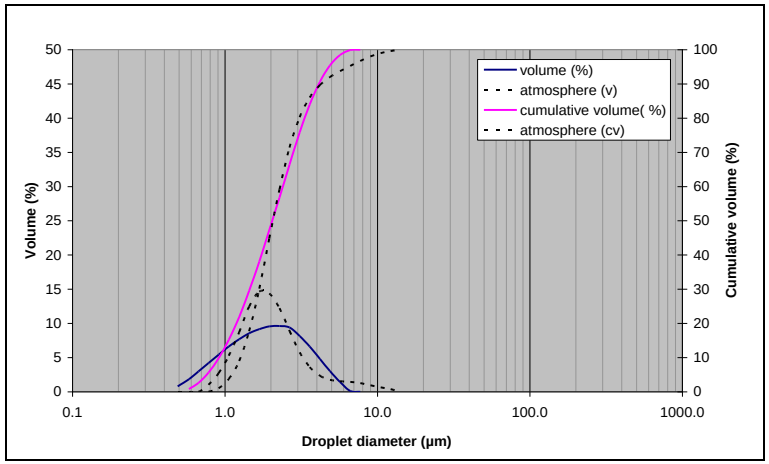

Parameter	Value
$d_{0.1}$	0.92
$d_{0.5}$	2.04
$d_{0.9}$	4.13
d_{32}	1.70
Δ	1.573
UI	0.487

FIGURE 5.26. DROPLET SIZE AND CUMULATIVE DROPLET SIZE DISTRIBUTION OF ATOMISED ETHYL LACTATE TRANSPORTED THROUGH 4MM BALLOTINI BY THE CIRRUS™ NEBULISER UNDER FIELD CAPACITY SATURATION CONDITIONS.

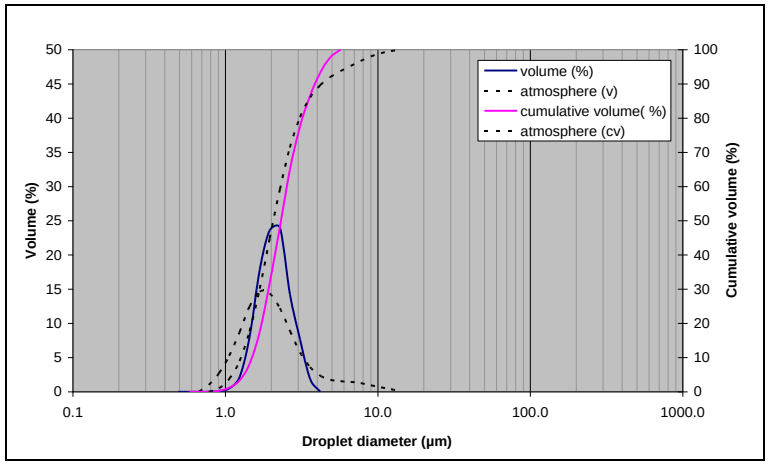

Parameter	*Value*
$d_{0.1}$	1.65
$d_{0.5}$	2.25
$d_{0.9}$	3.07
d_{32}	2.18
Δ	0.629
UI	0.198

FIGURE 5.27. DROPLET SIZE AND CUMULATIVE DROPLET SIZE DISTRIBUTION OF ATOMISED ETHYL LACTATE TRANSPORTED THROUGH 3MM BALLOTINI BY THE CIRRUS™ NEBULISER UNDER DRY CONDITIONS.

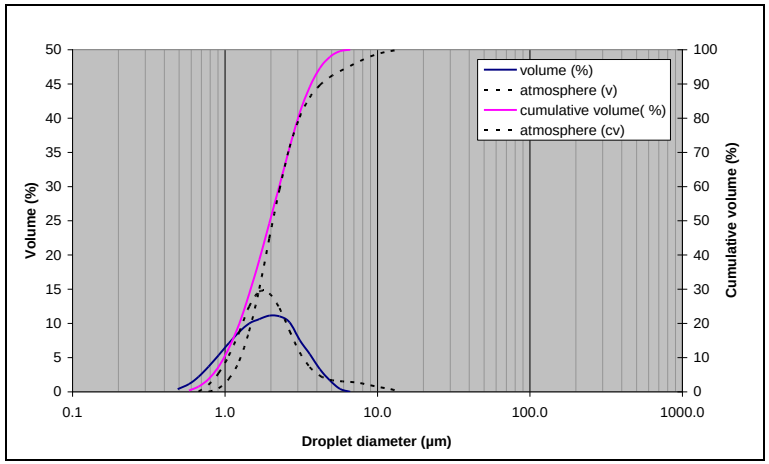

Parameter	*Value*
$d_{0.1}$	0.99
$d_{0.5}$	1.98
$d_{0.9}$	3.68
d_{32}	1.71
Δ	1.362
UI	0.426

FIGURE 5.28. DROPLET SIZE AND CUMULATIVE DROPLET SIZE DISTRIBUTION OF ATOMISED ETHYL LACTATE TRANSPORTED THROUGH 3MM BALLOTINI BY THE CIRRUS™ NEBULISER UNDER DRY CONDITIONS.

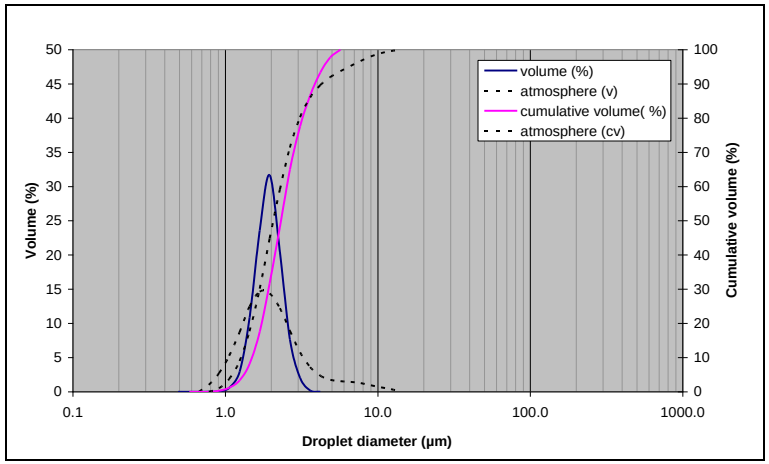

Parameter	Value
$d_{0.1}$	1.59
$d_{0.5}$	2.07
$d_{0.9}$	2.65
d_{32}	2.02
Δ	0.511
UI	0.157

FIGURE 5.29. DROPLET SIZE AND CUMULATIVE DROPLET SIZE DISTRIBUTION OF ATOMISED ETHYL LACTATE TRANSPORTED THROUGH 2MM BALLOTINI BY THE CIRRUS™ NEBULISER UNDER DRY CONDITIONS.

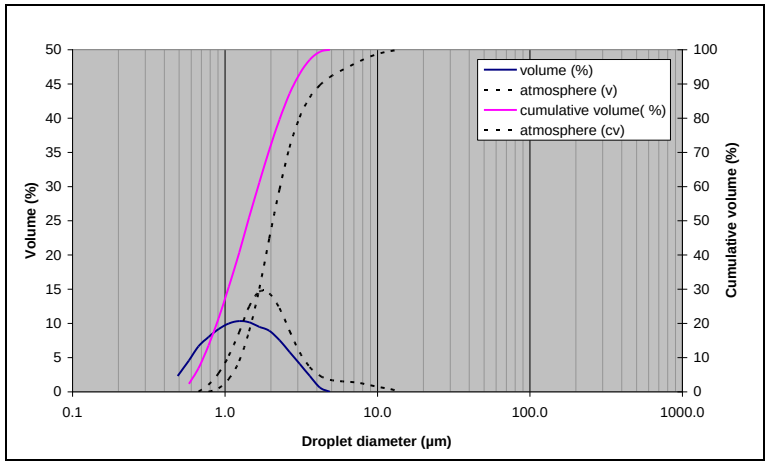

Parameter	Value
$d_{0.1}$	0.72
$d_{0.5}$	1.42
$d_{0.9}$	2.84
d_{32}	1.26
Δ	1.493
UI	0.462

FIGURE 5.30. DROPLET SIZE AND CUMULATIVE DROPLET SIZE DISTRIBUTION OF ATOMISED ETHYL LACTATE TRANSPORTED THROUGH 2MM BALLOTINI BY THE CIRRUS™ NEBULISER UNDER FIELD CAPACITY SATURATION CONDITIONS.

5.3.3. *Droplet size Distribution following Transportation through Fine-grained Gravel and Coarse-grained Sand*

In comparison with the results obtained for transportation through ballotini, the corresponding droplet size distribution measured following transportation of fine droplets of ethyl lactate or methanol released by the Microcirrus™ nebuliser through dry and wetted fine gravel or coarse sand size particles is shown in Figure 5.31. The results again are shown solely for the transportation of droplets released by the Microcirrus™ nebuliser. Several observations can be drawn from the data set compared with the results for ballotini:

1. the wetting of gravel and sand particles generally had the effect of reducing the $d_{0.1}$ $d_{0.5}$ and $d_{0.9}$ sizes for methanol and ethyl lactate, particularity $d_{0.9}$ size in the fine-grained gravel sample as shown in Figures 5.35, 5.39 and 5.43;

2. the $d_{0.9}$ values of substrate atomised by the Microcirrus nebuliser and transported through the fine gravel soil column samples increased when compared with release to atmosphere as supported by Figures 5.34 and 5.38. Similar to the results for ballotini the results would suggest that the porous media had the effect on coalescing the droplets into large droplets sizes;

3. the droplet size distribution appears remarkably similar for droplets of atomised liquids released into air compared with transportation through wetted coarse sand, this might suggest that there was negligible impaction or deposition of droplets on the surface of sand particles however further data would be needed on the volume or weight loss of injected liquid into the sand sample to confirm such a conclusion.

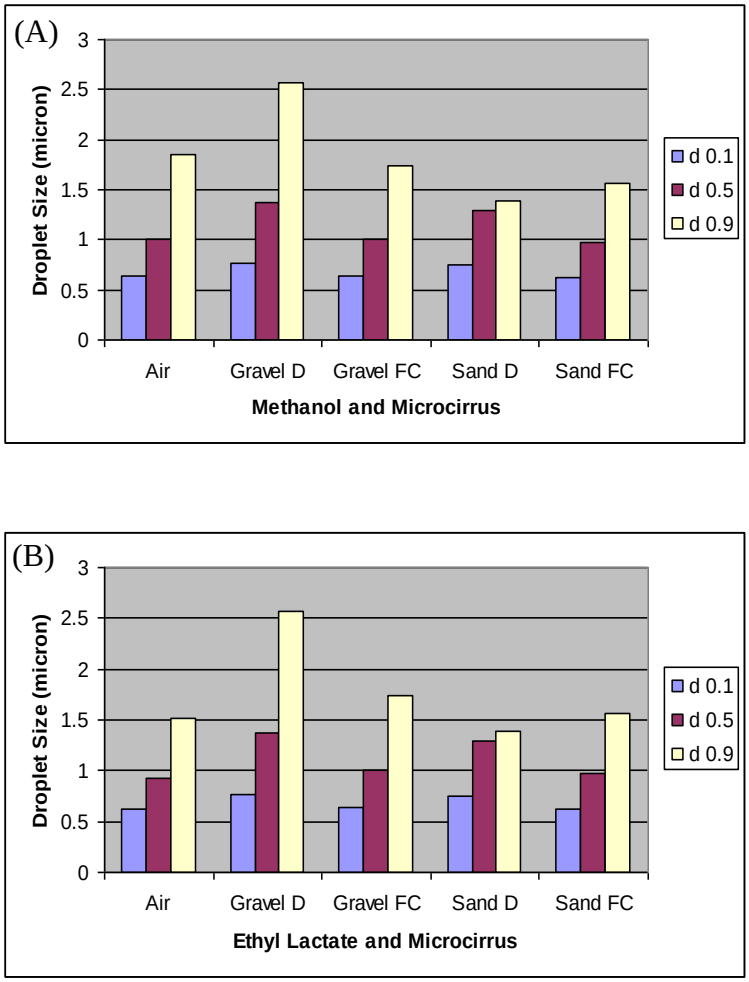

FIGURE 5.31. COMPARISON OF DROPLET SIZE DISTRIBUTION FOR TRANSPORTATION OF ATOMISED CARBON SUBSTRATE (A) ETHYL LACTATE AND (B) METHANOL WITH MICROCIRRUS™ THROUGH DRY (D) OR FIELD CONDITION (FC) FINE-GRAINED GRAVEL AND COARSE-GRAINED SAND.

In comparison with the data reviewed for the transportation of droplets produced by the Microcirrus™ nebuliser, a similar data set for droplets produced by the Cirrus™ nebuliser is shown in Figure 5.32 for transportation though sand and gravel. The most noticeable differences between the two data sets is the marked decrease in $d_{0.9}$ for droplets released by the Cirrus™ nebuliser when transported through gravel and sand compared with direct release to atmosphere. The $d_{0.9}$ diameter reduces from 4.75µm in air for methanol to 1.32µm in fully wetted, coarse-grained sand whereas a less pronounced and consistent decrease in droplet size took place for droplets produced by

the Microcirrus™ nebuliser. In contrast, $d_{0.1}$ barely changes when considering atomised methanol. Importantly, the results suggest that the maximum droplet size for transportation through coarse-grained sand is approximately 2.5µm.

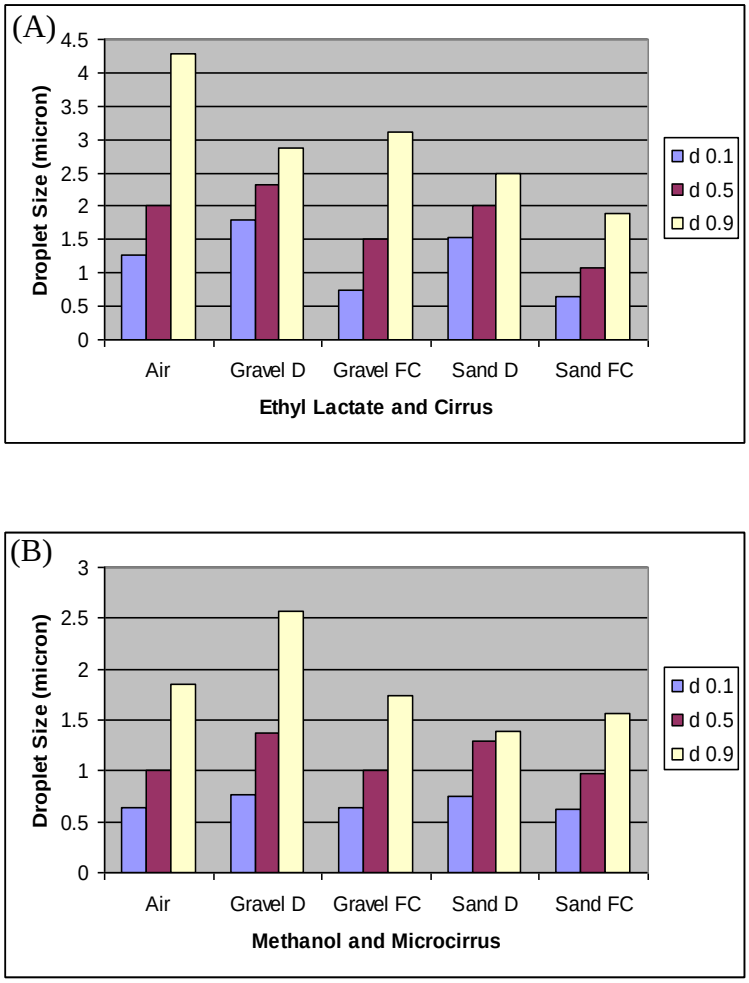

FIGURE 5.32. COMPARISON OF DROPLET SIZE DISTRIBUTION FOR TRANSPORTATION OF ATOMISED CARBON SUBSTRATE (A) ETHYL LACTATE AND (B) METHANOL WITH CIRRUS™ THROUGH DRY (D) OR FIELD SATURATED CONDITION (FC) FINE GRAVEL AND COARSE SAND.

Interestingly a diameter of 2.5µm is understood to be the droplet size that would typically be deposited in the trachea and alveoli of the human respiratory system when attempting to administer an atomised liquid drug solution as restated in Table 5.4.

TABLE 5.4. PREDICTED DEPOSITION OF INHALED ATOMISED DROPLETS IN THE HUMAN LUNG (after Intersurgical, 2003).

Particle MMAD	*Fate*
>5µm	Deposit in pharynx, larynx and upper respiratory airways.
2-5µm	Deposit in tracheobronchial airways.
0.5-2µm	Deposit in alveoli.
<0.5µm	Exhaled

It is perhaps also worth restating that the three mechanisms that govern the deposition of particles in the human lung (Schulz, 1998) would be as follows:

1. inertial impaction;
2. gravitational sedimentation;
3. Brownian diffusion.

These processes are further illustrated in Figure 5.49 which shows relationship between deposition fraction and droplet diameter (and hence droplet mass) in the human lung.

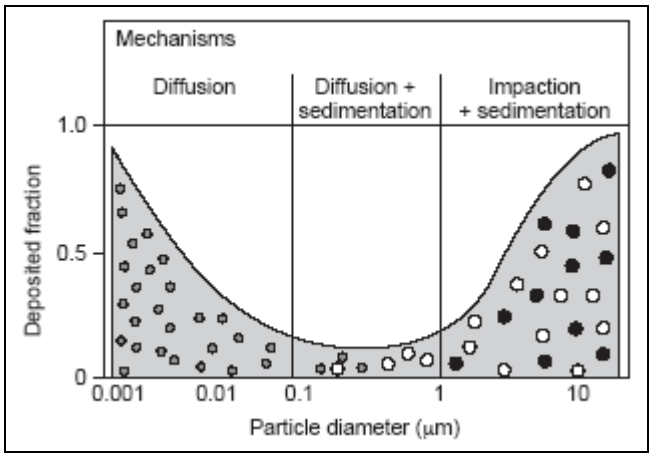

FIGURE 5.33. RELATIONSHIP BETWEEN DROPLET DEPOSITION AND DROPLET DIAMETER IN THE HUMAN LUNG (Schulz, 1998).

Inertial impaction is the predominant deposition mechanism for droplets >2µm, gravitational sedimentation is negligible for droplet diameters less than 0.5µm. This explains why most droplets below this diameter exit the lung upon expiration. The probability of deposition by this mechanism is highest in the alveolar region due to

relatively high residence times (Schulz, 1998). Hence, Brownian diffusion only significantly affects particles of diameter less than 0.5μm. Relatively long residence times due to low particle velocity means deposition by this mechanism is highest in the alveolar region of the lung (Schulz, 1998).

In comparison a granular soil could be described as containing pore spaces with sizes similar to those of the terminal regions of the lung, linked by tortuous flow paths. Table 5.5 restates the pore radius and waist radius of a group of spheres of identical radius, *r* for both cubical and rhombohedra packing arrangements (Coulson and Richardson, 1962).

TABLE 5.5. RELATIONSHIP BETWEEN PACKING ARRANGEMENT AND PORE WAIST RADIUS (Coulson and Richardson, 1962).

Packing Arrangement	Porosity	Pore radius	Waist radius
Cubical	47.6	0.700*r*	0.414*r*
Rhombohedral	25.9	0.288*r*	0.155*r*

A homogeneous soil of particle diameter 600μm for medium sand would have a pore diameter of 420μm and waist diameter of 249μm if packed in a *cubical* arrangement and a pore diameter of 173μm and waist diameter of 93μm if packed in a *rhombohedral* arrangement.

Figures 5.34 to 5.49 present the droplet size distribution of atomised methanol and ethyl lactate released by the Cirrus™ and Microcirrus™ nebuliser and transported through fine gravel and coarse sand under dry and field capacity conditions.

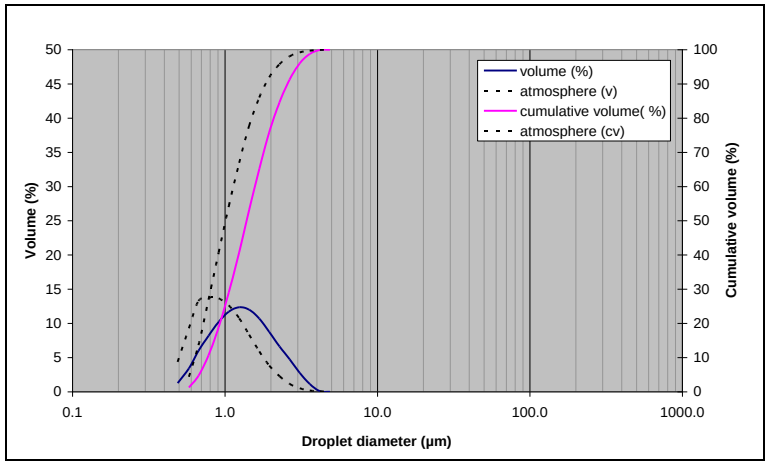

Parameter	*Value*
$d_{0.1}$	0.77
$d_{0.5}$	1.38
$d_{0.9}$	2.57
d_{32}	1.26
Δ	1.299
UI	0.399

FIGURE 5.34. DROPLET SIZE AND CUMULATIVE DROPLET SIZE DISTRIBUTION OF ATOMISED METHANOL TRANSPORTED THROUGH FINE GRAVEL BY THE MICROCIRRUS™ NEBULISER UNDER DRY CONDITIONS.

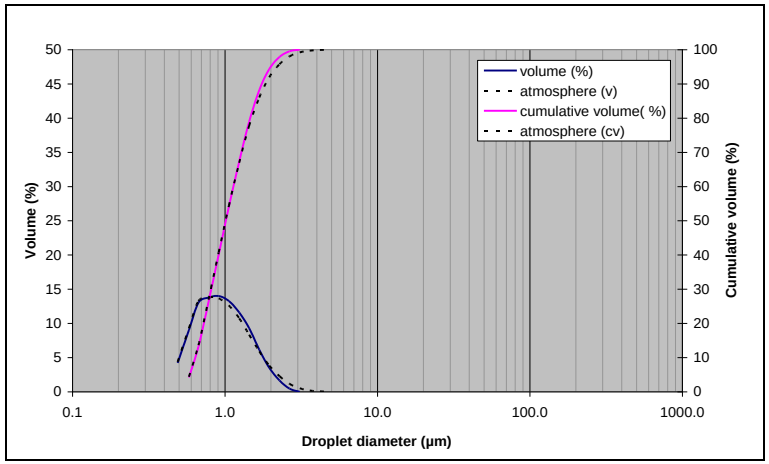

Parameter	*Value*
$d_{0.1}$	0.64
$d_{0.5}$	1.01
$d_{0.9}$	1.74
d_{32}	0.97
Δ	1.084
UI	0.341

FIGURE 5.35. DROPLET SIZE AND CUMULATIVE DROPLET SIZE DISTRIBUTION OF ATOMISED METHANOL TRANSPORTED THROUGH FINE GRAVEL BY THE MICROCIRRUS™ NEBULISER UNDER FIELD CAPACITY SATURATION CONDITIONS.

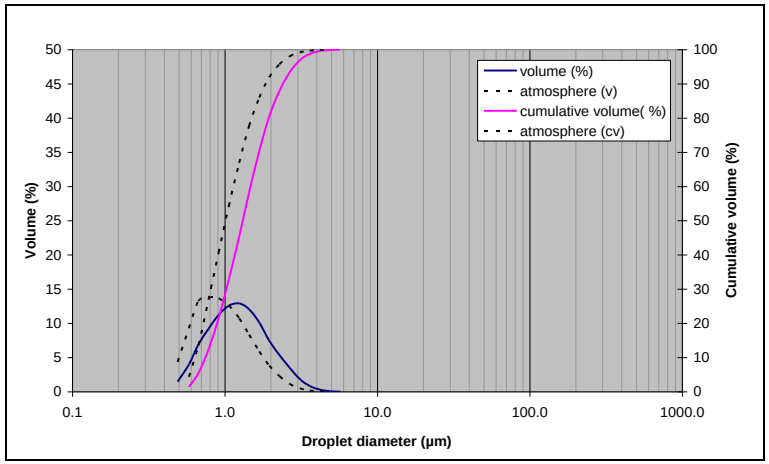

Parameter	*Value*
$d_{0.1}$	0.75
$d_{0.5}$	1.30
$d_{0.9}$	1.39
d_{32}	0.83
Δ	1.267
UI	0.394

FIGURE 5.36. DROPLET SIZE AND CUMULATIVE DROPLET SIZE DISTRIBUTION OF ATOMISED METHANOL TRANSPORTED THROUGH COARSE SAND BY THE MICROCIRRUS™ NEBULISER UNDER DRY CONDITIONS.

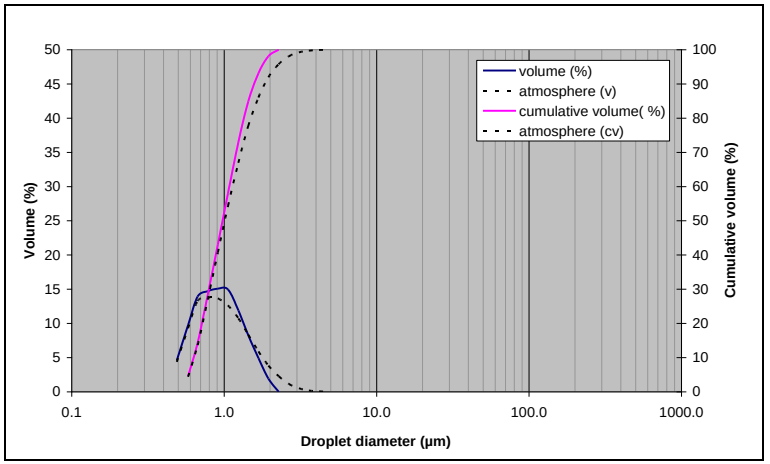

Parameter	*Value*
$d_{0.1}$	0.63
$d_{0.5}$	0.98
$d_{0.9}$	1.57
d_{32}	0.93
Δ	0.957
UI	0.295

FIGURE 5.37. DROPLET SIZE AND CUMULATIVE DROPLET SIZE DISTRIBUTION OF ATOMISED METHANOL TRANSPORTED THROUGH COARSE SAND BY THE MICROCIRRUS™ NEBULISER UNDER FIELD CAPACITY SATURATION CONDITIONS.

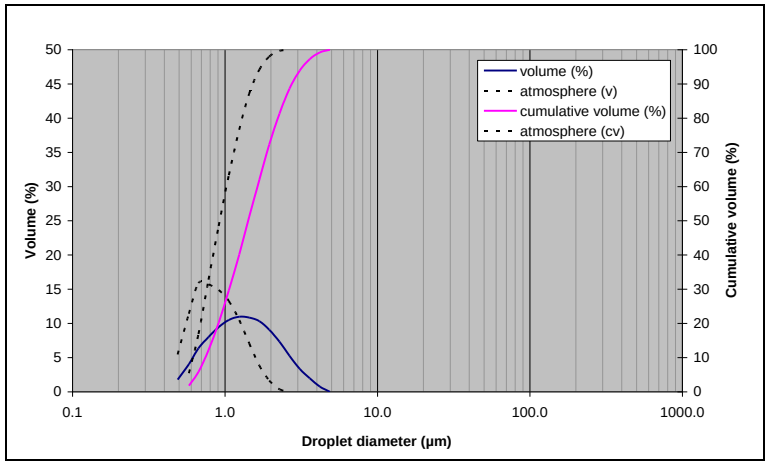

Parameter	*Value*
$d_{0.1}$	0.74
$d_{0.5}$	1.42
$d_{0.9}$	2.74
d_{32}	1.27
Δ	1.410
UI	0.439

FIGURE 5.38. DROPLET SIZE AND CUMULATIVE DROPLET SIZE DISTRIBUTION OF ATOMISED ETHYL LACTATE TRANSPORTED THROUGH FINE GRAVEL BY THE MICROCIRRUS™ NEBULISER UNDER DRY CONDITIONS.

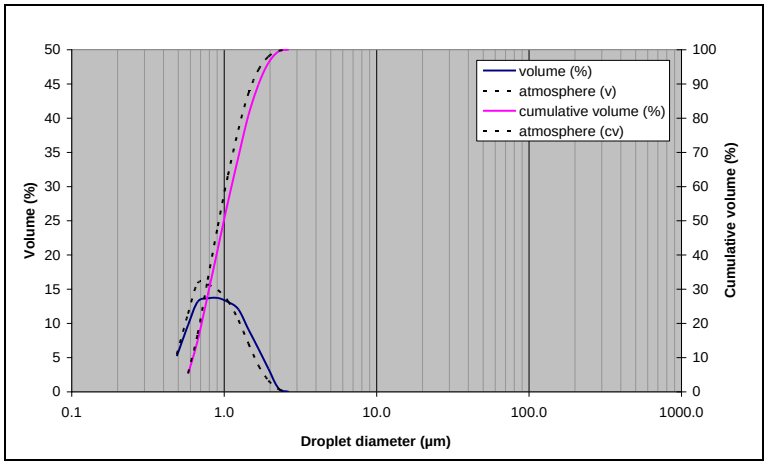

Parameter	*Value*
$d_{0.1}$	0.63
$d_{0.5}$	1.00
$d_{0.9}$	1.68
d_{32}	0.95
Δ	1.058
UI	0.327

FIGURE 5.39. DROPLET SIZE AND CUMULATIVE DROPLET SIZE DISTRIBUTION OF ATOMISED ETHYL LACTATE TRANSPORTED THROUGH FINE GRAVEL BY THE MICROCIRRUS™ NEBULISER UNDER FIELD CAPACITY SATURATION CONDITIONS.

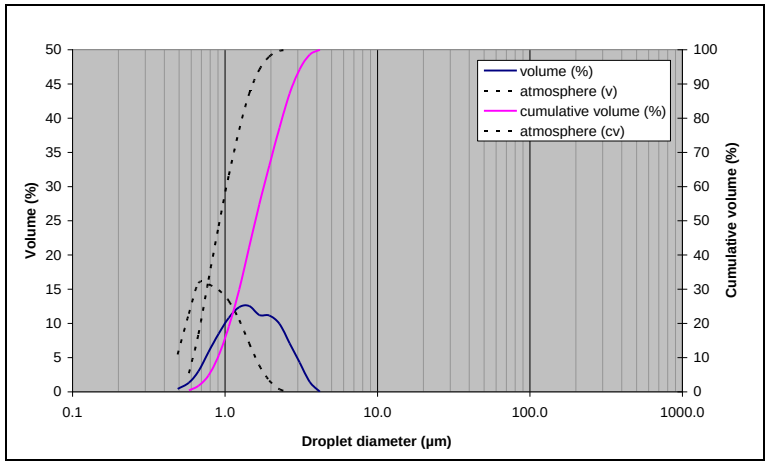

Parameter	*Value*
$d_{0.1}$	0.90
$d_{0.5}$	1.58
$d_{0.9}$	2.80
d_{32}	1.45
Δ	1.204
UI	0.373

FIGURE 5.40. DROPLET SIZE AND CUMULATIVE DROPLET SIZE DISTRIBUTION OF ATOMISED ETHYL LACTATE TRANSPORTED THROUGH COARSE SAND BY THE MICROCIRRUS™ NEBULISER UNDER DRY CONDITIONS.

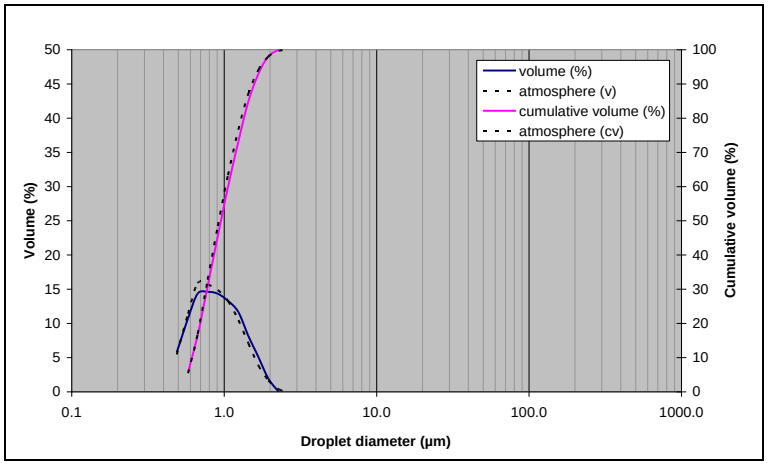

Parameter	*Value*
$d_{0.1}$	0.62
$d_{0.5}$	0.95
$d_{0.9}$	1.57
d_{32}	0.92
Δ	1.002
UI	0.312

FIGURE 5.41. DROPLET SIZE AND CUMULATIVE DROPLET SIZE DISTRIBUTION OF ATOMISED ETHYL LACTATE TRANSPORTED THROUGH COARSE SAND BY THE MICROCIRRUS™ NEBULISER UNDER FIELD CAPACITY SATURATION CONDITIONS.

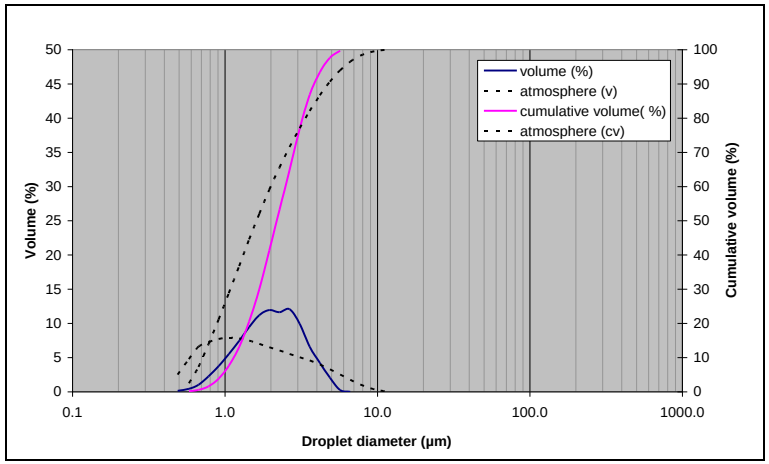

Parameter	*Value*
$d_{0.1}$	1.14
$d_{0.5}$	2.18
$d_{0.9}$	3.84
d_{32}	1.91
Δ	1.236
UI	0.439

FIGURE 5.42. DROPLET SIZE AND CUMULATIVE DROPLET SIZE DISTRIBUTION OF ATOMISED METHANOL TRANSPORTED THROUGH FINE GRAVEL BY THE CIRRUS™ NEBULISER UNDER DRY CONDITIONS.

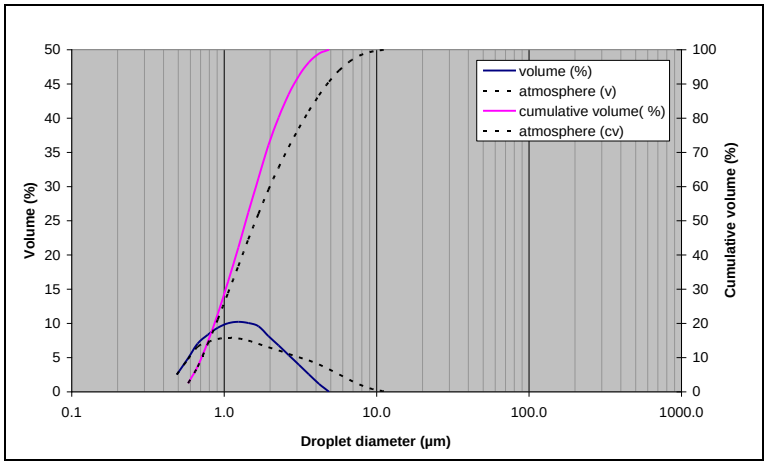

Parameter	*Value*
$d_{0.1}$	0.71
$d_{0.5}$	1.39
$d_{0.9}$	2.87
d_{32}	1.24
Δ	1.559
UI	0.327

FIGURE 5.43. DROPLET SIZE AND CUMULATIVE DROPLET SIZE DISTRIBUTION OF ATOMISED METHANOL TRANSPORTED THROUGH FINE GRAVEL BY THE CIRRUS™ NEBULISER UNDER FIELD CAPACITY SATURATION CONDITIONS.

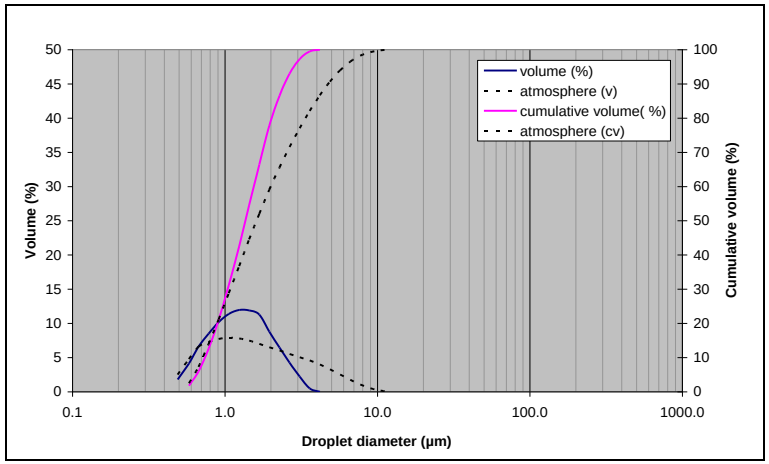

Parameter	Value
$d_{0.1}$	0.74
$d_{0.5}$	1.36
$d_{0.9}$	2.45
d_{32}	1.23
Δ	1.261
UI	0.389

FIGURE 5.44. DROPLET SIZE AND CUMULATIVE DROPLET SIZE DISTRIBUTION OF ATOMISED METHANOL TRANSPORTED THROUGH COARSE SAND BY THE CIRRUS™ NEBULISER UNDER DRY CONDITIONS.

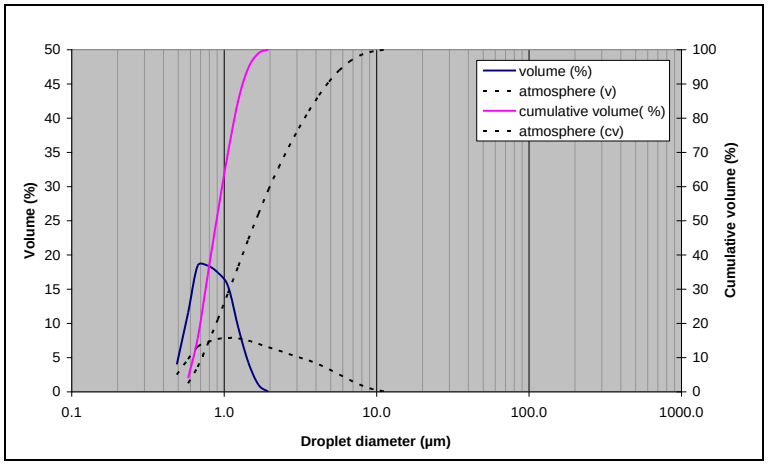

Parameter	Value
$d_{0.1}$	0.63
$d_{0.5}$	0.89
$d_{0.9}$	1.32
d_{32}	0.94
Δ	0.870
UI	0.769

FIGURE 5.45. DROPLET SIZE AND CUMULATIVE DROPLET SIZE DISTRIBUTION OF ATOMISED METHANOL TRANSPORTED THROUGH COARSE SAND BY THE CIRRUS™ NEBULISER UNDER FIELD CAPACITY SATURATION CONDITIONS.

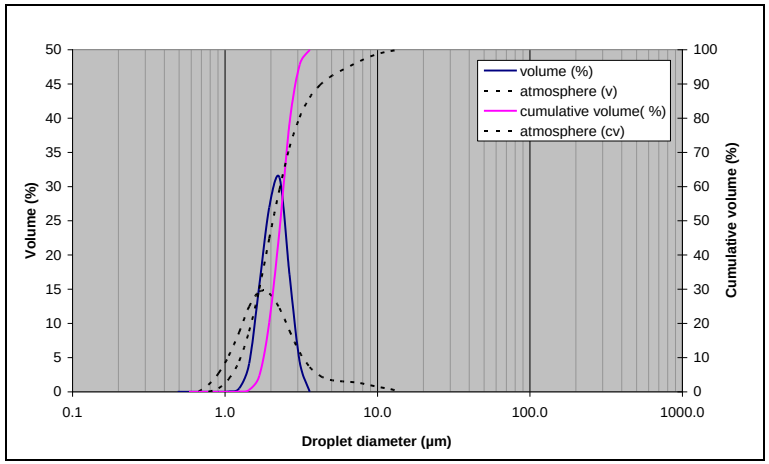

Parameter	*Value*
$d_{0.1}$	1.80
$d_{0.5}$	2.31
$d_{0.9}$	2.87
d_{32}	2.25
Δ	0.465
UI	0.154

FIGURE 5.46. DROPLET SIZE AND CUMULATIVE DROPLET SIZE DISTRIBUTION OF ATOMISED ETHYL LACTATE TRANSPORTED THROUGH FINE GRAVEL BY THE CIRRUS™ NEBULISER UNDER DRY CONDITIONS.

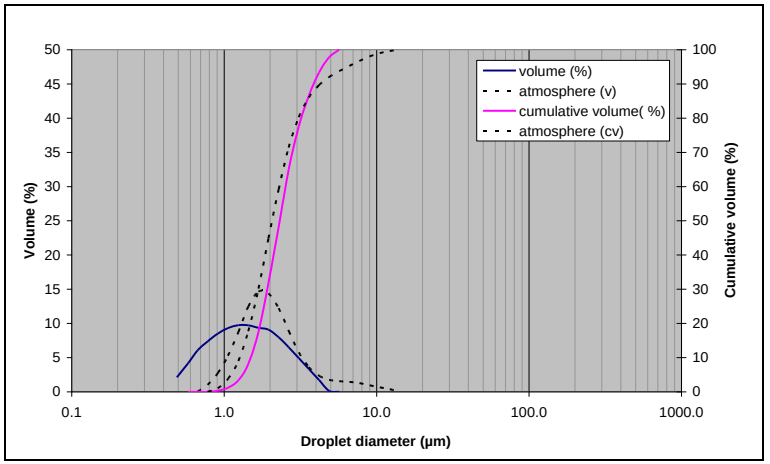

Parameter	*Value*
$d_{0.1}$	0.74
$d_{0.5}$	1.50
$d_{0.9}$	3.10
d_{32}	1.32
Δ	1.571
UI	0.484

FIGURE 5.47. DROPLET SIZE AND CUMULATIVE DROPLET SIZE DISTRIBUTION OF ATOMISED ETHYL LACTATE TRANSPORTED THROUGH FINE GRAVEL BY THE CIRRUS™ NEBULISER UNDER FIELD CAPACITY SATURATION CONDITIONS.

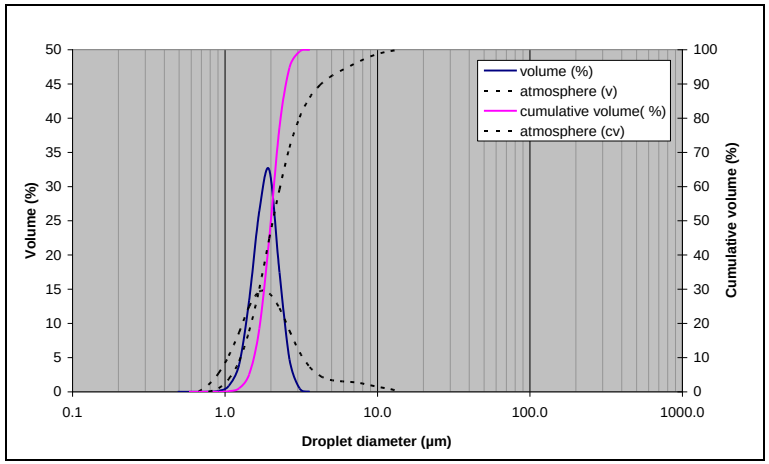

Parameter	Value
$d_{0.1}$	1.54
$d_{0.5}$	2.00
$d_{0.9}$	2.49
d_{32}	1.94
Δ	0.476
UI	0.154

FIGURE 5.48. DROPLET SIZE AND CUMULATIVE DROPLET SIZE DISTRIBUTION OF ATOMISED ETHYL LACTATE TRANSPORTED THROUGH COARSE SAND BY THE CIRRUS™ NEBULISER UNDER DRY CONDITIONS.

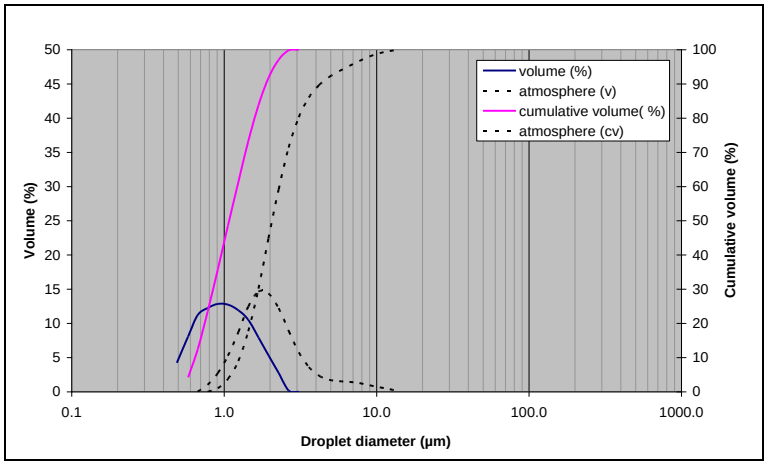

Parameter	Value
$d_{0.1}$	0.65
$d_{0.5}$	1.08
$d_{0.9}$	1.88
d_{32}	1.01
Δ	1.145
UI	0.356

FIGURE 5.49. DROPLET SIZE AND CUMULATIVE DROPLET SIZE DISTRIBUTION OF ATOMISED ETHYL LACTATE TRANSPORTED THROUGH COARSE SAND BY THE CIRRUS™ NEBULISER UNDER FIELD CAPACITY SATURATION CONDITIONS.

5.4. *Interim Conclusions*

The aforementioned experimental results provide convincing evidence for the possibility of transporting atomised carbon substrates through fine-grained gravel and coarse-grained sand under both dry and field conditions using Cirrus™ and Microcirrus™ medical jet nebulisers. In summary, there are two main outcomes from the test data.

1. The data demonstrate the feasibility of transporting atomised droplets of ethyl lactate and methanol through dry and fully wetted samples of gravel and sand size particles of soil and ballotini, which bodes well for the use of medical nebulisers to transport similar size droplets of liquid chemicals or for that matter bacterium through the vadose zone.

2. The droplet size distribution data indicate a maximum droplet size for transportation through wetted or dry sand and gravel of approximately 2.5µm, which coincidently agrees with the droplet size understood in medical literature to be deposited in the trachea and alveoli of the human respiratory system.

CHAPTER 6. MEDIUM-SCALE TEST COLUMN RESULTS

6.1. *Chapter Synopsis*

The following chapter presents the results from the medium-scale test column experiments described in Chapter 4.3. The tests aimed to determine the feasibility of using medical jet nebulisers to deliver droplets to a fully-saturated coarse-grained sand, after promising small-scale experiments in dry and field capacity saturated granular soil. The tests would also allow important design considerations to be made in advance of more detailed, larger-scale experiments. The tests assessed the vertical transportation of fine droplets through a fully-saturated granular material using medical jet nebulisers. Five sample ports were spaced vertically starting from the base of the column, as shown in Figure 4.10, to assess one-dimensional transport of the rhodamine WT. Lateral transportation of the tracer dye was not investigated during the medium-scale column experiments. The experiments were carried out between 21/08/2006 and 13/09/2006 after a period of preparation and commissioning of the column. Eight separate experiments are presented, four performed using a cirrus nebuliser, four performed using a Microcirrus nebuliser.

6.2. *Presentation of Medium-scale Column Test Results*

The results present the concentration of rhodamine water tracer measured in µg/l in sample levels A, B, C, D and E at 60, 120, 180 and 240 minutes after commencement of injection. Injection lasted for 180mins. The results are presented as a horizontal bar chart with RWT concentration plotted on the *x*-axis and sampling level on the *y*-axis. Due to the large range of RWT concentration measured across all the sample ports the results are plotted on a logarithmic *x*-axis.

A colour coding system was adopted in an attempt to improve the readability of the concentration results. The results were coded as described below:

- A measured RWT concentration of less than 1µg/l was deemed to be insufficient to show definite presence of the tracer in the column pore water. An increase in concentration of this magnitude could be attributed to other factors, particularly increased sediment in the sample or dirt on the sampling curvette. Measured concentrations of <1µg/l are characterised by a maroon bar on results charts.

- A measured RWT concentration of 1-10µg/l was deemed to show limited presence of the tracer as this class represents the minimum concentration required to show definite presence of RWT. Concentrations of this magnitude are characterised by a red bar on the results charts.

- A measured RWT concentration of 10-100µg/l was deemed to show moderate presence of the RWT solution and is characterised by an orange bar on the results charts.

- A measured RWT concentration of greater than 100µg/l was deemed to show relatively good presence and is characterised by a green bar on the results chart.

It must be noted that the maroon, red, orange and green indicators are not necessarily an indication of the expected quality of dechlorination . The coding system is used to give an indication of the *relative* presence of RWT in the column pore water facilitating the comparison of different tests.

The results also present the molar concentration of RWT in column pore water, calculated for each sample taken. To determine molar concentration, *C*, the number of moles of solute in each sample was first calculated using the following equation:

$$No\ of\ moles = \frac{mass\ of\ solute}{molar\ mass\ of\ solute} \qquad \text{(EQN 6.1)}$$

This allowed the molar concentration , C to be calculated using the equation:

$$C = \frac{v}{V} \qquad \text{(EQN 6.2)}$$

where v = no of moles of solute
V = volume of solution (m^3)

Molar concentration results are presented in two different forms. For each experiment, the molar concentration, C of RWT in sampled pore water is plotted on four separate graphs, one for each period of 60mins after injection. The y-axis uses a logarithmic scale to represent molar concentration in $\mu M/m^3$, the x-axis uses a linear scale to represent the distance, in mm, from the base of the column.

In addition, for each test, the molar concentration graphs described above have been used to construct cross-section drawings of the molar concentration distribution of RWT in the test column. The graphs were used to define the boundary between the different concentration classes shown below:

$$0\mu M/m^3 \leq C < 1\mu M/m^3$$
$$1\mu M/m^3 \leq C < 10\mu M/m^3$$
$$10\mu M/m^3 \leq C < 100\mu M/m^3$$
$$100\mu M/m^3 \leq C < 1000\mu M/m^3$$

Molar concentration graphs for all tests were examined as shown with the 60min graph from Test 1 shown below. Molar concentration boundaries were identified by noting the distance from the base of the column where the graph crosses the 1, 10 and $100\mu M/m^3$ lines on the x-axis. As all samples were taken from the internal boundary of the column, only vertical concentration boundaries can be plotted. Figures 6.1 and 6.2 illustrate how the cross-sectional drawings were constructed.

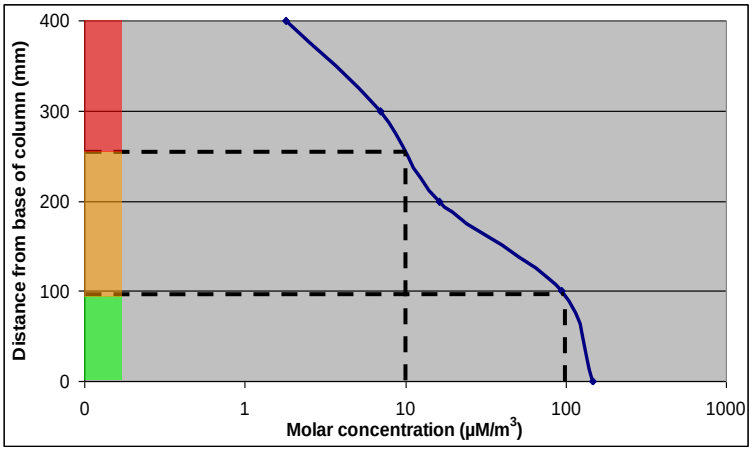

FIGURE 6.1. USING MOLAR CONCENTRATION GRAPHS TO DRAW DISTRIBUTION CROSS-SECTIONS.

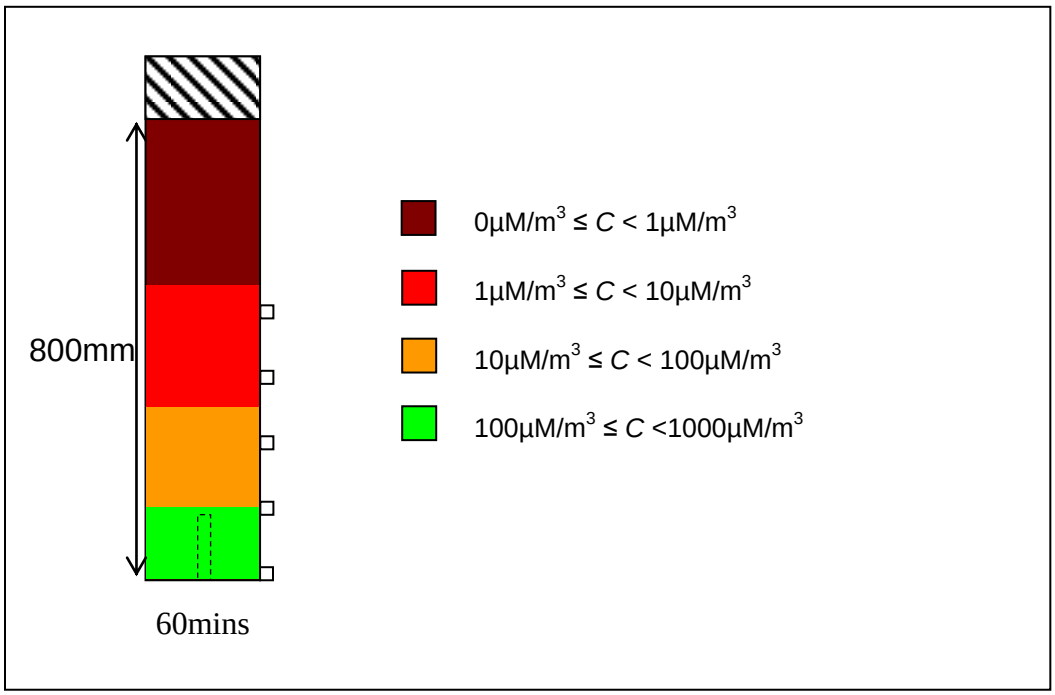

FIGURE 6.2. RESULTING CROSS-SECTIONAL VIEW OF MOLAR CONCENTRATION DISTRIBUTION IN COLUMN AT 60MINS.

It is clear that this graph does not cross the line representing 1µM/m^3 so it was necessary to extrapolate the data to plot this line on the cross-sectional distribution.

If the above procedure is repeated for each graph, the approximate boundaries for each molar concentration class can be plotted for each time period. This leads to a series of cross-sections for each test, making it easier to envisage the relative presence of the RWT and hence deposition of the tracer droplets in the column at the end of each 60min period.

6.3. *Test Results*

6.3.1. *Summary of Test Strategy*

Table 6.1 lists the design parameters of the eight tests carried out in the medium-scale column between 21/08/2006 and 13/09/2006. Each successive test altered either injection pressure, nebuliser type or injection pattern as detailed in Table 6.1.

TABLE 6.1. SUMMARY OF MEDIUM-SCALE TEST COLUMN DESIGN PARAMETERS.

Test	1	2	3	4	5	6	7	8
Date	21/08/2006	24/08/2006	30/08/2006	31/08/2006	04/09/2006	06/08/2006	11/09/2006	13/09/2006
Nebuliser	Cirrus	Cirrus	Cirrus	Cirrus	Microcirrus	Microcirrus	Microcirrus	Microcirrus
Nebuliser pressure (psi)	45	30	45	30	45	30	45	30
Nebuliser flowrate (l/min)	9	7	7	7	6	5	6	5
RWT concentration	20mg/l	20mg/l	20mg/l	20mg/l	20mg/l	20mg/l	20mg/l	20mg/l
Initial RWT mass (g)	242.84	244.36	270.70	260.35	198.64	206.96	169.31	160.58
Final RWT mass (g)	192.35	203.38	226.96	218.43	193.5	187.11	157.63	137.402
Total RWT injected (ml)	50.5	41.0	43.7	41.9	5.14	19.85	11.68	23.18
Injection pattern	Continuous	Continuous	Pulsed	Pulsed	Continuous	Continuous	Pulsed	Pulsed

6.3.2. *Test 1*

The results for Test 1 show an increase in RWT concentration at all sampling levels during the injection period. It can be seen that the highest concentration increases are at the base of the column, at sample levels D and E.

At 60mins, moderate presence of RWT is recorded at levels D and E with limited presence in all other levels. At 120mins RWT presence is now defined as good with moderate presence in level C and limited presence in levels A and B. At 180mins RWT concentration continues to increase at all levels with presence at level B now defined as moderate. At 240mins, 60mins after injection was ceased, tracer concentration is seen to decrease in levels B, C and D and increase in levels A and E.

Molar concentration plots, illustrated in Figure 6.3 shows an inversely proportional relationship between concentration and distance from the base of the column.

Figure 6.3 shows the molar concentration *C*, in µM/m^3, of rhodamine water tracer in pore water samples, in relation to the vertical distance from the base of medium-scale test column 1 at 0, 60, 120, 180 and 240mins after injection commenced.

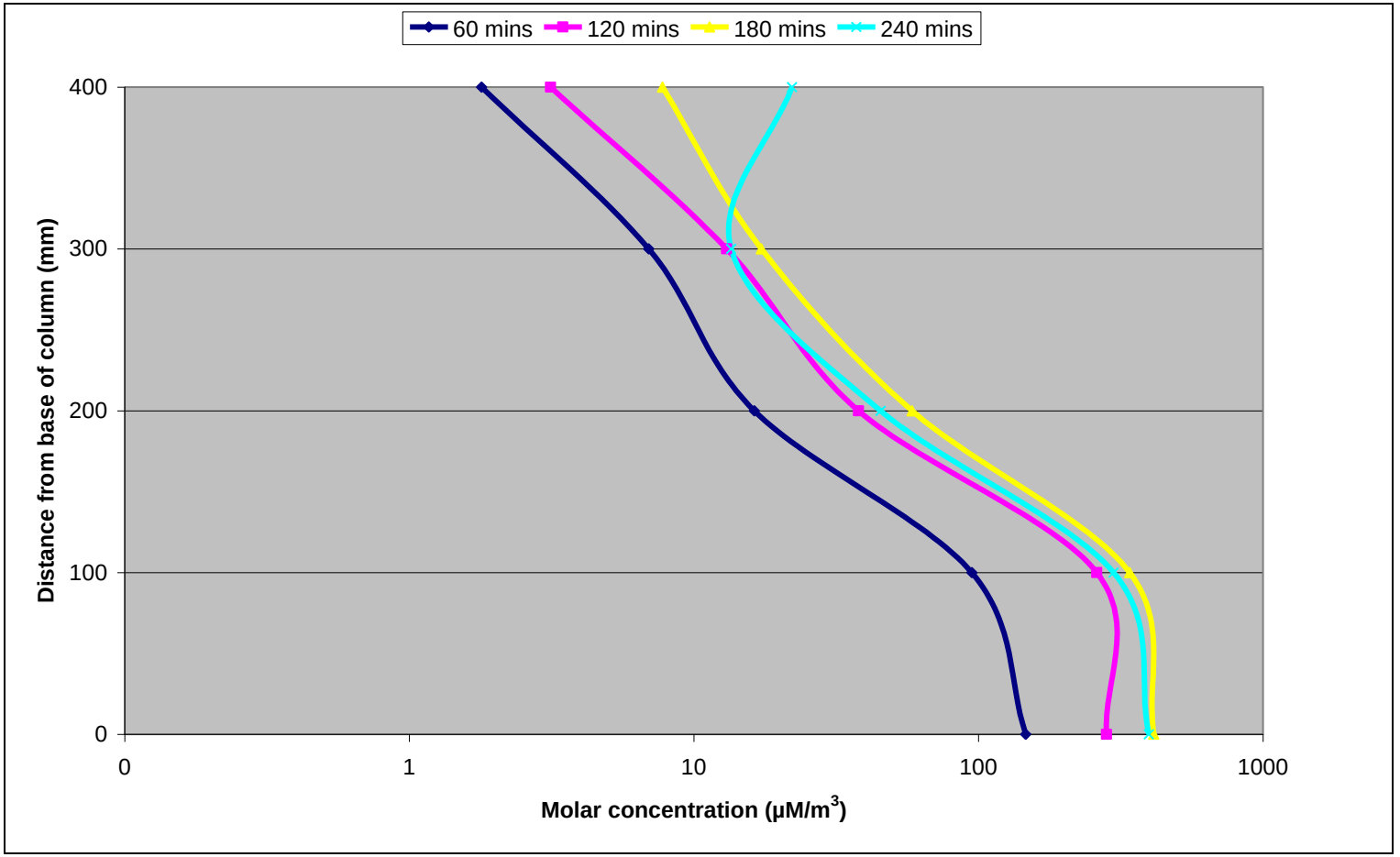

FIGURE 6.3. MOLAR CONCENTRATION OF RHODAMINE WATER TRACER IN MEDIUM-SCALE TEST COLUMN 8 AT 60, 120, 180 AND 240 MINUTES.

6.3.3. *Test 2*

The results for Test 2 show an increase in RWT concentration at all sampling levels during the injection period. It can be seen that the highest concentration increases are at the base of the column, at sampling levels D and E.

At 60mins, moderate presence of RWT is recorded at level E with limited presence at all other levels. At 120mins RWT increases at all levels. Sampling level E is now defined as exhibiting good presence of RWT, levels C and D show moderate presence and levels A and B show limited presence of the tracer.

Molar concentration plots, illustrated in Figure 6.4 generally show an inversely proportional relationship with distance from base of the column.

Figure 6.4 shows the molar concentration *C*, in μM/m^3, of rhodamine water tracer in pore water samples, in relation to the vertical distance from the base of medium-scale test column 2 at 0, 60, 120, 180 and 240mins after injection commenced.

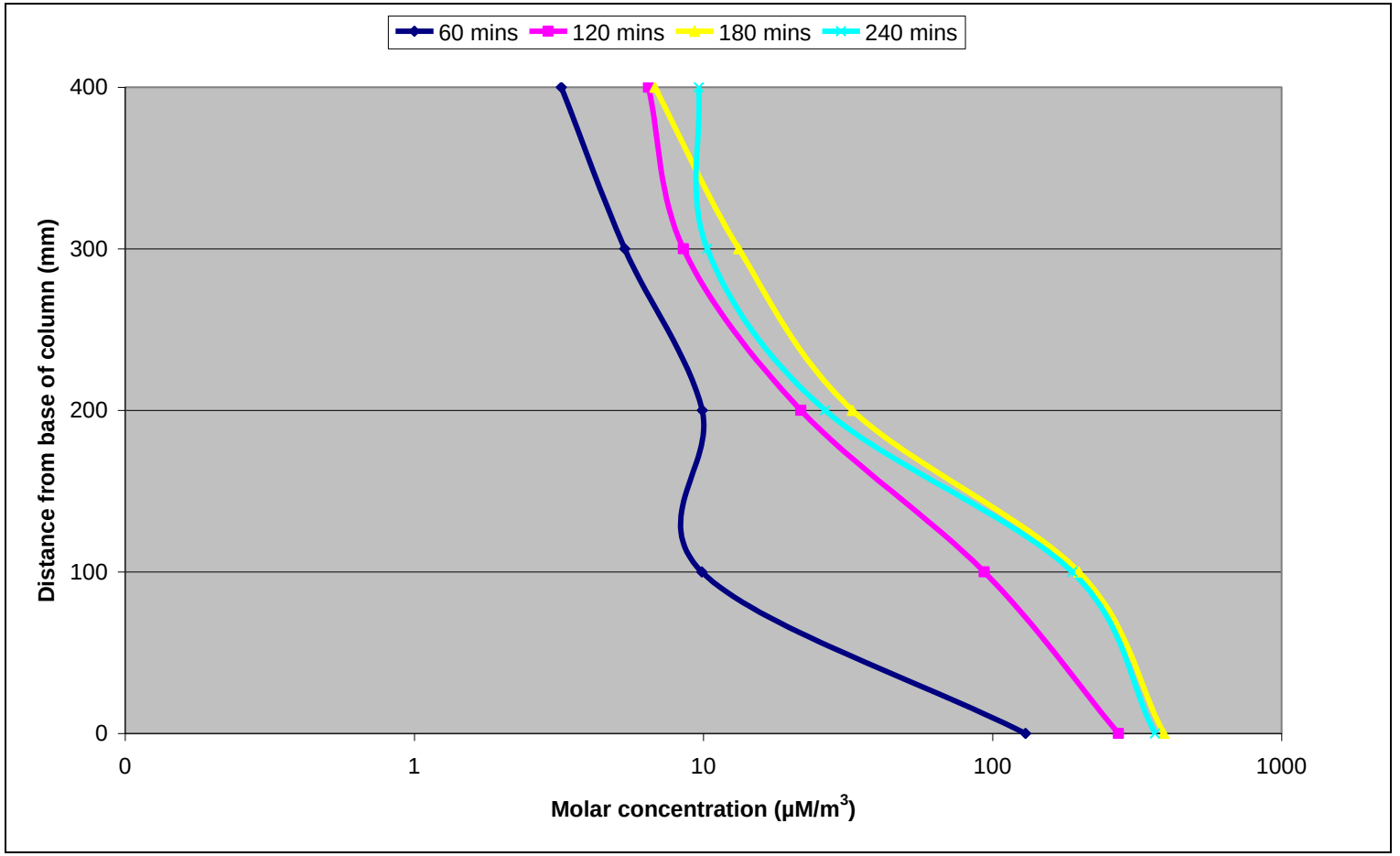

FIGURE 6.4. MOLAR CONCENTRATION OF RHODAMINE WATER TRACER IN MEDIUM-SCALE TEST COLUMN 8 AT 60, 120, 180 AND 240 MINUTES.

6.3.4. *Test 3*

The results for Test 3 show an increase in RWT concentration at all sampling levels during the injection period. It can be seen that the highest concentration increases are at the base of the column, at sample levels D and E. After 60mins, good presence of RWT is noted at these levels which continues to increase until 240mins.

At 60mins, moderate RWT presence is recorded at levels B, C, D and E with limited presence at level A. At 120mins an increase in RWT concentration can be seen in all sample levels. At level E, RWT presence is now defined as good with levels B, C, and D defined as moderate and level A showing limited presence. At 180mins levels D and E exhibit good presence, B and C show moderate presence and level A shows limited presence. At 240mins increase in RWT is noted in levels A, D and E with decreases in levels B and C.

Molar concentration plots, illustrated in Figure 6.5, generally show an inversely proportional relationship between concentration and distance from the base of the column.

Figure 6.5 shows the molar concentration *C*, in µM/m^3, of rhodamine water tracer in pore water samples, in relation to the vertical distance from the base of medium-scale test column 3 at 0, 60, 120, 180 and 240mins after injection commenced.

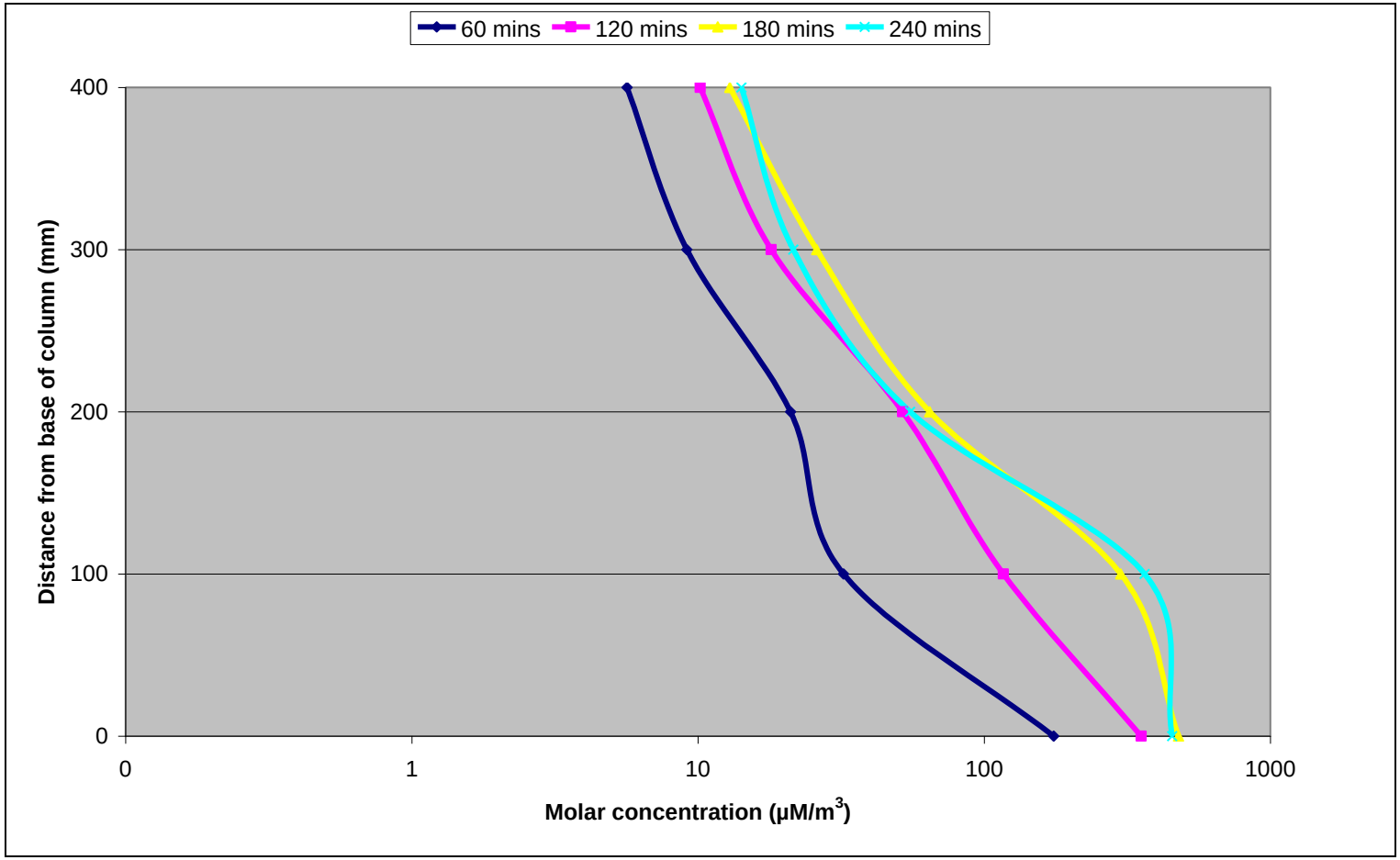

FIGURE 6.5. MOLAR CONCENTRATION OF RHODAMINE WATER TRACER IN MEDIUM-SCALE TEST COLUMN 8 AT 60, 120, 180 AND 240 MINUTES.

6.3.5. *Test 4*

The results for Test 4 show an increase in RWT concentration at all sampling levels during the injection period. It can be seen that the highest concentration increases are at the base of the column, at sample levels D and E.

At 60mins, moderate presence of RWT is recorded at levels D and E with limited presence in levels A, B and C. At 120mins, concentration increase can be seen at all levels with level E exhibiting good presence, levels B, C and D showing moderate presence and level A still showing limited presence. At 180mins further increases are recorded with level D now defined as exhibiting good presence. At 240mins concentration is recorded at level A with decreases in levels B, C, D and E.

Molar concentration plots, illustrated in Figure 6.6, show an inversely proportional relationship between concentration and distance from the base of the column.

Figure 6.6 shows the molar concentration *C*, in µM/m^3, of rhodamine water tracer in pore water samples, in relation to the vertical distance from the base of medium-scale test column 4 at 0, 60, 120, 180 and 240mins after injection commenced.

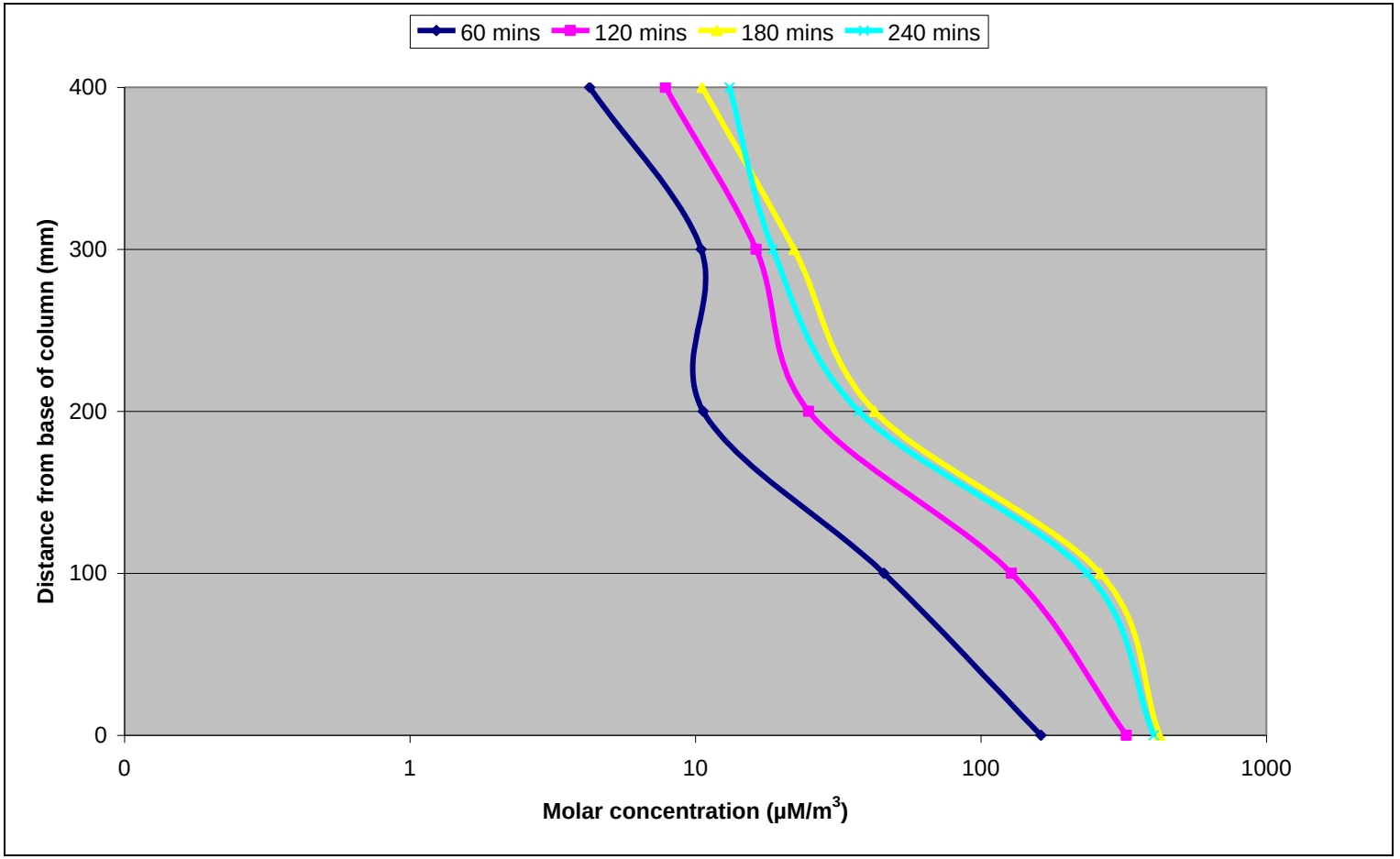

FIGURE 6.6. MOLAR CONCENTRATION OF RHODAMINE WATER TRACER IN MEDIUM-SCALE TEST COLUMN 8 AT 60, 120, 180 AND 240 MINUTES.

6.3.6. *Test 5*

The results for Test 5 show a somewhat erratic RWT concentration pattern with only the 240mins graph resembling any of the previous tests. It is also apparent that a relatively low volume of RWT was injected over the injection period. This was attributed to backpressure in the Microcirrus™ nebuliser restricting airflow through the nebuliser system, reducing atomisation and injection into the column.

At 60mins level E exhibits limited presence of RWT with levels A, B, C and D deemed to show no definite presence. At 120mins and 180mins only limited presence is recorded in sample level E however concurrent concentration increases are noted at this level. At 240mins sample levels B, C, D and E exhibit definite concentration increase however again the presence of RWT is only defined as limited.

Similarly, relative molar concentration plots, illustrated in Figures 6.7, show an erratic pattern with the exception of 240mins which shows an inversely proportional relationship between concentration and distance from the base of the column.

Figure 6.7 shows the molar concentration *C*, in μM/m^3, of rhodamine water tracer in pore water samples, in relation to the vertical distance from the base of medium-scale test column 5 at 0, 60, 120, 180 and 240mins after injection commenced.

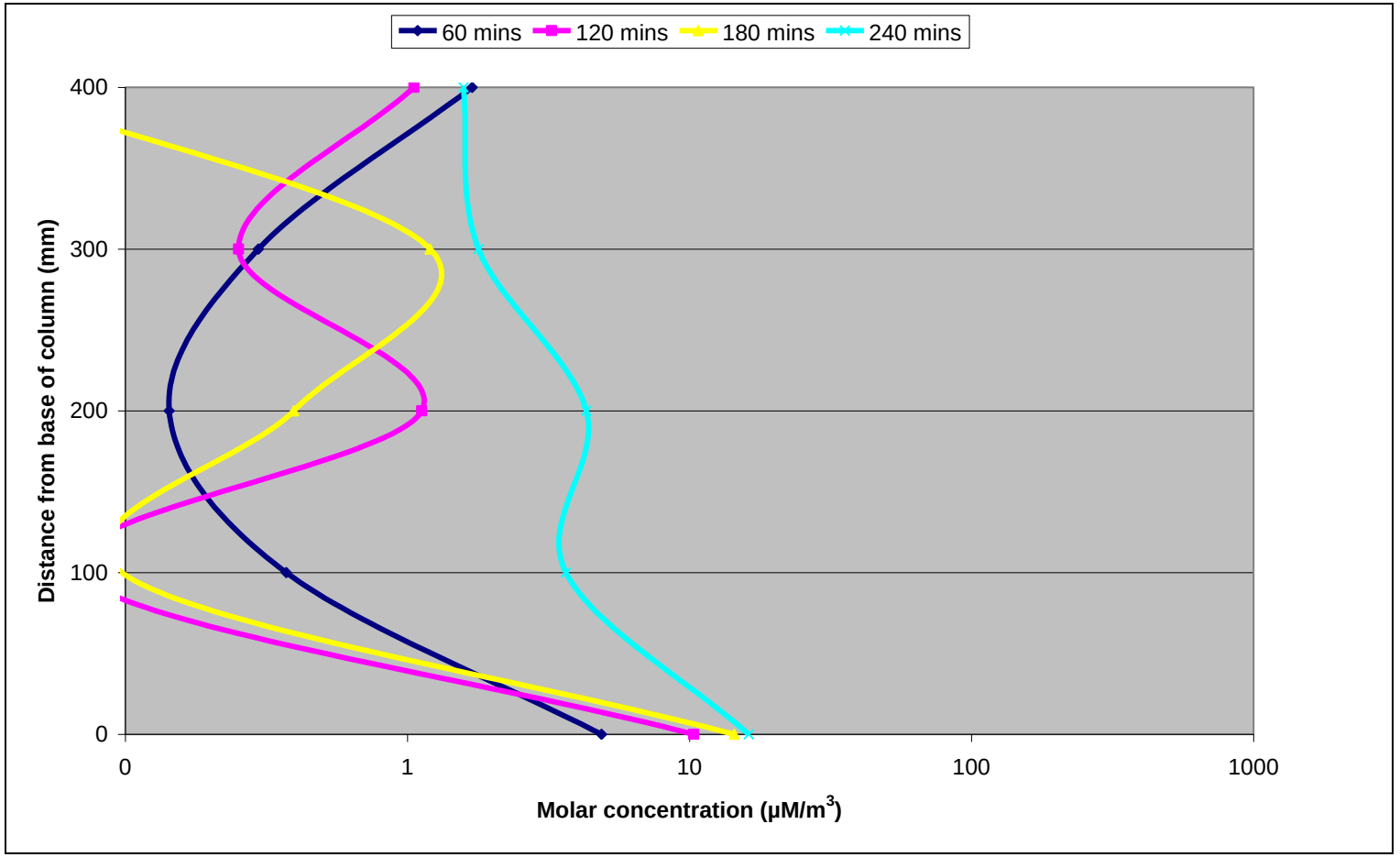

FIGURE 6.7. MOLAR CONCENTRATION OF RHODAMINE WATER TRACER IN MEDIUM-SCALE TEST COLUMN 5 AT 60, 120, 180 AND 240 MINUTES.

6.3.7. *Test 6*

The results for Test 6 show an increase in RWT concentration at all sampling levels during the injection period. It can be seen that the highest concentration increases are at the base of the column, at sample levels C, D and E.

At 60mins, level A shows no definite presence of RWT with limited presence recorded at levels B, C, D and E. At 120mins further increases are recorded at all levels with levels A, B and D showing limited presence of RWT and sample levels C and E exhibiting moderate presence. At 180mins further increases in concentration are recorded in sample levels B, C, D and E with level D now exhibiting moderate presence of RWT. At 240mins, slight increases in concentration are recorded at all sample levels.

Molar concentration plots, illustrated in Figure 6.8, generally show an inversely proportional relationship between concentration and distance from the base of the column however a slight increase is noted at 200mm before decreasing again.

Figure 6.8 shows the molar concentration *C*, in μM/m^3, of rhodamine water tracer in pore water samples, in relation to the vertical distance from the base of medium-scale test column 6 at 0, 60, 120, 180 and 240mins after injection commenced.

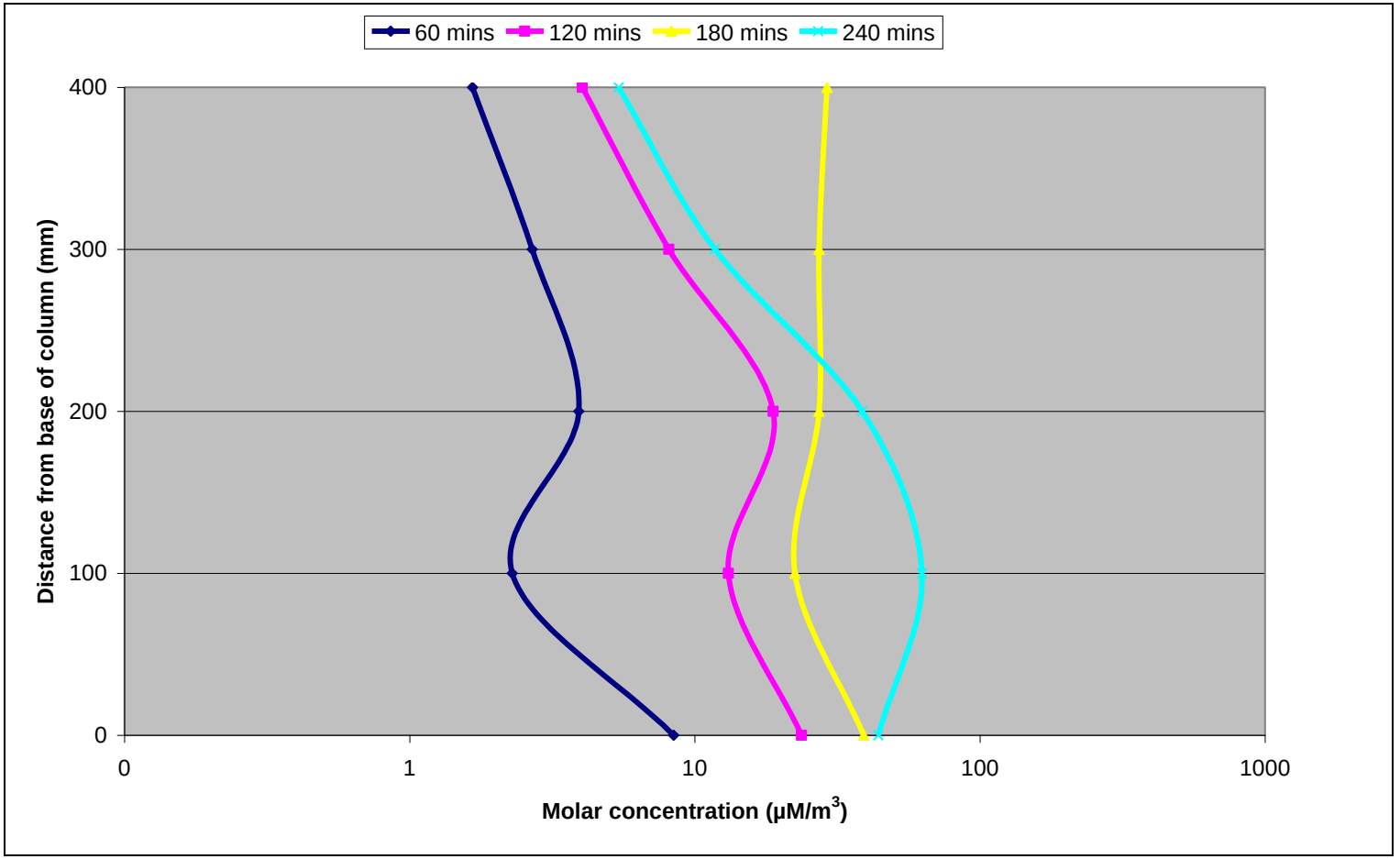

FIGURE 6.8. MOLAR CONCENTRATION OF RHODAMINE WATER TRACER IN MEDIUM-SCALE TEST COLUMN 8 AT 60, 120, 180 AND 240 MINUTES.

6.3.8. *Test 7*

The results for Test 7 show an increase in RWT concentration at all sampling levels during the injection period. It can be seen that the highest concentration increases are at the base of the column, at sample levels D and E.

At 60mins levels A and B show no definite presence of RWT in pore water and limited presence at levels C, D and E. At 120mins levels D and E now show moderate presence, levels B and C exhibit limited presence and level A still showing no definite presence of the RWT tracer. At 180mins further increases in concentration are recorded at all levels with level C now showing moderate presence of the tracer. At 240mins concentration increases are noted at sampling levels A, D and E and decreases at B and C.

Molar concentration plots, illustrated in Figures 6.9, generally show an inversely proportional relationship with distance from the base of the column however a slight increase can be seen at 200mm.

Figure 6.9 shows the molar concentration *C*, in µM/m^3, of rhodamine water tracer in pore water samples, in relation to the vertical distance from the base of medium-scale test column 7 at 0, 60, 120, 180 and 240mins after injection commenced.

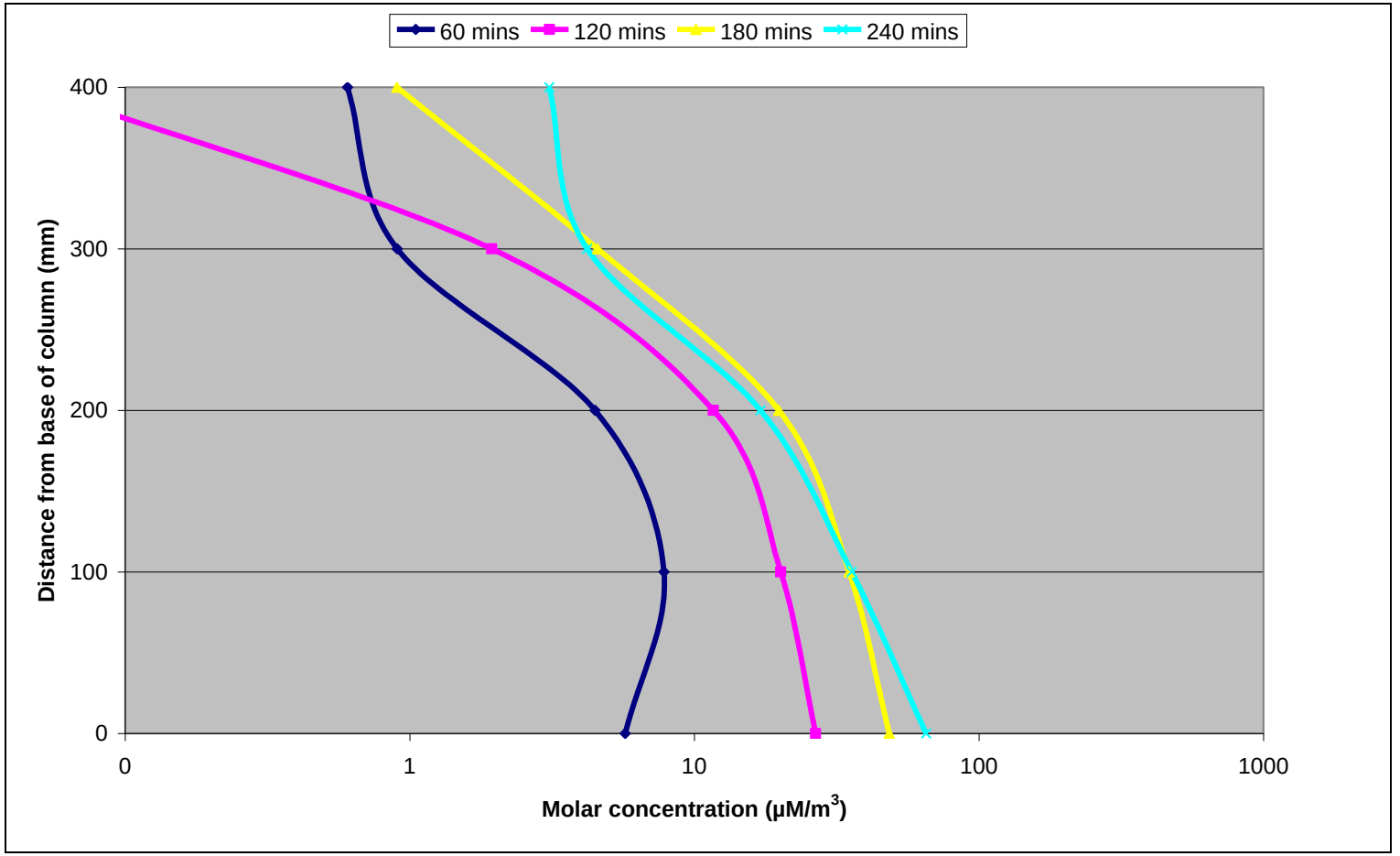

FIGURE 6.9. MOLAR CONCENTRATION OF RHODAMINE WATER TRACER IN MEDIUM-SCALE TEST COLUMN 8 AT 60, 120, 180 AND 240 MINUTES.

6.3.9. *Test 8*

The results for Test 8 show an increase in RWT concentration at all sampling levels during the injection period. It can be seen that the highest concentration increases are at the base of the column, at sample levels D and E.

At 60mins, level A shows no definite presence of RWT tracer, levels B and C show limited presence and levels D and E exhibiting moderate presence. At 120mins increases in concentration are recorded at all levels with levels A, B and C showing limited presence and levels D and E exhibiting moderate presence of RWT tracer. At 180mins further increases are noted at all levels with level C now showing moderate presence of the tracer. At 240mins, concentration increases are noted in levels A, C and E and decreases in levels B and D.

Molar concentration plots, illustrated in Figure 6.10, generally show an inversely proportional relationship with distance from the base of the column however a slight increase can be seen at 200mm.

Figure 6.10 shows the molar concentration *C*, in µM/m^3, of rhodamine water tracer in pore water samples, in relation to the vertical distance from the base of medium-scale test column 8 at 0, 60, 120, 180 and 240mins after injection commenced.

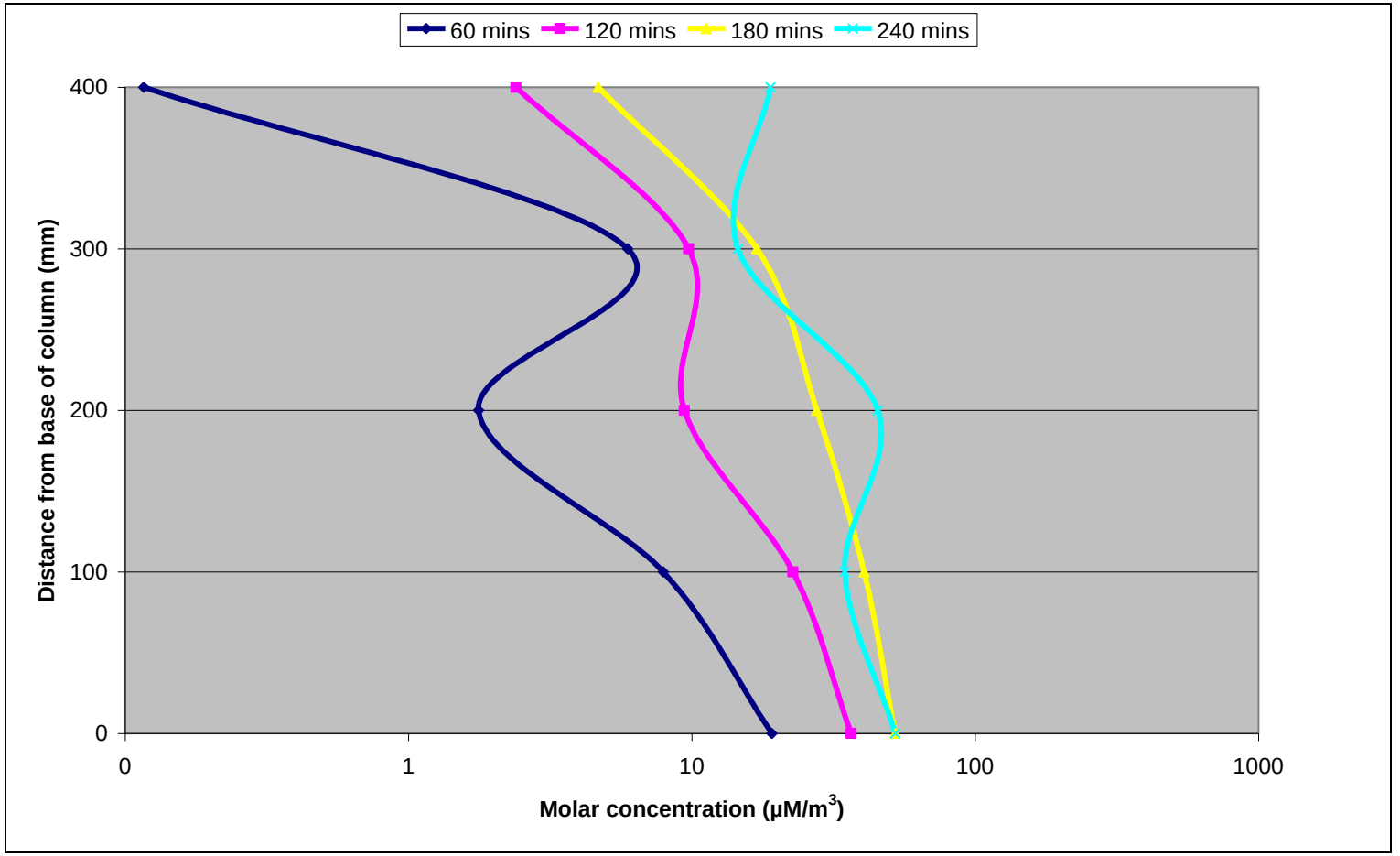

FIGURE 6.10. MOLAR CONCENTRATION OF RHODAMINE WATER TRACER IN MEDIUM-SCALE TEST COLUMN 8 AT 60, 120, 180 AND 240 MINUTES.

6.4. *Interim Conclusions*

The aforementioned experiments were designed to give provisional insight into the feasibility of using medical jet nebulisers to atomise and deliver fine droplets to fully-saturated coarse-grained sand, after promising results from small-scale droplet size distribution tests. The experiments also allowed design considerations to be made for planned large-scale column tests using the same granular material.

As anticipated, for both the Cirrus™ and Microcirrus™ nebuliser, rhodamine water tracer concentration and molar concentration plots suggest that the majority of the injected droplets are deposited at the base of the column, in the region directly surrounding the injection filter. In all eight test columns, a definite presence of RWT was measured at all sampling levels by the end of the injection period. Tests conducted with the Cirrus™ nebuliser indicated that this device achieved higher overall RWT concentrations in the column. This phenomenon is due, in part, to the fact that it releases a higher volume of droplets per minute, however the most likely explanation is that the Cirrus™ nebuliser has a droplet size distribution with a higher $d_{0.9}$ value relative to that of the Microcirrus™ nebuliser. As discussed in Chapter 5, larger droplets are more likely to be deposited in the pore spaces of granular material, leading to higher rates of deposition.

Maximum molar concentration differences between the bottom and top sampling levels in the column support this theory as the Microcirrus™ nebuliser appears to be able to deliver a more uniform RWT distribution when compared to the Cirrus™ nebuliser. This is possibly due to the fact that the Microcirrus™ nebuliser generally releases droplets with a smaller droplet size distribution, in particular a smaller $d_{0.9}$ value and these droplets are less likely to deposit in pore spaces and therefore penetrate greater distances from the injection filter.

While it was not possible to calculate the total volume of tracer deposited in the column, no droplets were seen to leave any of the test columns, suggesting that the deposition rate of droplets in fully-saturated media may be significantly higher than in dry or field condition media. This is possibly due to increased droplet deposition as a result of decreased pore space in the saturated soil as well as an increase in the vertical length of the sample.

Absolute molar concentration values do not compare favourably with the molar concentrations of various carbon substrates used in laboratory studies by researchers such as Freedman and Gossett (1989), De Bruin *et al* (1992), DiStefano *et al* (1992), Gerritse *et al* (1997) and Jayaraj *et al* (2003). It must be noted however that the volume of substrate injected in each test was relatively low compared to the anticipated injection volumes in a field installation. It is probable that a successful field installation would utilise a number of nebulisers to achieve significantly higher rates of substrate delivery. It is apparent from these tests however that medical jet nebulisers have the capability to transport gas bubbles in soil samples of coarse sand of vertical height approximately 1m, without the need for auxiliary gas flow into the column. Capillary pressures in these soils are relatively low and this, coupled with a hydrostatic pressure of approximately 10kPa, allows vertical transportation of the gas/droplet mixture. It remains to be seen how the nebulisers would perform at greater hydrostatic pressures and in finer grained material.

The results produced by the Microcirrus™ nebuliser were, at times, erratic. The Microcirrus™ nebuliser appears to perform relatively poorly when operated at continuous, relatively high air inlet pressures, as demonstrated in test column 5 when tracer concentrations during injection in the column were particularly inconsistent and final concentrations were found to be relatively low when compared to other tests. For this reason, the Cirrus™ nebuliser was selected for the planned large-scale column tests which are discussed in Chapter 7.

In summary, the experimental results recorded in this chapter indicate the possibility of using commercially available medical jet nebulisers to atomise and deliver fine droplets to a fully-saturated coarse grained sand on a relatively small scale. The deposition of droplets in the granular material appears to be relatively high, particularly in the region directly surrounding the injection filter, where tracer dye concentrations were typically two orders of magnitude higher than at the highest sample port of the column. This suggests that the droplets released by medical jet nebulisers may not be sufficiently small to efficiently penetrate the pore spaces of granular material under fully-saturated conditions. Another possibility is that the gas channels created in the granular media are not sufficiently large or stable to allow effective droplet transportation.

Large-scale column test results, described in Chapter 7, will establish the feasibility of atomising and transporting droplets using a greater number of medical nebulisers in series, on a scale that more realistically simulates anticipated field conditions.

CHAPTER 7. LARGE-SCALE TEST COLUMN RESULTS

7.1. *Chapter Synopsis*

The following chapter presents the results from the large-scale test column experiments described in Chapter 4.4. The experiments were carried out between 18/04/2007 and 29/05/2007 after a period of preparation and commissioning of the column. Six separate experiments are presented, all of which were carried out using the Cirrus™ nebuliser. The aim of the testing programme was to simulate, as closely as possible, the anticipated field conditions for the injection of fine droplets into a fully saturated granular soil. In this way, the feasibility of implementing medical jet nebulisers for the atomisation and delivery of carbon substrates to the subsurface could be assessed.

The column was flushed with clean water for a period of at least 24 hours between each test to ensure that all RWT was removed from the pore water prior to a new test commencing. Samples of the flushed water were taken at the end of the flushing process and analysed using the portable fluorometer to ensure that a return to steady had been achieved.

7.2. *Presentation of Large-Scale Test Column Results*

The results present the concentration of rhodamine water tracer (RWT) measured in µg/l in sample ports A, B, C, D and E at radial distances of 0, 200, 400 and 600mm. In addition the molar concentration of RWT is presented in $\mu M/m^3$ at each sample level. The results are presented as a horizontal bar chart with RWT concentration plotted on the *x*-axis. Due to the large range of RWT concentration in the sample ports, the results are plotted on a logarithmic *x*-axis.

A colour coding system was adopted in the same way as the medium-scale test column results in Chapter 6.

- A measured RWT concentration of less than 1µg/l was deemed to be insufficient to show definite presence of RWT solution in the pore water as an increase of this magnitude could be attributed to other factors, particularly increased sediment in the sample. Measured concentrations of <1µg/l are characterised by a maroon bar on results charts.

- RWT concentration of 1-10µg/l was deemed to show limited transportation of droplets and is characterised by a red bar on the results charts.

- RWT concentration of 10-100µg/l was deemed to show moderate transportation of the RWT solution and is characterised by an orange bar on the results charts.

- RWT concentration of greater than 100µg/l was deemed to show good transportation and is characterised by a green bar on the results chart.

It should be noted that the red, orange and green indicators are not an indication of the expected quality of bioremediation and purely illustrate the relative quality of droplet transportation.

The molar concentration of RWT was calculated for each sample taken in the same way as for the medium-scale column results in Chapter 6. Again, molar concentration results are presented in two different forms. For each experiment, the molar concentration, *C* of RWT in sample pore water is plotted on five separate graphs, one for each sampling level. The *y*-axis uses a logarithmic scale to represent molar concentration µM/m^3. The *x*-axis uses a linear scale to represent the distance, in mm, from the centre of the column. The maximum value on the *x*-axis is half the internal diameter of the column and therefore 600mm. The graphs are superimposed on a cross-sectional sketch of the large-scale test column.

In a similar way to Chapter 6, for each test presented, the graphs mentioned above have been used to construct cross-section drawings of the molar concentration distribution of RWT tracer in the large-scale test column. The graphs were used to define the boundary between the different concentration classes shown below which differ slightly from those in Chapter 6:

$$0\mu M/m^3 \leq C < 10\mu M/m^3$$

$$10\mu M/m^3 \leq C < 100\mu M/m^3$$

$$100\mu M/m^3 \leq C < 1000\mu M/m^3$$

$$1000\mu M/m^3 \leq C < 10000\mu M/m^3$$

As lateral and vertical data was available for this test, cross-sectional distributions have also been used to draw plan views as seen from the top or base of the column. This was achieved by locating the widest part of the molar concentration boundary for each class on the cross-section view and measuring its approximate diameter. This diameter was then used to construct a rough circle which was then superimposed on the plan view of the column.

Maximum molar concentration difference was found using the following formula:

$$1 - \frac{C_{max}}{C_{min}}$$

where C_{max} = maximum molar concentration in column
C_{min} = minimum molar concentration in column

In the same way as Chapter 6, the maximum molar concentration difference gives a good representation of the uniformity of droplet deposition in the large-scale column after the 5 hour injection period. As the maximum molar concentration difference tends towards zero, the tracer dye is more evenly distributed in the column.

7.3. *Test Results*

7.3.1. *Summary of Test Strategy*

Table 7.1 summarises the testing parameters for the large scale column experiments carried out between 10/05/2007 and 26/05/2007. Each successive test altered either the injection pressure or injection pattern as shown in Table 7.1.

TABLE 7.1. SUMMARY OF LARGE-SCALE TEST COLUMN DESIGN PARAMETERS.

Date	10/05/2007	18/04/2007	23/05/2007	21/05/2007	29/05/2007	26/05/2007
RWT concentration (µg/l)	1×10^6	1×10^6	1×10^6	1×10^6	1×10^6	1×10^6
RWT solution injected (g)	231.2	219.0	267.6	214.7	259.3	291.4
Nebuliser pressure (kPa)	300	300	400	400	500	500
Injection pressure (kPa)	30	30	41	41	0.54	0.54
Flowrate (l/min)	26	26	34	26	38	38
Injection time (mins)	300	300	300	300	300	300
Pore water displaced (l)	6.3	7.2	18.8	16.3	27.8	29.2
Injection pattern	Continuous	Pulsed	Continuous	Pulsed	Continuous	Pulsed

7.3.2. *Test 1*

The results indicate that, as predicted, the highest concentration of RWT tracer is found in the zone directly surrounding and vertically above the injection filter. Away from the filter the concentration appears to gradually decrease and is difficult to reliably measure at the surface of the column, particularly towards the levels A, B and C. Lateral distribution appears to be more limited than vertical distribution, most likely a result of the shape of the air plume in the column during the injection period.

At 0mm radial distance, limited RWT presence is recorded at levels C, D and E with levels A and B exhibiting no definite tracer presence. Interestingly, at 200mm radial distance levels B, C, D and E are now defined as having no definite presence of RWT and level A as having limited presence of the tracer. At 400mm radial distance levels D and E are defined as showing good presence of the tracer with all other levels defined as moderate presence. At 600mm radial distance, the centre of the column, levels C, D and E exhibit good presence of RWT and levels A and B show moderate presence.

The distribution again appears to show that the highest molar concentration of RWT in the column pore water is located in the region directly surrounding and vertically above the injection filter. This zone of over 1000µM/m^3 molar concentration extends vertically from the injection filter to around 550mm from the base of the column with an approximate maximum diameter of 300mm at level D. The zone of 100-1000µM/m^3 has an approximate maximum diameter of 600mm at level D and extends vertically from the base of the column to a central point just below level A. The zone of 10-100µM/m^3 has maximum approximate diameter of 750mm at the base of the column, extending vertically beyond level A.

Figure 7.1 shows the molar concentration in µM/m^3 of rhodamine water tracer in sample port levels A, B, C, D and E after five hours continuous injection in large-scale test column 1.

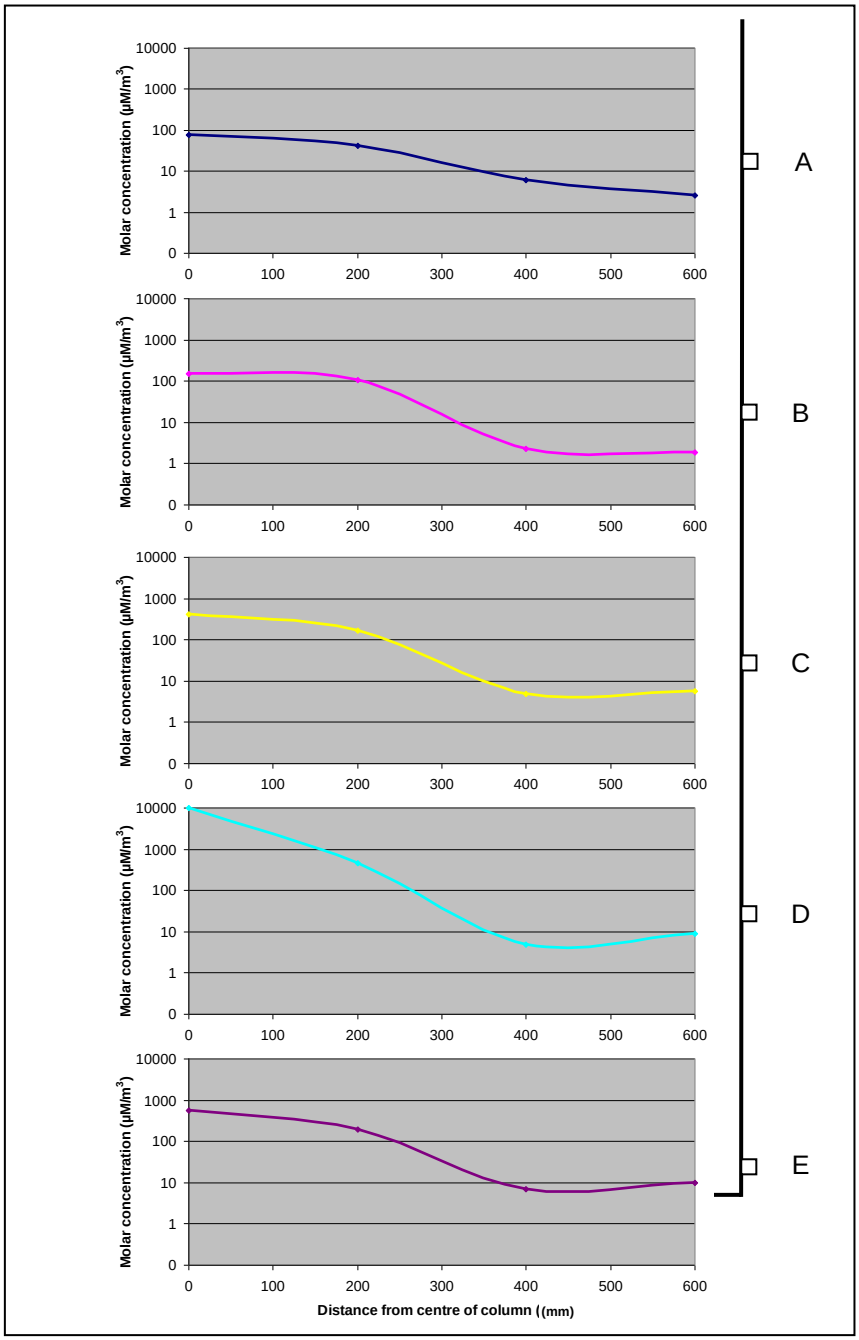

FIGURE 7.1. MOLAR CONCENTRATION OF RHODAMINE WATER TRACER IN SAMPLE LEVELS A, B, C, D AND E IN LARGE-SCALE TEST COLUMN 1.

Figure 7.2 shows the estimated molar concentration distribution of rhodamine water tracer, in µM/m^3, after five hours continuous injection in large-scale test column 1, in both plan and cross-section view.

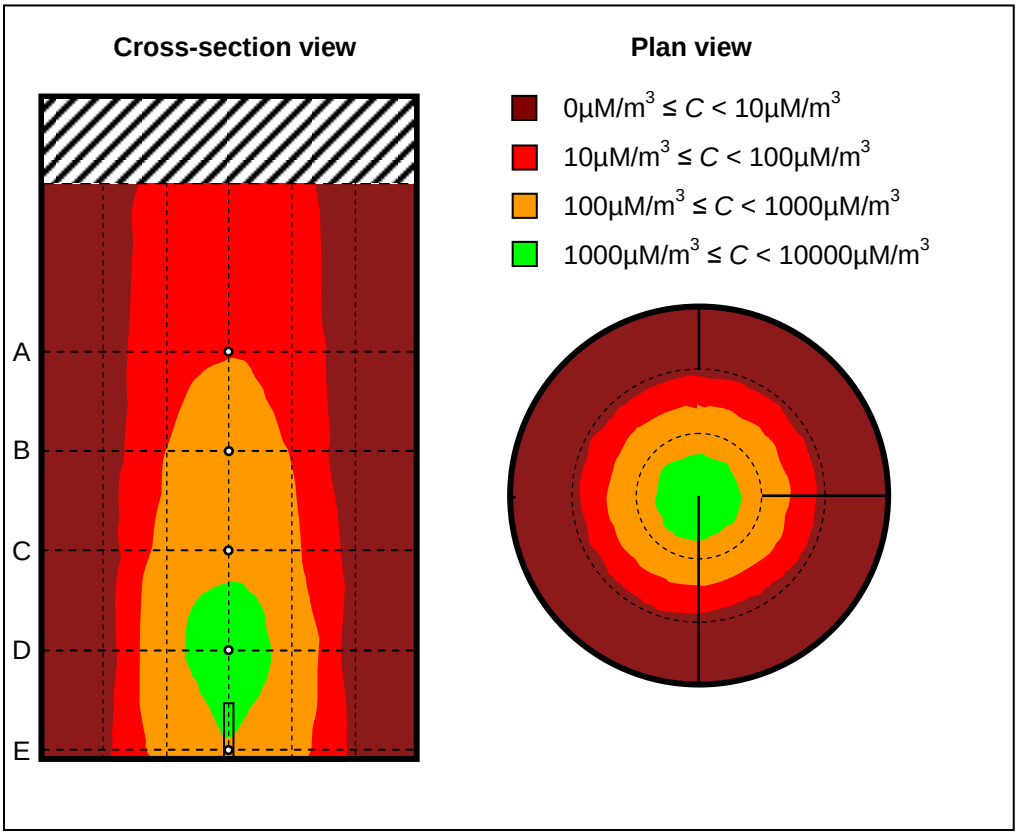

FIGURE 7.2. ESTIMATED MOLAR CONCENTRATION DISTRIBUTION OF RHODAMINE WATER TRACER IN LARGE-SCALE TEST COLUMN 1.

7.3.3. *Test 2*

At 0mm radial distance, limited RWT presence is recorded at levels D and E with all other levels exhibiting no definite tracer presence. At 200mm radial distance levels C, D and E are now defined as having moderate presence of RWT and levels A and B as having limited presence of the tracer. At 400mm radial distance levels D and E are now defined as showing good presence of the tracer with all other levels defined as moderate presence. At 600mm radial distance, the centre of the column, levels C, D and E exhibit good presence of RWT and levels A and B show moderate presence.

The distribution appears to show that the highest molar concentration of RWT in the column pore water is located in the region directly surrounding the injection filter. The zone of molar concentration greater than 1000µM/m^3 can be seen to have an approximate maximum diameter of 300mm at level D which extends vertically from the injection filter to around 500mm from the base of the column. The zone of molar concentration 100-1000µM/m^3 has an approximate maximum diameter of 800mm at the base of the column extending vertically to a central point some 100mm below level A. A zone of molar concentration 10-100µM/m^3 can be seen to spread to the walls of the column at its base, extending vertically to the top of the saturated zone however appearing to narrow above level D and then slightly widening again above level B.

Figure 7.3 shows the molar concentration in µM/m^3 of rhodamine water tracer in sample port levels A, B, C, D and E after five hours pulsed injection in large-scale test column 2.

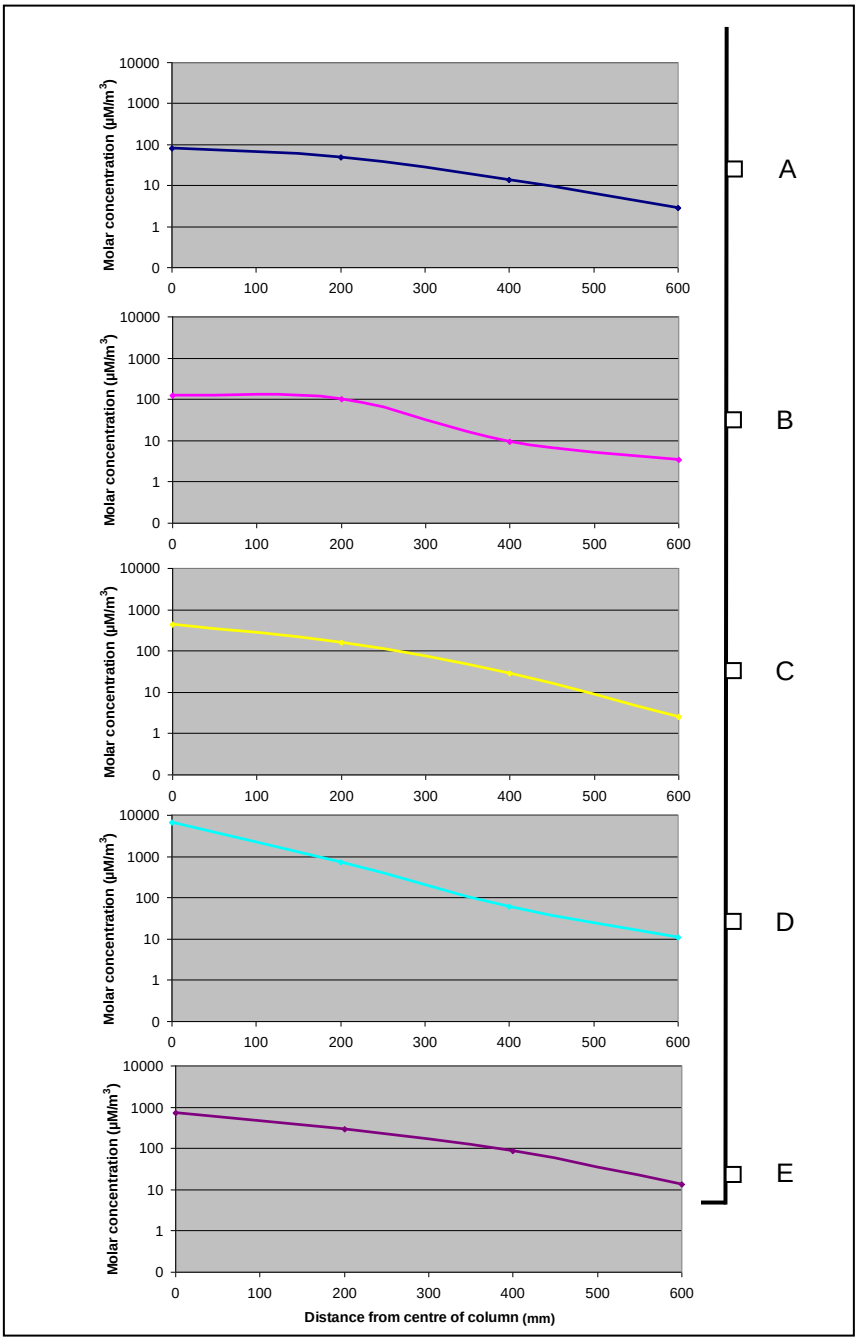

FIGURE 7.3. MOLAR CONCENTRATION OF RHODAMINE WATER TRACER IN SAMPLE LEVELS A, B, C, D AND E IN LARGE-SCALE TEST COLUMN 2.

Figure 7.4 shows the estimated molar concentration distribution of rhodamine water tracer, in $\mu M/m^3$, after five hours pulsed injection in large-scale test column 2, in both plan and cross-section view.

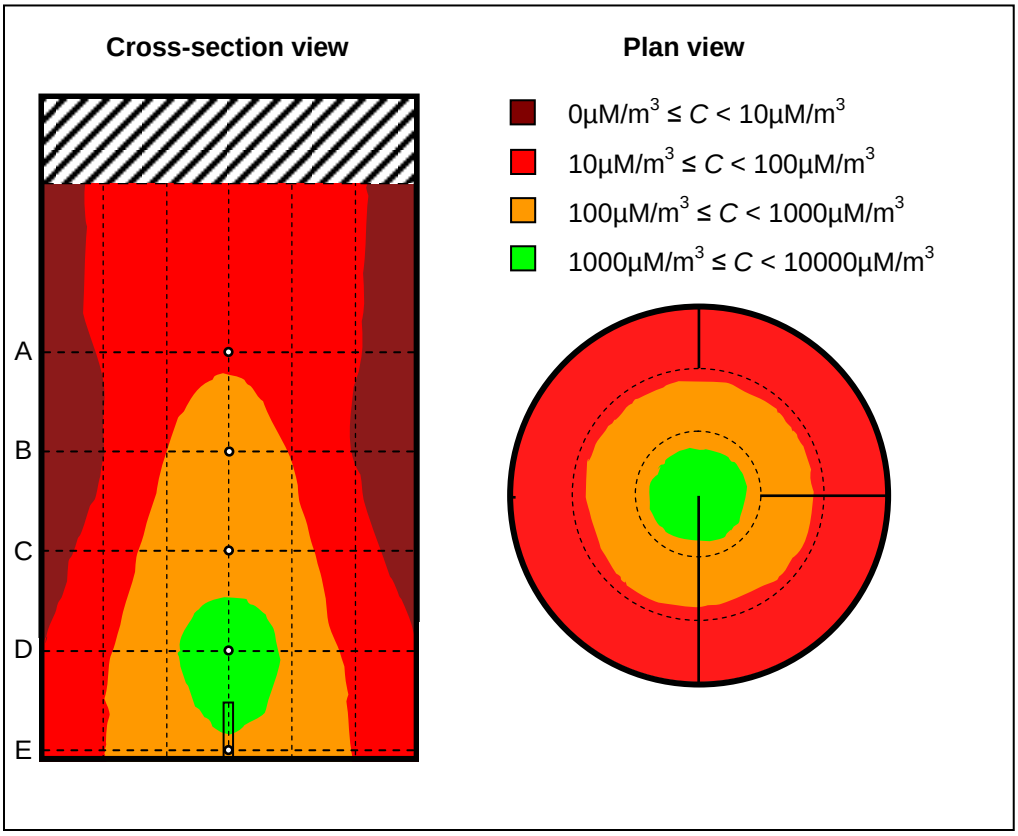

FIGURE 7.4. ESTIMATED MOLAR CONCENTRATION DISTRIBUTION OF RHODAMINE WATER TRACER IN LARGE-SCALE TEST COLUMN 2.

7.3.4. *Test 3*

At 0mm radial distance, limited RWT presence is recorded in all levels. At 200mm radial distance levels C, D show no definite presence of RWT with levels A, B and E exhibiting limited presence of the tracer. At 400mm radial distance levels C, D and E are defined as showing moderate presence of the tracer with level B defined as moderate presence and level a defined as limited presence. At 600mm radial distance, the centre of the column, levels C and D exhibit good presence, level E moderate presence and levels A and B show limited presence of RWT.

The distribution again appears to show that the highest molar concentration of RWT in the column pore water is located in the region directly surrounding the injection filter. No zone of molar concentration greater than 1000µM/m^3 can be seen for this test as this concentration was not detected in any sample ports. The zone of molar concentration 100-1000µM/m^3 has an approximate maximum diameter of 320mm at level D and can be seen to extend vertically from the injection filter to around 750mm above the base of the column. The zone of molar concentration 10-100µM/m^3 has an approximate maximum diameter of 830mm below level B and can be seen to extend vertically from the base of the column to a central point just above level A.

Figure 7.5 shows the molar concentration in µM/m^3 of rhodamine water tracer in sample port levels A, B, C, D and E after five hours continuous injection in large-scale test column 3.

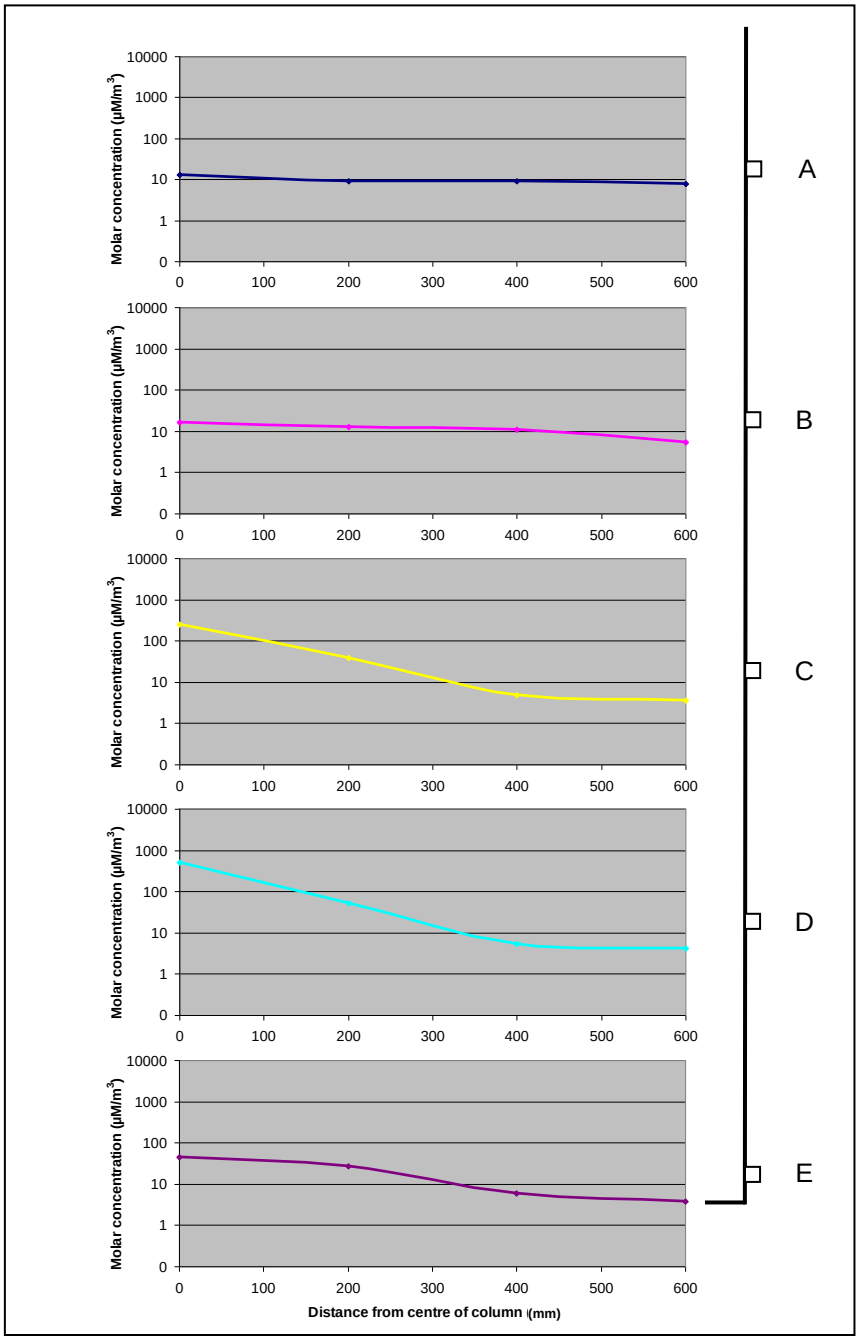

FIGURE 7.5. MOLAR CONCENTRATION OF RHODAMINE WATER TRACER IN SAMPLE LEVELS A, B, C, D AND E IN LARGE-SCALE TEST COLUMN 3.

Figure 7.6 shows the estimated molar concentration distribution of rhodamine water tracer, in $\mu M/m^3$, after five hours continuous injection in large-scale test column 3, in both plan and cross-section view.

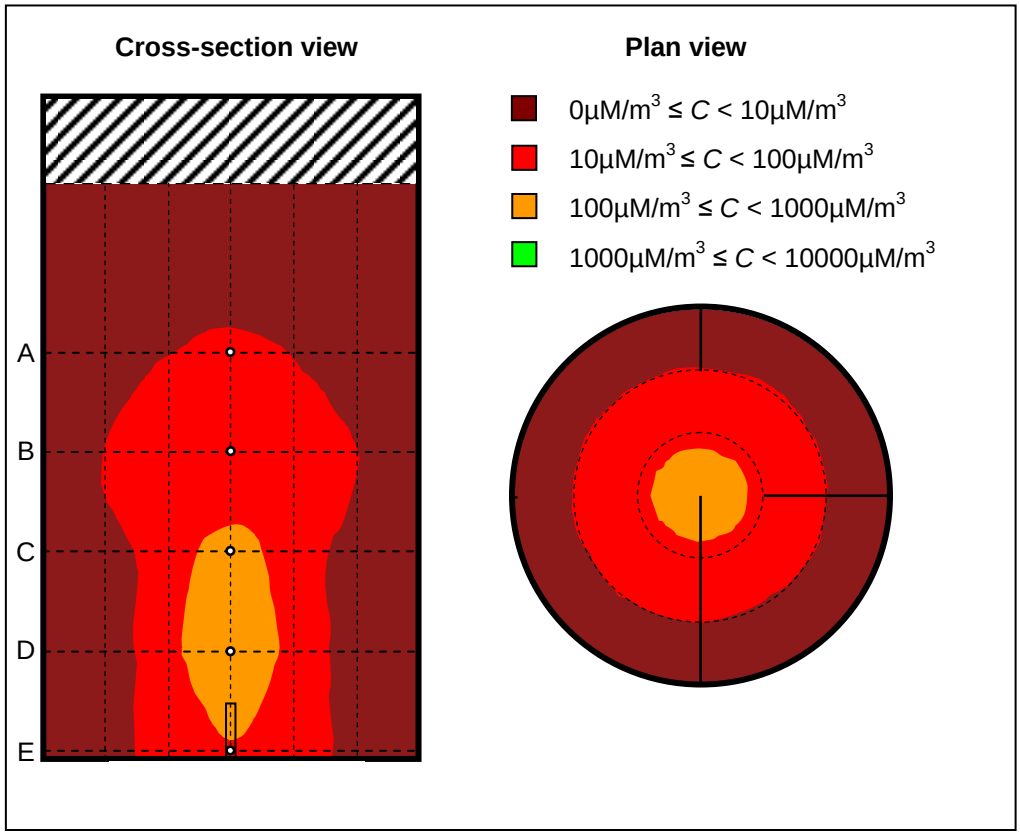

FIGURE 7.6. ESTIMATED MOLAR CONCENTRATION DISTRIBUTION OF RHODAMINE WATER TRACER IN LARGE-SCALE TEST COLUMN 3.

7.3.5. *Test 4*

At 0mm radial distance, limited tracer presence is recorded at levels C, D and E with levels A and B exhibiting no definite tracer presence. At 200mm radial distance all levels are defined as having limited presence of the RWT tracer. At 400mm radial distance level D is defined as showing moderate presence of the tracer with all other levels defined as limited presence. At 600mm radial distance, the centre of the column, level D exhibits good presence, levels A and B and C showing moderate presence and level E showing limited presence.

The distribution again appears to show that the highest molar concentration of RWT in the column pore water is located in the region directly surrounding the injection filter. The zone of molar concentration greater than 1000µM/m^3 can be seen to be somewhat smaller than the previous two tests. It has an approximate maximum diameter of 110mm at level D an extends vertically from the injection filter to around 400mm from the base of the column. The zone of molar concentration 100-1000µM/m^3 has an approximate maximum diameter of 500mm at level D and extends vertically from the injection filter to a central point approximately 20mm above level C. The zone of molar concentration 10-100µM/m^3 extends vertically from the base of the column to just above level A and has an approximate maximum diameter of 910mm just below level B.

Figure 7.7 shows the molar concentration in µM/m^3 of rhodamine water tracer solution in sample port levels A, B, C, D and E after five hours pulsed injection in large-scale test column 4.

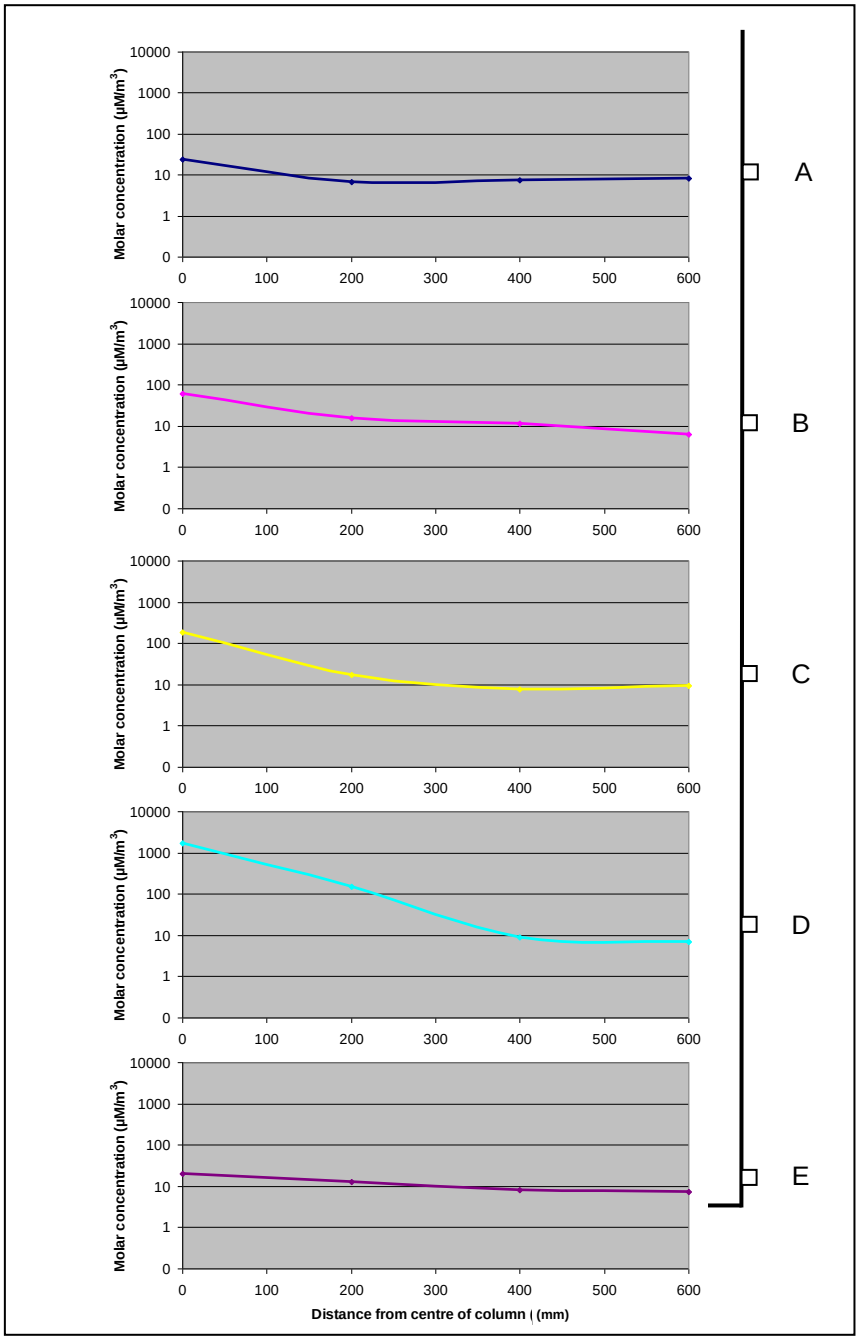

FIGURE 7.7. MOLAR CONCENTRATION OF RHODAMINE WATER TRACER IN SAMPLE LEVELS A, B, C, D AND E IN LARGE-SCALE TEST COLUMN 4.

Figure 7.8 shows the estimated molar concentration distribution of rhodamine water tracer, in µM/m^3, after five hours pulsed injection in large-scale test column 4, in both plan and cross-section view.

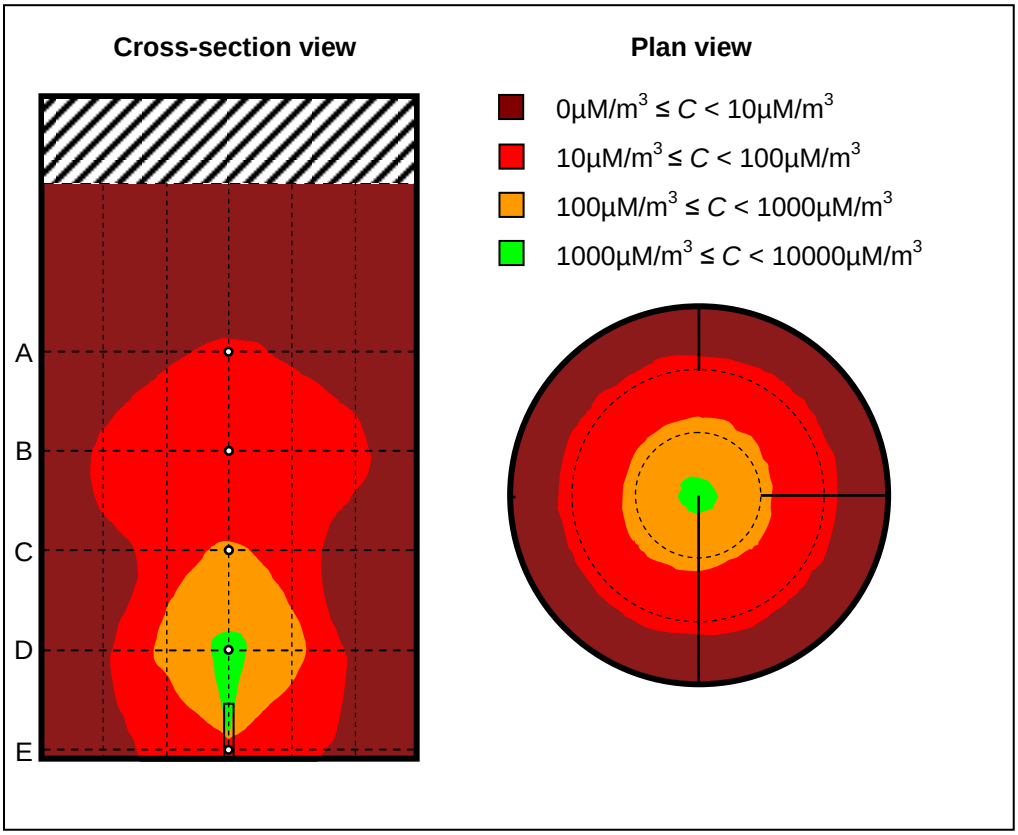

FIGURE 7.8. ESTIMATED MOLAR CONCENTRATION DISTRIBUTION OF RHODAMINE WATER TRACER IN LARGE-SCALE TEST COLUMN 4.

7.3.6. *Test 5*

At 0mm radial distance, limited RWT presence is recorded at level D with all other levels exhibiting no definite tracer presence. At 200mm radial distance levels A and E are defined as having limited presence of RWT with all other levels exhibiting no definite tracer presence. At 400mm radial distance levels C and D are now defined as showing moderate presence of the tracer with all other levels defined as limited presence. At 600mm radial distance, the centre of the column, level D exhibits good presence, level C and E show moderate presence and levels A and B show limited presence of RWT.

The distribution again appears to show that the highest molar concentration of RWT in the column pore water is located in the region directly surrounding the injection filter. There is no zone of molar concentration greater than 1000µM/m^3 as this concentration was not recorded in any sample port. The zone of 100-1000µM/m^3 has an approximate maximum diameter of 400mm at level D and extends vertically from the injection filter to a point 180mm above level D. The zone of 10-100µM/m^3 has an approximate maximum diameter of 720mm at the base of the column and extends vertically to a point above level A.

Figure 7.9 shows the molar concentration in µM/m^3 of rhodamine water tracer solution in sample port levels A, B, C, D and E after five hours continuous injection in large-scale test column 5.

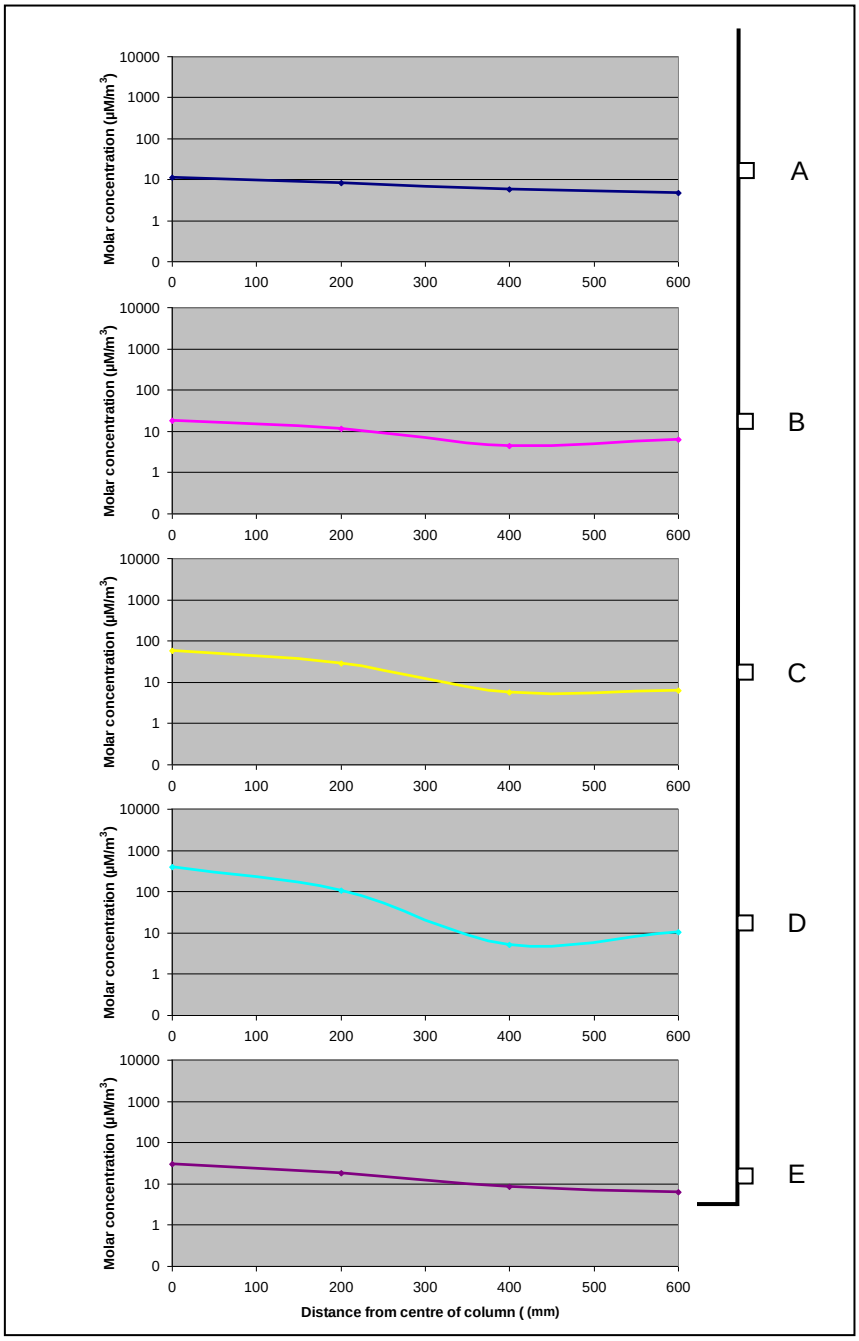

FIGURE 7.9. MOLAR CONCENTRATION OF RHODAMINE WATER TRACER IN SAMPLE LEVELS A, B, C, D AND E IN LARGE-SCALE TEST COLUMN 5.

Figure 7.10 shows the estimated molar concentration distribution of rhodamine water tracer, in µM/m^3, after five hours continuous injection in large-scale test column 5, in both plan and cross-section view.

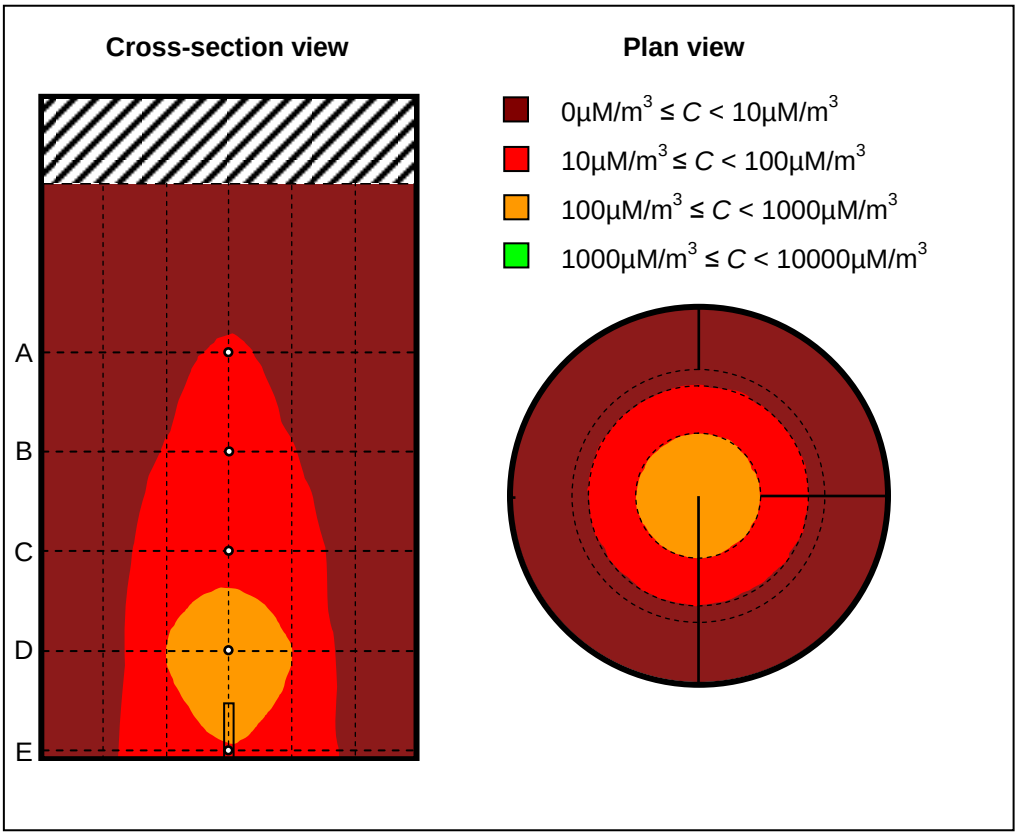

FIGURE 7.10. ESTIMATED MOLAR CONCENTRATION DISTRIBUTION OF RHODAMINE WATER TRACER IN LARGE-SCALE TEST COLUMN 5.

7.3.7. *Test 6*

At 0mm radial distance, limited RWT presence is recorded at levels C, D and E with levels A and B exhibiting no definite tracer presence. At 200mm radial distance levels B, C and D are defined as having limited presence of RWT and levels A and E as having no definite presence of the tracer. At 400mm radial distance levels C and D are now defined as showing moderate presence of the tracer with all other levels defined as limited presence. At 600mm radial distance, the centre of the column, level D exhibits good presence, levels B and C show moderate presence and levels A and E show limited presence of RWT.

The distribution again appears to show that the highest molar concentration of RWT in the column pore water is located in the region directly surrounding the injection filter. The small zone of molar concentration greater than 1000µM/m^3 can be seen to extend vertically from the injection filter to sampling level D with a maximum approximate of diameter of 30mm. The zone of molar concentration 100-1000µM/m^3 has an approximate maximum diameter of 450mm at level D and extends vertically from the injection filter to a central point just below level C. The zone of 10-100µM/m^3 has an approximate maximum diameter of 780mm at level D and extends from the base of the column to a point 150mm above level B.

Figure 7.11 shows the molar concentration in µM/m^3 of rhodamine water tracer in sample port levels A, B, C, D and E after five hours pulsed injection in large-scale test column 6.

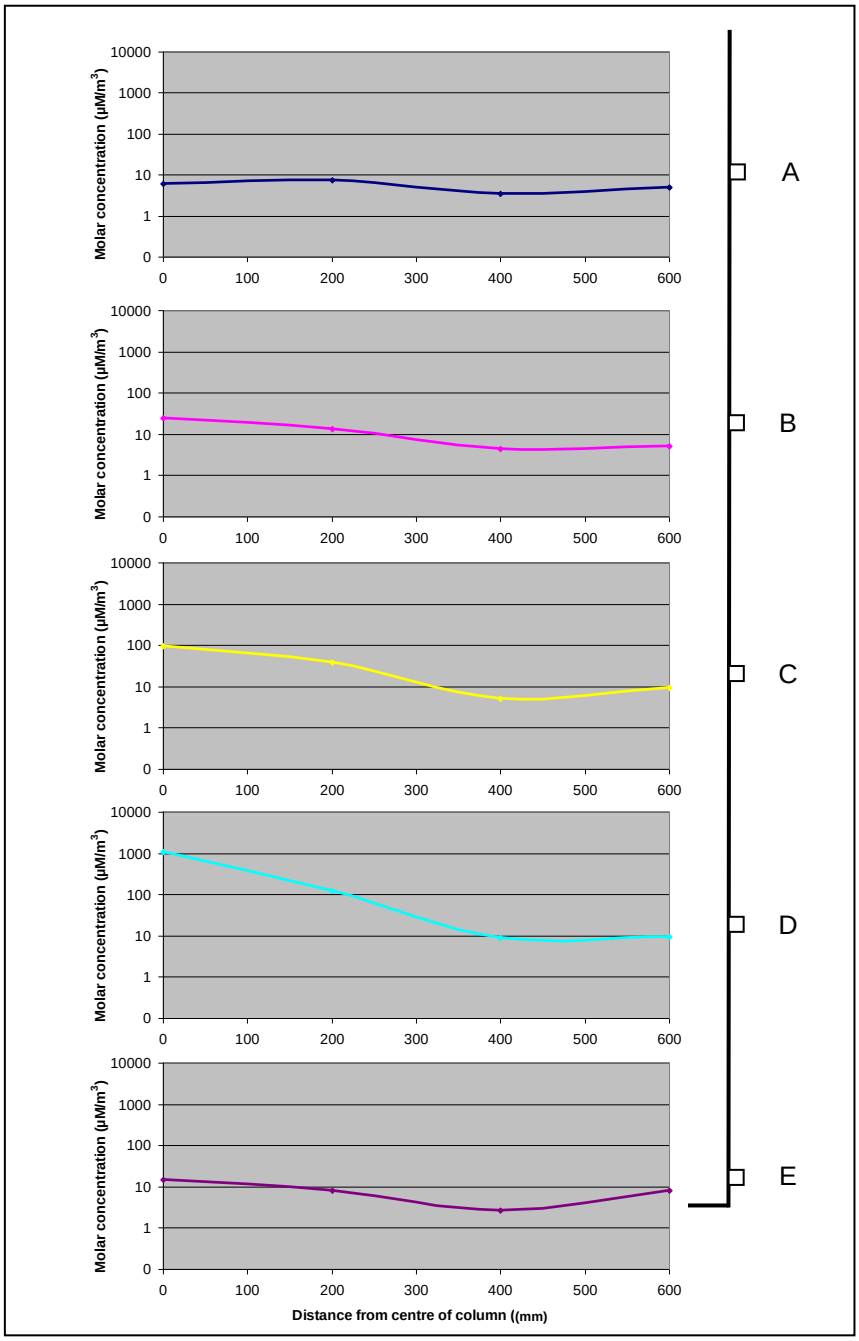

FIGURE 7.11. MOLAR CONCENTRATION OF RHODAMINE WATER TRACER IN SAMPLE LEVELS A, B, C, D AND E IN LARGE-SCALE TEST COLUMN 6.

Figure 7.12 shows the estimated molar concentration distribution of rhodamine water tracer, in µM/m^3, after five hours pulsed injection in large-scale test column 6, in both plan and cross-section view.

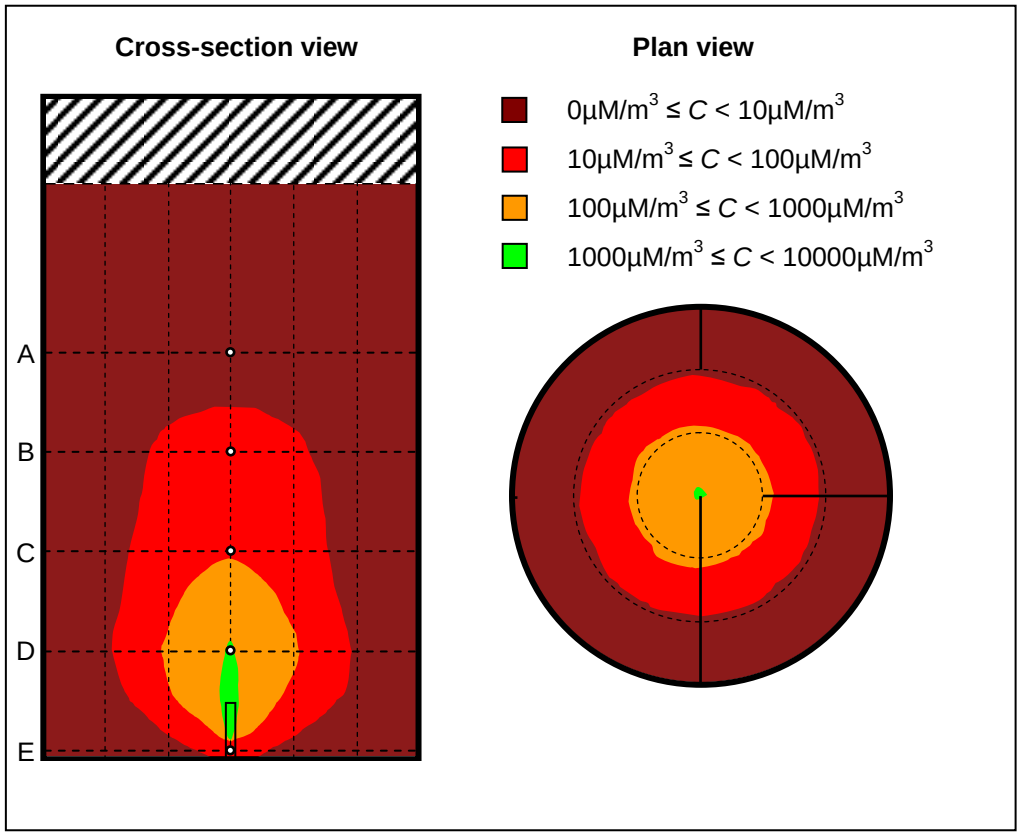

FIGURE 7.12. ESTIMATED MOLAR CONCENTRATION DISTRIBUTION OF RHODAMINE WATER TRACER IN LARGE-SCALE TEST COLUMN 6.

7.4. *Interim Conclusions*

The results from the large-scale test column illustrate the feasibility of using medical jet nebulisers to atomise and deliver fine droplets to a coarse-grained, fully saturated sand. As expected, the highest concentrations of rhodamine water tracer were located in the region directly surrounding and above the subsurface injection filter.

Test columns 1 and 2 record rhodamine water tracer concentrations greater than 1000µg/l in sample port D at 600mm radial distance. This magnitude of concentration is consistent with the concentration of methanol that was found to successfully stimulate reductive dechlorination of TCE, in laboratory studies carried out by Freedman and Gossett (1989) who found 2mg/l of methanol to be 13 times the required concentration to stimulate bioremediation. However the same results indicate a magnitude of molar concentration of lactate some two orders of magnitude lower than those used by De Bruin *et al* (1992) and Jayaraj *et al* (2003) in laboratory batch experiments who both used concentrations of 1mM ($1M/m^3$). Tests 1 and 2 also record molar concentrations some 2 to 3 orders of magnitude lower than the molar concentrations of lactate, formate, acetate and glucose that were found to be successful electron donors by Gerritse *et al* (1997).

Results from Tests 3, 4, 5 and 6 generally show an overall lower level of molar concentration than recorded in test columns 1 and 2. Sample results for each of the six tests indicate that, after a period of five hours injection, the highest concentration of rhodamine tracer is located generally in the region directly surrounding and vertically above the injection filter. This is supported by the fact that maximum molar concentration differences for all tests were in the region of 0.99, indicting that the tracer inside the column was exceptionally non-uniformly distributed. As the vertical and lateral distance from the injection filter increases, tracer concentration rapidly decreases and is often difficult to reliably measure at the lateral boundary of the column, particularly at sample levels A and B. This phenomenon would suggest that proportional deposition of droplets released from the Cirrus™ nebuliser is relatively high in coarse-grained saturated granular soil.

An increase in injection pressure appears to reduce the overall concentration levels in the column after the five hour injection period. This phenomenon is likely to be caused by the combined effect of two factors. As discussed in Chapter 2.4.2, an increase in air inlet pressure to the nebulisers results in a decrease in the mass median diameter of the

droplets released due to higher shear forces in the nebuliser's internal mixing chamber. In theory this should lead to greater droplet transportation through the soil and subsequent loss of very fine droplets from the top of the column to atmosphere. An increase in injection pressure should also lead to an increase in air channel density in the column, allowing a greater proportion of droplets to be transported through the soil matrix. This is supported by the fact that increasing nebuliser pressure markedly increases the volume of pore-water displaced from the column which is a direct indicator of the size of the air plume inside the column.

Molar concentration cross-section plots appear to indicate that lateral distribution of tracer in the column is limited to a greater degree than vertical distribution. This phenomenon is due to the fact that buoyancy forces tend to manipulate air channels towards the vertical, shaping the air plume and consequent location of air channels in the column. The shape of the zone in which RWT appears to have been deposited is in good agreement with the shapes of the air plumes observed by Ji *et al* (1993), McCray and Falta (1996), Elder and Benson (1999) and Reddy and Adams (2001) in laboratory tests performed in similar material to the sand used for the large-scale column tests.

Pulsing the injection of the atomised rhodamine tracer dye appears to create larger radii of influence, characterised by improved lateral distribution when compared to continuous injection. As discussed in Chapter 2.3.1.2, the observations of Boelsma *et al* show this is likely to be due to the theory that pulsing injection of air into the saturated soil creates a number of new air channels each time injection recommences, thus increasing the distribution of air channels and therefore droplet distribution in the column. These observations are supported by the fact that the volume of pore-water displaced, and hence the volume of the air plume during injection, was consistently larger for pulsed injection tests when compared to continuous injection tests at the same injection pressure. The additional benefit of pulsing gas injection into the subsurface is the encouragement of the redistribution of the contaminant in the groundwater aquifer which is beneficial to the bioremediation process (Boelsma *et al*, 2000).

To conclude, the aforementioned large-scale column experiment results have indicated that the injection of atomised liquid into a fully-saturated, coarse-grained sand is possible using medical jet nebuliser technology, however the distribution of the injected droplets is largely restricted to the region directly surrounding the injection filter. For all tests, the vertical, and particularly the lateral transportation, of rhodamine droplets in the column was noted to be somewhat limited. This suggests that the droplet size distribution released by the nebulisers is not sufficiently small to efficiently penetrate the pore spaces of a coarse-grained granular soil. Increasing the injection pressure appears to reduce the overall concentration levels in the column, a possible indicator that a proportion of droplets are being transported the entire length of the column and released to atmosphere. Pulsing the injection of the air appears to improve lateral distribution of the tracer droplets slightly however overall molar concentration differences, a measure of the non-uniformity of the tracer deposition, in the column are still relatively large.

CHAPTER 8. DISCUSSION AND CONCLUSIONS

8.1. *Chapter Synopsis*

This chapter analyses and discusses the results of the laboratory experiments presented in Chapters 5, 6 and 7. The aim of the research was to investigate the possibility of delivering atomised carbon substrate to the saturated subsurface to stimulate the in situ bioremediation of chlorinated solvents. It was anticipated that the droplet diameter required to penetrate the small, tortuous pore spaces of a medium-grained granular soil would have to be in the magnitude of 1-10μm. Medical jet nebulisers were identified as potential atomisers to satisfy the above requirements as they are specifically designed to produce droplets sufficiently small penetrate the alveolar regions of the human lung, having a similar diameter to pore sizes in medium-grained granular material.

Small-scale experiments focused on establishing the droplet size distribution of two atomised carbon substrates, methanol and ethyl lactate, having been transported through coarse and medium-grained granular material under dry and field capacity saturation conditions. Two separate medical jet nebulisers were used to atomise and deliver the substrates to the porous media.

Medium-scale experiments concentrated on quantifying the vertical transportation of atomised liquid through a fully saturated, medium-grained granular material using two separate medical jet nebulisers. A fluorescent tracer dye was used to determine the concentrations of transported droplets in pore water.

Large-scale experiments developed the work carried out in the medium-scale experiments to more realistically simulate anticipated conditions in a full-scale field installation. A large test column was designed and constructed to measure the vertical and lateral distribution of an atomised tracer dye in a fully-saturated, coarse-grained sand.

8.2. *Droplet Size Distribution Experiments*

A number of comparisons can be made about the atomisation and transportation of droplets from the two medical jet nebulisers, Microcirrus™ and Cirrus™ in different media. The simplest comparison is the range of droplet sizes using the parameters $d_{0.1}$, (the diameter at which 10% of the total volume of the spray is below), $d_{0.5}$, (the diameter at which 50% of the total volume of the spray is below), $d_{0.9}$, (the diameter at which 90% of the total volume of the spray is below).

A comparison of droplet sizes released by the Microcirrus™ and Cirrus™ nebulisers to atmosphere confirms that finer droplets were produced by Microcirrus™ nebuliser. The results show that atomisation of ethyl lactate produced a marginally finer droplet distribution than for methanol, however the $d_{0.1}$ size is equivalent. The most significant difference in droplet size is the type of nebuliser and not the substrate with the Microcirrus™ nebuliser producing the finer droplet size distribution.

The results for the transportation of atomised methanol and ethyl lactate transported through ballotini identify a number of features:

1. the $d_{0.9}$ value for droplets released to atmosphere is noticeably smaller when compared with atomised substrate transported through 3mm and 4mm ballotini, especially for ethyl lactate atomised by the Microcirrus nebuliser. This phenomenon could indicate that the droplets collided when transported through the ballotini to coalesce and become larger;

2. in contrast the $d_{0.1}$ size appears to be fairly consistent when released to atmosphere and when transported through dry or wetted ballotini;

3. wetting the ballotini to field condition did not appear to have a consistent affect on droplet size distribution. An exception is the transportation of methanol

droplets through wetted 4mm ballotini. In addition the $d_{0.9}$ size measured for transportation of methanol droplets through 2mm dry ballotini is noticeably low compared to similar measurements for transportation of atomised ethyl lactate through similar size ballotini.

These observations suggest that the main consequence of transporting atomised carbon substrate droplets through a coarse porous media is for droplets to coalesce into large size droplets and hence increase the $d_{0.9}$ size. Fully wetting the ballotini did not appear to significantly change the droplet size distribution except in one case (4mm, field ballotini). The results appear to confirm the feasibility of transporting a droplet size of 0.5 to 3.0µm through the pore spaces of coarse-grained sand.

In comparison with the results obtained for transportation through ballotini, the corresponding droplet size distribution measured following transportation of fine droplets of ethyl lactate or methanol released by the Microcirrus™ nebuliser through dry and wetted fine gravel or coarse sand size particles allow the following observations to be made:

1. the wetting of gravel and sand particles generally had the effect of reducing the $d_{0.1}$ $d_{0.5}$ and $d_{0.9}$ sizes for methanol and ethyl lactate, particularity $d_{0.9}$ size in the fine-grained gravel sample;

2. the $d_{0.9}$ values of substrate atomised by the Microcirrus nebuliser and transported through the fine gravel soil column samples increased when compared with release to atmosphere. Similar to the results for ballotini the results would suggest that the porous media had the effect on coalescing the droplets into large droplets sizes;

3. the droplet size distribution appears remarkably similar for droplets of atomised liquids released into air compared with transportation through wetted coarse

sand, this might suggest that there was negligible impaction or deposition of droplets on the surface of sand particles however further data would be needed on the volume or weight loss of injected liquid into the sand sample to confirm such a conclusion.

In comparison with the data reviewed for the transportation of droplets produced by the Microcirrus™ nebuliser, a similar data set for droplets produced by the Cirrus™ nebuliser was produced. The most noticeable differences between the two data sets is the marked decrease in $d_{0.9}$ for droplets released by the Cirrus™ nebuliser when transported through gravel and sand compared with direct release to atmosphere. Importantly, the results suggest that the maximum droplet size for transportation through coarse-grained sand is approximately 2.5µm. Interestingly a diameter of 2.5µm is understood to be the droplet size that would typically be deposited in the trachea and alveoli of the human respiratory system when attempting to administer an atomised liquid drug solution.

The droplet size distribution experimental results provide convincing evidence for the possibility of transporting atomised carbon substrates through fine-grained gravel and coarse-grained sand under both dry and field conditions using Cirrus™ and Microcirrus™ medical jet nebulisers. In summary, there are two main outcomes from the test data:

1. the data demonstrate the feasibility of transporting atomised droplets of ethyl lactate and methanol through dry and fully wetted samples of gravel and sand size particles of soil and ballotini, which bodes well for the use of medical nebulisers to transport similar size droplets of liquid chemicals or for that matter bacterium through the vadose zone.

2. the droplet size distribution data indicate a maximum droplet size for transportation through wetted or dry sand and gravel of approximately 2.5µm,

which coincidently agrees with the droplet size understood in medical literature to be deposited in the trachea and alveoli of the human respiratory system.

8.3. *Medium-scale Test Column Experiments*

The aforementioned experiments were designed to give provisional insight into the feasibility of using medical jet nebulisers to atomise and deliver fine droplets to fully-saturated coarse-grained sand, after promising results from small-scale droplet size distribution tests. The experiments also allowed design considerations to be made for planned large-scale column tests using the same granular material.

As anticipated, for both the Cirrus™ and Microcirrus™ nebuliser, rhodamine water tracer concentration and molar concentration plots suggest that the majority of the injected droplets are deposited at the base of the column, in the region directly surrounding the injection filter. In all eight test columns, a definite presence of RWT was measured at all sampling levels by the end of the injection period. Tests conducted with the Cirrus™ nebuliser indicated that this device achieved higher overall RWT concentrations in the column. This phenomenon is due, in part, to the fact that it releases a higher volume of droplets per minute, however the most likely explanation is that the Cirrus™ nebuliser has a droplet size distribution with a higher $d_{0.9}$ value relative to that of the Microcirrus™ nebuliser.

Maximum molar concentration differences between the bottom and top sampling levels in the column support this theory as the Microcirrus™ nebuliser appears to be able to deliver a more uniform RWT distribution when compared to the Cirrus™ nebuliser. This is possibly due to the fact that the Microcirrus™ nebuliser generally releases droplets with a smaller droplet size distribution, in particular a smaller $d_{0.9}$ value and these droplets are less likely to deposit in pore spaces and therefore penetrate greater distances from the injection filter.

While it was not possible to calculate the total volume of tracer deposited in the column, no droplets were seen to leave any of the test columns, suggesting that the deposition rate of droplets in fully-saturated media may be significantly higher than in dry or field condition media. This is possibly due to increased droplet deposition as a result of decreased pore space in the saturated soil as well as an increase in the vertical length of the sample.

Absolute molar concentration values in the medium-scale column do not compare favourably with the molar concentrations of various carbon substrates used in laboratory studies by researchers such as Freedman and Gossett (1989), De Bruin *et al* (1992), DiStefano *et al* (1992), Gerritse *et al* (1997) and Jayaraj *et al* (2003). It must be noted however that the volume of substrate injected in each test was relatively low compared to the anticipated injection volumes in a field installation. It is probable that a successful field installation would utilise a number of nebulisers to achieve significantly higher rates of substrate delivery. It is apparent from these tests however that medical jet nebulisers have the capability to transport gas bubbles in soil samples of coarse sand of vertical height approximately 1m, without the need for auxiliary gas flow into the column. Capillary pressures in these soils are relatively low and this, coupled with a hydrostatic pressure of approximately 10kPa, allows vertical transportation of the gas/droplet mixture. It remains to be seen how the nebulisers would perform at greater hydrostatic pressures and in finer grained material.

The results produced by the Microcirrus™ nebuliser were, at times, erratic. The Microcirrus™ nebuliser appears to perform relatively poorly when operated at continuous, relatively high air inlet pressures, as demonstrated in test column 5 when tracer concentrations during injection in the column were particularly inconsistent and final concentrations were found to be relatively low when compared to other tests. For this reason, the Cirrus™ nebuliser was selected for the planned large-scale column tests.

In summary, the experimental results recorded in this chapter indicate the possibility of using commercially available medical jet nebulisers to atomise and deliver fine droplets to a fully-saturated coarse grained sand on a relatively small scale. The deposition of droplets in the granular material appears to be relatively high, particularly in the region directly surrounding the injection filter, where tracer dye concentrations were typically two orders of magnitude higher than at the highest sample port of the column. This suggests that the droplets released by medical jet nebulisers may not be sufficiently small to efficiently penetrate the pore spaces of granular material under fully-saturated conditions. Another possibility is that the gas channels created in the granular media are not sufficiently large or stable to allow effective droplet transportation.

8.4. *Large-scale Test Column Experiments*

The aim of the large-scale test column experiments was to establish the possibility of injecting atomised liquids into a fully saturated granular material as close as possible to anticipated field conditions. Although the size of the column could not completely simulate the depth and radius of influence of an anticipated field pilot study it was still possible to draw valuable conclusions from the test results. The results from the large-scale test column illustrate the feasibility of using medical jet nebulisers to atomise and deliver fine droplets to a coarse-grained, fully saturated sand. As expected, the highest concentrations of rhodamine water tracer were located in the region directly surrounding and above the subsurface injection filter.

Test columns 1 and 2 record rhodamine water tracer concentrations greater than 1000µg/l in sample port D at 600mm radial distance. This magnitude of concentration is consistent with the concentration of methanol that was found to successfully stimulate reductive dechlorination of TCE, in laboratory studies carried out by Freedman and Gossett (1989) who found 2mg/l of methanol to be 13 times the required concentration to stimulate bioremediation. However the same results indicate a magnitude of molar concentration of lactate some two orders of magnitude lower than those used by De

Bruin *et al* (1992) and Jayaraj *et al* (2003) in laboratory batch experiments who both used concentrations of 1mM ($1M/m^3$). Tests 1 and 2 also record molar concentrations some 2 to 3 orders of magnitude lower than the molar concentrations of lactate, formate, acetate and glucose that were found to be successful electron donors by Gerritse *et al* (1997).

Results from Tests 3, 4, 5 and 6 generally show an overall lower level of molar concentration than recorded in test columns 1 and 2. Sample results for each of the six tests indicate that, after a period of five hours injection, the highest concentration of rhodamine tracer is located generally in the region directly surrounding and vertically above the injection filter. This is supported by the fact that maximum molar concentration differences for all tests were in the region of 0.99, indicting that the tracer inside the column was exceptionally non-uniformly distributed. As the vertical and lateral distance from the injection filter increases, tracer concentration rapidly decreases and is often difficult to reliably measure at the lateral boundary of the column, particularly at sample levels A and B. This phenomenon would suggest that proportional deposition of droplets released from the Cirrus™ nebuliser is relatively high in coarse-grained saturated granular soil.

An increase in injection pressure appears to reduce the overall concentration levels in the column after the five hour injection period. This phenomenon is likely to be caused by the combined effect of two factors. An increase in air inlet pressure to the nebulisers results in a decrease in the mass median diameter of the droplets released due to higher shear forces in the nebuliser's internal mixing chamber. In theory this should lead to greater droplet transportation through the soil and subsequent loss of very fine droplets from the top of the column to atmosphere. An increase in injection pressure should also lead to an increase in air channel density in the column, allowing a greater proportion of droplets to be transported through the soil matrix. This is supported by the fact that increasing nebuliser pressure markedly increases the volume of pore-water displaced

from the column which is a direct indicator of the size of the air plume inside the column.

Molar concentration cross-section plots appear to indicate that lateral distribution of tracer in the column is limited to a greater degree than vertical distribution. This phenomenon is due to the fact that buoyancy forces tend to manipulate air channels towards the vertical, shaping the air plume and consequent location of air channels in the column. The shape of the zone in which RWT appears to have been deposited is in good agreement with the shapes of the air plumes observed by Ji *et al* (1993), McCray and Falta (1996), Elder and Benson (1999) and Reddy and Adams (2001) in laboratory tests performed in similar material to the sand used for the large-scale column tests.

Pulsing the injection of the atomised rhodamine tracer dye appears to create larger radii of influence, characterised by improved lateral distribution when compared to continuous injection. As discussed in Chapter 2.3, the observations of Boelsma *et al* (2000) show this is likely to be due to the theory that pulsing injection of air into the saturated soil creates a number of new air channels each time injection recommences, thus increasing the distribution of air channels and therefore droplet distribution in the column. These observations are supported by the fact that the volume of pore-water displaced, and hence the volume of the air plume during injection, was consistently larger for pulsed injection tests when compared to continuous injection tests at the same injection pressure. The additional benefit of pulsing gas injection into the subsurface is the encouragement of the redistribution of the contaminant in the groundwater aquifer which is beneficial to the bioremediation process (Boelsma *et al*, 2000).

To conclude, the aforementioned large-scale column experiment results have indicated that the injection of atomised liquid into a fully-saturated, coarse-grained sand is possible using medical jet nebuliser technology, however the distribution of the injected droplets is largely restricted to the region directly surrounding the injection filter. For all tests, the vertical, and particularly the lateral transportation, of rhodamine droplets in the

column was noted to be somewhat limited. This suggests that the droplet size distribution released by the nebulisers is not sufficiently small to efficiently penetrate the pore spaces of a coarse-grained granular soil. Increasing the injection pressure appears to reduce the overall concentration levels in the column, a possible indicator that a proportion of droplets are being transported the entire length of the column and released to atmosphere. Pulsing the injection of the air appears to improve lateral distribution of the tracer droplets slightly however overall molar concentration differences, a measure of the non-uniformity of the tracer deposition, in the column are still relatively large.

It is likely however that the design of the test apparatus had an adverse impact on the experimental results as the boundary conditions in the large-scale column are not representative of anticipated conditions in a full-scale field installation. The presence of a solid boundary 600mm from the centre of the column will likely have prevented air channels from extending to their maximum possible radial distance from the injection point. This is turn will have led to droplet transportation and deposition in the saturated medium being significantly limited. While this boundary effect was unavoidable due to the constraints of laboratory testing, it must be noted that the distribution of atomised substrates in a full-scale field operation would likely be markedly improved, provided that other geological conditions were also favourable.

8.5. *Overall Conclusions and Implications for full-scale Field Testing*

The experiments carried out during this research have shown that droplets released by medical jet nebulisers can be transported through medium to coarse-grained granular soils under full saturation conditions. Droplet size distribution measurements using laser diffraction technology showed that the maximum droplets size that can be successfully transported through a granular soil is largely dependant on the diameter of the pore spaces in the material rather than the total path length taken by the droplets

The volume of <10µm droplets released by medical jet nebulisers is relatively small. This is due to the inherent design of the baffle system employed by the devices in order to produce such a small droplet size distribution. While the droplet size produced is sufficiently small to penetrate a medium-grained granular soil, the small volumes released prohibit the effectiveness of the devices as injection periods would have to be in the magnitude of hours to deliver sufficient substrate to the contaminated groundwater. As discussed previously, this length of injection would likely have the undesirable effect of striping contaminants from the saturated zone and releasing them to the vadose zone and atmosphere, representing a serious health risk.

A solution to this problem is to use a large number of nebulisers, thus increasing the volume of droplets. This solution however, would require a large volume of nitrogen gas to run the nebulisers as well as significant maintenance, with a likely result of raising running costs. In addition the pressure created by the large number of devices may be sufficient to initiate liquefaction of the soil, particularly at relatively shallow depths. Further experiments would be required to ascertain the effect on droplet size distribution when several nebulisers are used to transport droplets to the subsurface. It is likely that some droplet coalescence would occur prior to the spray reaching the subsurface due to the large number of droplets contained in a relatively small space. This could have the unwanted effect of making the majority of droplets too large to effectively penetrate the porous media in the subsurface, therefore negating the benefit of increasing the volume of substrate injected. Droplet size distribution measurements could be made using the laser diffraction particle sizer to determine the effect of using such a large number of nebulisers.

In their current form, medical jet nebulisers do not respond well to backpressure as liquid can be forced down the air inlet tubing. This could cause difficulties in situations where backpressure was high, i.e. at relatively deep depths or when soil permeability is low.

The current designs of the Microcirrus and Cirrus nebulisers are clearly suited to producing fine droplets that are able too penetrate the pore spaces of medium to coarse-grained granular material however they are currently not sufficiently robust or durable to withstand the pressure and duration of transporting sprays to the subsurface at significant depths. It is expected that a significant amount of backpressure could be created when sparging gas into a relatively fine-grained granular material or into an injection filter at significant depth below ground level. This would have the unwanted effect of forcing gas and/or liquid substrate back into the air inlet and significantly reducing the volume of droplets being produced by the nebulisers.

A solution to this potential problem would be to remanufacture the nebulisers using a more durable material such as stainless steel and install no return valves downstream of the air inlet points. This would increase the nebulisers resistance to high pressure as well as reducing the possibility of liquid returning into the air inlet due to backpressure.

CHAPTER 9. SUMMARY AND RECOMMENDATIONS FOR FUTURE WORK

9.1. *Summary*

A summary of the main findings of the research into the delivery of atomised substrates for in situ bioremediation of chlorinated solvents in the subsurface are presented below:

- small-scale experiments have proven the possibility of transporting atomised methanol and ethyl lactate through small columns of artificial and natural granular soil using medical jet nebulisers. A laser diffraction particle sizer was used to quantify droplet size distribution of transported aerosol. Transportation of atomised substrate was shown to occur under both dry and field capacity conditions;

- medium-scale experiments illustrated the possibility of transporting droplets through a fully-saturated, coarse-grained sand using medical jet nebulisers. A fluorescent tracer dye, rhodamine WT was used to quantify vertical distribution in a medium-scale test column during an injection period of three hours. Tracer concentration was found to be highest towards the base of the column, in the region directly surrounding the injection filter. The Cirrus nebuliser appeared to deliver droplets to the granular material more effectively than the Microcirrus nebuliser;

- large-scale column experiments showed the possibility atomising and delivering liquid droplets to fully-saturated granular soils. The vertical and lateral distribution of rhodamine WT was quantified in a large-scale test column after an injection period of five hours. The distribution of tracer was found to be generally restricted to the region directly surrounding the injection filter, potentially indicating that the droplet size distribution of aerosols released by

medical jet nebulisers is insufficiently small to effectively penetrate the pore spaces of a fully-saturated, coarse-grained sand.

9.2. *Recommendations for Future Work*

The following recommendations are made for any future experiments into the delivery of atomised carbon substrates for the in situ bioremediation of chlorinated solvents:

- investigation of the possibility of using alternative atomisation technology, such as high pressure humidifiers, to create a larger volume of <1µm droplets, thus potentially increasing the penetration of aerosol into granular soils as well as increasing the volume of substrate injected per minute. This would hopefully lead to increased distribution of the substrates in the subsurface as well as reducing the injection period which can be crucial to avoiding stripping the contaminant into the vadose zone. According to Taulbee and Yu (1975), Darquenne and Pavia (1994) and Schulz (1998) amongst others, the optimum particle size for minimum deposition in the human lung lies between 0.1 and 1µm;

- investigation of the possibility of delivering carbon substrates to the subsurface in the form of a vapour which is then allowed to condense in the subsurface under increased pressure to act as an electron donor. This technique has the potential to overcome the issue of droplet deposition in the region surrounding the injection filter as the substrate will be in the form of a vapour. Efficient methods of vapourising the substrates would need to be extensively investigated.

CHAPTER 10. REFERENCES

ALLMON. W. E, L. G. EVERETT, A. T. LIGHTNER, B. ALLEMAN, T. J. BOYD AND B. J. SPARGO. 1999. *Groundwater Circulating Well Technology Assessment*. Naval Research Laboratory

BALLAPRAGADA. B. S, H. D. STENSEL, J. A. PUHAKKA and J. F. FERGUSON. 1997. *Effect of Hydrogen on Reductive Dechlorination of Chlorinated Ethenes*. Environmental Science and Technology. 31: 1728-1734.

BAYVEL. L and Z. ORZECHOWSKI. 1993. *Liquid Atomisation*. Taylor and Francis.

BAKER. D. M and C. BENSON. 1996. *Review of Factors Affecting In Situ Air Sparging*. American Society of Civil Engineers.

COULSON. J. M and J. F. RICHARDSON. 1962. *Chemical Engineering – Volume 2*, Pergamon Press.

DAHMANI. J. W, A, AHLFELD. D. P, LIN. J. D and HILL III. E. 1993. *Laboratory Study of Air Sparging: Air Flow Visualization*. Ground Water Monitoring and Remediation (Fall). 115-126.

DARQUENNE. C and M. PAVIA. 1994. *One-dimensional Simulation of Aerosol Transport and Deposition in the Human Lung*. Journal of Applied Physiology. 77(6): 2889-2898.

DARQUENNE. C and M. PAVIA. 1996. *Two and Three-dimensional Simulations of Aerosol Transport and Deposition in Alveolar Zone of Human Lung*. Journal of Applied Physiology. 80(4):1401-1414.

DARQUENNE. C. 2001. *Heterogeneity of Aerosol Deposition in a Two-dimensional Model of Human Alveolated Ducts*. Journal of Aerosol Science. 33: 1261–1278.

DAVIES. C. N, J. HEYDER and M. C. SUBBA RAMU. 1972. *Breathing of Half-Micron Aerosols: 1 - Experimental*. Journal of Applied Physiology. 32(5): 591-600.

DE BRIUN. W. P, M. J. J. KOTTERMAN, M. A. POSTHUMUS, G. SCHRAA and A. J. B. ZEHNDER. 1992. *Complete Biological Reductive Transformation of Tetrachloroethene to Ethane*. Applied and Environmental Microbiology. 58(6): 1996-2000.

DISTEFANO. T. D, J. M. GOSSETT and S. H. ZINDER. 1992. *Hydrogen as an Electron Donor for Dechlorination of Tetrachloroethene by an Anaerobic Mixed Culture*. Applied and Environmental Microbiology. 58(11): 3622-3629.

DYER. M, E. MARNETTE, C. SCHUREN, K. van den BRINK and A. van LOON. (2003). *Full Scale Stimulation of Reductive Dechlorination Using the LINER® Technique*, 4th BGA Geoenvironmental Engineering Conference.

ELDER. C. R and C. H. BENSON. 1999. *Air Channel Formation, Size, Spacing and Tortuosity during Air Sparging*. Ground Water Monitoring and Remediation (Summer) 171-181.

ELDER. C. R, C. H. BENSON and G. R. EYKHOLT. 1999. *Modelling Mass Removal During In Situ Air Sparging*. Journal of Geotechnical and Geoenvironmental Engineering. 947-958.

FETZNER. S. 1998. *Bacterial Dehalogenation*. Applied Microbiology and Biotechnology. 50: 633-657.

FENNELL D. E and J. M. GOSSETT. 1997. *Comparison of Butyric Acid, Ethanol, Lactic Acid, and Propionic Acid as Hydrogen Donors for the Reductive Dechlorination of Tetrachloroethene*. Environmental Science and Technology. 31:918-926.

FIELD. J. A and R. SIERRA-ALVAREZ. 2004. *Biodegradability of Chlorinated Solvents and Related Chlorinated Aliphatic Compounds*. University of Arizona.

FREEDMAN. D. L and J. M. GOSSETT. 1989. *Biological Reductive Dechlorination of Tetrachloroethylene and Trichloroethylene to Ethylene under Methanogenic Conditions*. Applied and Environmental Microbiology. 55(9): 2144-2151.

GENNES. P. G. 1985. *Wetting: Statics and Dynamics*. Reviews of Modern Physics. 57(3): 827-861.

GERRITSE. J, O. DRZYZGA, G. KLOETSTRA, M. KEIJMEL, L. P. WIERSUM, R. HUTSON, M. D. COLLINS and J. C. GOTTSCHAL. 1999. *Influence of Different Electron Donors and Acceptors on Dehalorespiration of Tetrachloroethene by Desulfitobacterium frappieri TCE1*. Applied and Environmental Microbiology. 65(12): 5212-522.

GERRITSE. J, G. KLOETSTRA, A. BORGER, G. DALSTRA A. ALPHENAAR and J. C. GOTTSCHAL. 1997. *Complete Degradation of Tetrachloroethene in Coupled Anoxic and Oxic Chemostats*. Applied Microbiology Biotechnology. 48: 553-562.

GIBSON. S. A and G. W. SEWELL. 1992. *Stimulation of Reductive Dechlorination of Tetrachloroethene in Anaerobic Aquifer Microcosms by Addition of Short-Chain Organic Acids or Alcohols*. Applied and Environmental Microbiology. 58(4): 1392-1393.

HALOGENATED SOLVENTS INDUSTRY ALLIANCE INC. 1999. *Perchloroethylene White Paper*. Washington D.C.: Halogenated Solvents Industry Alliance, Inc.

HARKNESS. M. R, M. J. BRENNAN and A. A. BRACCO. 1998. *Stimulation of Complete Reductive Dechlorination of TCE in Strother Soil: Microcosm and Column Studies*. General Electric Company.

HESS. D. R. 2000. *Nebulizers: Principles and Performance.* Respiratory Care 45(6): 609-622.

HIDY. G. M. 1984. *Aerosols: An Industrial and Environmental Science*. Academic Press.

HINCHEE. R. E. 1994. *Air Sparging for Site Remediation*. Lewis.

JAYARAJ. J, R. S. MAKKAR and K. J. ROCKNE. 2003. *A New Electron Donor for Reductive Dechlorination of Perchloroethylene***.** Proceedings of the Seventh International In Situ and On-Site Bioremediation Symposium. A-35.

JI. W, A. DAHMANI, D. P. AHLFIED, J. D. LIN and E. HILL. 1993. *Laboratory Study of Air Sparging: Air Flow Visualization*. Groundwater Monitoring Review. Fall: 115-126.

KAO. C. M and J. PROSSER. 1999. *Intrinsic Bioremediation of Trichloroethylene and Chlorobenzene: Field and Laboratory Studies*. Journal of Hazardous Materials B69: 67-69

KEE. D. D and CHHABRA. 2002. *Transport Processes in Bubbles, Drops and Particles*. Taylor and Francis.

KENDRICK. A. H, E. C. SMITH and R. S. E. WILSON. 1997. *Selecting and Using Nebuliser Equipment*. Thorax. 52(2): S92-S101

KRAUSS. G, D. LAZIK and H. GEISTLINGER. 2003. *Gas Sparging for Bioremediation: Experimental Investigations of Gas Phase Distribution*. Proceedings of 2nd European Bioremediation Conference.

KUEPER. B. H, G. P. WEALTHALL, J. W. N. SMITH, S. A. LEHARNE and D. H. LERNER. 2003. *An Illustrated Handbook of DNAPL Transport and Fate in the Subsurface*. Environment Agency.

LEDERMULLER. R, R. STANGL and M. KNOCH. 2003. *Nebuliser Technology*. Pari GmbH.

LEFEBVRE. A. H. 1989. *Atomization and Sprays*. Hemisphere Publishing Corporation.

LUNDEGARD. P. D and D. LABRECQUE. 1995. *Air sparging in a sandy aquifer (Florence, Oregon, U.S.A.): Actual and apparent radius of influence*. Journal of Contaminant Hydrology. 19: 1-27.

MALVERN INSTRUMENTS LTD. 1997. *Getting Started*. Malvern Instruments. 1(3).

MASSEY. B. M. 1998. *Mechanics of Fluids*. Nelson Thornes.

MAYMÓ-GATELL. X, Y CHIEN, J. M. GOSSETT and S. H. ZINDER. 1997. *Isolation of a Bacterium that Reductively Dechlorinates Tetrachloroethene to Ethene*. Science. 276: 1568-1571.

McCALLION. O. N. M, K. M. G. TAYLOR, P. A. BRIDGES, M. THOMAS and A. J. TAYLOR. 1996. *Jet Nebulisers for Pulmonary Drug Delivery*. International Journal of Pharmaceutics. 130:1-11.

MERTENS. J. A. 2000. *Vapor Degreasing with Solvents*. Metal Finishing. 98(6) 43-51.

MORAN. M. J. 2005. *Occurrence and Implications of Selected Chlorinated Solvents in Ground Water and Source Water in the United States and in Drinking Water in 12 Northeast and Mid-Atlantic States, 1993–2002*. US Geological Survey.

MUERS. M. F. 1997. *Overview of Nebuliser Treatment*. Thorax. 52(2): S25–S30.

NERBRINK. O, M. DAHLBACK and H.C. HANSSON. 1994. *Why do Medical Nebulizers Differ in their Output and Particle Size Characteristics?*. Journal of Aerosol Medicine; 7(3): 259-276.

O'CALLAGHAN. C and P. W. BARRY. 1997. *The Science of Nebulised Drug Delivery*. Thorax. 52(2): S31–S44.

PARSONS CORPORATION. 2004. *Principles and Practices of Enhanced Anaerobic Bioremediation of Chlorinated Solvents*.

PULS. R. W. 1998. *Permeable Reactive Barrier Technologies for Contaminant Remediation*. USEPA Technology Innovation Office.

QIAN. J and C. K. LAW. 1997. *Regimes of Coalescence and Separation in Droplet Collision*. Journal of Fluid Mechanics; 331: 59-80.

RAYLEIGH. 1878. *On the Instability of Jets*. Proceedings of the London Mathematical Society. 10(1):4-13.

REDDY. K. R and J. A. ADAMS. 2001. *Effects of Soil Heterogeneity on Airflow Patterns and Hydrocarbon Removal during in situ Air Sparging*. Journal of Geotechnical and Geoenvironmental Engineering. 127(3): 234-247.

ROOSEVELT. S. E and M. Y. CORAPCIOGLU. 1998. *Air Bubble Migration in a Granular Porous Medium: Experimental Studies*. Water Resources Research. 34(5): 1131-1142.

SABATINI. D. A and T. A. Austin. 1991. *Characteristics of Rhodamine WT and Fluorescein as Adsorbing Ground-Water Tracers*. Groundwater. 29(3): 341-349.

SAFFMAN. P. G. 1965. *The Lift on a Small Sphere in a Slow Shear Flow*. Journal of Fluid Mechanics. 22: 385-400.

SCHMIDT. R, R. DEZEEUW, L. HENNING, and D. TRIPPLER. 2001. *State Programs to Clean Up Drycleaners*. State Coalition for Remediation of Drycleaners.

SEMER. R., J. A. ADAMS and K.R. REDDY. 1998. *An experimental investigation of air flow patterns in saturated soils during air sparging*. Geotechnical and Geological Engineering. 16(1).

SHULZ. H. 1998. *Mechanisms and Factors Affecting Intrapulmonary Particle Deposition: Implications for Efficient Inhalation Therapies*. PSTT. 1(8): 336-344.

SIRIGNANO. W. A. 1999. *Fluid Dynamics and Transport of Droplets and Sprays*. Cambridge University Press.

STECKEL. H and F. ESKANDAR. 2003. *Factors Affecting Aerosol Performance During Nebulization with Jet and Ultrasonic Nebulizers*. European Journal of Pharmaceutical Sciences. 19: 443–455.

TAULBEE. D. B and C. P. YU. 1975. *A Theory of Aerosol Deposition in the Human Respiratory Tract*. Journal of Applied Physiology. 38(1): 77-85.

TAYLOR. G and M. GUMBLETON. 2004. *Aerosols for Macromolecule Delivery*. American Journal of Drug Delivery 2(2): 1-14.

USEPA. 1998. *Field Applications of In Situ Remediation Technologies: Ground-Water Circulation Wells*. USEPA Technology Innovation Office.

USEPA. 2000. *Engineered Approaches to In Situ Bioremediation of Chlorinated Solvents: Fundamentals and Field Applications*. USEPA Technology Innovation Office.

USEPA. 2002. *Field Applications of In Situ Remediation Technologies: Permeable Reactive Barriers*. USEPA Technology Innovation Office.

USEPA. 2004. *In Situ Thermal Treatment of Chlorinated Solvents: Fundamentals and Field Applications*. USEPA Technology Innovation Office.

USEPA. 2001. *A Citizen's Guide to Bioremediation*. USEPA Technology Innovation Office.

USEPA. 2004. *Site Characterization Technologies for DNAPL Investigations*. USEPA Technology Innovation Office.

VASUDEVAN. D, R. FIMMEN and A. FRANCISCO. 2001. *Tracer-Grade Rhodamine WT: Structure of Constituent Isomers and their Sorption Behaviour*. Environmental Science and Technology *35*, 4089-4096.

WESTRICK, J. J., J. W. MELLO and R. F. THOMAS. 1984. *The Groundwater Supply Survey*. Journal of the American Water Works Association. 76(5): 52-59.

WHEELER. S. J. 1988. *A Conceptual Model for Soils Containing Large Gas Bubbles*. Geotechnique. 38(3). 389-397.

WHEELER. S. J. 1990. *Movement of Large Gas Bubbles in Unsaturated Fine-Grained Sediments*. Marine Geotechnology. 9. 113-129.

Turner Designs. 2004. *Aquafluor Users Manual*.

CHAPTER 11. APPENDICES

11.1. *Droplet Size Distribution Results*

11.1.1. *Droplet size distribution results for Figure 5.1*

Size low	*In %*	*Size high*	*Under %*	*Representative diameters*	
0.49	4.37	0.58	4.37	$d_{0.1}$	0.64
0.58	9.28	0.67	13.65	$d_{0.5}$	1.01
0.67	13.27	0.78	26.92	$d_{0.9}$	1.85
0.78	13.77	0.91	40.69	d_{32}	0.97
0.91	13.65	1.06	54.34	Δ	1.196
1.06	12.62	1.24	66.96	*UI*	0.379
1.24	10.73	1.44	77.69		
1.44	8.34	1.68	86.03		
1.68	5.90	1.95	91.94		
1.95	3.82	2.28	95.75		
2.28	2.28	2.65	98.05		
2.65	1.17	3.09	99.21		
3.09	0.51	3.60	99.73		
3.60	0.20	4.19	99.93		
4.19	0.07	4.88	100.00		
4.88	0.00	5.69			

11.1.2. *Droplet size distribution results for Figure 5.2*

Size low	*In %*	*Size high*	*Under %*	*Representative diameters*	
0.49	5.46	0.58	5.46	$d_{0.1}$	0.62
0.58	11.42	0.67	16.88	$d_{0.5}$	0.92
0.67	15.89	0.78	32.77	$d_{0.9}$	1.52
0.78	15.70	0.91	48.47	d_{32}	1.01
0.91	14.89	1.06	63.36	Δ	0.975
1.06	13.25	1.24	76.61	*UI*	0.308
1.24	10.46	1.44	87.07		
1.44	7.08	1.68	94.15		
1.68	3.83	1.95	97.98		
1.95	1.65	2.28	99.63		
2.28	0.37	2.65	100.00		
2.65	0.00	3.09			

11.1.3. *Droplet size distribution results for Figure 5.3*

Size low	*In %*	*Size high*	*Under %*	*Representative diameters*	
0.49	2.51	0.58	2.51	$d_{0.1}$	0.72
0.58	4.78	0.67	7.29	$d_{0.5}$	1.61
0.67	6.59	0.78	13.88	$d_{0.9}$	4.75
0.78	7.25	0.91	21.13	d_{32}	1.39
0.91	7.72	1.06	28.85	Δ	2.510
1.06	7.91	1.24	36.76	*UI*	0.768
1.24	7.80	1.44	44.56		
1.44	7.47	1.68	52.02		
1.68	7.00	1.95	59.02		
1.95	6.51	2.28	65.53		
2.28	6.02	2.65	71.55		
2.65	5.52	3.09	77.07		
3.09	5.04	3.60	82.11		
3.60	4.57	4.19	86.68		
4.19	3.99	4.88	90.67		
4.88	3.29	5.69	93.96		
5.69	2.53	6.63	96.49		
6.63	1.76	7.72	98.25		
7.72	1.06	9.00	99.31		
9.00	0.52	10.48	99.83		
10.48	0.17	12.21	100.00		
12.21	0.00	14.22			

11.1.4. *Droplet size distribution results for Figure 5.4*

Size low	*In %*	*Size high*	*Under %*	*Representative diameters*	
0.49	0.00	0.58	0.00	$d_{0.1}$	1.26
0.58	0.00	0.67	0.00	$d_{0.5}$	2.06
0.67	0.00	0.78	0.00	$d_{0.9}$	4.28
0.78	1.02	0.91	1.02	d_{32}	1.98
0.91	2.72	1.06	3.74	Δ	1.465
1.06	5.27	1.24	9.01	*UI*	0.498
1.24	8.71	1.44	17.72		
1.44	12.44	1.68	30.16		
1.68	14.65	1.95	44.81		
1.95	14.37	2.28	59.18		
2.28	12.22	2.65	71.40		
2.65	8.87	3.09	80.27		
3.09	5.76	3.60	86.03		
3.60	3.60	4.19	89.63		
4.19	2.35	4.88	91.98		
4.88	1.75	5.69	93.73		
5.69	1.55	6.63	95.28		
6.63	1.45	7.72	96.73		
7.72	1.28	9.00	98.01		
9.00	0.96	10.48	98.97		
10.48	0.66	12.21	99.62		
12.21	0.38	14.22	100.00		
14.22	0.00	16.57			

11.1.5. *Droplet size distribution results for Figure 5.5*

Size low	*In %*	*Size high*	*Under %*	*Representative diameters*	
0.49	3.44	0.58	3.44	$d_{0.1}$	0.67
0.58	6.59	0.67	10.03	$d_{0.5}$	1.21
0.67	9.19	0.78	19.22	$d_{0.9}$	2.40
0.78	10.21	0.91	29.43	d_{32}	1.12
0.91	10.93	1.06	40.36	Δ	1.433
1.06	11.14	1.24	51.50	*UI*	0.444
1.24	10.85	1.44	62.35		
1.44	10.19	1.68	72.54		
1.68	8.47	1.95	81.01		
1.95	6.91	2.28	87.92		
2.28	5.22	2.65	93.14		
2.65	3.60	3.09	96.74		
3.09	2.29	3.60	99.03		
3.60	0.97	4.19	100.00		
4.19	0.00	4.88			

11.1.6. *Droplet size distribution results for Figure 5.6*

Size low	*In %*	*Size high*	*Under %*	*Representative diameters*	
0.49	3.78	0.58	3.78	$d_{0.1}$	0.66
0.58	7.18	0.67	10.96	$d_{0.5}$	1.17
0.67	9.88	0.78	20.84	$d_{0.9}$	2.35
0.78	10.69	0.91	31.53	d_{32}	1.09
0.91	11.19	1.06	42.72	Δ	1.446
1.06	11.18	1.24	53.90	*UI*	0.447
1.24	10.68	1.44	64.58		
1.44	9.86	1.68	74.44		
1.68	8.11	1.95	82.55		
1.95	6.32	2.28	88.87		
2.28	4.65	2.65	93.52		
2.65	3.25	3.09	96.77		
3.09	2.16	3.60	98.93		
3.60	1.08	4.19	100.00		
4.19	0.00	4.88			

11.1.7. *Droplet size distribution results for Figure 5.7*

Size low	*In %*	*Size high*	*Under %*	*Representative diameters*	
0.49	3.58	0.58	3.58	$d_{0.1}$	0.67
0.58	6.83	0.67	10.41	$d_{0.5}$	1.19
0.67	9.46	0.78	19.87	$d_{0.9}$	2.36
0.78	10.41	0.91	30.28	d_{32}	1.10
0.91	11.04	1.06	41.32	Δ	1.417
1.06	11.18	1.24	52.50	*UI*	0.436
1.24	10.81	1.44	63.31		
1.44	10.11	1.68	73.42		
1.68	8.42	1.95	81.84		
1.95	6.82	2.28	88.66		
2.28	5.23	2.65	93.89		
2.65	3.63	3.09	97.52		
3.09	2.03	3.60	99.55		
3.60	0.44	4.19	100.00		
4.19	0.00	4.88			

11.1.8. *Droplet size distribution results for Figure 5.8*

Size low	*In %*	*Size high*	*Under %*	*Representative diameters*	
0.49	4.36	0.58	4.36	$d_{0.1}$	0.64
0.58	8.24	0.67	12.60	$d_{0.5}$	1.08
0.67	11.25	0.78	23.85	$d_{0.9}$	1.97
0.78	11.99	0.91	35.84	d_{32}	1.02
0.91	12.38	1.06	48.22	Δ	1.226
1.06	12.29	1.24	60.51	*UI*	0.379
1.24	11.85	1.44	72.36		
1.44	9.76	1.68	82.12		
1.68	7.47	1.95	89.59		
1.95	5.39	2.28	94.98		
2.28	3.47	2.65	98.45		
2.65	1.55	3.09	100.00		
3.09	0.00	3.60			

11.1.9. *Droplet size distribution results for Figure 5.9*

Size low	*In %*	*Size high*	*Under %*	*Representative diameters*	
0.49	3.40	0.58	3.40	$d_{0.1}$	0.67
0.58	6.51	0.67	9.91	$d_{0.5}$	1.22
0.67	9.07	0.78	18.98	$d_{0.9}$	2.44
0.78	10.09	0.91	29.07	d_{32}	1.12
0.91	10.80	1.06	39.87	Δ	1.453
1.06	11.02	1.24	50.89	*UI*	0.447
1.24	10.76	1.44	61.65		
1.44	10.14	1.68	71.79		
1.68	8.49	1.95	80.28		
1.95	6.98	2.28	87.26		
2.28	5.46	2.65	92.72		
2.65	3.94	3.09	96.66		
3.09	2.43	3.60	99.09		
3.60	0.91	4.19	100.00		
4.19	0.00	4.88			

11.1.10. *Droplet size distribution results for Figure 5.10*

Size low	*In %*	*Size high*	*Under %*	*Representative diameters*	
0.49	4.70	0.58	4.70	$d_{0.1}$	0.64
0.58	8.84	0.67	13.54	$d_{0.5}$	1.04
0.67	12.00	0.78	25.54	$d_{0.9}$	1.83
0.78	12.78	0.91	38.32	d_{32}	0.98
0.91	13.32	1.06	51.64	Δ	1.144
1.06	13.58	1.24	65.22	*UI*	0.354
1.24	11.70	1.44	76.92		
1.44	9.13	1.68	86.05		
1.68	6.50	1.95	92.55		
1.95	4.49	2.28	97.04		
2.28	2.48	2.65	99.52		
2.65	0.47	3.09	100.00		
3.09	0.00	3.60			

11.1.11. *Droplet size distribution results for Figure 5.11*

Size low	*In %*	*Size high*	*Under %*	*Representative diameters*	
0.49	0.05	0.58	0.05	$d_{0.1}$	1.28
0.58	0.19	0.67	0.24	$d_{0.5}$	2.54
0.67	0.52	0.78	0.76	$d_{0.9}$	4.6
0.78	1.45	0.91	2.21	d_{32}	2.19
0.91	2.60	1.06	4.81	Δ	1.304
1.06	4.01	1.24	8.82	*UI*	0.403
1.24	5.66	1.44	14.48		
1.44	7.48	1.68	21.96		
1.68	9.29	1.95	31.25		
1.95	10.68	2.28	41.93		
2.28	11.21	2.65	53.14		
2.65	11.76	3.09	64.89		
3.09	11.66	3.60	76.55		
3.60	9.13	4.19	85.68		
4.19	6.78	4.88	92.46		
4.88	4.69	5.69	97.14		
5.69	2.40	6.63	99.54		
6.63	0.46	7.72	100.00		
7.72	0.00	9.00			

11.1.12. *Droplet size distribution results for Figure 5.12*

Size low	*In %*	*Size high*	*Under %*	*Representative diameters*	
0.49	0.37	0.58	0.37	$d_{0.1}$	0.99
0.58	1.07	0.67	1.44	$d_{0.5}$	1.95
0.67	2.11	0.78	3.55	$d_{0.9}$	3.58
0.78	3.62	0.91	7.17	d_{32}	1.70
0.91	5.34	1.06	12.51	Δ	1.326
1.06	7.15	1.24	19.66	*UI*	0.418
1.24	8.89	1.44	28.55		
1.44	10.31	1.68	38.86		
1.68	11.19	1.95	50.05		
1.95	11.28	2.28	61.33		
2.28	11.23	2.65	72.56		
2.65	9.97	3.09	82.53		
3.09	7.67	3.60	90.20		
3.60	5.04	4.19	95.24		
4.19	2.95	4.88	98.19		
4.88	1.40	5.69	99.59		
5.69	0.40	6.63	99.99		
6.63	0.01	7.72	100.00		
7.72	0.00	9.00			

11.1.13. *Droplet size distribution results for Figure 5.13*

Size low	*In %*	*Size high*	*Under %*	*Representative diameters*	
0.49	0.10	0.58	0.10	$d_{0.1}$	1.20
0.58	0.32	0.67	0.42	$d_{0.5}$	2.37
0.67	0.77	0.78	1.19	$d_{0.9}$	4.24
0.78	1.85	0.91	3.04	d_{32}	2.05
0.91	3.16	1.06	6.20	Δ	1.281
1.06	4.71	1.24	10.91	*UI*	0.397
1.24	6.47	1.44	17.38		
1.44	8.32	1.68	25.70		
1.68	10.06	1.95	35.76		
1.95	11.24	2.28	47.00		
2.28	11.56	2.65	58.55		
2.65	12.28	3.09	70.83		
3.09	10.78	3.60	81.61		
3.60	7.91	4.19	89.52		
4.19	5.49	4.88	95.01		
4.88	3.44	5.69	98.45		
5.69	1.53	6.63	99.98		
6.63	0.02	7.72	100.00		
7.72	0.00	9.00			

11.1.14. *Droplet size distribution results for Figure 5.14*

Size low	*In %*	*Size high*	*Under %*	*Representative diameters*	
0.49	0.31	0.58	0.31	$d_{0.1}$	0.96
0.58	1.09	0.67	1.40	$d_{0.5}$	1.77
0.67	2.37	0.78	3.77	$d_{0.9}$	3.11
0.78	4.17	0.91	7.94	d_{32}	1.58
0.91	6.30	1.06	14.24	Δ	1.213
1.06	8.54	1.24	22.78	*UI*	0.376
1.24	10.61	1.44	33.39		
1.44	12.15	1.68	45.54		
1.68	12.86	1.95	58.40		
1.95	12.43	2.28	70.83		
2.28	10.39	2.65	81.22		
2.65	8.51	3.09	89.73		
3.09	5.55	3.60	95.28		
3.60	3.15	4.19	98.43		
4.19	1.34	4.88	99.77		
4.88	0.23	5.69	100.00		
5.69	0.00	6.63			

11.1.15. *Droplet size distribution results for Figure 5.15*

Size low	*In %*	*Size high*	*Under %*	*Representative diameters*	
0.49	0.02	0.58	0.02	$d_{0.1}$	1.23
0.58	0.12	0.67	0.14	$d_{0.5}$	2.21
0.67	0.45	0.78	0.59	$d_{0.9}$	3.64
0.78	1.51	0.91	2.10	d_{32}	1.98
0.91	3.00	1.06	5.10	Δ	1.091
1.06	4.94	1.24	10.04	*UI*	0.343
1.24	7.29	1.44	17.33		
1.44	9.84	1.68	27.16		
1.68	12.17	1.95	39.33		
1.95	13.32	2.28	52.65		
2.28	13.58	2.65	66.23		
2.65	13.06	3.09	79.29		
3.09	10.09	3.60	89.38		
3.60	5.96	4.19	95.33		
4.19	3.36	4.88	98.69		
4.88	1.29	5.69	99.98		
5.69	0.02	6.63	100.00		
6.63	0.00	7.72			

11.1.16. *Droplet size distribution results for Figure 5.16*

Size low	*In %*	*Size high*	*Under %*	*Representative diameters*	
0.49	0.76	0.58	0.76	$d_{0.1}$	0.85
0.58	2.12	0.67	2.88	$d_{0.5}$	1.60
0.67	3.91	0.78	6.79	$d_{0.9}$	2.91
0.78	5.90	0.91	12.69	d_{32}	1.43
0.91	7.96	1.06	20.65	Δ	1.285
1.06	9.85	1.24	30.50	*UI*	0.399
1.24	11.30	1.44	41.80		
1.44	12.06	1.68	53.86		
1.68	11.96	1.95	65.82		
1.95	10.89	2.28	76.71		
2.28	8.82	2.65	85.53		
2.65	7.00	3.09	92.53		
3.09	4.48	3.60	97.01		
3.60	2.32	4.19	99.33		
4.19	0.67	4.88	100.00		
4.88	0.00	5.69			

11.1.17. *Droplet size distribution results for Figure 5.17*

Size low	*In %*	*Size high*	*Under %*	*Representative diameters*	
0.49	1.91	0.58	1.91	$d_{0.1}$	0.75
0.58	3.84	0.67	5.75	$d_{0.5}$	1.43
0.67	5.86	0.78	11.61	$d_{0.9}$	3.03
0.78	7.89	0.91	19.50	d_{32}	1.30
0.91	9.50	1.06	29.00	Δ	1.595
1.06	10.57	1.24	39.57	*UI*	0.499
1.24	10.99	1.44	50.56		
1.44	10.66	1.68	61.22		
1.68	9.58	1.95	70.80		
1.95	7.84	2.28	78.64		
2.28	6.56	2.65	85.20		
2.65	5.40	3.09	90.60		
3.09	3.89	3.60	94.49		
3.60	2.54	4.19	97.03		
4.19	1.55	4.88	98.58		
4.88	0.85	5.69	99.43		
5.69	0.38	6.63	99.81		
6.63	0.15	7.72	99.96		
7.72	0.04	9.00	100.00		
9.00	0.00	10.48			

11.1.18. *Droplet size distribution results for Figure 5.18*

Size low	*In %*	*Size high*	*Under %*	*Representative diameters*	
0.49	4.30	0.58	4.30	$d_{0.1}$	0.64
0.58	9.15	0.67	13.45	$d_{0.5}$	1.01
0.67	13.10	0.78	26.55	$d_{0.9}$	1.69
0.78	13.92	0.91	40.47	d_{32}	0.96
0.91	14.39	1.06	54.86	Δ	1.043
1.06	14.48	1.24	69.34	*UI*	0.327
1.24	11.78	1.44	81.12		
1.44	8.52	1.68	89.64		
1.68	5.43	1.95	95.07		
1.95	3.04	2.28	98.11		
2.28	1.48	2.65	99.59		
2.65	0.40	3.09	100.00		
3.09	0.00	3.60			

11.1.19. *Droplet size distribution results for Figure 5.19*

Size low	*In %*	*Size high*	*Under %*	*Representative diameters*	
0.49	2.29	0.58	2.29	$d_{0.1}$	0.71
0.58	5.10	0.67	7.39	$d_{0.5}$	1.29
0.67	7.85	0.78	15.24	$d_{0.9}$	2.50
0.78	9.45	0.91	24.69	d_{32}	1.18
0.91	10.77	1.06	35.46	Δ	1.394
1.06	11.51	1.24	46.97	*UI*	0.432
1.24	11.53	1.44	58.50		
1.44	10.80	1.68	69.30		
1.68	9.40	1.95	78.70		
1.95	7.53	2.28	86.23		
2.28	5.77	2.65	92.00		
2.65	4.03	3.09	96.03		
3.09	2.37	3.60	98.40		
3.60	1.16	4.19	99.56		
4.19	0.40	4.88	99.96		
4.88	0.02	5.69	100.00		
5.69	0.00	6.63			

11.1.20. *Droplet size distribution results for Figure 5.20*

Size low	*In %*	*Size high*	*Under %*	*Representative diameters*	
0.49	3.07	0.58	3.07	$d_{0.1}$	0.68
0.58	5.95	0.67	9.02	$d_{0.5}$	1.25
0.67	8.45	0.78	17.47	$d_{0.9}$	2.41
0.78	9.71	0.91	27.18	d_{32}	1.14
0.91	10.69	1.06	37.87	Δ	1.377
1.06	11.20	1.24	49.07	*UI*	0.424
1.24	11.24	1.44	60.31		
1.44	10.94	1.68	71.25		
1.68	9.28	1.95	80.53		
1.95	7.25	2.28	87.78		
2.28	5.57	2.65	93.35		
2.65	3.90	3.09	97.25		
3.09	2.22	3.60	99.47		
3.60	0.54	4.19	100.00		
4.19	0.00	4.88			

11.1.21. *Droplet size distribution results for Figure 5.21*

Size low	*In %*	*Size high*	*Under %*	*Representative diameters*	
0.49	8.98	0.58	8.98	$d_{0.1}$	0.58
0.58	14.77	0.67	23.75	$d_{0.5}$	0.85
0.67	17.46	0.78	41.21	$d_{0.9}$	1.39
0.78	16.33	0.91	57.54	d_{32}	0.83
0.91	14.23	1.06	71.77	Δ	0.951
1.06	11.44	1.24	83.21	*UI*	0.292
1.24	8.49	1.44	91.70		
1.44	5.05	1.68	96.75		
1.68	2.44	1.95	99.19		
1.95	0.82	2.28	100.00		
2.28	0.00	2.65			

11.1.22. *Droplet size distribution results for Figure 5.22*

Size low	*In %*	*Size high*	*Under %*	*Representative diameters*	
0.49	5.33	0.58	5.33	$d_{0.1}$	0.62
0.58	9.98	0.67	15.31	$d_{0.5}$	0.98
0.67	13.42	0.78	28.73	$d_{0.9}$	1.62
0.78	14.06	0.91	42.79	d_{32}	0.93
0.91	14.34	1.06	57.13	Δ	1.008
1.06	14.25	1.24	71.38	*UI*	0.309
1.24	11.77	1.44	83.15		
1.44	8.68	1.68	91.83		
1.68	5.62	1.95	97.45		
1.95	2.56	2.28	100.00		
2.28	0.00	2.65			

11.1.23. *Droplet size distribution results for Figure 5.23*

Size low	*In %*	*Size high*	*Under %*	*Representative diameters*	
0.49	0.00	0.58	0.00	$d_{0.1}$	1.49
0.58	0.00	0.67	0.00	$d_{0.5}$	2.31
0.67	0.00	0.78	0.00	$d_{0.9}$	3.86
0.78	0.31	0.91	0.31	d_{32}	2.20
0.91	0.90	1.06	1.21	Δ	1.024
1.06	2.15	1.24	3.36	*UI*	0.311
1.24	4.80	1.44	8.15		
1.44	9.41	1.68	17.56		
1.68	14.17	1.95	31.73		
1.95	16.46	2.28	48.19		
2.28	16.81	2.65	65.00		
2.65	12.63	3.09	77.63		
3.09	8.98	3.60	86.61		
3.60	6.72	4.19	93.33		
4.19	4.46	4.88	97.79		
4.88	2.21	5.69	100.00		
5.69	0.00	6.63			

11.1.24. *Droplet size distribution results for Figure 5.24*

Size low	*In %*	*Size high*	*Under %*	*Representative diameters*	
0.49	0.80	0.58	0.80	$d_{0.1}$	0.92
0.58	1.83	0.67	2.63	$d_{0.5}$	2.04
0.67	2.99	0.78	5.62	$d_{0.9}$	4.13
0.78	4.20	0.91	9.82	d_{32}	1.70
0.91	5.43	1.06	15.25	Δ	1.573
1.06	6.62	1.24	21.87	*UI*	0.487
1.24	7.68	1.44	29.55		
1.44	8.55	1.68	38.10		
1.68	9.15	1.95	47.25		
1.95	9.57	2.28	56.82		
2.28	9.62	2.65	66.44		
2.65	9.40	3.09	75.84		
3.09	8.15	3.60	83.99		
3.60	6.61	4.19	90.60		
4.19	4.80	4.88	95.40		
4.88	3.04	5.69	98.44		
5.69	1.44	6.63	99.88		
6.63	0.13	7.72	100.00		
7.72	0.00	9.00			

11.1.25. *Droplet size distribution results for Figure 5.25*

Size low	*In %*	*Size high*	*Under %*	*Representative diameters*	
0.49	0.00	0.58	0.00	$d_{0.1}$	1.65
0.58	0.00	0.67	0.00	$d_{0.5}$	2.25
0.67	0.00	0.78	0.00	$d_{0.9}$	3.07
0.78	0.02	0.91	0.02	d_{32}	2.18
0.91	0.11	1.06	0.13	Δ	0.6296
1.06	0.50	1.24	0.63	*UI*	0.1981
1.24	2.18	1.44	2.81		
1.44	8.01	1.68	10.82		
1.68	17.84	1.95	28.66		
1.95	23.59	2.28	52.25		
2.28	24.01	2.65	76.25		
2.65	14.26	3.09	90.51		
3.09	7.61	3.60	98.12		
3.60	1.88	4.19	100.00		
4.19	0.00	4.88			

11.1.25. *Droplet size distribution results for Figure 5.26*

Size low	*In %*	*Size high*	*Under %*	*Representative diameters*	
0.49	0.39	0.58	0.39	$d_{0.1}$	0.99
0.58	1.13	0.67	1.52	$d_{0.5}$	1.98
0.67	2.19	0.78	3.71	$d_{0.9}$	3.68
0.78	3.68	0.91	7.39	d_{32}	1.71
0.91	5.36	1.06	12.75	Δ	1.362
1.06	7.11	1.24	19.86	*UI*	0.426
1.24	8.74	1.44	28.60		
1.44	9.99	1.68	38.59		
1.68	10.62	1.95	49.21		
1.95	11.14	2.28	60.35		
2.28	11.02	2.65	71.37		
2.65	10.16	3.09	81.53		
3.09	7.57	3.60	89.10		
3.60	5.51	4.19	94.61		
4.19	3.30	4.88	97.91		
4.88	1.66	5.69	99.57		
5.69	0.43	6.63	100.00		
6.63	0.00	7.72			

11.1.27. *Droplet size distribution results for Figure 5.27*

Size low	*In %*	*Size high*	*Under %*	*Representative diameters*	
0.49	0.00	0.58	0.00	$d_{0.1}$	1.59
0.58	0.00	0.67	0.00	$d_{0.5}$	2.07
0.67	0.00	0.78	0.00	$d_{0.9}$	2.65
0.78	0.01	0.91	0.01	d_{32}	2.02
0.91	0.09	1.06	0.10	Δ	0.511
1.06	0.59	1.24	0.69	*UI*	0.158
1.24	2.94	1.44	3.63		
1.44	10.82	1.68	14.45		
1.68	23.59	1.95	38.04		
1.95	31.67	2.28	69.72		
2.28	20.43	2.65	90.15		
2.65	7.62	3.09	97.77		
3.09	2.04	3.60	99.81		
3.60	0.19	4.19	100.00		
4.19	0.00	4.88			

11.1.28. *Droplet size distribution results for Figure 5.28*

Size low	*In %*	*Size high*	*Under %*	*Representative diameters*	
0.49	2.32	0.58	2.32	$d_{0.1}$	0.72
0.58	4.57	0.67	6.89	$d_{0.5}$	1.42
0.67	6.64	0.78	13.53	$d_{0.9}$	2.84
0.78	8.01	0.91	21.54	d_{32}	1.26
0.91	9.18	1.06	30.72	Δ	1.493
1.06	9.98	1.24	40.70	*UI*	0.461
1.24	10.34	1.44	51.04		
1.44	10.16	1.68	61.20		
1.68	9.49	1.95	70.69		
1.95	8.93	2.28	79.62		
2.28	7.55	2.65	87.17		
2.65	5.81	3.09	92.98		
3.09	4.08	3.60	97.06		
3.60	2.34	4.19	99.40		
4.19	0.61	4.88	100.00		
4.88	0.00	5.69			

11.1.29. *Droplet size distribution results for Figure 5.29*

Size low	*In %*	*Size high*	*Under %*	*Representative diameters*	
0.49	1.27	0.58	1.27	$d_{0.1}$	0.77
0.58	3.42	0.67	4.69	$d_{0.5}$	1.38
0.67	6.00	0.78	10.69	$d_{0.9}$	2.57
0.78	8.19	0.91	18.88	d_{32}	1.26
0.91	10.22	1.06	29.10	Δ	1.2990
1.06	11.72	1.24	40.82	*UI*	0.3987
1.24	12.36	1.44	53.18		
1.44	12.00	1.68	65.18		
1.68	10.70	1.95	75.88		
1.95	8.75	2.28	84.63		
2.28	6.62	2.65	91.25		
2.65	4.77	3.09	96.01		
3.09	2.77	3.60	98.78		
3.60	1.14	4.19	99.92		
4.19	0.08	4.88	100.00		
4.88	0.00	5.69			

11.1.30. *Droplet size distribution results for Figure 5.30*

Size low	*In %*	*Size high*	*Under %*	*Representative diameters*	
0.49	4.22	0.58	4.22	$d_{0.1}$	0.64
0.58	9.03	0.67	13.25	$d_{0.5}$	1.01
0.67	13.03	0.78	26.28	$d_{0.9}$	1.74
0.78	13.78	0.91	40.06	d_{32}	0.97
0.91	14.00	1.06	54.06	Δ	1.0840
1.06	13.28	1.24	67.34	*UI*	0.3409
1.24	11.59	1.44	78.94		
1.44	9.29	1.68	88.23		
1.68	6.13	1.95	94.36		
1.95	3.51	2.28	97.87		
2.28	1.67	2.65	99.54		
2.65	0.46	3.09	100.00		
3.09	0.00	3.60			

11.1.31. *Droplet size distribution results for Figure 5.31*

Size low	*In %*	*Size high*	*Under %*	*Representative diameters*	
0.49	8.98	0.58	8.98	*d0.1*	0.58
0.58	14.77	0.67	23.75	*d0.5*	0.85
0.67	17.46	0.78	41.21	*d0.9*	1.39
0.78	16.33	0.91	57.54	*d32*	0.83
0.91	14.23	1.06	71.77	*Δ*	0.9513
1.06	11.44	1.24	83.21	*UI*	0.2924
1.24	8.49	1.44	91.70		
1.44	5.05	1.68	96.74		
1.68	2.44	1.95	99.18		
1.95	0.82	2.28	100.00		
2.28	0.00	2.65			

11.1.32. *Droplet size distribution results for Figure 5.32*

Size low	*In %*	*Size high*	*Under %*	*Representative diameters*	
0.49	8.98	0.58	8.98	$d_{0.1}$	0.58
0.58	14.77	0.67	23.75	$d_{0.5}$	0.85
0.67	17.46	0.78	41.21	$d_{0.9}$	1.39
0.78	16.33	0.91	57.54	d_{32}	0.83
0.91	14.23	1.06	71.77	Δ	0.9513
1.06	11.44	1.24	83.21	*UI*	0.2924
1.24	8.49	1.44	91.70		
1.44	5.05	1.68	96.74		
1.68	2.44	1.95	99.18		
1.95	0.82	2.28	100.00		
2.28	0.00	2.65			

11.1.33. *Droplet size distribution results for Figure 5.33*

Size low	*In %*	*Size high*	*Under %*	*Representative diameters*	
0.49	1.79	0.58	1.79	$d_{0.1}$	0.74
0.58	4.04	0.67	5.83	$d_{0.5}$	1.42
0.67	6.36	0.78	12.19	$d_{0.9}$	2.74
0.78	8.00	0.91	20.19	d_{32}	1.27
0.91	9.45	1.06	29.64	Δ	1.4100
1.06	10.49	1.24	40.13	*UI*	0.4398
1.24	10.97	1.44	51.10		
1.44	10.85	1.68	61.95		
1.68	10.32	1.95	72.27		
1.95	9.06	2.28	81.33		
2.28	7.32	2.65	88.65		
2.65	5.25	3.09	93.90		
3.09	3.35	3.60	97.26		
3.60	1.98	4.19	99.24		
4.19	0.76	4.88	100.00		
4.88	0.00	5.69			

11.1.34. *Droplet size distribution results for Figure 5.34*

Size low	*In %*	*Size high*	*Under %*	*Representative diameters*	
0.49	5.22	0.58	5.22	$d_{0.1}$	0.63
0.58	9.78	0.67	15.00	$d_{0.5}$	1.00
0.67	13.17	0.78	28.16	$d_{0.9}$	1.68
0.78	13.66	0.91	41.82	d_{32}	0.95
0.91	13.71	1.06	55.53	Δ	1.0580
1.06	13.13	1.24	68.65	*UI*	0.3273
1.24	12.06	1.44	80.71		
1.44	9.16	1.68	89.87		
1.68	6.27	1.95	96.14		
1.95	3.38	2.28	99.52		
2.28	0.48	2.65	100.00		
2.65	0.00	3.09			

11.1.35. *Droplet size distribution results for Figure 5.35*

Size low	*In %*	*Size high*	*Under %*	*Representative diameters*	
0.49	0.43	0.58	0.43	$d_{0.1}$	0.90
0.58	1.34	0.67	1.77	$d_{0.5}$	1.58
0.67	3.02	0.78	4.79	$d_{0.9}$	2.80
0.78	5.82	0.91	10.61	d_{32}	1.45
0.91	8.49	1.06	19.10	Δ	1.2040
1.06	10.81	1.24	29.91	*UI*	0.3733
1.24	12.38	1.44	42.29		
1.44	12.55	1.68	54.84		
1.68	11.22	1.95	66.06		
1.95	11.15	2.28	77.21		
2.28	9.94	2.65	87.15		
2.65	7.11	3.09	94.26		
3.09	4.28	3.60	98.55		
3.60	1.45	4.19	100.00		
4.19	0.00	4.88			

11.1.36. *Droplet size distribution results for Figure 5.36*

Size low	*In %*	*Size high*	*Under %*	*Representative diameters*	
0.49	5.79	0.58	5.79	$d_{0.1}$	0.62
0.58	10.77	0.67	16.56	$d_{0.5}$	0.95
0.67	14.35	0.78	30.91	$d_{0.9}$	1.57
0.78	14.62	0.91	45.53	d_{32}	0.92
0.91	14.34	1.06	59.87	Δ	1.0020
1.06	13.29	1.24	73.16	*UI*	0.3121
1.24	11.65	1.44	84.81		
1.44	8.19	1.68	93.00		
1.68	5.06	1.95	98.07		
1.95	1.93	2.28	100.00		
2.28	0.00	2.65			

11.1.37. *Droplet size distribution results for Figure 5.37*

Size low	*In %*	*Size high*	*Under %*	*Representative diameters*	
0.49	0.14	0.58	0.14	$d_{0.1}$	1.14
0.58	0.44	0.67	0.58	$d_{0.5}$	2.18
0.67	1.02	0.78	1.60	$d_{0.9}$	3.84
0.78	2.27	0.91	3.87	d_{32}	1.91
0.91	3.76	1.06	7.63	Δ	1.2360
1.06	5.51	1.24	13.14	*UI*	0.3865
1.24	7.45	1.44	20.59		
1.44	9.46	1.68	30.05		
1.68	11.21	1.95	41.26		
1.95	11.95	2.28	53.21		
2.28	11.63	2.65	64.84		
2.65	12.08	3.09	76.92		
3.09	9.94	3.60	86.86		
3.60	6.58	4.19	93.44		
4.19	4.22	4.88	97.66		
4.88	2.06	5.69	99.73		
5.69	0.27	6.63	100.00		
6.63	0.00	7.72			

11.1.38. *Droplet size distribution results for Figure 5.38*

Size low	*In %*	*Size high*	*Under %*	*Representative diameters*	
0.49	2.52	0.58	2.52	$d_{0.1}$	0.71
0.58	4.92	0.67	7.44	$d_{0.5}$	1.39
0.67	7.05	0.78	14.49	$d_{0.9}$	2.87
0.78	8.32	0.91	22.81	d_{32}	1.24
0.91	9.36	1.06	32.17	Δ	1.5590
1.06	10.02	1.24	42.20	*UI*	0.4777
1.24	10.24	1.44	52.44		
1.44	10.05	1.68	62.49		
1.68	9.58	1.95	72.07		
1.95	8.14	2.28	80.21		
2.28	6.77	2.65	86.98		
2.65	5.36	3.09	92.35		
3.09	3.96	3.60	96.31		
3.60	2.55	4.19	98.86		
4.19	1.14	4.88	100.00		
4.88	0.00	5.69			

11.1.39. *Droplet size distribution results for Figure 5.39*

Size low	*In %*	*Size high*	*Under %*	*Representative diameters*	
0.49	1.81	0.58	1.81	$d_{0.1}$	0.74
0.58	4.13	0.67	5.94	$d_{0.5}$	1.36
0.67	6.60	0.78	12.54	$d_{0.9}$	2.45
0.78	8.49	0.91	21.03	d_{32}	1.23
0.91	10.18	1.06	31.21	Δ	1.2610
1.06	11.39	1.24	42.60	*UI*	0.3892
1.24	11.97	1.44	54.57		
1.44	11.89	1.68	66.46		
1.68	11.27	1.95	77.73		
1.95	8.81	2.28	86.54		
2.28	6.47	2.65	93.01		
2.65	4.26	3.09	97.27		
3.09	2.23	3.60	99.50		
3.60	0.50	4.19	100.00		
4.19	0.00	4.88			

11.1.40. *Droplet size distribution results for Figure 5.40*

Size low	*In %*	*Size high*	*Under %*	*Representative diameters*	
0.49	4.02	0.58	4.02	$d_{0.1}$	0.63
0.58	11.56	0.67	15.58	$d_{0.5}$	0.89
0.67	18.43	0.78	34.01	$d_{0.9}$	1.32
0.78	18.44	0.91	52.45	d_{32}	0.87
0.91	17.42	1.06	69.87	Δ	0.7688
1.06	15.45	1.24	85.32	*UI*	0.2464
1.24	9.33	1.44	94.65		
1.44	4.32	1.68	98.97		
1.68	1.03	1.95	100.00		
1.95	0.00	2.28			

11.1.41. *Droplet size distribution results for Figure 5.41*

Size low	*In %*	*Size high*	*Under %*	*Representative diameters*	
0.49	0.00	0.58	0.00	$d_{0.1}$	1.80
0.58	0.00	0.67	0.00	$d_{0.5}$	2.31
0.67	0.00	0.78	0.00	$d_{0.9}$	2.87
0.78	0.00	0.91	0.00	d_{32}	2.25
0.91	0.00	1.06	0.01	Δ	0.4654
1.06	0.05	1.24	0.06	*UI*	0.1537
1.24	0.52	1.44	0.58		
1.44	4.13	1.68	4.71		
1.68	15.60	1.95	20.31		
1.95	26.95	2.28	47.26		
2.28	31.29	2.65	78.55		
2.65	17.09	3.09	95.64		
3.09	4.36	3.60	100.00		
3.60	0.00	4.19			

11.1.42. *Droplet size distribution results for Figure 5.42*

Size low	*In %*	*Size high*	*Under %*	*Representative diameters*	
0.49	2.12	0.58	2.12	$d_{0.1}$	0.74
0.58	4.17	0.67	6.29	$d_{0.5}$	1.50
0.67	6.06	0.78	12.35	$d_{0.9}$	3.10
0.78	7.37	0.91	19.72	d_{32}	1.32
0.91	8.50	1.06	28.22	*Δ*	1.5710
1.06	9.32	1.24	37.54	*UI*	0.4841
1.24	9.74	1.44	47.28		
1.44	9.72	1.68	57.00		
1.68	9.35	1.95	66.35		
1.95	9.08	2.28	75.43		
2.28	7.97	2.65	83.40		
2.65	6.50	3.09	89.90		
3.09	4.91	3.60	94.81		
3.60	3.32	4.19	98.13		
4.19	1.73	4.88	99.86		
4.88	0.14	5.69	100.00		
5.69	0.00	6.63			

11.1.43. *Droplet size distribution results for Figure 5.43*

Size low	*In %*	*Size high*	*Under %*	*Representative diameters*	
0.49	0.00	0.58	0.00	$d_{0.1}$	1.54
0.58	0.00	0.67	0.00	$d_{0.5}$	2.00
0.67	0.00	0.78	0.00	$d_{0.9}$	2.49
0.78	0.01	0.91	0.01	d_{32}	1.94
0.91	0.15	1.06	0.16	Δ	0.4762
1.06	0.89	1.24	1.05	*UI*	0.1542
1.24	4.05	1.44	5.10		
1.44	13.40	1.68	18.50		
1.68	26.44	1.95	44.94		
1.95	32.44	2.28	77.38		
2.28	17.45	2.65	94.83		
2.65	4.69	3.09	99.52		
3.09	0.48	3.60	100.00		
3.60	0.00	4.19			

11.1.44. *Droplet size distribution results for Figure 5.44*

Size low	*In %*	*Size high*	*Under %*	*Representative diameters*	
0.49	4.24	0.58	4.24	$d_{0.1}$	0.65
0.58	8.08	0.67	12.32	$d_{0.5}$	1.08
0.67	11.20	0.78	23.51	$d_{0.9}$	1.88
0.78	12.25	0.91	35.76	d_{32}	1.01
0.91	12.85	1.06	48.61	Δ	1.1450
1.06	12.75	1.24	61.35	*UI*	0.3562
1.24	11.92	1.44	73.27		
1.44	10.51	1.68	83.78		
1.68	7.93	1.95	91.71		
1.95	5.35	2.28	97.06		
2.28	2.76	2.65	99.82		
2.65	0.18	3.09	100.00		
3.09	0.00	3.60			

11.2. *Medium-Scale Test Column Results*

11.2.1. *Test 1*

Time (mins)	*A*	*B*	*C*	*D*	*E*
0	0.000	0.000	0.000	0.000	0.000
15	0.573	1.602	3.530	2.101	12.52
30	1.040	2.066	4.310	11.74	34.06
45	0.403	2.590	6.702	32.04	58.52
60	1.018	3.930	9.252	53.75	83.06
75	1.288	4.102	13.40	86.36	100.2
90	0.947	6.148	16.55	113.6	124.6
105	2.255	6.094	19.53	127.8	142.8
120	1.778	7.382	21.47	147.6	159.8
135	2.376	7.738	24.94	164.2	174.2
150	3.013	8.709	27.99	180.6	194.2
165	3.124	8.910	29.53	189.3	214.3
180	4.402	9.790	33.16	192.9	234.2
195	12.35	7.509	25.35	180.9	233.0
210	13.51	8.418	27.31	180.6	231.1
225	11.95	8.133	24.99	175.0	223.7
240	12.54	7.669	25.68	169.2	224.8

Time (mins)	*A*	*B*	*C*	*D*	*E*
0	0.000	0.000	0.000	0.000	0.000
15	1.011	2.825	6.226	3.706	22.09
30	1.834	3.644	7.602	20.72	60.08
45	0.711	4.568	11.82	56.52	103.2
60	1.795	6.931	16.32	94.81	146.5
75	2.272	7.235	23.64	152.3	176.9
90	1.670	10.84	29.19	200.4	219.9
105	3.977	10.75	34.45	225.4	252.0
120	3.136	13.02	37.87	260.4	282.0
135	4.191	13.65	43.99	289.6	307.4
150	5.314	15.36	49.37	318.6	342.7
165	5.510	15.71	52.09	333.9	378.1
180	7.764	17.27	58.49	340.3	413.2
195	21.79	13.24	44.71	319.1	411.1
210	23.83	14.85	48.17	318.6	407.8
225	21.08	14.34	44.08	308.7	394.7
240	22.12	13.53	45.30	298.5	396.6

11.2.2. *Test 2*

Time (mins)	*A*	*B*	*C*	*D*	*E*
0	0.000	0.000	0.000	0.000	0.000
15	1.178	0.544	2.967	0.000	14.78
30	1.437	1.039	4.075	0.059	35.37
45	1.545	1.435	5.683	1.259	55.58
60	1.827	3.031	5.614	5.596	73.68
75	2.113	2.620	8.401	14.73	99.69
90	2.065	4.174	10.12	25.95	114.8
105	2.880	4.045	11.16	39.50	139.1
120	3.662	4.836	12.32	53.09	154.5
135	4.120	5.700	13.88	64.80	165.0
150	3.888	6.314	14.98	85.38	182.9
165	3.750	6.530	16.69	97.58	205.3
180	3.853	7.510	18.55	112.8	221.9
195	4.378	6.762	14.31	82.38	220.0
210	5.487	6.500	14.30	97.40	210.2
225	5.238	6.112	14.09	107.0	175.7
240	5.473	5.849	14.94	107.0	206.8

Time (mins)	*A*	*B*	*C*	*D*	*E*
0	0.000	0.000	0.000	0.000	0.000
15	2.078	0.959	5.233	0.000	26.07
30	2.534	1.832	7.187	0.104	62.39
45	2.725	2.531	10.02	2.220	98.03
60	3.222	5.346	9.901	9.870	130.0
75	3.727	4.621	14.82	25.98	175.8
90	3.642	7.362	17.85	45.77	202.5
105	5.079	7.134	19.68	69.67	245.3
120	6.459	8.529	21.73	93.64	272.5
135	7.266	10.05	24.48	114.3	291.0
150	6.857	11.14	26.42	150.6	322.6
165	6.614	11.52	29.43	172.1	362.1
180	6.796	13.25	32.71	198.9	391.4
195	7.721	11.93	25.24	145.3	388.0
210	9.677	11.46	25.22	171.8	370.7
225	9.238	10.78	24.85	188.7	309.9
240	9.653	10.32	26.35	188.7	364.7

11.2.3. *Test 3*

Time (mins)	*A*	*B*	*C*	*D*	*E*
0	0.000	0.000	0.000	0.000	0.000
15	1.250	1.055	3.548	0.000	14.28
30	2.563	2.775	8.081	2.154	41.71
45	2.812	4.303	11.43	6.425	68.51
60	3.201	5.182	11.94	18.29	99.10
75	3.781	5.582	17.37	29.25	128.6
90	3.799	8.302	21.65	44.97	157.8
105	5.310	8.392	25.74	57.71	175.0
120	5.770	10.21	29.42	66.20	200.4
135	6.170	10.82	30.27	80.43	216.1
150	7.220	12.97	32.74	102.3	232.3
165	7.220	13.57	35.64	137.1	252.9
180	7.330	14.74	36.58	170.0	270.7
195	8.270	13.64	33.53	192.1	263.2
210	9.020	13.16	32.86	201.4	263.2
225	8.940	12.56	31.66	204.4	256.1
240	8.040	12.20	31.26	206.1	257.0

Time (mins)	*A*	*B*	*C*	*D*	*E*
0	0.000	0.000	0.000	0.000	0.000
15	2.205	1.861	6.258	0.000	25.19
30	4.520	4.894	14.25	3.799	73.57
45	4.960	7.589	20.16	11.33	120.8
60	5.646	9.139	21.06	32.25	174.8
75	6.669	9.845	30.64	51.58	226.8
90	6.700	14.64	38.19	79.30	278.3
105	9.365	14.80	45.40	101.8	308.6
120	10.18	18.01	51.89	116.7	353.4
135	10.88	19.09	53.39	141.8	381.1
150	12.73	22.88	57.75	180.5	409.7
165	12.73	23.94	62.86	241.8	446.0
180	12.93	26.00	64.52	299.9	477.4
195	14.59	24.06	59.14	338.8	464.2
210	15.91	23.21	57.96	355.2	464.2
225	15.77	22.16	55.84	360.5	451.7
240	14.18	21.52	55.14	363.5	453.3

11.2.4. *Test 4*

Time (mins)	*A*	*B*	*C*	*D*	*E*
0	0.000	0.000	0.000	0.000	0.000
15	0.776	0.543	2.097	7.103	17.30
30	1.466	2.736	3.776	13.43	37.64
45	1.671	4.527	4.843	18.76	60.42
60	2.413	5.941	6.039	25.92	91.98
75	3.008	7.183	7.755	35.46	108.5
90	3.169	7.606	10.23	45.07	128.8
105	3.989	8.797	12.19	60.03	158.5
120	4.454	9.255	14.13	72.52	183.0
135	4.756	10.51	17.36	87.38	203.0
150	5.201	11.38	19.57	104.1	222.4
165	5.699	11.84	21.62	133.8	231.1
180	5.976	12.56	24.08	148.3	239.5
195	6.993	12.16	20.09	137.7	233.9
210	6.854	11.71	22.19	145.2	232.6
225	7.515	11.84	21.52	143.5	228.3
240	7.461	10.60	21.15	133.1	228.7

Time (mins)	*A*	*B*	*C*	*D*	*E*
0	0.000	0.000	0.000	0.000	0.000
15	1.369	0.958	3.698	12.53	30.50
30	2.586	4.825	6.660	23.69	66.38
45	2.947	7.984	8.542	33.09	106.6
60	4.256	10.48	10.65	45.72	162.2
75	5.305	12.67	13.68	62.55	191.3
90	5.589	13.41	18.04	79.50	227.1
105	7.035	15.52	21.50	105.9	279.5
120	7.856	16.32	24.92	127.9	322.7
135	8.388	18.53	30.61	154.1	358.0
150	9.173	20.06	34.51	183.5	392.2
165	10.05	20.89	38.13	235.9	407.5
180	10.54	22.14	42.47	261.5	422.3
195	12.33	21.44	35.43	242.8	412.5
210	12.09	20.64	39.13	256.0	410.2
225	13.25	20.87	37.95	253.0	402.6
240	13.16	18.69	37.30	234.7	403.3

11.2.5. *Test 5*

Time (mins)	*A*	*B*	*C*	*D*	*E*
0	0.000	0.000	0.000	0.000	0.000
15	0.637	0.000	0.000	0.000	0.000
30	0.160	0.000	0.000	0.000	0.000
45	1.101	0.088	0.273	0.354	1.787
60	0.962	0.168	0.081	0.211	2.763
75	0.411	0.178	0.288	0.000	3.446
90	0.068	0.307	0.595	0.318	3.687
105	0.538	0.103	0.762	0.519	5.239
120	0.599	0.143	0.638	0.038	5.863
135	0.505	0.277	0.669	0.724	6.348
150	0.457	0.599	0.603	1.162	6.912
165	0.157	0.377	0.679	0.393	7.937
180	0.018	0.683	0.224	0.055	8.177
195	0.817	0.813	1.064	1.947	9.207
210	1.266	1.651	1.745	1.696	9.197
225	1.087	1.310	1.695	2.074	8.447
240	0.896	1.013	2.443	2.067	9.207

Time (mins)	*A*	*B*	*C*	*D*	*E*
0	0.000	0.000	0.000	0.000	0.000
15	1.123	0.000	0.000	0.000	0.000
30	0.282	0.000	0.000	0.000	0.000
45	1.942	0.155	0.481	0.624	3.152
60	1.697	0.296	0.143	0.372	4.873
75	0.725	0.314	0.508	0.000	6.078
90	0.120	0.541	1.049	0.561	6.503
105	0.949	0.182	1.344	0.915	9.240
120	1.056	0.252	1.125	0.067	10.34
135	0.891	0.489	1.180	1.277	11.20
150	0.806	1.056	1.064	2.049	12.19
165	0.277	0.665	1.198	0.693	14.00
180	0.032	1.205	0.395	0.097	14.42
195	1.441	1.434	1.877	3.434	16.24
210	2.233	2.912	3.078	2.991	16.22
225	1.917	2.310	2.989	3.658	14.90
240	1.580	1.787	4.309	3.646	16.24

11.2.6. *Test 6*

Time (mins)	*A*	*B*	*C*	*D*	*E*
0	0.000	0.000	0.000	0.000	0.000
15	0.648	0.000	0.000	0.000	0.000
30	0.959	0.000	0.000	0.000	0.000
45	1.098	0.217	1.298	0.397	1.500
60	0.942	1.524	2.222	1.298	4.783
75	1.381	2.084	4.302	1.547	6.743
90	1.336	3.800	6.712	4.520	8.823
105	1.442	3.466	8.602	4.909	11.20
120	2.288	4.600	10.67	7.438	13.43
135	3.064	5.576	14.33	9.698	15.88
150	3.318	7.099	16.63	12.54	17.41
165	3.119	7.339	19.36	15.16	20.03
180	1.815	6.429	16.48	12.73	22.17
195	2.472	5.724	15.47	19.69	23.64
210	3.617	6.599	18.00	25.67	24.44
225	3.103	6.849	19.61	31.28	24.07
240	3.065	6.679	21.90	35.50	24.97

Time (mins)	*A*	*B*	*C*	*D*	*E*
0	0.000	0.000	0.000	0.000	0.000
15	1.143	0.000	0.000	0.000	0.000
30	1.691	0.000	0.000	0.000	0.000
45	1.937	0.383	2.289	0.700	2.646
60	1.661	2.688	3.919	2.289	8.436
75	2.436	3.676	7.587	2.728	11.89
90	2.356	6.702	11.84	7.972	15.56
105	2.543	6.113	15.17	8.658	19.76
120	4.035	8.113	18.82	13.12	23.69
135	5.404	9.834	25.28	17.10	28.01
150	5.852	12.52	29.33	22.13	30.71
165	5.501	12.94	34.15	26.75	35.33
180	3.201	11.34	29.07	22.47	39.11
195	4.360	10.10	27.29	34.74	41.70
210	6.379	11.64	31.75	45.29	43.11
225	5.473	12.08	34.59	55.18	42.46
240	5.406	11.78	38.63	62.63	44.04

11.2.7. *Test 7*

Time (mins)	*A*	*B*	*C*	*D*	*E*
0	0.000	0.000	0.000	0.000	0.000
15	0.000	0.000	0.000	0.502	0.725
30	0.102	0.000	0.000	1.398	0.948
45	0.011	0.081	2.022	2.778	1.585
60	0.343	0.512	2.539	4.431	3.241
75	0.059	0.041	3.559	5.661	5.712
90	0.079	0.830	4.802	7.763	8.700
105	0.082	0.998	6.149	9.609	12.13
120	0.027	1.101	6.610	11.40	15.12
135	0.412	1.170	8.201	13.11	19.07
150	0.379	2.162	9.695	15.28	22.06
165	0.220	2.015	10.95	17.56	24.87
180	0.511	2.591	11.25	19.85	27.45
195	1.370	2.245	9.315	20.55	30.74
210	2.311	2.842	9.375	20.34	34.74
225	2.075	2.669	9.225	19.24	36.35
240	1.752	2.381	9.695	20.24	37.00

Time (mins)	*A*	*B*	*C*	*D*	*E*
0	0.000	0.000	0.000	0.000	0.000
15	0.000	0.000	0.000	0.885	1.279
30	0.180	0.000	0.000	2.466	1.672
45	0.019	0.143	3.566	4.900	2.795
60	0.605	0.903	4.478	7.815	5.716
75	0.104	0.072	6.277	9.984	10.07
90	0.139	1.464	8.469	13.69	15.34
105	0.145	1.760	10.84	16.95	21.40
120	0.048	1.942	11.66	20.12	26.67
135	0.727	2.064	14.46	23.14	33.64
150	0.668	3.813	17.10	26.97	38.91
165	0.388	3.554	19.30	30.99	43.87
180	0.901	4.570	19.83	35.03	48.42
195	2.416	3.960	16.43	36.26	54.22
210	4.076	5.012	16.53	35.89	61.28
225	3.660	4.707	16.27	33.95	64.12
240	3.090	4.199	17.10	35.71	65.26

11.2.8. *Test 8*

Time (mins)	*A*	*B*	*C*	*D*	*E*
0	0.000	0.000	0.000	0.000	0.000
15	0.000	0.000	0.000	0.776	0.000
30	0.000	0.000	0.000	2.348	0.000
45	0.000	2.733	0.578	2.946	6.722
60	0.066	3.368	1.001	4.496	10.87
75	0.025	4.080	0.708	6.420	13.66
90	0.537	4.967	2.287	8.561	16.42
105	0.006	6.045	4.381	11.39	18.78
120	1.357	5.527	5.334	12.89	20.71
135	0.707	6.685	7.984	14.53	22.19
150	1.400	7.346	9.761	17.58	25.58
165	1.998	8.320	12.26	20.28	27.72
180	2.650	9.619	15.64	22.98	29.60
195	9.650	8.275	14.25	17.01	30.42
210	12.67	7.674	18.94	17.72	30.87
225	11.22	9.065	23.41	19.19	30.19
240	10.74	8.238	25.70	19.65	29.64

Time (mins)	*A*	*B*	*C*	*D*	*E*
0	0.000	0.000	0.000	0.000	0.000
15	0.000	0.000	0.000	1.369	0.000
30	0.000	0.000	0.000	4.141	0.000
45	0.000	4.820	1.019	5.196	11.86
60	0.116	5.940	1.765	7.930	19.16
75	0.044	7.196	1.249	11.32	24.08
90	0.947	8.760	4.034	15.10	28.95
105	0.011	10.66	7.727	20.09	33.11
120	2.393	9.748	9.408	22.74	36.52
135	1.247	11.79	14.08	25.63	39.13
150	2.469	12.96	17.22	31.01	45.11
165	3.524	14.67	21.62	35.77	48.88
180	4.674	16.97	27.59	40.53	52.20
195	17.02	14.59	25.13	30.00	53.64
210	22.35	13.53	33.41	31.26	54.44
225	19.79	15.99	41.29	33.85	53.24
240	18.94	14.53	45.33	34.66	52.27

11.3. *Large-scale Column Results*

11.3.1. *Test 1*

T_0				
	0	**200**	**400**	**600**
A	1.430	0.933	0.770	3.406
B	1.279	0.393	15.71	13.42
C	1.200	1.225	4.963	18.14
D	1.923	0.269	1.224	20.05
E	0.990	1.210	0.574	6.693

T_5				
	0	**200**	**400**	**600**
A	1.652	7.610	27.33	45.36
B	1.913	5.265	57.72	71.88
C	1.432	16.53	88.91	249.1
D	6.234	35.43	402.4	3840
E	7.690	50.07	164.5	417.3

$T_5 - T_0$				
	0	**200**	**400**	**600**
A	0.222	6.677	26.56	41.95
B	0.634	4.872	42.01	58.46
C	0.232	15.305	83.95	231.0
D	4.311	35.161	401.2	3820
E	6.700	48.86	163.9	410.6

$\mu mol/m^3$				
	0	**200**	**400**	**600**
A	2.914	13.42	48.20	80.00
B	3.374	9.286	101.8	126.8
C	2.526	29.15	156.8	439.3
D	10.99	62.49	709.7	6773
E	13.56	88.31	290.1	736.0

11.3.2. *Test 2*

T_0				
	0	**200**	**400**	**600**
A	0.698	1.183	2.974	2.215
B	0.703	1.005	5.581	1.282
C	1.507	1.812	1.273	3.746
D	1.019	2.396	1.709	2.605
E	0.606	3.112	1.718	2.048

T_5				
	0	**200**	**400**	**600**
A	1.464	3.408	23.49	43.80
B	1.084	1.281	61.39	84.15
C	3.207	2.777	97.11	232.3
D	5.089	2.790	262.3	5722
E	5.677	3.874	112.8	312.6

$T_5 - T_0$				
	0	**200**	**400**	**600**
A	0.766	2.225	20.52	41.58
B	0.381	0.276	55.81	82.87
C	1.700	0.965	95.84	228.6
D	4.070	0.394	260.6	5719
E	5.071	0.762	111.1	310.6

$\mu mol/m^3$				
	0	**200**	**400**	**600**
A	2.582	6.011	41.43	77.24
B	1.912	2.259	108.3	148.4
C	5.656	4.898	171.3	409.7
D	8.975	4.921	462.6	10091
E	10.01	6.833	198.9	551.3

11.3.3. *Test 3*

T_0				
	0	**200**	**400**	**600**
A	3.677	2.323	1.377	3.297
B	2.671	1.488	5.171	3.422
C	2.783	2.731	5.448	9.122
D	2.788	2.855	3.735	6.658
E	2.753	3.300	5.336	2.777

T_5				
	0	**200**	**400**	**600**
A	4.652	4.166	3.834	13.42
B	3.512	6.513	8.675	35.16
C	5.257	4.339	9.798	104.2
D	3.904	5.059	84.28	960.0
E	4.155	4.658	7.103	11.66

$T_5 - T_0$				
	0	**200**	**400**	**600**
A	0.975	1.843	2.457	10.12
B	0.841	5.025	3.504	31.74
C	2.474	1.608	4.350	95.08
D	1.116	2.204	80.55	953.3
E	1.402	1.358	1.767	8.883

$\mu mol/m^3$				
	0	**200**	**400**	**600**
A	8.205	7.348	6.762	23.67
B	6.194	11.49	15.30	62.01
C	9.272	7.653	17.28	183.8
D	6.885	8.923	148.6	1693
E	7.328	8.215	12.53	20.56

11.3.4. *Test 4*

T_0				
	0	**200**	**400**	**600**
A	2.046	1.975	4.561	3.906
B	0.953	2.170	5.857	3.426
C	0.741	2.536	3.245	6.197
D	0.991	2.226	2.982	1.915
E	0.866	1.854	2.823	1.674

T_5				
	0	**200**	**400**	**600**
A	4.461	5.101	5.306	7.458
B	3.071	6.105	7.348	9.206
C	2.094	2.834	22.27	139.6
D	2.417	3.047	30.17	293.6
E	2.119	3.454	15.75	25.06

$T_5 - T_0$				
	0	**200**	**400**	**600**
A	2.415	3.126	0.745	3.552
B	2.118	3.935	1.491	5.780
C	1.353	0.298	19.03	133.4
D	1.426	0.821	27.19	291.7
E	1.253	1.600	12.93	23.39

$\mu mol/m^3$				
	0	**200**	**400**	**600**
A	7.868	8.997	9.358	13.15
B	5.416	10.77	12.96	16.24
C	3.693	4.998	39.28	246.2
D	4.263	5.374	53.21	517.8
E	3.737	6.092	27.78	44.20

11.3.5. *Test 5*

T_0				
	0	**200**	**400**	**600**
A	2.567	1.124	2.284	1.229
B	2.416	1.447	2.502	1.659
C	4.037	0.679	1.456	6.452
D	3.644	1.360	1.141	7.573
E	3.654	0.523	3.204	5.856

T_5				
	0	**200**	**400**	**600**
A	2.878	2.003	4.249	3.432
B	2.891	2.523	7.732	13.69
C	5.428	2.874	21.93	55.24
D	5.273	5.173	69.42	628.0
E	4.665	1.522	4.484	8.372

$T_5 - T_0$				
	0	**200**	**400**	**600**
A	0.311	0.879	1.965	2.203
B	0.475	1.076	5.230	12.03
C	1.391	2.195	20.47	48.79
D	1.629	3.813	68.28	620.4
E	1.011	0.999	1.280	2.516

$\mu mol/m^3$				
	0	**200**	**400**	**600**
A	5.076	3.533	7.494	6.053
B	5.099	4.450	13.64	24.15
C	9.573	5.069	38.68	97.43
D	9.300	9.124	122.4	1108
E	8.228	2.684	7.908	14.77

11.3.6. *Test 6*

T_0				
	0	**200**	**400**	**600**
A	2.419	1.319	2.655	3.821
B	2.707	1.933	2.319	4.689
C	3.081	2.856	3.872	5.119
D	2.137	2.350	3.323	4.164
E	3.340	3.753	5.142	4.340

T_5				
	0	**200**	**400**	**600**
A	2.745	3.198	4.660	6.327
B	3.497	2.489	6.576	10.52
C	3.602	3.281	15.90	32.82
D	5.763	2.904	59.52	228.2
E	3.563	4.893	10.48	16.92

$T_5 - T_0$				
	0	**200**	**400**	**600**
A	0.326	1.879	2.005	2.506
B	0.790	0.556	4.257	5.831
C	0.521	0.425	12.03	27.70
D	3.626	0.554	56.20	224.0
E	0.223	1.140	5.338	12.58

$\mu mol/m^3$				
	0	**200**	**400**	**600**
A	4.841	5.640	8.219	11.16
B	6.168	4.390	11.60	18.55
C	6.353	5.787	28.04	57.88
D	10.16	5.122	105.0	402.5
E	6.284	8.630	18.48	29.84